ALMA MATER STUDIORUM - UNIVERSITÀ DI BOLOGNA

SCUOLA DI INGEGNERIA E ARCHITETTURA

DICAM

CORSO DI LAUREA MAGISTRALE IN INGEGNERIA PER L'AMBIENTE E IL TERRITORIO

CURRICULUM

"EARTH RESOURCES ENGINEERING"

MASTER THESIS

in

MODELLISTICA IDROLOGICA M

The impact of spatial representation on flood hazard assessment: a comparison between 1D, quasi-2D and fully 2D hydrodynamic models of Rio Marano (Rimini)

CANDIDATO   RELATORE

Giacomo Negretto   Chiar.mo Prof. Attilio Castellarin

                                                   CORRELATORI

                                          Dott. Ing. Davide Sormani

                                          Dott. Ing. Alessio Domeneghetti

Abstract

Hydraulic modelling of floods allows to simulate flood propagation in natural channels and floodplains, representing an important instrument for flood hazard assessment. In this project, using the software HEC-RAS, four hydraulic models were constructed and compared through a case study on Marano stream (Rimini). The models include a one-dimensional model, with extended cross sections to represent the floodplain flow; a 1D model, with floodplain represented as hydrostatic *Storage Areas*; a coupled 1D/2D model, with a 1D representation of the main channel flow and a 2D representation of the flow within the floodplain and a fully 2D model, with both main channel and floodplains represented through a two-dimensional hydrodynamic numerical scheme. Firstly, 1D steady flow simulations were performed to get a conservative estimate of the maximum water levels along the stream, for flood discharges with return periods equal to 20, 50, 100, 200 years. The results enabled to identify the flood-prone areas and to test the hydraulic adequacy of the structures. Secondly, unsteady flow simulations were performed with all four hydraulic models, to assess flood peaks reductions associated to the flood wave routing (T = 20, 50, 100, 200 years). Furthermore, the floodplain inundation dynamics resulting from each model were compared. The results of the steady flow simulations showed that six bridges are inadequate and most of the natural floodplains of the stream are inundated proportionally to the flood discharge considered. Concerning the unsteady flow simulations, each model returned different results in terms of flood peak reduction and floodplain inundation dynamics. Hydrometric observations are needed to assess which of the four models return the most reliable results. However, the 1D model with extended cross section resulted inadequate for modeling channel-floodplain interactions and floodplain inundation dynamics. The 1D model with hydrostatic *Storage Areas* resulted to be suitable for assessing the flood peak reduction induced by the introduction of levees separating the floodplain from the main channel. Regarding the coupled 1D/2D model, the results showed that the elevation profile of the structure coupling 1D and 2D flow areas has a large impact on model results. The 2D model returned the most detailed information regarding flood propagation in both main channel and floodplains.

Sommario

La modellazione idraulica permette di simulare la propagazione delle piene nell'alveo naturale e nelle aree golenali, rappresentando un importante strumento per la valutazione del rischio di alluvione. In questo studio, utilizzando il software HEC-RAS, sono stati sviluppati e confrontati quattro modelli idraulici del torrente Marano (Rimini). I modelli utilizzati sono: un modello monodimensionale, nel quale le sezioni trasversali sono state allungate per rappresentare il flusso nelle aree golenali; un modello monodimensionale, nel quale le aree golenali sono state rappresentate come aree idrostatiche (*Storage Areas*); un modello quasi bidimensionale, nel quale il flusso nell'alveo è stato rappresentato in una dimensione e il flusso nelle aree golenali in due dimensioni; e un modello completamente bidimensionale, nel quale entrambi i flussi sono stati rappresentati tramite uno schema numerico bidimensionale. Innanzitutto, eseguendo le simulazioni 1D in moto stazionario, si sono stimati conservativamente i massimi livelli idrici lungo il torrente, per tempi di ritorno di 20, 50 ,100 e 200 anni. I risultati hanno permesso di identificare le aree inondabili e di valutare l'adeguatezza idraulica dei manufatti. Successivamente, utilizzando tutti e quattro i modelli idraulici, si sono eseguite le simulazioni in moto non stazionario per quantificare la laminazione di onde di piena di progetto (T = 20, 50, 100, 200 anni). Le simulazioni in moto non stazionario sono inoltre servite per studiare le diverse dinamiche di inondazione delle aree golenali associate ai quattro modelli considerati. I risultati delle analisi in moto stazionario hanno mostrato che la maggior parte delle aree golenali del torrente vengono inondate proporzionalmente alla portata di piena considerata; inoltre si sono rilevati sei ponti inofficiosi. Per quanto riguarda le analisi in moto non stazionario, ciascun modello ha restituito risultati differenti sia in termini di laminazione dell'onda di piena di progetto, che in termini di dinamiche di inondazione delle aree golenali. Sono quindi necessarie osservazioni idrometriche al fine di valutare quale modello restituisca i risultati più attinenti al caso reale. Tuttavia, il modello 1D con sezioni allungate, è risultato inadeguato per rappresentare le interazioni tra alveo e aree golenali. Si sottolinea invece come il modello 1D con *Storage Areas* possa essere adatto per studiare la laminazione dell'onda di piena indotta dall'introduzione di argini golenali. Riguardo al modello quasi-2D, si è notato come il profilo altimetrico della struttura collegante l'area a flusso 1D e l'area a flusso 2D, influisca significativamente sui risultati del modello. Il modello completamente 2D ha invece restituito i risultati più dettagliati in termini di propagazione della piena sia nell'alveo che nelle aree golenali.

Table of contents

1. Introduction

Floods are among the world most impacting natural hazards. An increase in floods as a direct consequence of climate change, is expected in the future. Italy, with its peculiar geomorphology and geographical location, is likely to be strongly affected by the effects of climate change. Indeed, flood events have been numerous already over the past fifty years. In Figure 1 is reported a map from the "Istituto di Ricerca per la Protezione Idrogeologica (IRPI)" in the "Rapporto Periodico sul rischio posto alla Popolazione italiana da Frane e Inondazioni", showing the flood events causing victims or missing from 1968 to 2018.
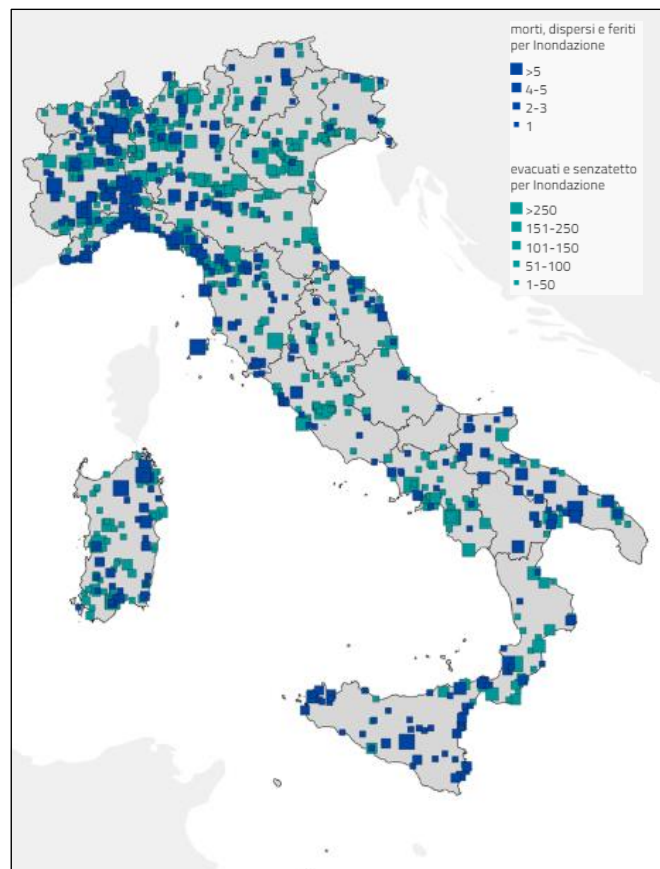
Figure 1: Map of the flood events from 1968 to 2018 (IRPI, CNR)

So far, in Italy as in many other countries in the world, structural measures, as reshaping of river beds, levees and weirs, have been widely adopted. But as a matter of fact, observing the map reported above, these measures did not contribute to prevent floods from causing victims or missing. To reduce the number of structural measures while also reducing the costs, promoting a sustainable development of territories; it must be understood that the security, availability and beauty of a river basin depend first and foremost on the uses to which is intended for (*LEGAMBIENTE, 2007*).

Data provided by ISPRA (*Rapporto Consumo Suolo, 2018*) show that artificial soil coverage has increased at national level, from 2.7%, estimated for the 1950's, to 7,75% (considering water bodies), estimated for 2017. The level of soil sealing within 150 m from the water bodies is 7.6%, and 11.6% of the artificial soil coverage is located at flood hazard areas with return periods between 100 and

200 years. These data clearly indicate, that the improper land management and excessive urban development and sprawling may increase flood risk dramatically.

In this context, hydraulic modelling of floods is becoming increasingly important, since allow to simulate flood propagation in natural channels and in floodplains, representing an important instrument for flood hazard assessment. In particular, hydraulic models can provide flood inundation maps which include the maximum inundation extent, flood depth distribution and flood velocity distribution. A more accurate identification of flood prone areas characterized by high-risk level can help planners and flood-risk managers to improve preparedness and design interventions. Moreover, the European Floods Directive emphasizes the importance of flood risk communication with the people involved, stimulating their involvement in the development of flood management plans. In this respect, detailed 2D flood maps, might allow non-expert public a first perception of flood impact.

Over the last decades, the performances of hydraulic models have improved greatly as a result of more powerful computers and of the improved detail of the input data (e.g. land use, topography). There are different ways to model river hydraulics. 1D models represents the river and the surrounding floodplains by using cross sections, modelling the flow in one dimension. These models perform well when the flow is confined in a straight river even during flood event. For rivers, having a winding pattern and complex floodplains, a two-dimension flow representation, showing the 2D flow paths and the local velocities during river flooding, is preferred.

This Master Thesis focuses on the representation of the hydraulic behavior of the Marano stream, a water body which flows through the municipalities of Coriano, Rimini and Riccione. In particular, the analysis considers the stretch of the stream between Ospedaletto (Rimini, *cross section 36.5*) and the stream's mouth located in Riccione (Rimini, *cross section 0*).

We performed both steady and unsteady flow simulations by using the software Hec-Ras, developed by the US Army Corps of Engineers (*HEC-RAS, Hydraulic Reference Manual, 2016*). The steady flow simulations were used to get a conservative estimate of the maximum water levels along the stream, for flood discharges with return periods equal to 20, 50, 100, 200 years, provided by the River Basin Authority within the river basing management plan ("Piano di Bacino"). The results were also used to delineate flood prone areas and test the hydraulic adequacy of the structures. The unsteady flow simulations have enabled the assessment of the flood peaks reductions and of the floodplain inundation dynamics, instead; the unsteady flow analysis consider the same return periods of the steady flow ones. Since the Marano catchment is ungauged we adopted a regionalization method (*Majone et al. (2000a; 2000b)*) for identifying synthetic flood hydrographs (also referred to as design hydrographs), which is illustrated in chapter 8.1.

The hydraulic behavior of the stream was studied using four different models:

- A 1D model with extended cross sections to represent the floodplain flow;
- A 1D model with floodplains represented as hydrostatic *Storage Areas*, which are hydraulically connected to the main channel;
- A coupled 1D/2D model, with a 1D representation of the main channel flow and a 2D representation of the flow within the floodplain;
- A fully 2D model with both main channel and floodplains represented through a two-dimensional hydrodynamic numerical scheme.

In conclusion, a comparison between the results of the four models is shown, explaining advantages and disadvantages of each approach.

2. The Marano stream

The Marano stream is a waterbody flowing into the Adriatic Sea, after crossing the municipalities of Montescudo, Coriano, Rimini and Riccione. The main channel is 27 km long, with source located on the Mount Ghelfa (628 m a.s.l.), in the province of San Marino, and mouth located in the town of Riccione. The catchment of the Marano stream has a total area of 60.4 km^2 and it is adjacent to the catchments of the Melo and Conca rivers on the orographic right side; and of the Marecchia and Ausa rivers on the orographic left side. The catchment areas for each crossed municipality are shown in Table 1.

Province	Municipality	Area (km^2)
Rimini	Coriano	17.60
	Rimini	12.30
	Montescudo	6.50
	Riccione	3.10
San Marino		18.00
Pesaro	Sassofeltrio	1.80
	Montegrimano	1.10
Total		60.4

Table 1: Catchment areas for each crossed municipality

The first stretch of the stream is mainly straight with natural embankments, it is few dozen wide and it has significant slopes until the town of Ospedaletto (Rimini). From here, the slopes decrease (<1%) and the profile of the stream becomes winding creating large meanders along which discontinuous levees are present. The last downstream stretch is canalized, still with discontinuous levees. The stream flows into the Adriatic Sea with a north oriented estuary.

The Marano is characterized by a torrential hydrological regime; therefore, during the summer period, it has mostly zero discharges.

Along the stream there are many river banks collapsed, unclassified levees, buildings and infrastructures at flood risk. The last downstream stretch can be considered as the one at the highest flood risk, since, if the levees are breached, the urban area of Riccione is flooded.

The sediment transport is mainly in suspension, since the catchment is mainly composed by clays, silts and sands. Along the first stretch of the stream there are mainly limestone, chalk and sandstones outcrops. During floods periods, the stream path is constantly modified, the water erodes the levees on one side, depositing alluvial materials on the opposite side and vice versa. Nevertheless, the bottom sediment transport is quantitatively limited.

The land use in the catchment is respectively: 35% arable land, 12% permanent crops, 6% pasture and meadow, 5% woods, 11% other uses.

The present study focuses on the meandering stretch of the stream showed in Figure 1, not considering the first upstream stretch.
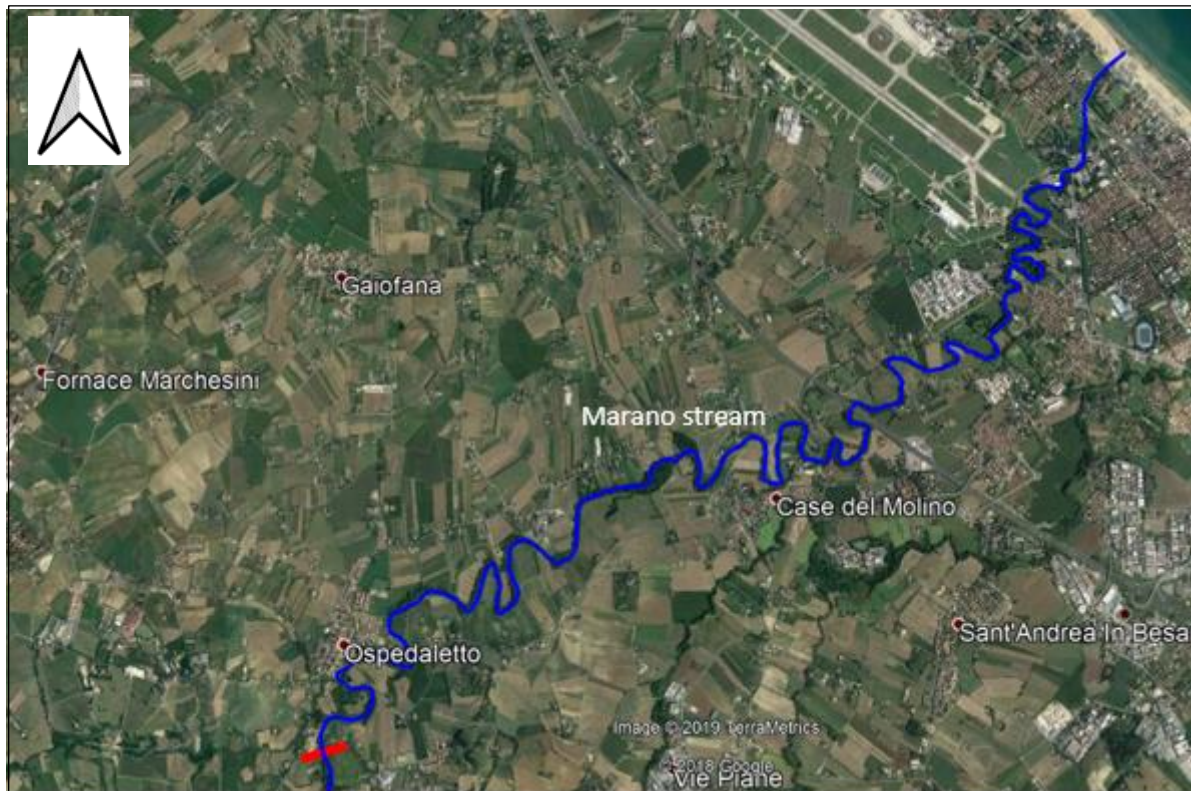
Figure 2: Stretch of the stream analyzed, in red the first upstream cross section (36.5)

Figure 3: Detail of the drainage area at the closing section of Ospedaletto

Table 2 illustrates the characteristics of the catchment at the upstream section and at the mouth.

Section	Drainage Area (km²)	Mean elevation of the catchment (m.a.s.l.)	Elevation at the outlet (m.a.s.l.)	Main channel length (km)
Ospedaletto (Coriano)	54.27	228.63	36.14	16.79
Mouth	60.4	209	-0.6	27

Table 2: Catchment characteristics

3. HEC-RAS Modeling system

The HEC-RAS software was developed at the hydrologic engineering center by the U.S. Army Corps of Engineers. This modeling system is designed to perform one-dimensional, two-dimensional or combined 1D and 2D hydraulic calculations for a network of natural and constructed channels, overbank and floodplain areas or levee protected areas. In this Master Thesis, two components of HEC-RAS software (5.0.5) were used. Firstly, by means of a 1D steady flow simulation, water surface profiles for steady gradually varied flow were computed, using the results to evaluate the flooded areas and the hydraulic adequacy of the structures. Secondly, the flood wave propagation and the natural flood peak reduction were evaluated by means of 1D, quasi-2D and 2D unsteady flow simulations.

3.1 Geometric data

The first step to develop the hydraulic model is to enter geometric data, they consist of:

- Background map (optional);
- Information on the connectivity of the stream system;
- Cross-section data, consisting of altitude of the terrain, Main channel bank station, Ineffective flow area, Obstruction Area and Levee;
- Left, central and right cross sections distances;
- Energetic loss coefficients (Manning's values and contraction and expansion coefficients);
- Hydraulic structures data (Bridge/Culvert, Inline Structures, Lateral Structures, Storage Areas and 2D Flow Areas).

3.2 Steady flow water surface profiles (1D)

For the steady flow computation, the following assumptions are made:

- The water density is assumed to be constant;
- Flow is steady;
- Flow is gradually varied (at each cross section the pressure distribution is hydrostatic, making an exception at hydraulic structures where the flow can be rapidly varied, at this location the momentum equation is used);
- Flow is one dimensional (velocity components in direction different from that of the flow are not considered);
- River channels have slopes less than 1:10 (the vertical pressure head is approximated as the depth of the water measured perpendicular to the channel bottom).

3.2.2 Equations

The water surface profiles are computed from one cross section to the next solving the Energy equation iteratively:

$$Z_2 + Y_2 + \frac{a_2 V_2^2}{2g} = Z_1 + Y_1 + \frac{a_1 V_1^2}{2g} + h_e$$

Where:

Z_1, Z_2 are the elevation of the main channel inverts;

Y_1, Y_2 are the depth of water at cross sections;

V_1, V_2 are the average velocities;

a_1, a_2 are the velocity weighting coefficients computed as:

$$a = \frac{\sum Q_i v_i^2}{Q v^2}$$

g is the gravitational acceleration;

h_e is the energy head loss
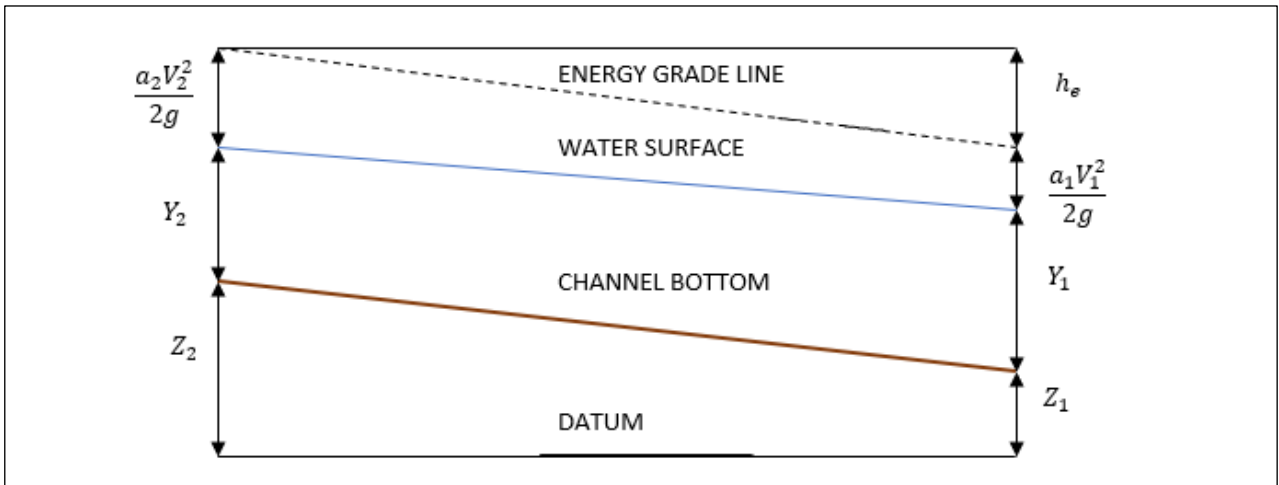
Figure 4: Representation of the Energy equation

The equation for the energy head loss includes the friction losses and the contraction or expansion losses and is written as follows:

$$h_e = L\bar{S}_f + C \left| \frac{a_2 V_2^2}{2g} - \frac{a_1 V_1^2}{2g} \right|$$

Where:

L is the discharge weighted reach length;

$\bar{S}_f$ is the friction slope between two section;

C is the expansion or contraction loss coefficient.

The discharge weighted reach length, L, is computed as:

$$L = \frac{L_{lob} \bar{Q}_{lob} + L_{ch} \bar{Q}_{ch} + L_{rob} \bar{Q}_{rob}}{\bar{Q}_{lob} + \bar{Q}_{ch} + \bar{Q}_{rob}}$$

Where:

L_{lob}, L_{ch}, L_{rob} are the cross section reach lengths in the left overbank, main channel and right overbank;

$\bar{Q}_{lob}$, $\bar{Q}_{ch}$, $\bar{Q}_{rob}$ are the average flows between sections for the left overbank, main channel and right overbank

The friction slope at each cross section is computed from the Manning's equation, so that the friction slope between two cross section is given by:

$$\bar{S}_f = \left(\frac{Q_1 + Q_2}{K_1 + K_2}\right)^2$$

Where:

Q_1, Q_2 are the average flow in the two cross sections;

K_1, K_2 are the conveyances in the two cross sections computed as follows:

$$K = \frac{1.486}{n} AR^{2/3}$$

Where:

n is the Manning's roughness coefficient;

A is the flow area;

R is the hydraulic radius.

If in a section different values of Manning's roughness coefficient are present, the software subdivides it as shown below:
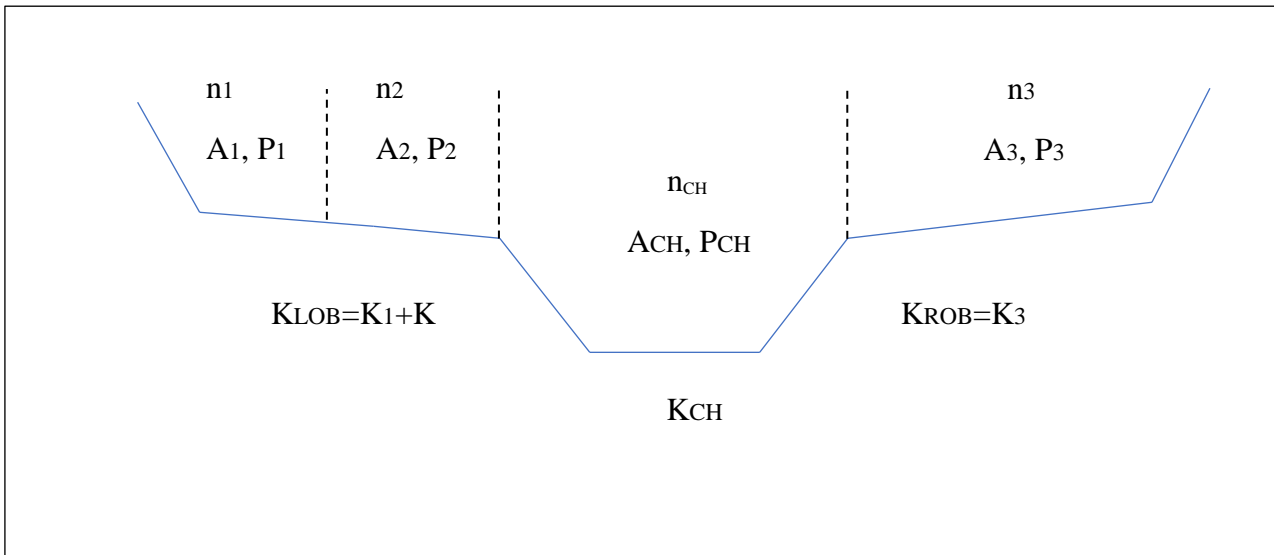
Figure 5: Conveyance Subdivision

The computational procedure to determine the unknown water surface at a cross section is as follows:

1. Assume a water surface elevation at the upstream cross section (for subcritical profile), or downstream (for supercritical profile).
2. Determine the total conveyance and the velocity head at the corresponding cross section.
3. Compute $\bar{S}_f$ and h_e.
4. Compute WS2.

8

5. Compare WS2 with WS1 assumed at the first step, repeat the steps until the difference is within the defined tolerance (0.003m).

The iterative procedure to assume a water surface elevation is the following:

- The first water surface assumption is the projection of the previous cross section's water surface depth onto the cross section of interest.
- The second trial water surface elevation is computed as follows:

$$WSnew = WSassumed + 0.70(WScomputed - WSassumed)$$

- The following trials are based on "Secant" method:

$$WS_i = WS_{i-2} - \frac{(WS^c_{i-2} - WS_{i-2})(WS_{i-2}-WS_{i-1})}{WS^c_{i-2} - WS_{i-2} + WS_{i-1} - WS^c_{i-1}}$$

If the denominator becomes too small (less than 1.0E-2), the secant method fails. In this case a new guess is made computing the average of the assumed and computed water surfaces from the previous iteration.

The program is limited by a maximum number of iterations. During the iterations, the program keeps track of the water surface producing the minimum error between the assumed and the computed value. If the maximum number of iterations is reached before a balanced water surface is computed, the program computes the critical depth. After that, if the minimum of the difference between assumed and computed water surface is smaller than 0.1 m and this water surface is on the correct side of critical depth, the program uses this water surface as the final answer. Otherwise, if the minimum of the difference between assumed and computed water surface is greater than 0.1 m or the water surface is on the wrong side of critical depth, the program uses the critical depth. Usually, when the Energy Equation cannot be balanced, there is an inadequate number of cross sections or bad cross section data. However, this can be due to an attempt of the program to compute a subcritical water surface when the flow regime is supercritical.

Critical depth is the elevation for which the total energy head is a minimum. The total energy head is defined as:

$$H = WS + \frac{aV^2}{2g}$$
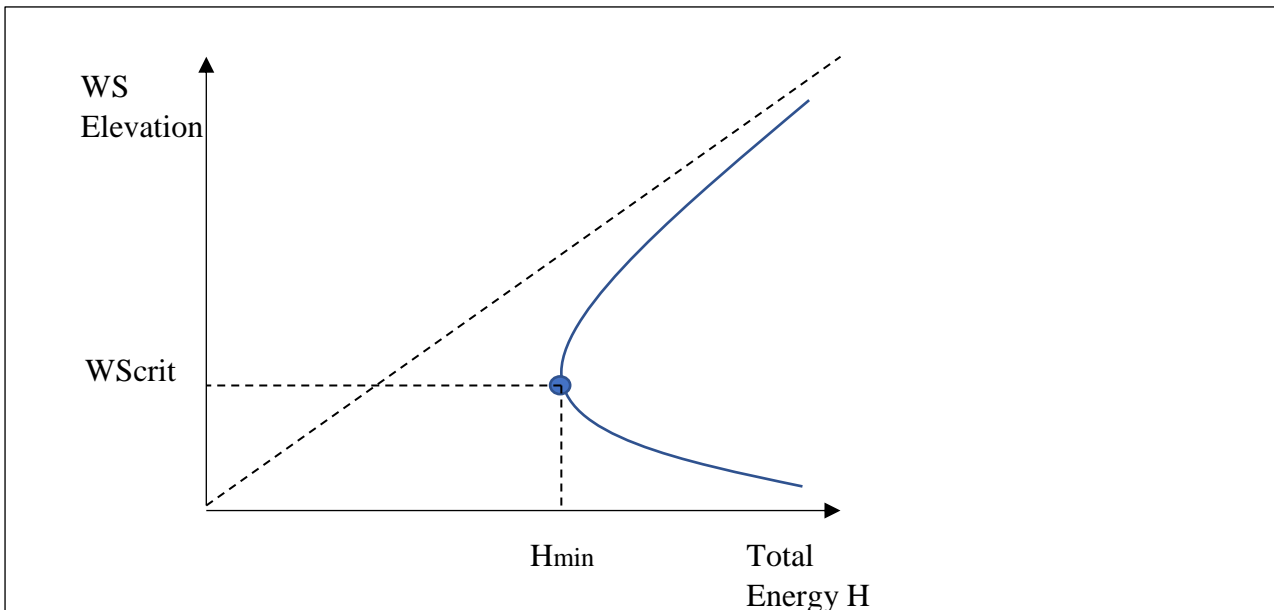
Figure 6: Total Energy Head vs Water Surface Elevation

The program can compute the critical depth with two methods, a "parabolic" method or a "secant" method. The parabolic method is the fastest, but it can individuate a single minimum energy. Since for most cross sections there is only one minimum on the energy curve, the parabolic method is set as the default method. The parabolic method determines three values of total energy head for the corresponding values of water surface evenly spaced. The water surface that corresponds to the minimum value of total energy head, is defined by the parabola passing through the three points on the H versus WS elevation plane and it is used for the next assumption of WS elevation. The iterative procedure stops when the change in WS elevation is smaller than 0.003 m and the total energy head has not changed more than 0.003 m.

Occasionally, there can be more than one minimum on the total energy curve. This can occur at cross section having breaks in the total energy curve due to levees, ineffective flow areas or very wide and flat overbanks. In these cases is advisable to use the secant method. This method subdivides the cross section in 30 intervals and creates a table containing the WS elevation and the total energy head for each of these intervals. After that, the program searches the value in the table having a lower energy in respect of the values above and below it, this interval is identified as a local minimum. Then, the program keeps searching others local minimum (two is the maximum) in the table. If the program finds more than one local minimum, it chooses as final answer the WS elevation with the lowest energy. If the local minimum is due to an interruption of the energy curve then the program identifies as critical depth the one associated to the next lowest value of energy. If the critical depth is located at the top of the section, this is not a critical depth. Thus, the program doubles the height of the section extending vertical walls at the extremes of the section and try again.

When the water surface passes through the critical depth is no more possible to apply the energy equation. Indeed, the energy equation can be applied only to gradually varied flow and the transition through critical depth is a rapidly varying flow situation. This is the case of significant changes in channels slope, bridge constrictions, drop structures, weirs and stream junction. At drop structures and weirs empirical equations are used, while in other situations the momentum equation is needed.

The momentum equation is derived from Newton's second law of motion:

$$\sum F_x = ma$$

Applying the equation just written to a body of water located between two cross sections, the change in momentum over a unit time is written as follows:

$$P_2 - P_1 + W_x - F_f = Q\rho\Delta V_x$$

Where:

P is the hydraulic pressure at section 1 and 2;

W_x is the force exerted by the weight of water in the X direction;

F_f is the force due to external friction losses between section 2 and 1;

Q is the discharge;

ρ is the density of water;

ΔV_x is the change on velocity between section 2 and 1, in the X direction.
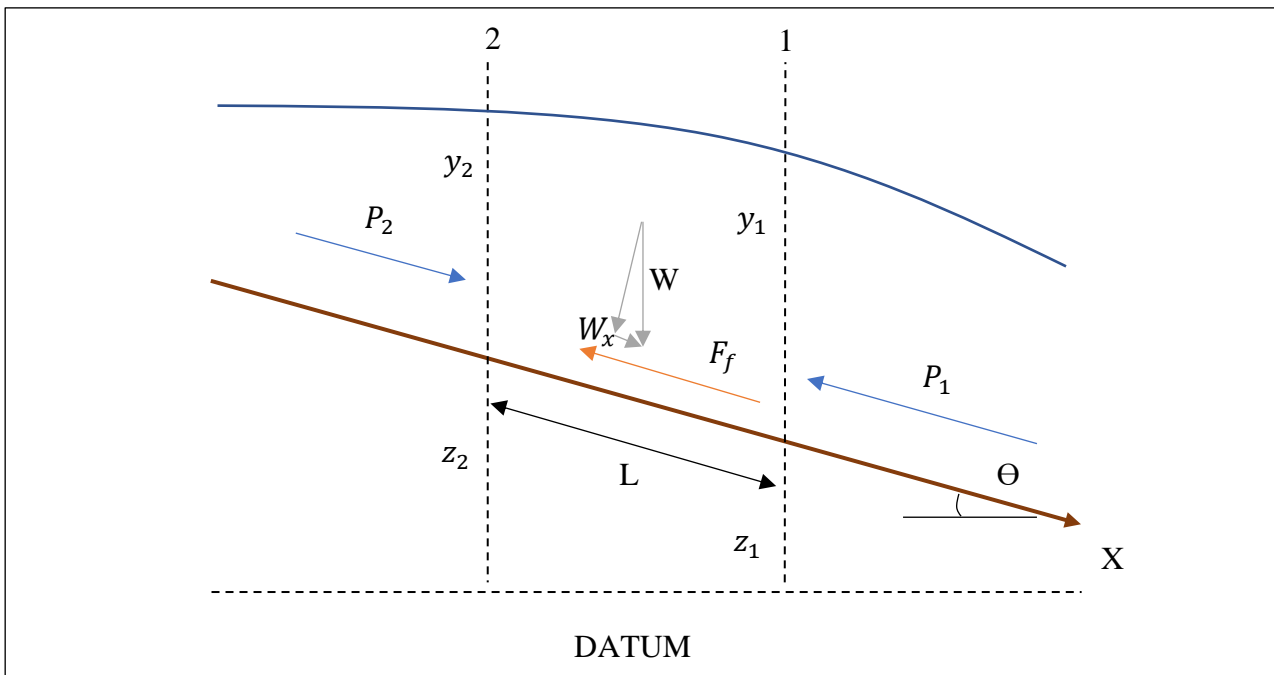
Figure 7: Application of the momentum principle

The force due to hydrostatic pressure in the X direction is:

$$P = \gamma A \bar{Y} cos\Theta$$

Where:

γ is the unit weight of water;

A is the wetted area at the cross section;

$\bar{Y}$ is the distance between the water surface and the centroid of the cross section.

The weight of water force is:

$$W = \gamma \left(\frac{A_1 + A_2}{2}\right) L$$

$$sin\theta = \frac{z_2 - z_1}{L} = S_0$$

$$W_x = W sin\theta$$

Where:

L is the distance between the cross sections along the X axis;

S_0 is the slope of the channel.

The force due to the external friction is:

$$F_f = \tau \bar{P} L$$

Where:

τ is the shear stress;

$\bar{P}$ is the average wetted perimeter between the cross sections.

$$\tau = \gamma \bar{R} \bar{S}_f$$

Where:

$\bar{R}$ is the average hydraulic radius;

$\bar{S}_f$ is the friction slope.

Therefore:

$$F_f = \gamma \left(\frac{A_1 + A_2}{2}\right) \bar{S}_f L$$

Knowing that:

$$ma = Q\rho\Delta v_x = Q\rho(\beta_1 v_1 - \beta_2 v_2)$$

Where:

β is the momentum coefficient that accounts for a varying velocity distribution in irregular channels.

Substituting the terms listed above in the equation:

$$P_2 - P_1 + W_x - F_f = Q\rho\Delta V_x$$

The final momentum equation is obtained:

$$\frac{Q_2^2 \beta_2}{gA_2} + A_2 \bar{Y}_2 + \left(\frac{A_1 + A_2}{2}\right) LS_0 - \left(\frac{A_1 + A_2}{2}\right) L\bar{S}_f = \frac{Q_1^2 \beta_1}{gA_1} + A_1 \bar{Y}_1$$

3.2.3 Boundary conditions

Boundary conditions are needed to establish the starting water surface at the end of the river system. Before starting the simulation, the program needs to know which is the flow regime. The computation starts at a cross section with known initial conditions and continues upstream for a subcritical flow regime or downstream for a supercritical flow regime, in case of mixed flow regime boundary conditions must be entered at all the ends of the river system.

The program has four available types of boundary conditions:

- Known water surface elevation;
- Critical depth;
- Normal depth, computed with the Manning's equation: $Q = KS_f^{1/2}$ (S_f average slope of the energy gradeline);
- Rating curve;

3.3   Unsteady flow hydrodynamics (1D)

3.3.1 Equations

The flow in a stream can be described by two dependable variables, flow discharge Q, or velocity V, and water surface elevation $z = z_0 + h$. These variables are involved in two partial differential equations that can be obtained from the principle of conservation of mass and momentum.

Considering the elementary volume shown in figure:
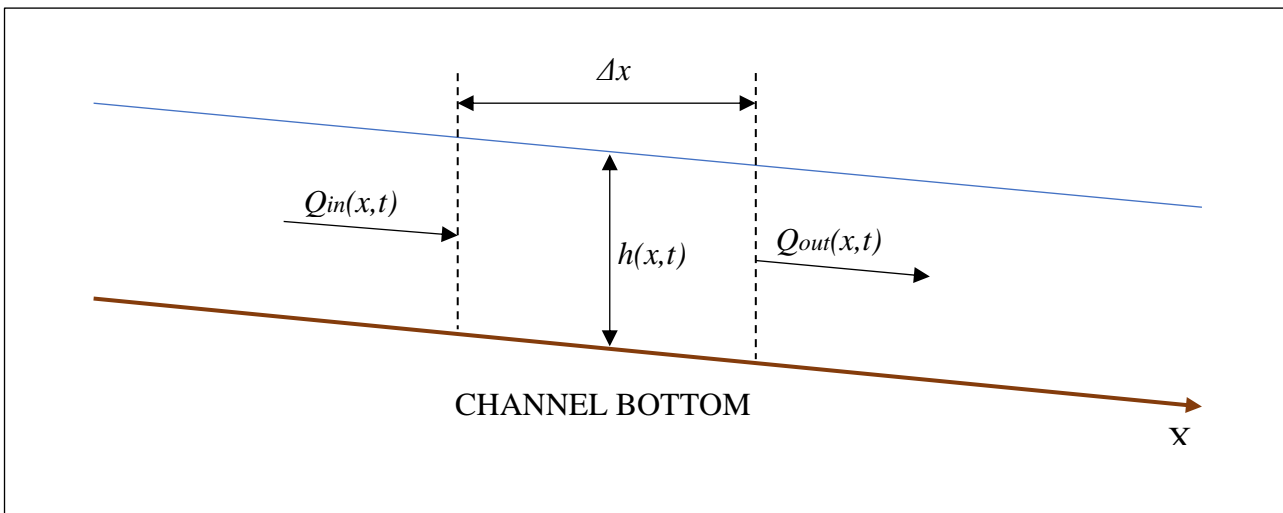
Figure 8: Elementary control volume

the total flow area A_T for the control volume, is obtained summing the active area A and the off-channel storage area S.

The unsteady flow equations, valid under the same assumption made for the steady flow equation, are the following:

- **Continuity Equation**: for a control volume as the one shown in Figure 5, the net rate of flow into the volume is equal to the rate of change of storage inside the volume. The rate of flow entering the control volume is written as:

$$Q - \frac{\partial Q}{\partial x}\frac{\Delta x}{2}$$

The rate of flow leaving the control volume as:

$$Q + \frac{\partial Q}{\partial x}\frac{\Delta x}{2}$$

and the rate of change in storage as:

$$\frac{\partial A_T}{\partial t}\Delta x$$

The change in mass in the control volume is obtained as:

$$\rho\frac{\partial A_T}{\partial t}\Delta x = \rho\left[\left(Q - \frac{\partial Q}{\partial x}\frac{\Delta x}{2}\right) - \left(Q + \frac{\partial Q}{\partial x}\frac{\Delta x}{2}\right) + Q_I\right]$$

Q_I being the lateral inflow to the control volume and ρ the fluid density. Dividing by Δx and considering the water density constant in time, the final form of the continuity equation is written as:

$$\frac{\partial A_T}{\partial t} + \frac{\partial Q}{\partial x} - q_I = 0$$

Where q_I is the lateral inflow per unit length.

- **Momentum Equation:** the net rate of momentum entering the volume (momentum flux) plus the sum of all external forces acting on the volume is equal to the rate of accumulation of momentum. The external forces considered are: pressure, gravity and friction.

Pressure force:

$$F_P = \rho g A \frac{\partial h}{\partial x}\Delta x$$

Gravitational force:

$$F_g = -\rho g A \sin\theta\, \Delta x \approx -\rho g A \frac{\partial z_0}{\partial x}\,\Delta x$$

Where:

z_0 is the invert elevation.

Friction force:

$$F_f = -\rho g A S_f \Delta x$$

The momentum flux entering the control volume is written as:

$$\rho\left[QV - \frac{\partial QV}{\partial x}\frac{\Delta x}{2}\right]$$

14

While the momentum flux leaving the control volume is written as:

$$\rho \left[QV + \frac{\partial QV}{\partial x} \frac{\Delta x}{2} \right]$$

Thus, the net rate of momentum entering control volume is:

$$-\rho \frac{\partial QV}{\partial x} \Delta x$$

Lastly, the rate of accumulation of momentum is written as:

$$\rho \Delta x \frac{\partial Q}{\partial t}$$

Now, is possible to write the momentum equation:

$$\rho \Delta x \frac{\partial Q}{\partial t} = -\rho \frac{\partial QV}{\partial x} \Delta x - \rho g A \frac{\partial h}{\partial x} \Delta x - \rho g A \frac{\partial z_0}{\partial x} \Delta x - \rho g A S_f \Delta x$$

Knowing that the water surface elevation z is equal to $z_0 + h$, dividing the expression by $\rho \Delta x$ and rearranging the terms, the final form of the momentum equation is obtained as follows:

$$\frac{\partial Q}{\partial t} + \frac{\partial QV}{\partial x} + g A \left(\frac{\partial z}{\partial x} + S_f \right) = 0$$

When the water in the river rises above the main channel banks, it inundates the floodplain and fills the storage area. A further increase in the water level causes floodplain to convey water downstream along a path shorter than the main channel's one. As the river stage decreases, water moves back to the main channel.
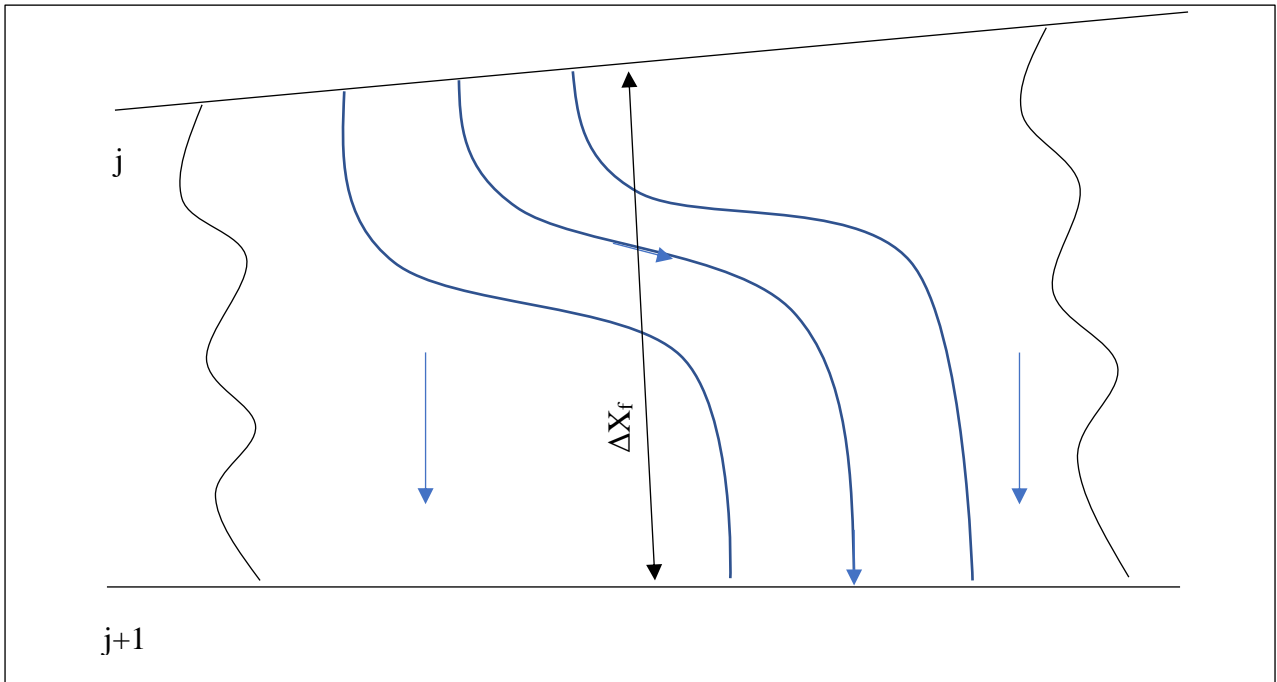
Figure 9: Channel and Floodplain flows

Usually, since the main direction of flow is along the channel, the scheme (Figure 6) can be approximated by a one-dimensional flow. A common approach foresees that the flow in the

floodplain is ignored, considering possible only the storage. This approach is suitable for large leveed river having floodplain highly vegetated or real storage areas. Another approach proposed by Fread (1976) and Smith (1978) is that of divide the system in two different channels, writing the continuity and momentum equation for both. The exchange of momentum between the channel and the floodplain is neglected, assuming at each cross sections a horizontal water surface normal the flow direction. Therefore, the discharge can be distributed according to conveyance:

$$Q_c = \Phi Q$$

$$Q_f = (1 - \Phi)Q$$

Where:

Q_c is the flow in the channel;

Q_f is the flow in the floodplain;

Q is the total flow;

Φ is equal to $\dfrac{K_c}{(K_c + K_f)}$

Where:

K_c is the conveyance in the channel;

K_f is the conveyance in the floodplain.

The continuity and momentum equation can now be written as follows:

$$\frac{\partial A}{\partial t} + \frac{\partial(\Phi Q)}{\partial x_c} + \frac{\partial[(1 - \Phi)Q]}{\partial x_f} = 0$$

$$\frac{\partial Q}{\partial t} + \frac{\partial(\Phi^2 Q^2/A_c)}{\partial x_c} + \frac{\partial[(1 - \Phi)^2 Q^2/A_f)}{\partial x_f} + gA_c\left(\frac{\partial Z}{\partial x_c} + S_f\right) + gA_f\left(\frac{\partial z}{\partial x_f} + S_{ff}\right) = 0$$

Where the subscripts c and f stand for channel and floodplain.

The program solves the two equations approximated to finite differences for both channel and floodplain.

- **Continuity equation:**

$$\frac{\Delta Q_c}{\Delta x_c} + \frac{\Delta A_c}{\Delta t} = \bar{q}_f$$

$$\frac{\Delta Q_f}{\Delta x_f} + \frac{\Delta A_f}{\Delta t} + \frac{\Delta S}{\Delta t} = \bar{q}_c + \bar{q}_I$$

Where:

S is the storage from non-conveying portions of cross section;

$\bar{q}_I$ is the average lateral inflow per unit length of floodplain;

$\bar{q}_c$ and $\bar{q}_f$ are the exchanges of water between the channel and the floodplain. Assuming:

$$\Delta x_c q_c = -q_f \Delta x_f$$

- **Momentum equation:**

$$\frac{\Delta Q_c}{\Delta t} + \frac{\Delta(V_c Q_c)}{\Delta x_c} + g\bar{A}_c\left(\frac{\Delta z}{\Delta x_c} + \bar{S}_{fc}\right) = M_f$$

$$\frac{\Delta Q_f}{\Delta t} + \frac{\Delta(V_f Q_f)}{\Delta x_f} + g\bar{A}_f\left(\frac{\Delta z}{\Delta x_f} + \bar{S}_{ff}\right) = M_c$$

Where:

M_f and M_c are the momentum fluxes per unit distance exchanged between the channel and the floodplain. Assuming:

$$\Delta M_c x_c = -\Delta x_f M_f$$

The friction force defined by the last two terms of the equation can be written as follow:

$$g\bar{A}\bar{S}_f \Delta x_e = g\bar{A}_c\bar{S}_{fc}\Delta x_c + g\bar{A}_f\bar{S}_{ff}\Delta x_f$$

Where:

Δx_e is the equivalent flow path;

S_f is the friction slope for the entire cross section;

$A = \bar{A}_c + \bar{A}_f$

The convective terms can be expressed as follows:

$$\Delta(\beta V Q) = \Delta(Q_c Q_c) + \Delta(V_f Q_f)$$

Where β is a velocity distribution factor defined as:

$$\beta = \frac{(V_c Q_c + V_f Q_f)}{QV}$$

3.3.2 Implicit finite difference scheme

The four-point implicit scheme or Preissmann scheme (Figure 7), is the most used and successful method for solving the one-dimensional unsteady flow equations.
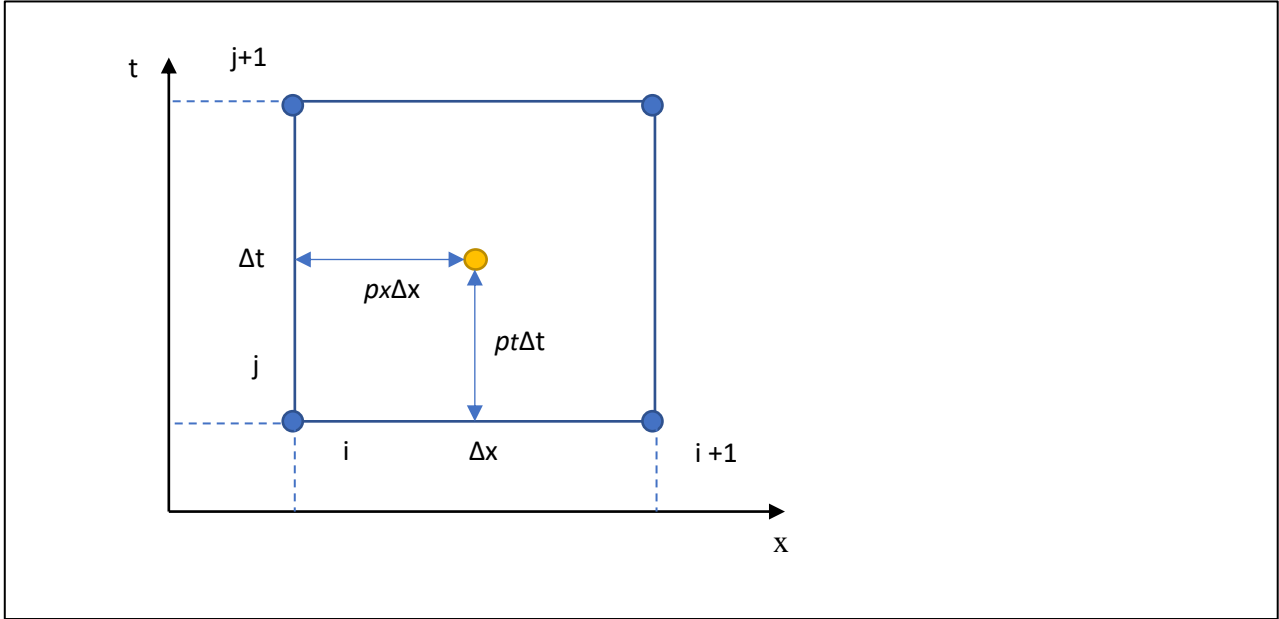
Figure 10: Preissmann scheme

Using this scheme, space derivatives and function values are assessed at a point $(n + p_t)\Delta t$, inside the computational cell. Therefore, values at $(n + 1)\Delta t$ are present into all terms in the equations. The program solves a system of simultaneous equations the solution of which is influenced from the entire reach. As a consequence, the time step can be significantly larger compared to the explicit numerical scheme.

Being f a generic function:

$$\frac{\partial f}{\partial t} \approx p_x \frac{f_{i+1}^{j+1} - f_{i+1}^{j}}{\Delta t} + (1 - p_x)\frac{f_i^{j+1} - f_i^{j}}{\Delta t}$$

$$\frac{\partial f}{\partial x} \approx p_t \frac{f_{i+1}^{j+1} - f_i^{j+1}}{\Delta t} + (1 - p_t)\frac{f_{i+1}^{j} - f_i^{j}}{\Delta t}$$

$$f \approx p_t p_x f_{i+1}^{j+1} + p_x(1 - p_t)f_{i+1}^{j} + (1 - p_x)p_t f_i^{j+1} + (1 - p_x)(1 - p_t)f_i^{j}$$

The stability of a numerical method indicates how evolve the errors during the computation. In particular:

- The method is unstable if the errors increase for any kind of Δt and Δx.
- The method is unconditionally stable if the errors do not increase for any kind of Δt and Δx.
- The method is conditionally stable if the errors do not increase for specific values of Δt and Δx. The condition of *Courant-Friedrichs-Lewy* must be verified:

$$\Delta t \leq \frac{\Delta x}{v + \sqrt{gh}}$$

Where:

v is the flow mean velocity;

$\sqrt{gh}$ is the small perturbation's propagation velocity.

Von Neumann stability analyses (Fread (1974), Ligget and Cunge (1975), show that for $0.5 < p_t \leq 1.0$ the implicit scheme is unconditionally stable, while for $p_t = 0.5$ is conditionally stable and for $p_t < 0.5$ is unstable. The same authors performed a convergence analysis showing that numerical dumping increase when $\lambda/\Delta t$ decreases, being λ the length of a wave in a hydraulic simulation. Therefore, in simulation in which the length of a wave is long enough with respect to spatial distances, convergence is not a problem.

Other practical factors may contribute to the instability of the numerical method. Dramatic changes in channel cross sections or in channel slope, flood wave characteristics and hydraulic structures as levees, bridges, culverts and weirs. Usually the stability problems are mostly associated to these practical factors, overshadowing any considerations about p_t. For this reason, the accuracy and the stability of any model application has to be tested by a sensitivity study with different time and space intervals.

The continuity and momentum equations are non-linear. Solving a non-linear system of equations by means of implicit finite difference scheme is slow and can experience convergence problems. Therefore, a technique of linearization is applied to the equations (Ligget and Cunge, 1975; Chen, 1973).

The assumptions for the linearization are the following:

- If $f \cdot f \gg \Delta f \cdot \Delta f$, then $\Delta f \cdot \Delta f = 0$;
- If $f = f(Q, z)$, then Δf can be approximated by the first term of the Taylor Series:

$$\Delta f_j = \left(\frac{\partial f}{\partial Q}\right)\Delta Q_j + \left(\frac{\partial f}{\partial z}\right)\Delta z_j$$

- If Δt is small, then certain variables can be treated explicitly:

$$f_i^{j+1} = f_i^j$$

The second assumption is applied to the friction slope, S_f and Area, A. The third assumption is applied to the velocity, V; in the convective term; the velocity distribution factor, β; the equivalent flow path, x_e; and the flow distribution factor, Φ.

3.3.3 Initial and boundary conditions

A river reach has N computational nodes and $2N – 2$ finite difference equations. Two additional equations are needed, having $2N$ unknowns. The boundary conditions provide these equations. For subcritical flow regime, the boundary condition for the geometric variable must be known downstream and for cinematic variable upstream; while for supercritical flow regime both variables must be known upstream.

The upstream boundary condition for the cinematic variable, Q, is a flow hydrograph. Whereas, the boundary condition for the geometric variable, h, may be:

- A stage hydrograph (can be used as either an upstream or downstream boundary condition);

- A flow hydrograph (can be used as either an upstream or downstream boundary condition);
- A single-valued rating curve (can be used as a downstream boundary condition).
  Being a single valued relationship and not reflecting any loop in the rating, it may introduce errors in the vicinity of the rating curve. Therefore, the single-valued rating curve has to be entered sufficiently downstream with respect to the study area in order to not introducing in it any errors.
- Normal depth from Manning's equation (can be used as downstream boundary condition).
  It counts the same assumption made in the previous point. In fact, the slope of the water surface used in Manning's equation may be a good estimation of the friction slope but it is hard to obtain ahead time.

To start the simulation the program needs an initial condition, this is accomplished by fixing the initial discharge at the beginning of the simulation. By doing this, the program can compute the starting water elevation along the reach assuming steady flow water conditions.

3.3.4 Solution of the system of linear equations

For each time step, a system of linear equations composed by the finite difference equations, the external and internal boundary conditions and the storage area equations has to be solved:

$$Ax = b$$

Where:

A is the coefficient matrix;
x is the column vector of unknowns;
b is the column vector of constants.

For a single channel without storage area, the coefficient matrix has a band width of five. This kind of matrix is easily solved using a banded matrix solver. Unfortunately, for network problems, the banded structure is destroyed by sparse terms associated to boundary conditions and storage areas. Consequently, the parse terms of systems with hundreds of cross sections and many reaches, represent an important numerical problem to solve.
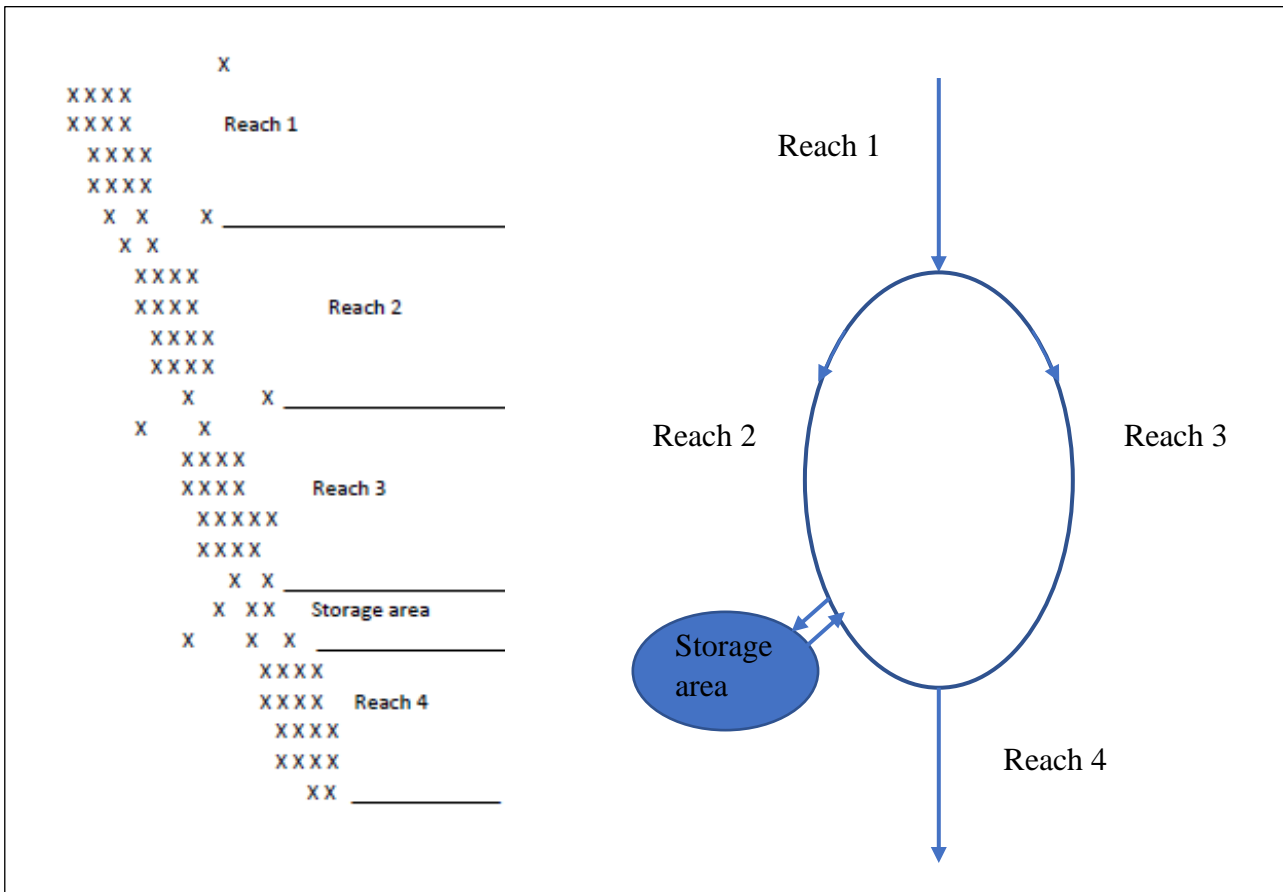
Figure 11: Example of matrix for a river system

HEC-RAS uses a storage algorithm for sparse matrixes named "Skyline". This algorithm takes advantage of the fact that in any sparse matrix the non-zero element are located to the left of the diagonal and in a column above the diagonal. These inverted "L shaped" structures are stored in a vector, occupying a minimum amount of the total storage. Elements outside the "L" structures are considered zero, while the elements inside the "L" structures are accessed by row and column numbers. As a result of this, the Skyline vector works as the original matrix.

3.4 Unsteady flow hydrodynamics (2D)

3.4.1 Equations

For channel and flood modeling, the Navier-Stokes equations are simplified in the Shallow Water (SW) equations. These equations are valid under the following assumptions:

- Incompressible flow;
- Hydrostatic pressure;
- Turbulent motion is approximated by eddy viscosity (equations are Reynolds averaged);
- The vertical length scale is much smaller than the horizontal length scale, the vertical velocity is small and the pressure is hydrostatic.

In some shallow flows the gravity term and the bottom friction terms of the momentum equation, are predominant in respect to unsteady, advection and viscous term. Consequently, this last three terms

can be disregarded so that the momentum equation becomes the two-dimensional form of the Diffusion Wave Approximation. The combination of this equation with the mass conservation results in a one equation model named Diffusion Wave Approximation if the Shallow Water equations (DSW).

- **Mass Conservation equation**:

$$\frac{\partial H}{\partial t} + \frac{\partial(hu)}{\partial x} + \frac{\partial(hv)}{\partial y} + q = 0$$

Where:

$H(x, y, t)$ is the water surface elevation equal to the bottom surface elevation $z(x, y)$ plus the water depth $h(x, y, t)$;

u and v are the velocity components in the x and y direction;

q is a source/sink flux term.

In vector form the equations becomes:

$$\frac{\partial H}{\partial t} + \nabla \cdot hV + q = 0$$

Where:

$V = (u, v)$ is the velocity vector.

The integral form is written as follows:

$$\frac{\partial}{\partial t} + \iiint_{\Omega} d\Omega + \iint_{S} V \cdot n dS + Q = 0$$

Where:

Ω is the volumetric region representing the three-dimensional space occupied by the fluid;

S represents the side boundaries;

Q represents any flow crossing the bottom surface (infiltration) or the top water surface (rain/evaporation).

Nowadays, airborne remote sensing can provide very high-resolution topographic data but, often, the data are too dense to run a simulation in a feasible time. By using a relatively new approach called sub-grid bathymetry it is possible to incorporate the fine resolution topography in the computation, keeping an acceptable computational time. A relatively coarse computational grid and a high-resolution underlaying topography are used. The mass conservation equation is discretized with a finite volume technique and the fine grid details are accounted for by parameters which represent multiple integrals over volumes and face areas. Following this approach, the mass conservation equation takes into account the high-resolution topography of each discrete cell. Some important information of the fine bathymetry such as hydraulic radius, volume and cross-sectional area are stored in the computational grid cell. All the others fine topography details are lost but in many cases

the water surface is smoother than the bathymetry therefore, a coarser grid is a good representation of the spatial variability of the free surface elevation.

Assuming that, the triple integral of the mass conservation equation is a function of the water surface elevation H and the following discretization can be done:

$$\frac{\partial}{\partial t}\iiint_{\Omega} d\Omega = \frac{\Omega(H^{n+1}) - \Omega(H^n)}{\Delta t}$$

Assuming that, the grid cells have a polygonal shape the double integral of the mass conservation equation can be written as:

$$\iint_{S} V \cdot n\, dS = \sum_{k} V_k \cdot n_k A_k(H)$$

Where:

V_k is the average velocity at face k;

n_k is the unit normal vector at face k;

$A_k(H)$ is the area of face k as a function of water surface elevation.
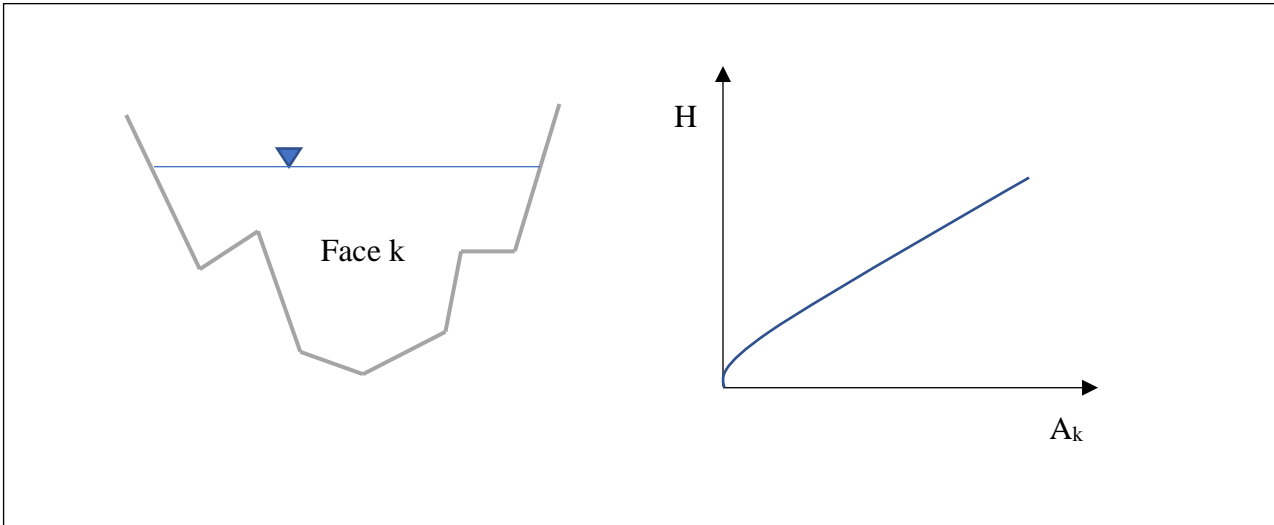
Figure 12: Cell face terrain data and hydraulic property table

Substituting the last two terms in the integral form of the mass conservation equation yields the sub-grid bathymetry mass conservation equation:

$$\frac{\Omega(H^{n+1}) - \Omega(H^n)}{\Delta t} + \sum_{k} V_k \cdot n_k A_k(H) + Q = 0$$

If the cell volume and face area as function of H are unknowns, the classical "box scheme" can be used computing $\Omega(H) = P \cdot h$ and $A_k(H) = l_k \cdot h$, where P is the cell area and l_k the length of the edge k (without any dependency of H).

- **Momentum conservation equation:**

$$\frac{\partial u}{\partial t} + u\frac{\partial u}{\partial x} + v\frac{\partial u}{\partial y} = -g\frac{\partial H}{\partial x} + v_t\left(\frac{\partial^2 u}{\partial x^2} + \frac{\partial^2 u}{\partial y^2}\right) - c_f u + fv$$

$$\frac{\partial v}{\partial t} + u\frac{\partial v}{\partial x} + v\frac{\partial v}{\partial y} = -g\frac{\partial H}{\partial y} + v_t\left(\frac{\partial^2 v}{\partial x^2} + \frac{\partial^2 v}{\partial y^2}\right) - c_f v + fu$$

Where:

u and v are the velocities in x and y direction;

g is the gravitational acceleration;

v_t is the horizontal eddy viscosity;

c_f is the bottom friction coefficient;

f is the Coriolis parameter.

On the left side of the equation are present the acceleration terms, while on the right side are present the internal or external forces acting on the fluid.

The differential vector form of the momentum equation is written as follows:

$$\frac{\partial V}{\partial t} + V \cdot \nabla V = -g\nabla H + v_t\nabla^2 V - c_f V + fk \times V$$

The terms of the equation are:

- **Acceleration.** The Eulerian acceleration can be written in the Lagrangian form:

$$\frac{DV}{Dt} = \frac{\partial V}{\partial t} + V \cdot \nabla V$$

- **Gravity.** When the flow surface is not horizontal a pressure gradient is produced by the weight of the water columns having different heights.

- **Eddy viscosity.** Turbulent flow mixing is modeled as a gradient isotropic diffusion process. The eddy viscosity coefficient represents the diffusion rate and is written as follows:

$$v_t = Dhu_*$$

Where D is a non-dimensional empirical mixing coefficient and u_* is the shear velocity, computed as:

$$u_* = \sqrt{gRS} = \frac{n\sqrt{g}}{R^{1/6}}|V|$$

Where R is the hydraulic radius and S is the energy slope computed with Chèzy formula and then simplified with Manning's equation.

The empirical mixing coefficient varies with geometry and bottom/wall surface.

D	Mixing Intensity	Geometry and Surface
0.11 to 0.26	Little mixing	Straight channel, smooth surface
0.30 to 0.77	Moderate mixing	Gentle meanders, moderate surface irregularities
2.0 to 5.0	Strong mixing	Strong meanders, rough surface

Table 3:Eddy Viscosity transverse mixing coefficients

- **Bottom Friction.** Using the Chèzy formula and further simplifying with the Manning's equation, the bottom friction coefficient is obtained:

$$c_f = \frac{g|V|}{C^2 R} = \frac{n^2 g|V|}{R^{4/3}}$$

Where:

C is the Chèzy coefficient and n is the empirical roughness coefficient.

- **Coriolis Effect.** The apparent horizontal force felt by any object on the Earth is proportional to the Coriolis parameter written as follows:

$$f = 2\omega \sin\varphi$$

Where:

$\omega = 0.00007292115855306587/s$ id the sidereal angular velocity of the Earth and φ is the latitude.

As earlier introduced in this chapter, in shallow frictional and gravity controlled flow, unsteady, advection, turbulence and Coriolis terms of the full momentum equation can be disregarded obtaining a simplified equation named ***Diffusion-Wave form of the Momentum Equation:***

$$\frac{n^2|V|V}{(R(H))^{\frac{4}{3}}} = -\nabla H$$

Dividing both sides of the equation by the square root of their norm, the equation becomes:

$$V = \frac{-(R(H))^{2/3}}{n} \frac{\nabla H}{|\nabla H|^{1/2}}$$

Therefore, this equation can be used in place of the full momentum equation when the velocity can be determined by a balance between barotropic pressure gradient and bottom friction. In this case, the substitution of the last written equation in the mass conservation equation yields the differential form of the ***Diffusion-Wave Approximation of the Shallow Water (DSW) equations***, reducing the system of equations to:

$$\frac{\partial H}{\partial t} - \nabla \cdot \beta \nabla H + q = 0$$

Where:

$$\beta = \frac{(R(H))^{5/3}}{n|\nabla H|^{1/2}}$$

If detailed bathymetry information is available, the Diffusion Wave form of the momentum equation can be substituted into the sub-grid bathymetry form of the continuity equation obtaining:

$$\frac{\Omega(H^{n+1}) - \Omega(H^n)}{\Delta t} - \sum_k \alpha \nabla H \cdot n + Q = 0$$

Where:

$$\alpha = \alpha(H) = \frac{(R(H))^{\frac{2}{3}} A_k(H)}{n|\nabla H|^{1/2}}$$

3.4.2 Numerical methods

The first step to solve efficiently the equation by means of a numerical method, is the domain subdivision into non-overlapping polygons forming a grid. HEC-RAS does not require a structured or orthogonal grid but, the absence of orthogonality can affect the computational time speed. Each grid cell must be convex and by default, a limit of 8 sides for each polygonal cell is set. The grid definition is very important since the solution stability and accuracy depend much on its characteristics.

In addition to the regular grid, a dual grid must be defined. This is necessary given the differential form of the relationship between variables and since in the equations there are second order derivatives terms. The dual grid defines a correspondence between its nodes and the regular grid cells and between regular grid nodes and dual grid cells as well
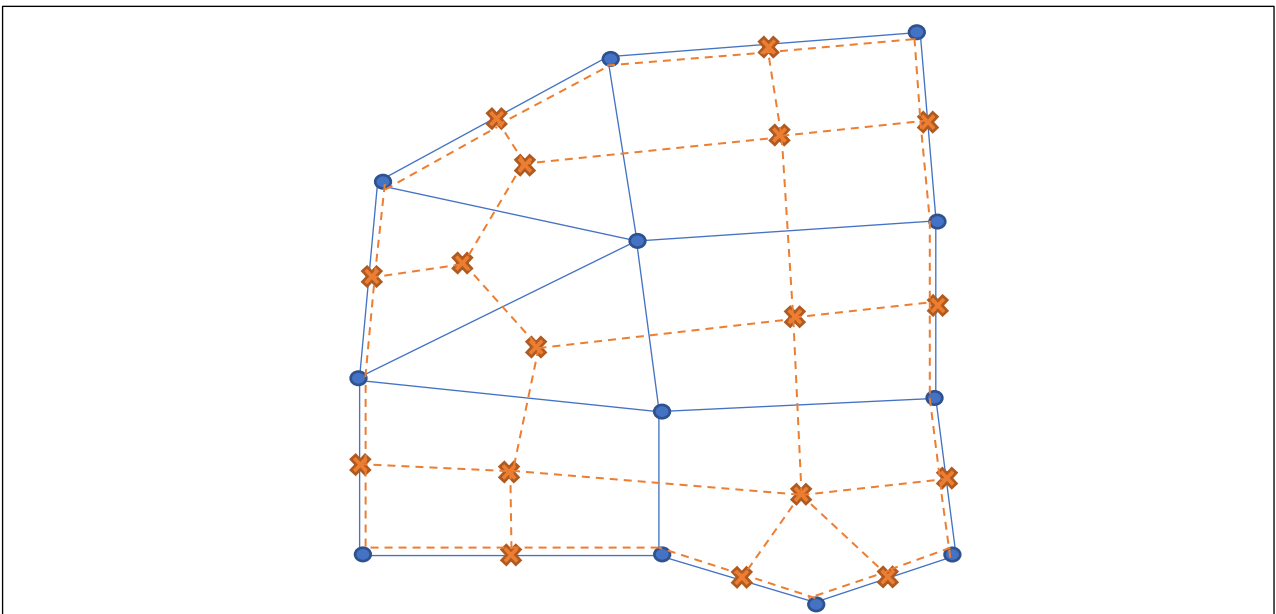
Figure 13: Regular grid and dual grid

As shown above (Figure 9), the dual nodes are in one-to-one correspondence with the normal grid cells and boundary edges. This is useful when defining boundary conditions as the boundary edges are treated as topological artificial cells having no area.

The water surface elevation is computed at the grid cell center, the velocity perpendicular to the cell face (driving the flow transfer across the face), and the velocity vector at the cell face points.

The program uses a hybrid discretization scheme in which finite differences and finite volumes are combined taking advantage of orthogonality where this exists.

- *Finite Difference Approximations*
  This technique is used to discretize the volume derivative in time as follows:
  $$\frac{\partial \Omega}{\partial t} \approx \frac{\Omega(H^{n+1}) - \Omega(H^n)}{\Delta t}$$

  Finite differences are used to approximate the normal water surface derivative only in the case in which the grid is locally orthogonal, which means that the direction n' determined by the cell center must be orthogonal to the face between the cells.
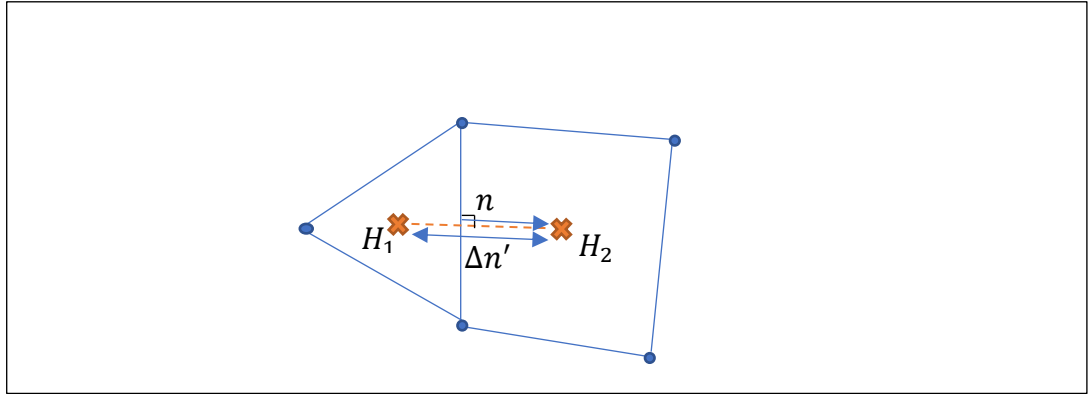
Figure 14: Locally orthogonal grid

  The approximation is written as follows:
  $$\nabla H \cdot n' = \frac{\partial H}{\partial n'} \approx \frac{H_2 - H_1}{\Delta n'}$$

  If the face between the cell is not orthogonal the normal water surface derivative is split as the sum of finite difference and finite volume approximation.

- *Finite Volume Approximations*
  The finite volume approximation is used to discretize the normal water derivative when the grid is not locally orthogonal. The approximation of the gradient term ∇H at a grid face, consists in averaging its value over dual cells. Applying the Gauss' divergence theorem the following formula is obtained:
  $$\nabla H \approx \frac{\oint_L H n dL}{A'}$$
  Where:
  L is the dual cells boundary;
  A' is the area of the dual cells.

Since the dual cells are polygons, the line integral can be written as a sum over the dual cell faces. The dual face k' joining dual nodes j_1 and j_2 gives a contribution to the line integral equal to:

$$\frac{n_{k'} l_{k'} (H_1 + H_2)}{2}$$

Where:

$l_{k'}$ is the length of the dual face k';

$n_{k'}$ is the unit outward normal vector at dual face k';

H_1 and H_2 is the water elevation at cell center j_1 and j_2.
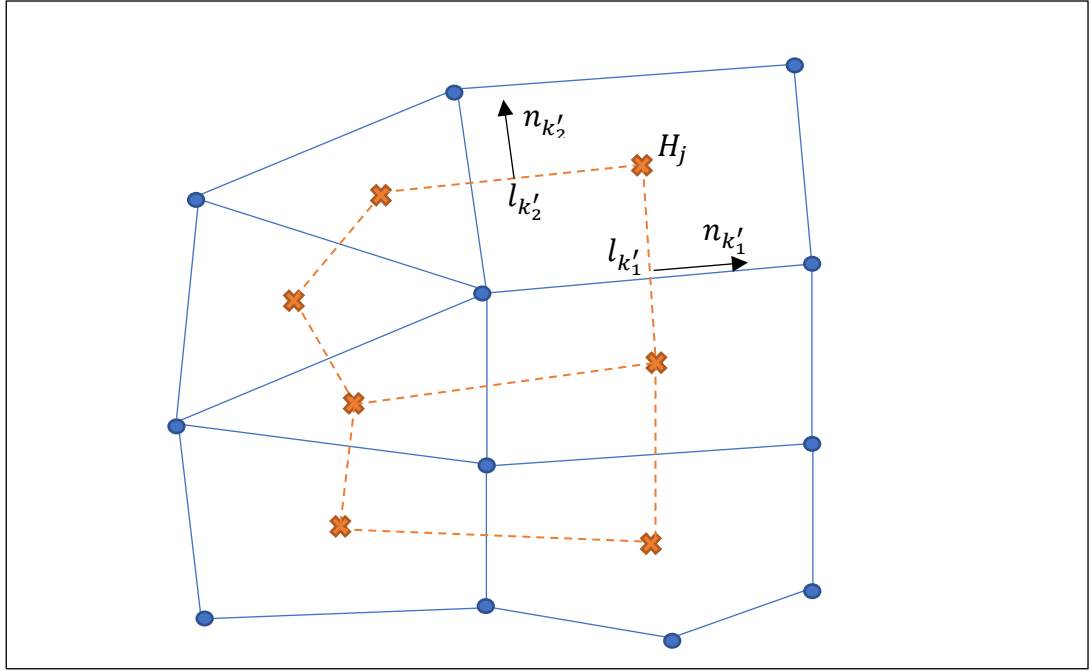
Figure 15: Cell and dual cell final volume approximation

The finite volume approximation of the gradient can be written as a sum over all dual nodes around the calculation face:

$$\nabla H \approx \sum_j c_j H_j$$

Where:

H_j is the water elevation at cell j;

c_j is a vector constant equal to $\frac{(n_{k'_1} l_{k'_1} + n_{k'_2} l_{k'_2})}{2A'}$.

Therefore, the directional derivatives in an arbitrary direction T' can be computed with the formula:

$$\frac{\partial H}{\partial T'} = \nabla H \cdot T' \approx \sum_j c'_j H_j$$

Where:

$$c'_j = \frac{(n_{k'_1} l_{k'_1} + n_{k'_2} l_{k'_2}) \cdot T'}{2A'}$$

- *Hybrid Discretization*

  As already stated, If the face between the cell is not orthogonal, the normal water surface derivative is split as the sum of finite difference (first term on the right-hand side) and finite volume approximation (second term on the right-hand side):

$$\frac{\partial H}{\partial n} = (n \cdot n')\frac{\partial H}{\partial n'} + (n \cdot T')\frac{\partial H}{\partial T'}$$

Where:

n is the direction normal to a face;

$T = k \times n$ is the direction orthogonal to n;

n' is the direction determined by the cells centers on both sides of the face;

$T' = k \times n'$ is the direction orthogonal to n'.

Following this approach, a linear formula on H is derived:

$$\nabla H \cdot n = \frac{\partial H}{\partial n} \approx \sum_j c'_{j'} H_j$$

Where the coefficients $c'_{j'}$ combine the finite difference terms $\pm 1/\Delta n'$ and the finite volume terms c'_j.

3.4.3 Initial and Boundary Conditions

For a 2D flow area, different initial condition can be set:

1. **Dry Initial Condition**
2. **Single Water Surface Elevation:** cells having a lower terrain elevation than the user established water surface elevation will be wet.
3. **Restart File Option for Initial Condition:** it contains a water surface elevation for every cell and velocities for each cell face. This condition can be used if a previous run has been made and the "write out a Restart File" option was selected.
4. **Ramp Up Option:** it allows to run a model with a warm-up period. This option consists in running a series of time steps with constants inflow, keeping all the boundary conditions constant as they were at the beginning of the simulation.

In addition to initial condition, external boundary conditions must be set at all the edges of the domain for each time step. In the program there are five available types of boundary condition:

1. **Flow Hydrograph:** it can be used for putting flow into (positive values) or taking flow out (negative values) of a 2D flow area. For this type of boundary condition, it is needed the energy slope. This is used to compute, along the boundary condition line and for each time step, the normal depth. The program then computes a flow distribution in the cross section. At each time step only the cells having a water surface elevation higher than their outer boundary face terrain will receive water. Nevertheless, the cells can evenly receive water if the computed normal depth water surface is higher than the boundary face elevation data along the boundary condition line.

2. **Stage Hydrograph:** it can be used for bringing flow into a 2D flow area in the case the water surface elevation of the stage hydrograph is higher than the cell water surface elevation. Otherwise, if the water surface elevation of the stage hydrograph is lower than the cell water surface elevation, flow will be taken out. The flow is computed on a per cell basis.
3. **Normal Depth:** it can be used only for taking flow out of a 2D flow area. Along with normal depth, it is required the definition of the friction slope for that area, which is used in Manning's equation to compute a normal depth for each given flow. It is computed on a per cell basis.
4. **Rating Curve:** it can be used only for taking out flow of a 2D flow area and is computed on a per cell basis.
5. **Precipitation:** it can be used to enter rainfall excess (rainfall minus losses due to infiltration or interception) into a 2D flow area. It is entered equally to all cells of the 2D flow area.

3.4.4 Numerical solver of DSW equations

As it has been described in the previous chapter, time derivatives of the DSW equations are discretized using finite differences, while for spatial derivatives discretization a hybrid approximation technique is used. The contribution of variables at time steps *n* and *n+1* are weighted by means of the generalized Crank-Nicholson method.

The sub-grid bathymetry form of the continuity equation can be rearranged by taking advantage of the linear formula on H:

$$\Omega(H^{n+1}) + \sum_j a_j \left((1 - p_t)H_j^n + p_t H_j^{n+1} \right) = d$$

Where:

a_j are coefficients function of term Δt, c'_j, and α, remembering that $\alpha = \alpha(H) = \frac{(R(H))^{\frac{2}{3}} A_k(H)}{n |\nabla H|^{1/2}}$ and c'_j, combine the finite difference terms $\pm 1/\Delta n'$ and the finite volume terms c'_j;

$d = \Omega(H^n) - \Delta t Q$.

The equation can be rewritten moving to the right-hand side all the terms referred to time step $n + 1$ and grouping terms that refer to the same cell:

$$\Omega(H^{n+1}) + p_t \sum_j a_j H_j^{n+1} = d - (1 - p_t) \sum_j a_j H_j^n$$

This equation is written for each cell in the domain, obtaining a system of equation that can be written in the following compact vector notation:

$$\Omega(H) + \psi H = b$$

Where:

Ω is the vector of all cell volumes;

H is the vector of all cell water elevation at time $n + 1$;

Ψ is the coefficient matrix;

b is the right-hand side vector.

In case the coefficients are lagged, the bathymetric relationship $\Omega(H)$ cause non-linearity in the system of equation. Another bathymetric relationship $P(H)$, representing the diagonal matrix of cell wet surface areas, gives the Jacobian of Ω with respect to H. Knowing this information the system of equation can be solved using the following iterative formula:

$$H^{m+1} = H^m - (P(H^m) + \psi)^{-1}(\Omega(H^m) + \psi H^m - b)$$

Where m is the iteration index.

The coefficients a_j are a function of water surface elevation. Therefore, since it is used the Crank-Nicholson method, the coefficients a_j will be evaluated at time $n + p_t$, $H = (1 - p_t)H_j^n + p_t H_j^{n+1}$. This creates a circular dependency on the solution of the system of equations corrected through iteration.

The linearized scheme is unconditionally stable for $0.5 \leq p_t \leq 1$, it is second order accurate in space while time accuracy depends on the p_t chosen ($p_t = 1$ first order accurate, $p_t = 0.5$ second order accurate). For $p_t = 0.5$ it is obtained the Crank-Nicholson scheme (central differences in time and spatial derivatives evaluated at $n + 0.5$), which is stable if:

$$\frac{\Delta t}{\Delta x^2} < \frac{1}{2 - 4p_t}$$

While, for $p_t = 1$ the scheme is implicit and it corresponds to using backward differences in time and evaluating the spatial derivatives at step $n + 1$.

Solution Algorithm:

1. Pre-processing of the geometry along with local orthogonality and sub-grid bathymetry.
2. Solution starts with the initial condition H^0.
3. For step $n + 1$ boundary conditions are implemented.
4. Initial guess $H^{n+1} = H^n$.
5. The solver computes the p_t-averaged water elevation $H = (1 - p_t)H_j^n + p_t H_j^{n+1}$ and sub-grid bathymetry quantities depending on it.
6. The solver computes the coefficients a_j and create the system of equations $\Omega(H) + \psi H = b$
7. The system of equations is solved iteratively considering the boundary conditions and a candidate solution H^{n+1} is obtained.
8. If the residual is larger than the given tolerance (and the maximum number of iterations has not been reached) the solver goes back to step 5, differently it continues with step 9.
9. Accepted H^{n+1}, the solver computes the velocities V^{n+1} with the formula $V = \frac{-(R(H))^{2/3}}{n} \frac{\nabla H}{|\nabla H|^{1/2}}$, taking advantage of the linear formula on H.
10. The solver proceeds with the next time step n, repeating the steps from step 3; otherwise it ends.

3.5 Model's computational steps

3.5.1 Geometric pre-processing

To speed the unsteady flow calculations, all the geometric data are processed into hydraulic tables and rating curves, such that the program, during the iterations, interpolates the hydraulic variables from the tables avoiding the calculation of the variables at each iteration.

For each cross section, tables of elevation versus area, conveyance and storage are created. The hydraulic tables are created for both main channel and floodplain. There is a minimum (21) and a maximum (100) number of points which can be stored in the hydraulic tables. Furthermore, an interval for spacing the points has to be set and is up to the user ensure that the combination of number of points and space interval include all the possible stages occurring during the simulation.

The hydraulic structures are processed into families of rating curves (headwater versus flow and tailwater versus flow). The user can define the number of points on the free-flow rating curve (maximum 100 points), the number of submerged curves to be processed (maximum of 60) and the limits on the extent of the curves.

3.5.2 Unsteady flow simulation

The unsteady flow simulation is composed by three steps. First, data are read from HEC-DSS (Hec-Ras data storage system) and converted into the computational interval set by the user. Afterwards, the program reads the hydraulic tables generated during the geometric pre-processing together with the initial conditions, boundary conditions and the flow data. At last, the program performs the unsteady flow calculations, writing the stage and flow hydrographs for each specified node.

3.5.3 Post-processing

After the simulation, it is possible to run the post-processor in order to compute detailed hydraulic information for user specified time lines during the simulation. By default, the post-processor returns detailed output for the maximum stage water profile occurred during the entire simulation at each cross section.

3.6 Hydraulic modeling of the structures

3.6.1 Modeling bridges

The flow energy losses caused by structure (bridges, culverts) are computed in three parts:

- losses due to the expansion of flow occurring in the reach just downstream from the structure;
- losses at the structure itself;
- losses due to the contraction of flow occurring in the reach just upstream of the structure.

To compute the energy losses the program requires four cross sections defined by the user, generating other two cross sections inside of the bridge structure.
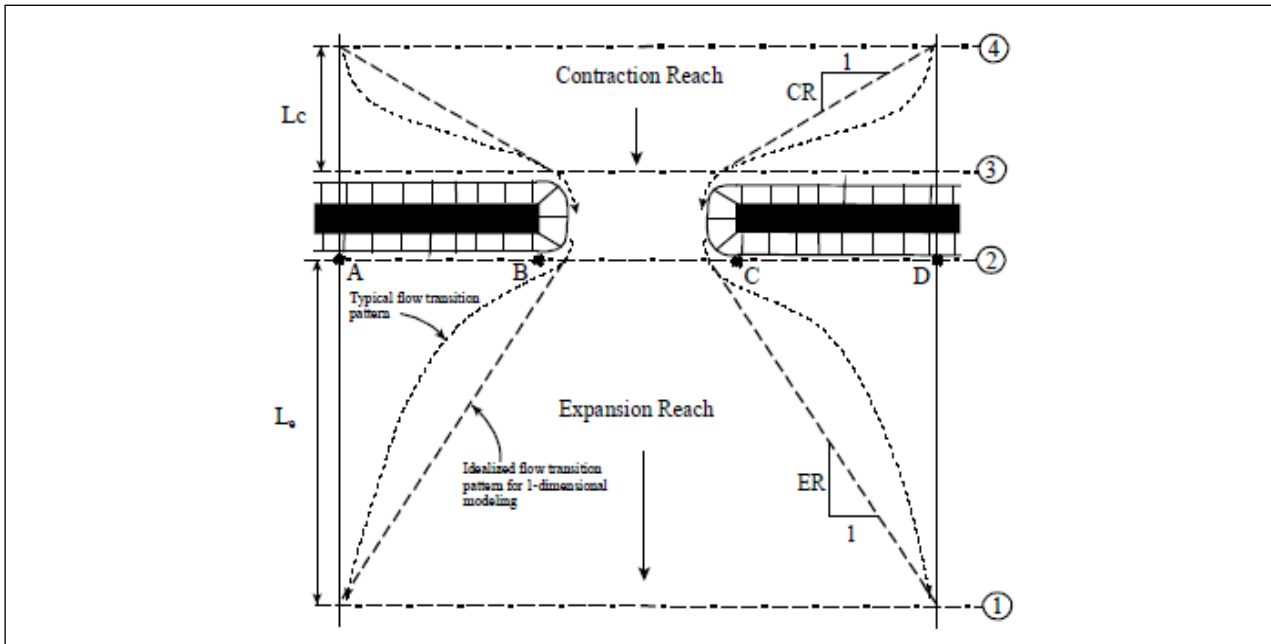
Figure 16: Cross sections locations at a bridge

The first cross section should be located downstream of the structure, at such a distance (L_e) that the flow is not influenced by the structure (flow fully expanded). The expansion reach length L_e varies depending on the magnitude of flow, the velocity of flow, the degree and shape of constriction. There are tabulated values of expansion ratios (ER), available for different degrees of constriction, different slopes and different ratios of the overbank roughness to main channel roughness, which multiplied by the average obstruction length (A to B and C to D) return L_e.

The second cross section is usually located a short distance downstream of the bridge. There must be enough space to allow flow expansion.

The third cross section should be located a short distance upstream of the bridge such that there is enough space for the abrupt acceleration and contraction of the flow occurring in the area close to the opening. The distance varies with the size of the bridge opening.

At the second and third cross sections must be defined the ineffective flow areas at each side of the bridge opening. This is accomplished in the cross section data editor.

The fourth cross section is located upstream from the bridge, where the flow lines are almost parallel. Generally, the distance along which flow contraction occurs is shorter that the distance for flow expansion. It is suggested by the Corps of Engineers to locate the cross section one times the average length of the side constriction caused by the structure abutments (average distance from A to B and from C to D).

In Hec-Ras the bridge geometry is defined by the bridge deck and roadway, sloping abutments, if necessary, and piers. Additionally, it is required the distance of the bridge's face from the upstream cross section as well as the width of the deck.

Concerning the energy losses, Manning's equation is used to compute friction losses: a weighted friction slope is multiplied by a weighted reach length between the cross sections. The expansion and contraction losses are calculated multiplying a coefficient by the absolute value of the change in velocity head between subsequent cross sections.

Hec-Ras allows to model low flow (class A, B and C), high flow and combined flow.

3.6.1.1 Low flow computations

Low flow is defined by the open channel flow through the bridge opening. Firstly, the program identifies the class of flow by means of the momentum equation, calculating the momentum at critical depth inside the bridge at the upstream and downstream ends. The controlling section in the bridge will be the end having the higher momentum. The class of flow is selected by comparing the momentum of the controlling section with the momentum of the flow downstream of the bridge (for subcritical profile) or with the momentum of the flow upstream of the bridge (for supercritical profile).

Class A low flow: if the momentum downstream is greater than the critical depth momentum inside the bridge, the flow is completely subcritical and is considered as class A low flow. Energy losses from cross section 3 to 4 and from 1 to 2 are computed in the same way: the friction losses summed to the contraction losses (from cross section 3 to 4) or to the expansion losses (from cross section 1 to 2).

To compute losses through the bridge (from cross section 2 to 3), there are four available methods:

- Energy Equation: the bridge is treated as a cross section except for the fact that the area of the bridge below the water surface is subtracted from the total area, increasing the wetted perimeter where the water is in contact with the bridge. As previously mentioned, two additional cross section inside the bridge, named BD (Bridge Downstream) and BU (Bridge Upstream), are automatically generated. The program then computes the energy balance between cross section 2 and BD, BD and BU, BU and 3.
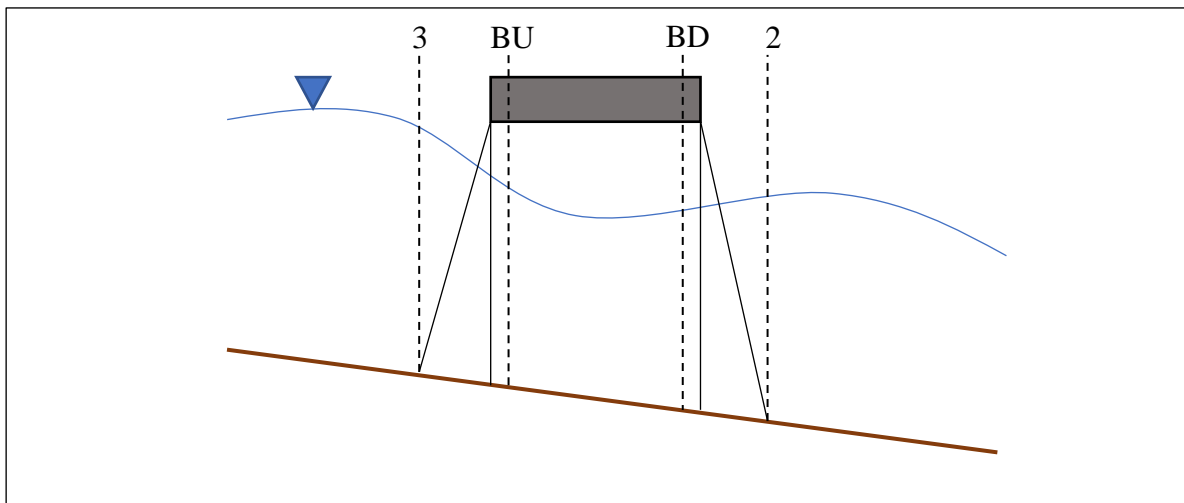
Figure 17: Additional cross sections near the bridge

- Momentum Balance Method: the program performs a momentum balance between the four cross sections as with the energy equation.
- Yarnell Equation: the program computes the change in water surface from section 2 to section 3 using an empirical equation based on 2600 lab experiments varying the shape of the piers, the width, the length, the angle and the flow rate.
- FHWA WSPRO Method: the program computes the water surface profile through the bridge by solving the energy equation iteratively.

Class B low flow: if the momentum downstream is less than the critical depth momentum at the controlling section inside the bridge, the program assumes that the constriction causes the flow to pass through critical depth so that a hydraulic jump occurs at a certain distance downstream. Class B low flow can exist for both subcritical and supercritical profiles. In both cases the program uses the momentum equation to compute the upstream and downstream water surfaces, if the momentum equation does not converge on an answer, the program switches to an energy-based method.

Class C low flow: If the water surface through the bridge is completely supercritical the flow is class C. The program computes the water surface through the bridge by means of the energy equation or the momentum equation.

3.6.1.2 High flow computations

The high flow occurs when the water comes into contact with the maximum low chord of the bridge deck. The program computes high flows by the energy equation, following the same procedure used for low flows; or by applying two separate equations for pressure or weir flow.

Pressure flow: when the flow comes into contact with the upstream side of the bridge, the program solves for orifice flow. If only the upstream side of the bridge is in contact with the water, the following equation (FHWA, 1978) is used:

$$Q = C_d A_{BU} \sqrt{2g} \left(Y_3 - \frac{Z}{2} + \frac{a_3 V_3^2}{2g} \right)^{\frac{1}{2}}$$

Where:

Q is the total discharge through the bridge opening;

C_d is the coefficient of discharge for pressure flow;

A_{BU} is the net area of the bridge opening at section BU;

Y_3 is the hydraulic depth at section 3;

Z is the vertical distance between the highest point of the low chord and the mean river bed elevation at section BU.
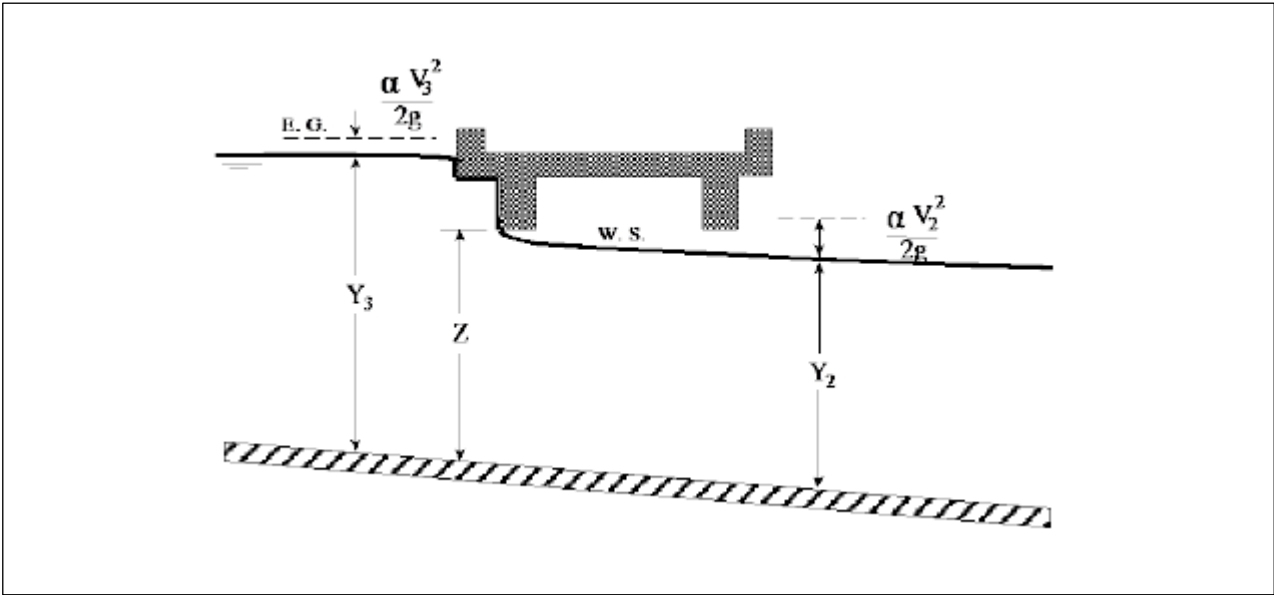
Figure 18: Pressure flow (upstream side)

When either the upstream and the downstream side of the bridge are in contact with the water surface, the program uses the standard full flowing orifice equation:

$$Q = CA\sqrt{2gH}$$

Where:

C is the coefficient of discharge for fully submerged pressure flow;

H is the difference between the energy gradient elevation upstream and the water surface elevation downstream;

A is the net area of the bridge opening.
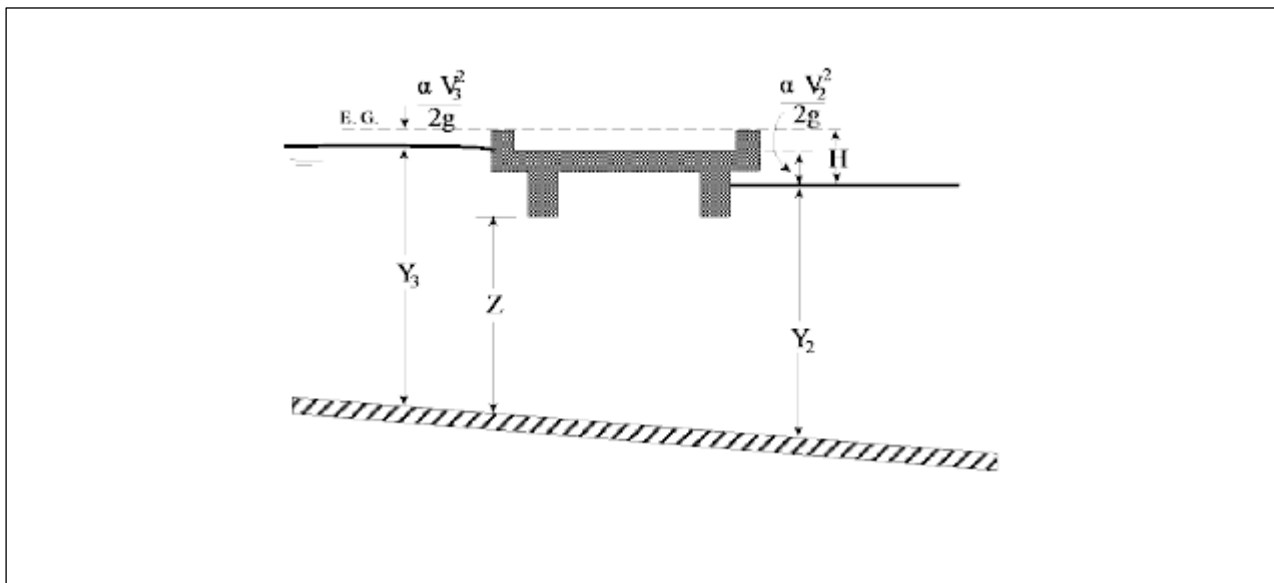
Figure 19: Pressure flow (upstream and downstream sides submerged)

Weir flow: when the water flows over the bridge the program uses the weir equation:

$$Q = CLH^{\frac{3}{2}}$$

Where:

Q is the total flow over the weir;

C is the coefficient of discharge for weir flow;

L is the length of the weir;

H is the difference between energy upstream and road crest.
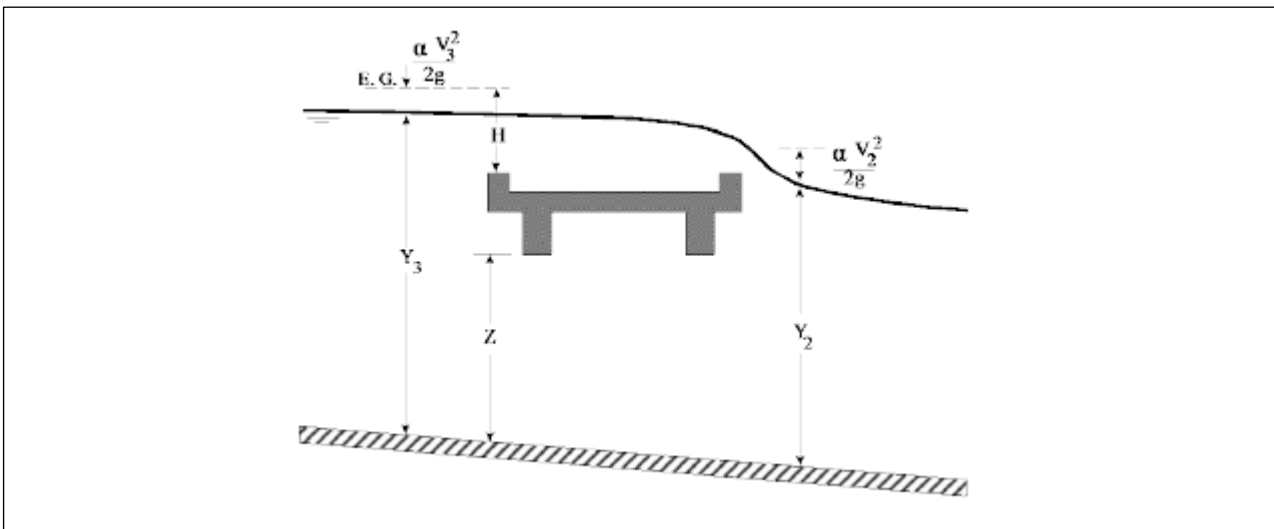
Figure 20: Weir flow

3.6.1.3 Combination flow

If low flow or pressure flow occur with weir flow, the program iterates to determine the amount of each flow type. The iteration stops when the low flow method (or pressure flow method) and the weir flow method have the same energy upstream of the bridge at section 3. Flow combination is computed with the energy and Yarnell low flow method.

3.6.2 Modeling culverts

Bridge modeling and culvert modeling are very similar in Hec-Ras except that the FHWA standard equations are used to compute inlet control losses at the structure. The layout of the cross sections, the location of the ineffective flow areas and the loss coefficients selection are the same as for bridges.

Flow in culverts can be divided into:

Inlet control flow: it occurs when the flow capacity of the entrance is less than the flow capacity of the culvert barrel, in this case the control section of the culvert is located just inside the entrance of the culvert. At this location or close to it, the water surface passes through critical depth and downstream the flow is supercritical.

Outlet control flow: it occurs when the culvert flow capacity is constrained by downstream flow condition or by the culvert barrel flow capacity.

The program computes the upstream energy needed to produce a given flow rate through the culvert, for both inlet control flow and outlet control flow. The higher upstream energy controls the flow in the culvert. For Inlet control flow, the program computes the upstream energy considering the culvert inlet as a sluice gate or as a weir. For Outlet control flow, to compute the upstream energy, an energy balance between downstream and upstream cross section is performed. If the computed upstream energy of inlet control flow is higher than the upstream energy of outlet control flow, the program checks, performing additional computations, if the inlet control flow energy can cause the pressurization of the culvert barrel. If low flow is present through the entire length of the culvert barrel, the inlet control flow is valid. If the flow pressurizes the culvert barrel by going through a hydraulic jump inside the barrel, the program considers the upstream energy computed for the outlet control flow (assuming a full flowing barrel).

3.6.3 Modeling inline and lateral structures

In Hec-Ras it is possible to model inline and lateral structures such as gated spillways and overflow weirs. The layout of the cross sections, the location of the ineffective flow areas and the loss coefficients selection are the same as for bridges and culverts.

Inline gated spillways can be modeled as radial gates, sluice gates, overflow gates or using a family of rating curves defined by the user. Both submerged and unsubmerged condition at the inlet and at the outlet of the gates can be model. If the upstream water surface is greater or equal to 1.25 times the height of the gate opening, the program uses the gate flow equations. If the upstream water surface is between 1.0 and 1.25 time the gate opening, two upstream heads are computed by the program, one with weir flow equation and the other with gate flow equation. Next, the program computes a linear weighted average of the two values. Otherwise, if the upstream water surface is equal or less than 1.0 times the gate opening, the program applies the weir flow. Furthermore, at the same cross section, the program can model overflow weir, which could represent the top of the structure (gate openings) and embankment. In Hec-Ras, the overflow weir can be defined as broad crested, ogee shaped or sharp crested and the standard weir equation is used to compute the flow.

Hec-Ras is capable to model lateral weirs, gated spillways and culverts. A minimum of two cross sections, one upstream and one downstream of the structure must be defined. Gated spillways or culverts are modeled as described previously. To model lateral weir, when the water surface and the weir segment are parallel, the program uses the standard weir equation. Otherwise, if the water surface across the weir and/or the weir have a slope, it is used a general equation derived by integrating the standard weir equation between the sloping segments.

3.6.4 Modeling storage areas

Storage areas are regions in which water can be diverted into or from and are represented as polygons drawn by the user. Storage areas can be located upstream of a reach as an upstream boundary condition, laterally to a reach, or downstream of a reach as a downstream boundary condition. Storage areas can be connected to a river by means of a lateral structure, otherwise storage areas can be connected to each other by using a storage area connection (weir, gated spillways, weir and gated spillways or a weir and culverts). To enter information about the volume of the storage area, two option are available. The first option is to enter the area of the storage and a minimum elevation, the program then computes the volume by simply multiplying the area by the depth assuming the storage

area to have the same area at all the elevations. The second and best option is to enter an elevation versus volume curve.

3.6.5 Modeling 2D flow areas

Hec-Ras is capable of performing two-dimensional flow modeling and combined 1D and 2D flow modeling. Firstly, in Ras Mapper (a portion of Hec-Ras software in which GIS operations can be performed), a horizontal coordinate projection must be established. Secondly, a terrain model has to be developed in order to compute and represent 2D flow. This is accomplished by importing terrain data in Ras Mapper. Next, from within the Geometry editor, 2D flow areas polygons have to be drawn and it is possible and recommended to draw break lines to better represents any significant barrier to flow (levees, natural embankments, roads, hydraulic structures). The 2D computational mesh is developed on regular intervals by means of the 2D Flow Area editor, assigning a dx and dy cell spacing. Cell density can be increased or decreased, by adding, moving or delating cell centers. In Hec-Ras, the mesh can be structured or unstructured, if it is structured the program takes advantage of the orthogonality between cell faces during the numerical discretization. In the case of a combined 1D/2D model, it must be entered a connection between 1D elements and 2D flow areas (lateral structure or inline structure). As for combined 1D/2D model, the program allows to connect 2D flow areas by using a 2D flow area hydraulic connection (weir, gated spillways, weir and gated spillways or a weir and culverts).

4. Geometry definition for the Marano stream

In a previous study project on this stream (*Stambazzi, 2017*), three geometric datasets, obtained from three different field surveys (1996, 2003, 2016), were used to define the geometry (cross sections and hydraulic structures) of a 1D hydraulic model in Hec-Ras. For this study, the "Agenzia regionale per la sicurezza territoriale e la protezione civile" provided a Lidar relief (2008) with a resolution of 1m x 1m, to allow 2D flow modelling as well as floodplains inundation mapping.

It is necessary to emphasize that the laser employed in Lidar survey is not able to penetrate water and even if a green laser (λ=532nm, able to penetrate water) was employed, it would not provide the amount of details generated by field measurements. Consequently, field measurements were used to represent the main channel geometry, whereas the Lidar relief to represent overbank areas.

In the following chapters the procedure to define the geometry of the four hydraulic models used is illustrated.

4.1 1D hydraulic model

Firstly, terrain data (Lidar) was imported in Ras Mapper, setting the horizontal coordinate projection. Subsequently, the geometry of the 1D hydraulic model (186 cross sections, 11 bridges and 1 culvert), created by Stambazzi, were imported in the new geometry file. Cross sections were then interpolated maintaining a maximum distance of 50 meters.

Using a tool of Ras Mapper, the cross sections main channel was interpolated and merged with the Lidar creating a combined channel and overbank terrain model. Afterwards, the cross sections and the hydraulic structures were associated to the new terrain model updating the cross sections attributes (*River Stations, Bank Stations, Reach length* and *Elevation profile*) required by the program. *Levees* were added in order to ensure that water flows out of the river section only when the water level rises above the levee level.
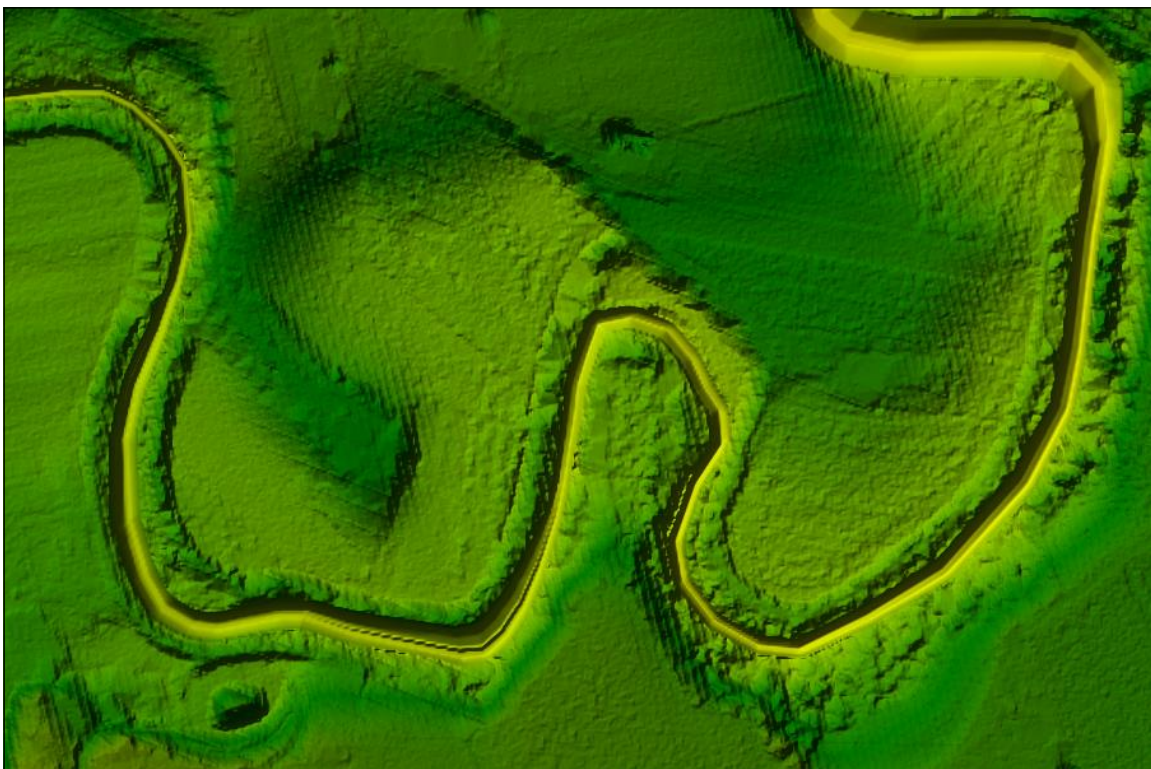
Figure 21: Detail of the combined channel and overbank terrain model

Where it was deemed necessary, cross sections were extended to represent the floodplain flow. Figure 22 shows a stretch of the stream as an example.
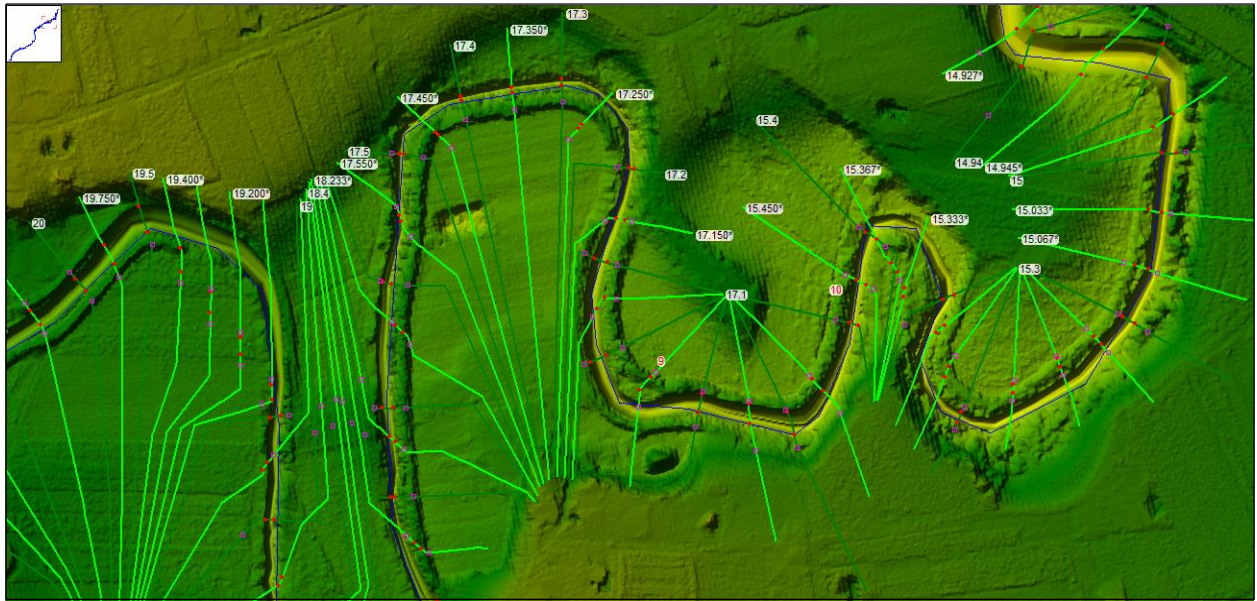
Figure 22: 1D model with extended cross sections (in light green the cross sections interpolated)

4.2 1D hydraulic model with storage areas

In the second hydraulic model, 38 *Storage Areas* were entered in correspondence of floodplain meanders. For each *Storage Area* an elevation versus volume relationship was computed, based on the underlying terrain profile. The *Storage Areas* were then connected to the main channel by means of *Lateral Structures,* defined by the elevations data of the levees, placed between the main channel and the areas. The extended cross sections were truncated in correspondence of the beginning of the *Storage Areas.* Figure 23 shows a stretch of the stream as an example.

Figure 23: 1D model with Storage Areas

4.3 Coupled 1D/2D hydraulic model

In the third hydraulic model the *Storage Areas* were turned into *2D Flow Areas.* A computational mesh was created for each area on a regular interval of 10 meters in both *x* and *y* directions. The *2D Flow Areas* are connected to the main channel by the same *Lateral Structures* used in the model with the *Storage Areas.* Figure 24 shows a stretch of the stream as an example.

Figure 24: Coupled 1D/2D hydraulic model

4.4 2D hydraulic model

A unique *2D flow area polygon* was drawn on the combined channel and overbank terrain model, making sure that the boundaries of the polygon are not reached by the water. Then, *break lines* were drawn to align computational cells with the stream centerline, levees, natural embankments and hydraulic structures. In this way, cell faces are kept perpendicular to the main flow direction by also taking account of the barriers to the flow. The computational mesh was then generated on regular interval (*dx=10m* and *dy=10m*), increasing cells density (*dx=5m* and *dy=5m)* in correspondence of the *break lines* and of the hydraulic structures. In Figure 25, a stretch of the stream is shown as an example.

Figure 25: 2D Model

Since it is not possible to use Hec-Ras bridge modeling capabilities in 2D hydraulic model, it was decided to model only the five critical bridges (the ones resulted inadequate from 1D steady and unsteady flow simulations). In particular, *2D flow area hydraulic connections* (gates and weir or culverts and weir, depending on the shape of the bridge) were used, reproducing the bridge geometry as well as possible. However, it is underlined that gates and culverts hydraulic routines use a partially different computational method. In Figure 26, the two geometrical representations of the bridge of Via Tortona are shown as an example.
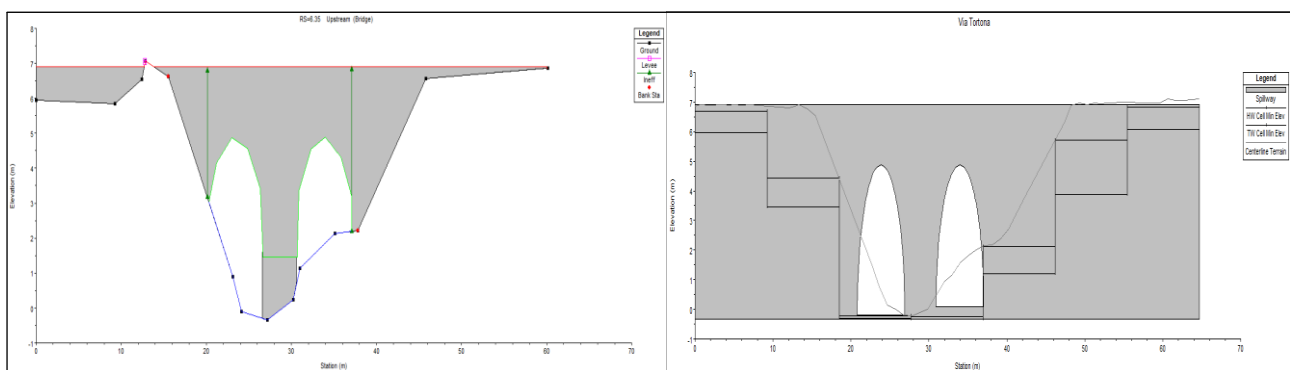
Figure 26: Bridge of Via Tortona, as it is represented in the 1D model (bridge) on the left and in the 2D model (culverts and weir) on the right

To enter boundary conditions, two *boundary condition lines* were drawn, one upstream in correspondence of the cross section 36.5 and one downstream in correspondence of the mouth of the stream.

Since Hec-Ras does not compute flow rates for 2D hydraulic models, three *2D flow area hydraulic connections* were drawn in correspondence of three cross sections of the 1D hydraulic model. By entering the terrain profile data in the *Embankment Station/Elevation Table* and selecting the *Normal 2D Equation* as *Overflow Computational Method*, Hec-Ras is forced to use the 2D equations over the terrain defined by the 2D connection line, considering it as a weir when instead it is a normal cross section. At these cross sections, it will be possible to compare flow rates resulting from 1D and 2D hydraulic simulations; since, according to the results of a trial 2D simulation, flow results almost entirely mono dimensional.

Lastly, *2D Flow Areas Connections* were entered to obtain flow results in correspondence of the *Lateral Structures* defined in the previous models. These connections are defined by the elevations data of the levees such as the *Lateral Structures* and can be modeled using either weir flow equation or 2D equations.

5. Roughness definition of the Marano stream

The Manning's coefficients were determined visually during field surveys and with the help of satellites images from Google Earth, taking the values of Table 4 (*Chow, 1959*) as a reference. The coefficients will be then calibrated comparing the results of steady flow simulations with the hydrometric data collected during the flood event occurred on 5 and 6 February 2015

Type of Channel and Description	Minimum	Normal	Maximum
Natural streams			
1. Main Channels			
a. Clean, straight, full stage, no rifts or deep pools	0.025	0.030	0.033
b. same as above, but more stones and weeds	0.030	0.035	0.040
c. clean, winding, some pools and shoals	0.033	0.040	0.045
d. same as above, but some weeds and stones	0.035	0.045	0.050
e. same as above, lower stages, more ineffective slopes and sections	0.040	0.048	0.055
f. same as "d" with more stones	0.045	0.050	0.060
g. sluggish reaches, weedy, deep pools	0.050	0.070	0.080
h. very weedy reaches, deep pools, or floodways with heavy stand of timber and underbrush	0.075	0.100	0.150
2. Mountain streams, no vegetation in channel, banks usually steep, trees and brush along banks submerged at high stages			
a. bottom: gravel, cobbles, and few boulders	0.030	0.040	0.050

	0.040	0.050	0.070
b. bottom: cobbles with large boulders	0.040	0.050	0.070
3. Floodplains			
a. Pasture, no brush			
1. short grass	0.025	0.030	0.035
2. high grass	0.030	0.035	0.050
b. Cultivated areas			
1. no crop	0.020	0.030	0.040
2. mature row crops	0.025	0.035	0.045
3. mature field crops	0.030	0.040	0.050
c. Brush			
1. scattered brush, heavy weeds	0.035	0.050	0.070
2. light brush and trees, in winter	0.035	0.050	0.060
3. light brush and trees, in summer	0.040	0.060	0.080
4. medium to dense brush, in winter	0.045	0.070	0.110
5. medium to dense brush, in summer	0.070	0.100	0.160
d. Trees			
1. dense willows, summer, straight	0.110	0.150	0.200
2. cleared land with tree stumps, no sprouts	0.030	0.040	0.050
3. same as above, but with heavy growth of sprouts	0.050	0.060	0.080
4. heavy stand of timber, a few down trees, little undergrowth, flood stage below branches	0.080	0.100	0.120
5. same as above, with flood stage reaching branches	0.100	0.120	0.160

Table 4: Manning's roughness coefficients

From the mouth of the stream to the footbridge (section 2.15), the main channel can be classified as clean, straight, full stage and without pools; the banks are characterized by light brushes and trees and the floodplains by scattered brush and heavy weeds. Therefore, values of Manning's coefficients equal to 0.03, 0.06 and 0.05 m$^{-1/3}$ s were assigned respectively to the main channel, banks and floodplains.
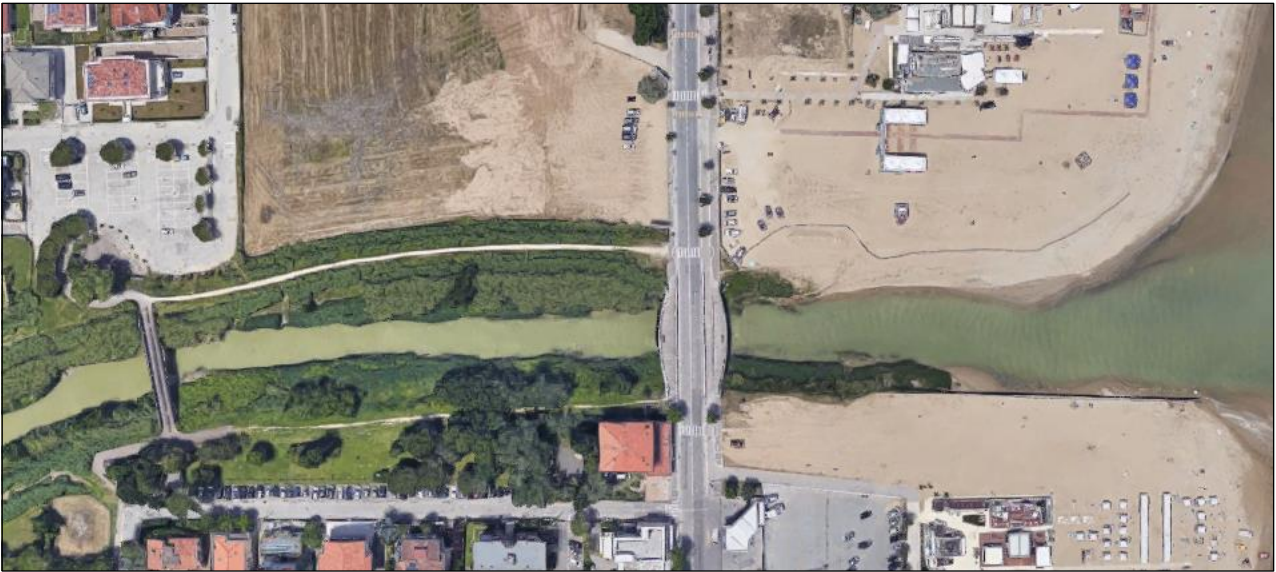
Figure 27: First stretch from the mouth to the footbridge (section 2.15)

For the second stretch, from the footbridge (section 2.15) to the first upstream section (section 36.5), the central main channel roughness was increased to 0.04 $m^{-1/3}$, since the pattern become winding and some pools and shoals are present. Moreover, the floodplain roughness was changed in correspondence of: eight areas characterized by heavy stand of timber (n=0.100 $m^{-1/3}$ s), seven areas characterized by medium to dense brush (n=0.070 $m^{-1/3}$ s), two areas characterized by light brush and trees (n=0.060 $m^{-1/3}$ s) and one cemented area (n=0.01 $m^{-1/3}$ s).

Figure 28: Picture taken at the bridge of the SP 31 (second stretch)

Marano stream

Figure 29: Detail of a floodplain characterized by heavy stand of timber

6. Meteorological event of 5 and 6 February 2015

As previously mentioned, there are no historical hydrometric data of the Marano stream. Therefore, the field observations collected during the particularly intense meteorological event, occurred on 5 and 6 February 2015, were used as a reference.

From the early morning of 5 February until 6 February afternoon the Emilia-Romagna region was hit by extensive and persistent precipitations, particularly focused on the eastern and central areas. The province of Bologna, Forlì-Cesena, Ravenna and Rimini were the most affected, with 150 mm of cumulated rainfall at the central-eastern river basins. Figure 26 shows the cumulated rainfall on the region, for mountain areas, since pluviometers do not record snowfall, the data has to be coupled with snowfall maps.
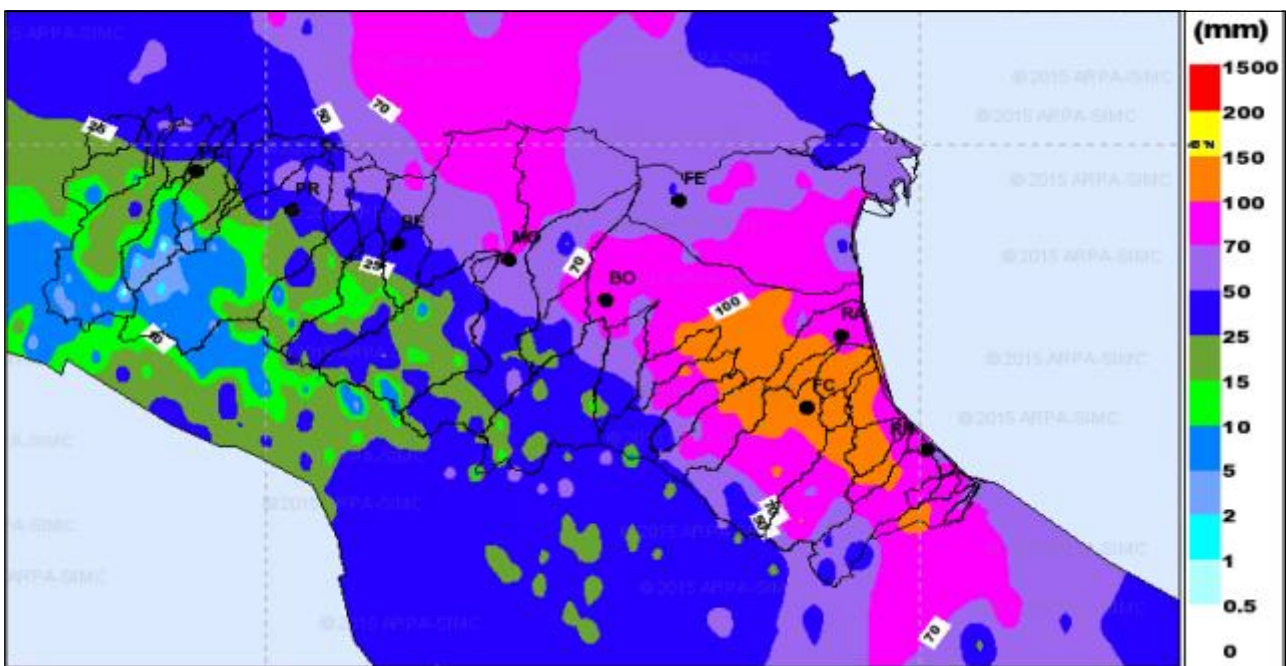
Figure 30: Cumulated rainfall on the Emilia-Romagna region during 5 and 6 February (ARPAE)

Hourly rainfall intensities did not exceed 25 mm/h, but the small sizes of the river basins caused a quick response to the precipitation, producing flood waves of remarkable volumes. Because of the different precipitation peaks, the flood waves are characterized by subsequent peaks which have summed up at the downstream river sections, generating the highest water stages ever recorded.

The highest peak discharges have been recorded at the small foothills river basins such as the one of the Uso stream, located north of the Marano stream.
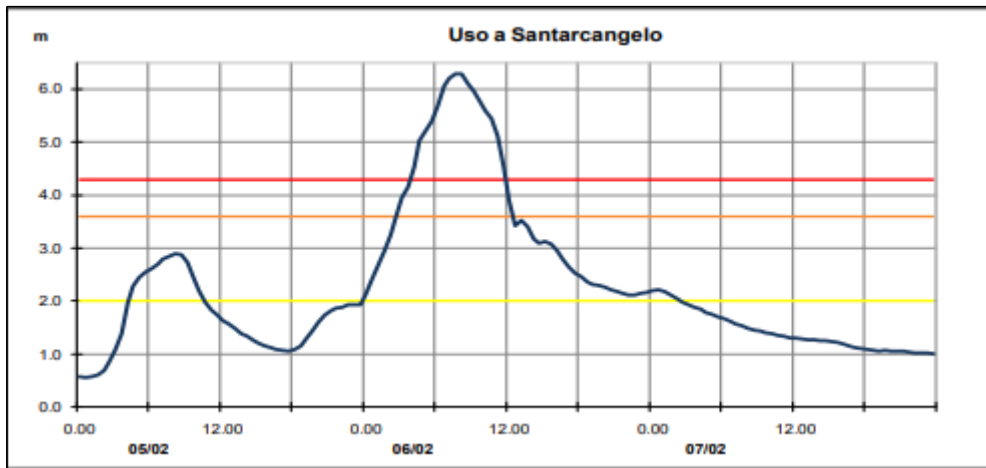
Figure 31: Stage hydrograph of Uso stream recorded at a downstream section

The three thresholds illustrated in Figure 31 represent respectively: a non-remarkable flood wave (flow in the main channel) in yellow, a flood wave with limited erosional and sediment transport phenomena (floodplains activation) in orange, and lastly a remarkable flood wave with widespread erosional and sediment transport phenomena (water stages in proximity of the levee safety margin) in red.

As it is illustrated in Figure 31, even though the two subsequent peaks of the flood wave associated with the two rainfall events remained separated, the water stages remained above the red threshold for 9 hours, with a very slow recession considering the river basin dimension.

The extensive and persistent precipitation caused widespread flooding of the secondary hydraulic network of the region (urban sewage system, drainage channels and flooding of the underpasses), aggravated by the strong swells which induced extensive backwater effects along the coastline.

Figure 32 shows some pictures of the flood event taken at the most critical points along the Marano stream.
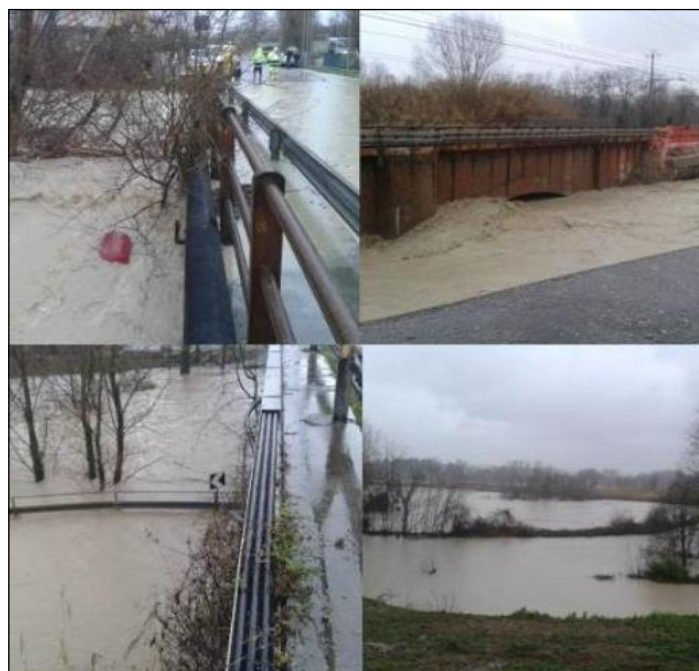
Figure 32: From the upper left corner clockwise: the bridge of via Tortona, the bridge of the railway line, flooded area at Coriano, the bridge of SS16 with viale Saluzzo underneath it

7. Steady flow hydraulic analysis of the Marano stream

The steady flow hydraulic analysis was run with the 1D hydraulic model. The aim of the analysis is determining the maximum water levels for design floods with a return period of 20, 50, 100 and 200 years; in order to assess the flood prone areas and the hydraulic adequacy of the structures present along the Marano stream.

The technical legislation on the constructions (*NTC 2008*) states that for the hydraulic analysis of bridges it must be considered a design flood with a return period not lower than 200 years and it must be ensured a freeboard not lower than 0.5 times the energy grade line or not lower than 1.5 m. For not straight intrados, the freeboard must be ensured for 2/3 of the span of the bridge and generally for 40 m in case of spans equal or longer than this value.

7.1 Design floods estimation

The "Autorità di Bacino Marecchia-Conca" provided the regionalized design floods associated to four return periods (20, 50, 100, 200), at the upstream cross section (36.5) of the stream. It is underlined that the design floods were recently recalculated further to a mistake in the drainage area at the closing section of Ospedaletto (Rimini).

The modified VA.PI. regionalization was used to estimate the design floods. This technique uses the index flood Q_I, which is the typical flood of a section whose return period remained constant within a homogeneous region (characterized by homogeneous geomorphoclimatic and rainfall characteristics); and the growth curve q_T' of the flood peaks, which follows a Gumbel probabilistic distribution and expresses the floods relationship with the return periods.

The design flood is given by the following expression:

$$Q(T) = Q_I \cdot q_T'$$

where:

Q_I is the index flood;

$q_T' = u' - \frac{1}{\alpha'} \ln(T)$, with u' and α' are the model parameters.

If flood historical measurements are available, the index flood is considered equal to the statistical mean. But if, as in this case, no flood measurements are available, the index flood can be indirectly estimated by means of a multiregression model. A multiple linear regression is a simple method to statistically regionalize hydrological information as catchment attributes and flood quantiles. In this case, it correlates, using linear or non-linear equations, the index flood, which is the dependent variable, with the explanatory variables, which are the geomorphoclimatic and rainfall characteristics of the homogeneous area:

$$\ln(Q_I) = A_0 + A_1 \cdot \ln(w_1) + \cdots + A_n \cdot \ln(w_n) + \varepsilon$$

where:

A_i are the model parameters;

w_i are the explanatory variables of the model;

ε is the model error.

The model parameters are estimated by means of a stepwise regression analysis, which consists in testing the dependent variable with each explanatory variable. First, a significance level is set, then for each regression a p-value and a R^2 value are computed. R^2 is a measure of the performance of the regression, while the p-value tests the null hypothesis (the explanatory variables has correlation with the dependent variable, p-value lower than the significance level) with the alternative hypothesis (the explanatory variables has no correlation with the dependent variable, p-value higher than the significance level). All the one predictor models are tested and the one returning the lowest p-value and the highest R^2 value is chosen as first predictor. Then, all two predictors models, having the first predictor fixed, are tested. The procedure goes on until there is no justifiable reason to enter or remove any other predictor. The model parameters will be the intercept and the angular coefficient of the best multi predictor model.

In this case, the index flood is defined by two different expressions related to the extension of the catchment area. These expressions are function of the following variables: length of the main channel, catchment mean altitude with respect to the closing section, mean altitude with respect to the mean sea level, mean annual precipitation averaged over the catchment, average of the yearly 24 hours peaks rainfall averaged over the catchment, return periods of interest and exponents of the rainfall depth-duration-frequency curves.

Concerning the growth curve q'_T definition, the Gumbel cumulative distribution function of a random variables X, is given by:

$$F_X(x) = \exp\big(-\exp\big(-\alpha(x - u)\big)\big), x \geq 0$$

where:

$F_X(x) = P(X \leq x)$, where $P(X \leq x)$ is the probability that the random variable X is less than or equal to x;

$\alpha(x) = \dfrac{1.283}{\sigma(x)}$, scale parameter of the distribution, function of the mean squared error $\sigma(x)$;

$u(x) = \mu(x) - 0.0450\sigma(x)$, position parameter, function of the mean $\mu(x)$;

The cumulative distribution function $F(x)$ is equal to $\dfrac{T-1}{T}$ and in this case x is equal to Q_T, therefore the inverse function is written as:

$$Q_T = u - \frac{1}{\alpha}\ln\left(\ln\left(\frac{T}{T-1}\right)\right)$$

For $T > 20 \; years, \; \ln\left(\frac{T}{T-1}\right) \approx \frac{1}{T}$, obtaining:

$$Q_T = u - \frac{1}{\alpha}\ln(T)$$

which divided by the index flood Q_I, returns:

$$q'_I = u' - \frac{1}{\alpha'}\ln(T)$$

Where:

$u' = \frac{u}{Q_I}$;

$\alpha' = \alpha Q_I.$

The growth curve of the modified VA.PI. regionalization method follows the Two Component Extreme Value distribution function, TCEV (*Rossi et al., 1984*). This distribution function assumes that the annual maximum flood quantiles come from two different populations related to different meteorological phenomena. This hypothesis is justified by the presence of one or more outliers in many historical data series, making them seem heterogeneous with respect to the other data. The cumulative distribution function of the TCEV model is composed of two components (populations), each of which is described by a Gumbel distribution:

$$F_X(x) = \exp\left(-\lambda_1 \cdot exp\left(-\frac{x}{\theta_1}\right) - \lambda_2 \cdot exp\left(-\frac{x}{\theta_2}\right)\right), \qquad x \geq 0$$

Where:

λ are the parameters expressing the average number of independents events above a threshold;

θ are the position parameters of the distribution related to the two populations;

the subscripts 1 and 2 refer respectively to the most frequent events (base component) and to the extreme events (extraordinary component).

By considering the standardized variable $y = \frac{x}{\theta_1} - ln\lambda_1$, the cumulative distribution function can be written as follows:

$$F_Y(y) = \exp\left(- exp(-y) - \Lambda \cdot exp\left(-\frac{y}{\theta}\right)\right)$$

where:

$\Lambda = \left(\frac{\lambda_2}{\lambda_1}\right)^{-\theta}$;

$\theta = \frac{\theta_2}{\theta_1}.$

The TCEV distribution, with respect to the mono-component distribution, better represents flood peaks that are generated by different physical phenomena and it is able to account for most of the characteristics of real flood data, as the large variability of the sample skewness coefficient (*Singh, 1998*).

7.2 Boundary conditions

For the steady flow simulation, a mixed flow regime was imposed. As previously mentioned, the first upstream cross section (36.5), is located just upstream of Ospedaletto, location at which the "Autorità di Bacino" computed the flood peaks with the method described above. The flow data was entered at the first upstream cross section (36.5) and were assumed constant along the entire stream. This assumption was made, since the area of the downstream inter-basin is limited (10.3% of the total drainage area).

Section	Q_{20} (m^3/s)	Q_{50} (m^3/s)	Q_{100} (m^3/s)	Q_{200} (m^3/s)
36.5	134	170	199	230

Table 5: Flood discharges for the four return periods (Autorità di Bacino Marecchia-Conca)

A normal depth, considering $S_f = 0.005$, and a constant water stage of 1.49 m (resulting from the simultaneous effect of the flood wave and the tide with a return period of 10 years (*Idroser, 1982*)) was set respectively as upstream and downstream boundary conditions.

7.3 Steady flow simulations results

Below, are presented and commented the steady flow simulation results, moving from downstream to upstream (in legend are shown the steady flow profiles associated to Q_{20}, Q_{50}, Q_{100} and Q_{200} with a blue line of increasing thickness; and the velocities distribution represented by a yellow blurring to blue with increasing velocities; in some cases, due to the change of flow regime, the profile associated to lower discharges are higher than the ones associated to higher discharges):

- In a stretch 100 m long, located just before the pedestrian bridge, the discharge Q_{200} floods the area on the right orographic sides.
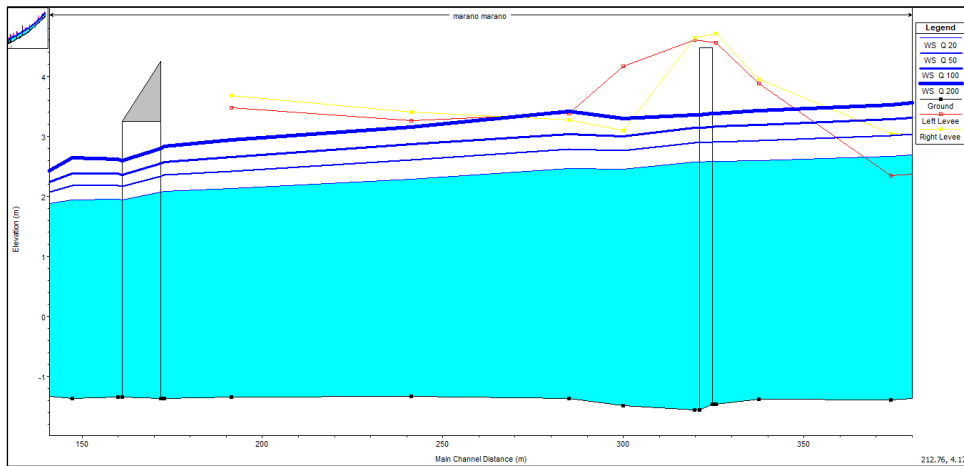
Figure 33: Longitudinal profile of the stretch between the first downstream bridge (section 1.05 BR) and the pedestrian bridge (section 2.15 BR)
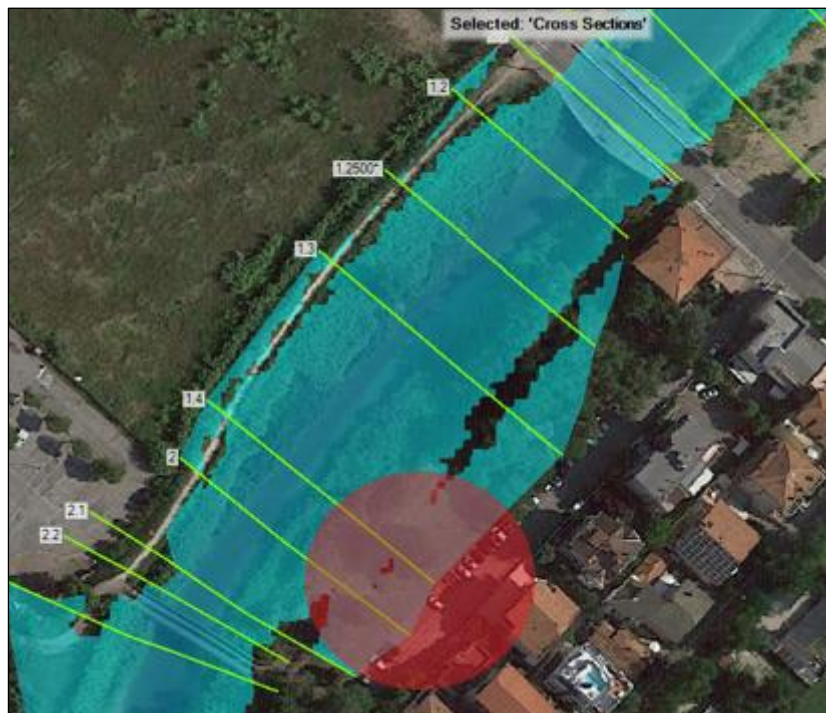
Figure 34: Flooded area highlighted in red (Q_{200})

- The stretch located between the pedestrian bridge (section 2.15 BR) and the bridge of the railway line (section 3.15 BR) underwent a heightening of the levees of circa 1 m, therefore, discharges Q_{50}, Q_{100} and Q_{200}, which result flooding, would be contained.
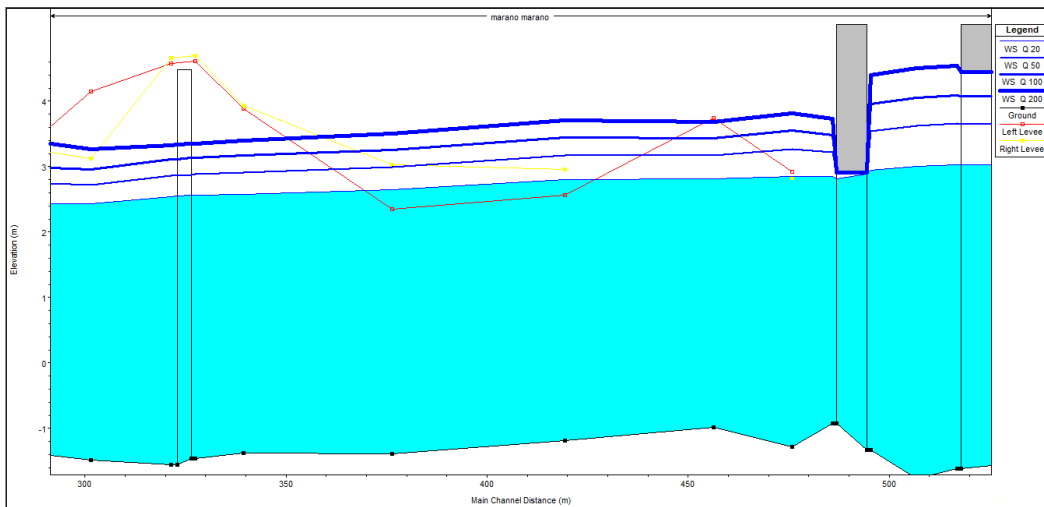
Figure 35: Longitudinal profile of the stretch between the pedestrian bridge (section 2.15 BR) and the bridge of the railway line (section 3.15 BR)

- The pedestrian bridge, for discharge Q_{100} , has a freeboard lower than 1.5 m.
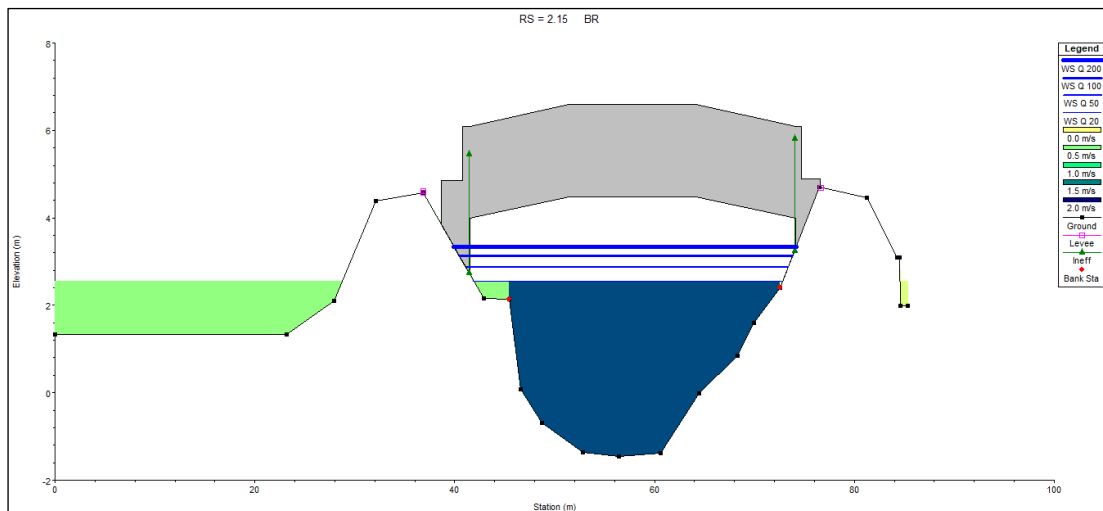
Figure 36: Cross section of the pedestrian bridge (section 2.15 BR)

- The bridge of the railway line (section 3.15 BR) results inadequate, since the flow reaches the intrados for each investigated discharge. The result was confirmed by the 2015 event.
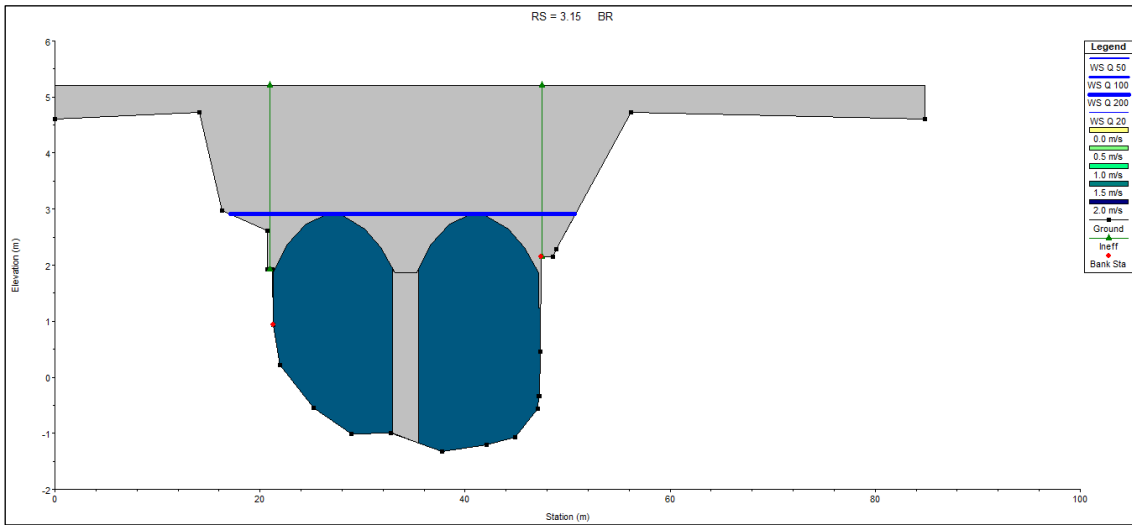
Figure 37: Cross section of the bridge of the railway line (section 3.15 BR)
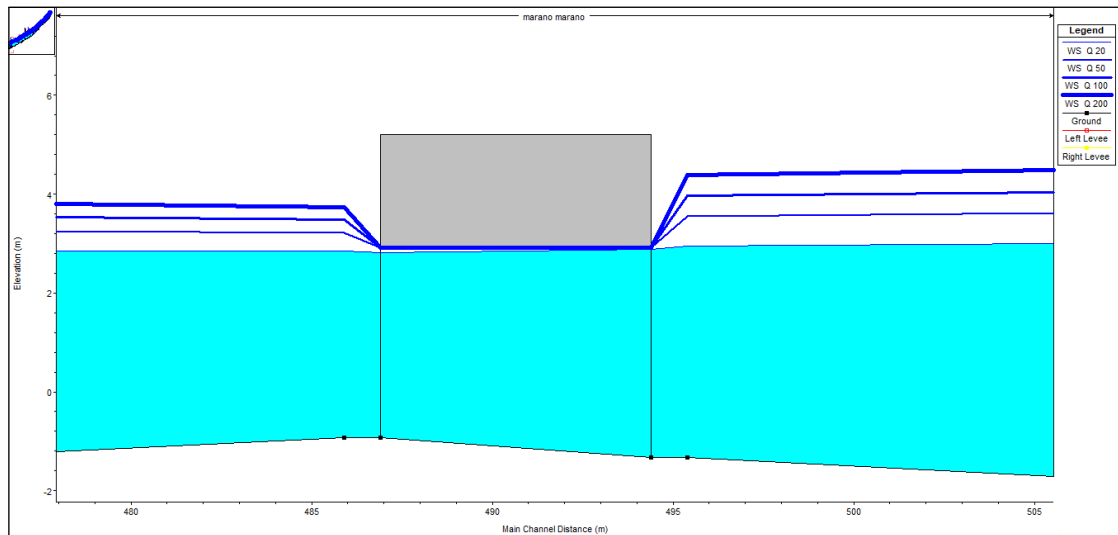
Figure 38: Longitudinal profile of the bridge of the railway line (section 3.15 BR)

- The bridge of the Viale Portofino (section 3.45 BR) results inadequate, the discharge Q_{200} reaches the intrados, whereas, for the other discharges, results a freeboard lower than 1.5 m.
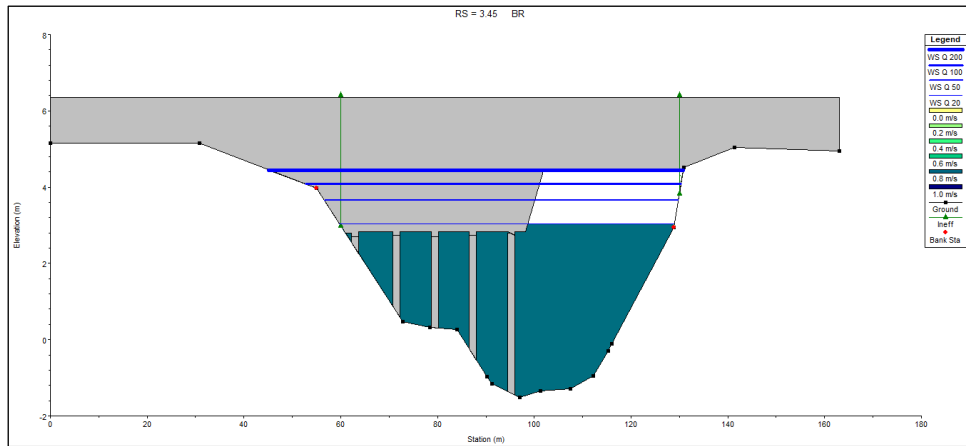
Figure 39: Cross section of the bridge of Viale Portofino (section 3.45 BR)
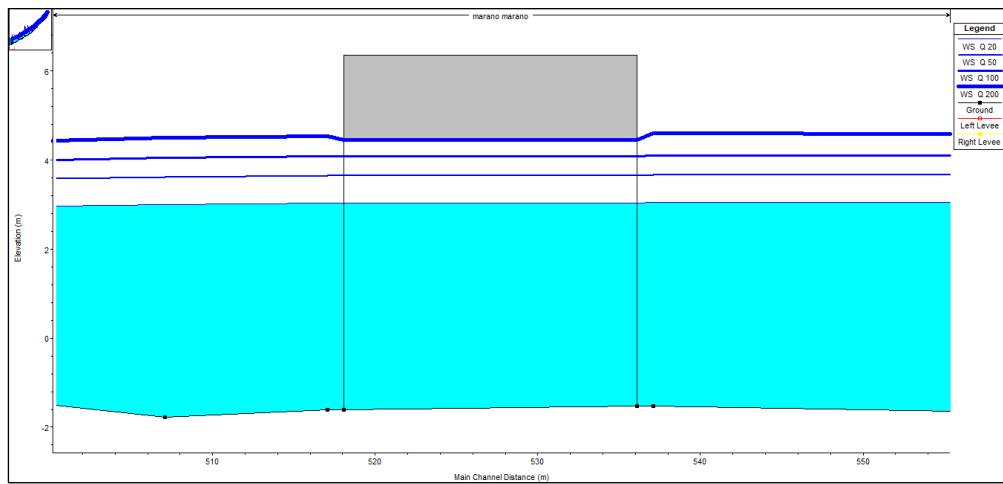
Figure 40: Longitudinal profile of the bridge of Viale Portofino (section 3.45 BR)

- The discharge Q_{100} floods a residential area just upstream of the bridge of Viale Portofino (section 3.45 BR).
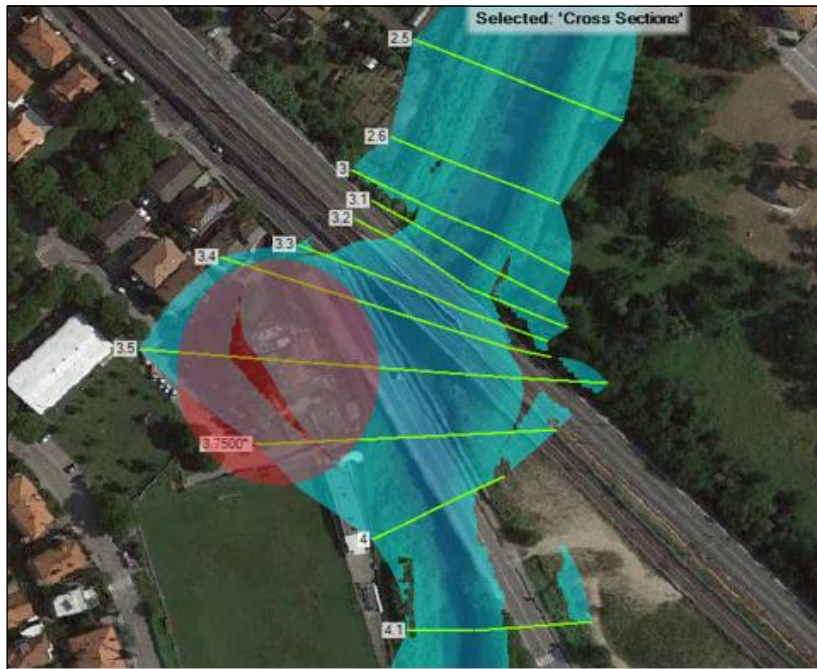
Figure 41: Flooded residential area highlighted in red (Q_{200})
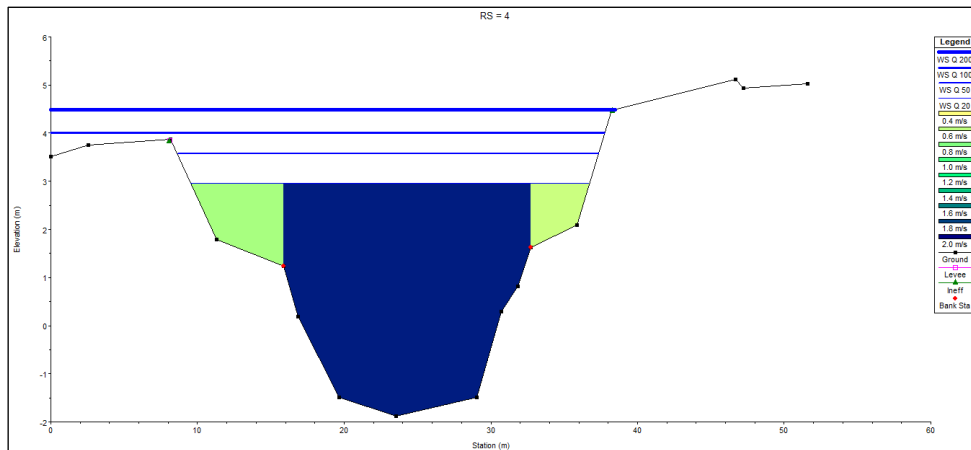
Figure 42: Cross section 4, upstream of the bridge of Viale Portofino

- Downstream of the bridge of the SS 16 (section 5.45 BR), a go-kart track located on the orographic left side is flooded for discharges equal to Q_{100}. On the orographic right side, the discharge Q_{200} floods a productive area.
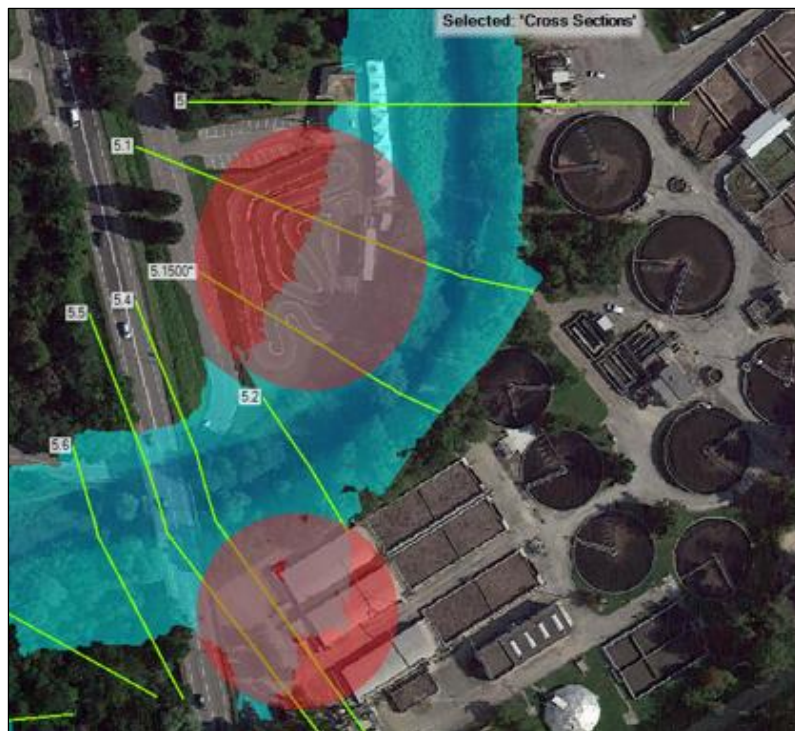
Figure 43: Flooded areas highlighted in red (Q_{200})
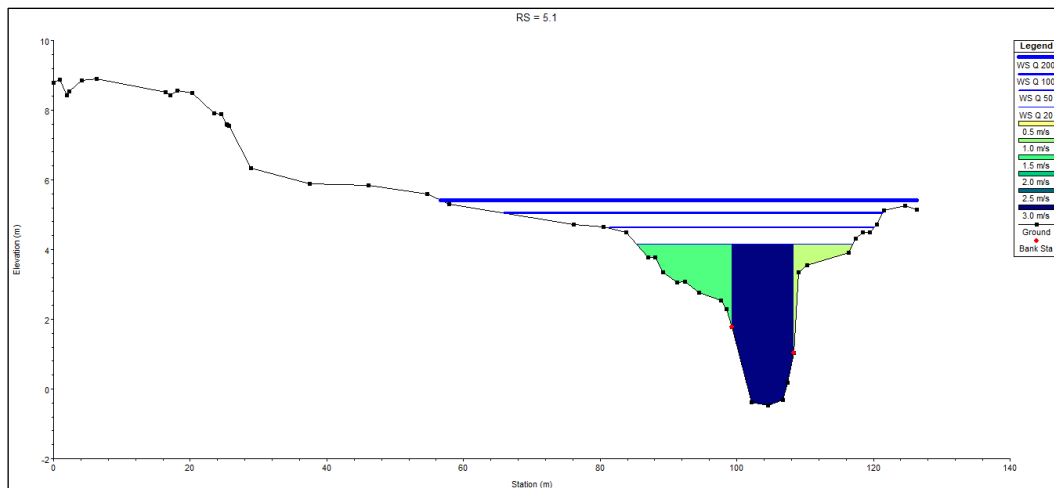
Figure 44: River cross section at the go-kart track
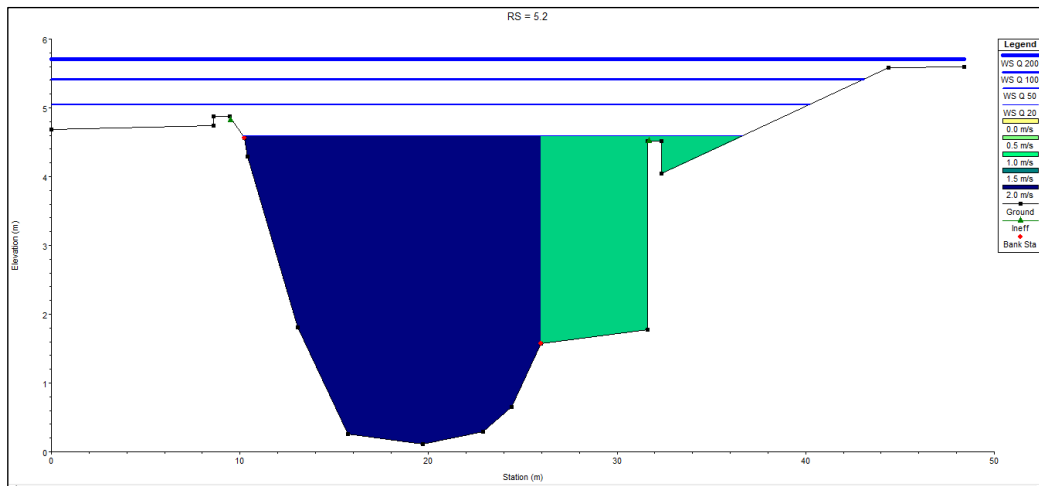
Figure 45: Cross section in correspondence of the productive area

- The bridge of the SS 16 (section 5.45 BR) results well dimensioned, but the street (Viale Saluzzo) located below it, on the orographic left side, is flooded for discharges equal to Q_{50}.
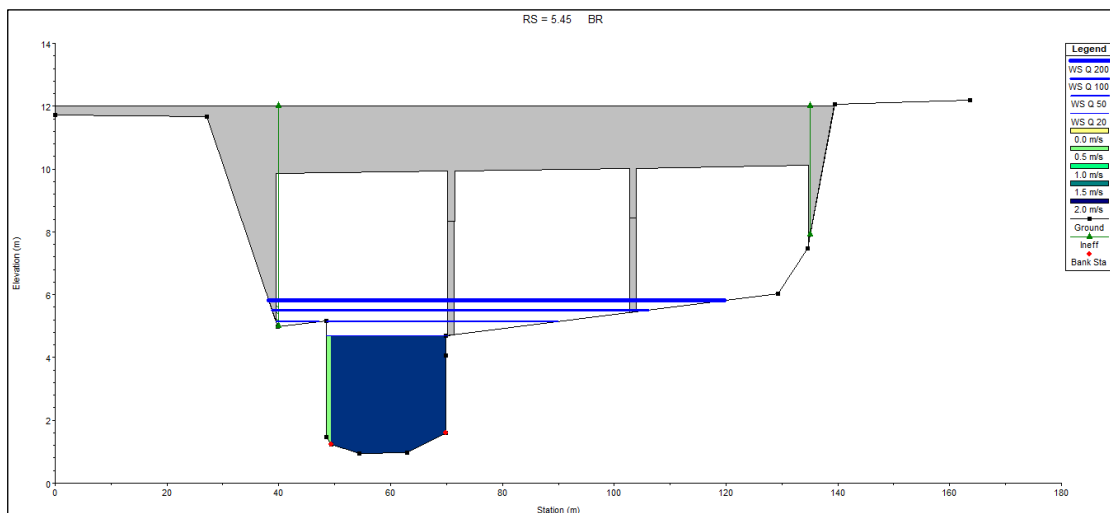
Figure 46: Cross section of the bridge of the SS 16 (section 5.45 BR)

- A beverage warehouse located downstream of the bridge of Via Tortona, is flooded for discharges equal to Q_{100}. The result was confirmed by the 2015 event.
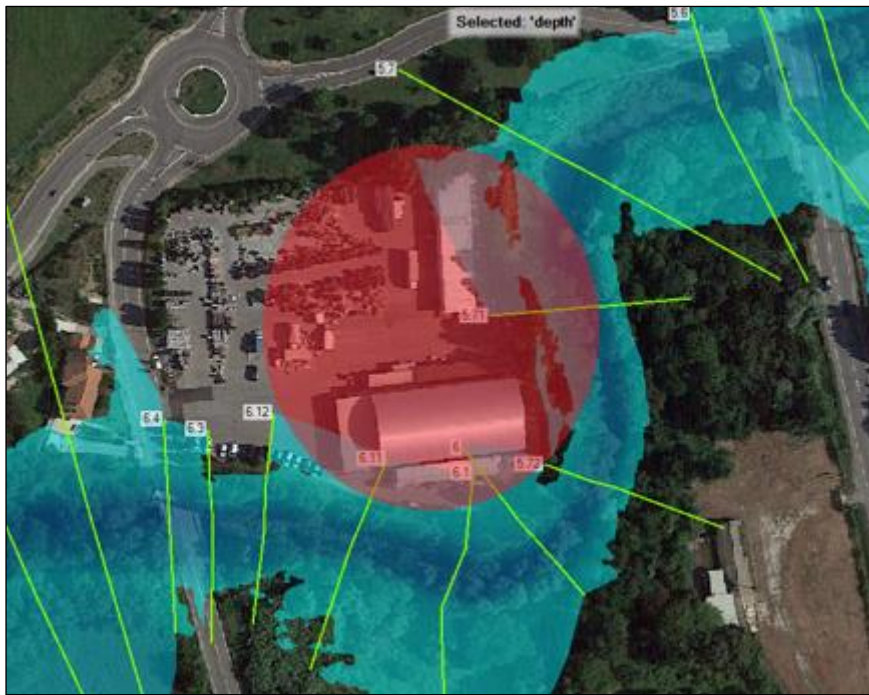
Figure 47: Flooded area highlighted in red (Q_{200})
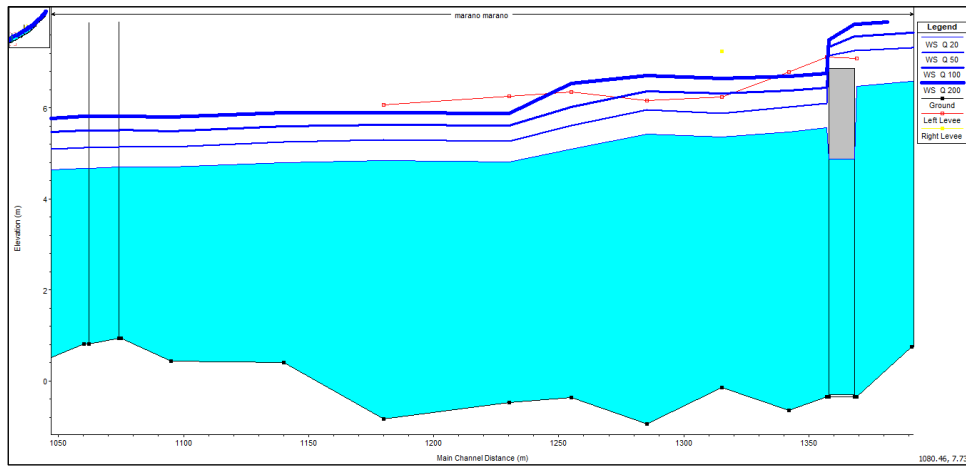
Figure 48: Longitudinal profile of the stretch between the SS 16 bridge and the Via Tortona bridge

- The bridge of Via Tortona (section 6.35 BR) is completely submerged for discharges equal to Q_{50}, while the discharge Q_{20} results reaching the intrados.
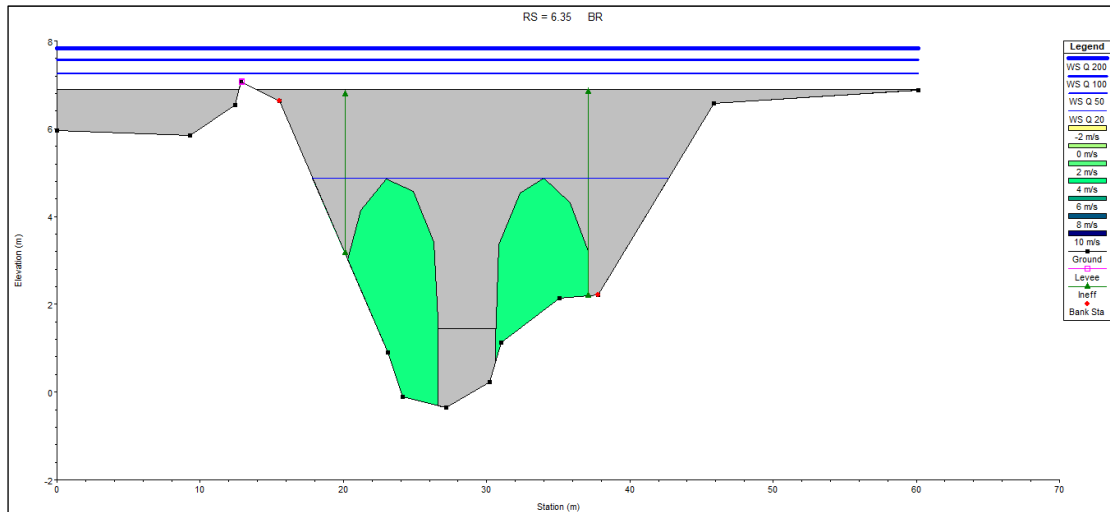
Figure 49: Cross section of the bridge of Via Tortona (section 6.35 BR)

- The meandering area between the bridge of Via Tortona (section 6.35 BR) and the bridge of Via San Lorenzo (section 11.65 BR) is flooded. The result was confirmed by the 2015 event.
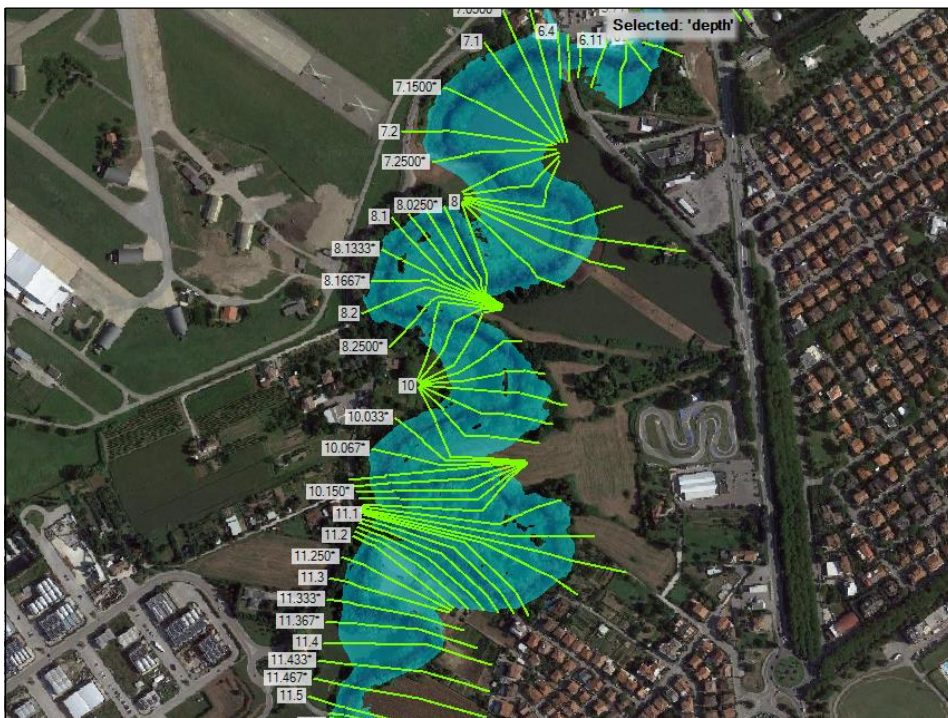
Figure 50: Flooded meandering area (Q_{200}) between the bridge of Via Tortona (section 6.35 BR) and the bridge of Via San Lorenzo (section 11.65 BR)
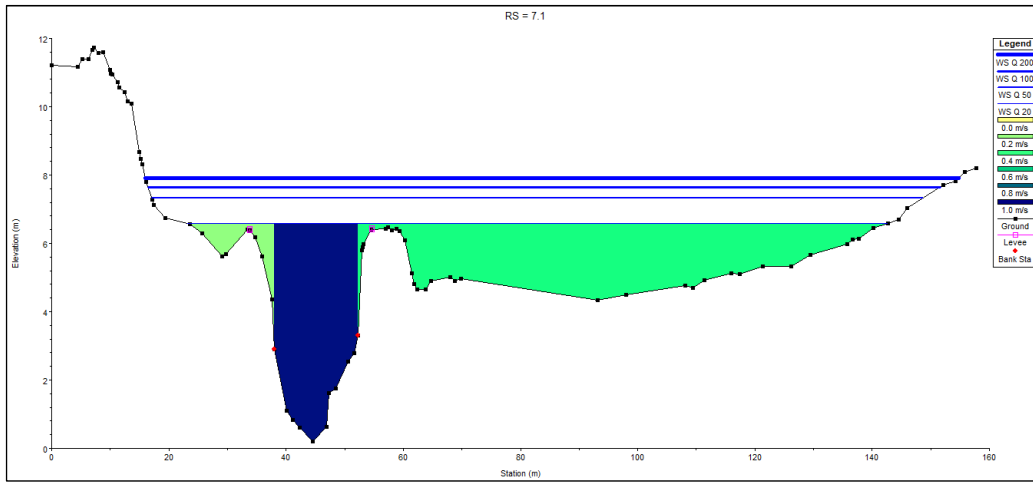
Figure 51: Cross section 7.1
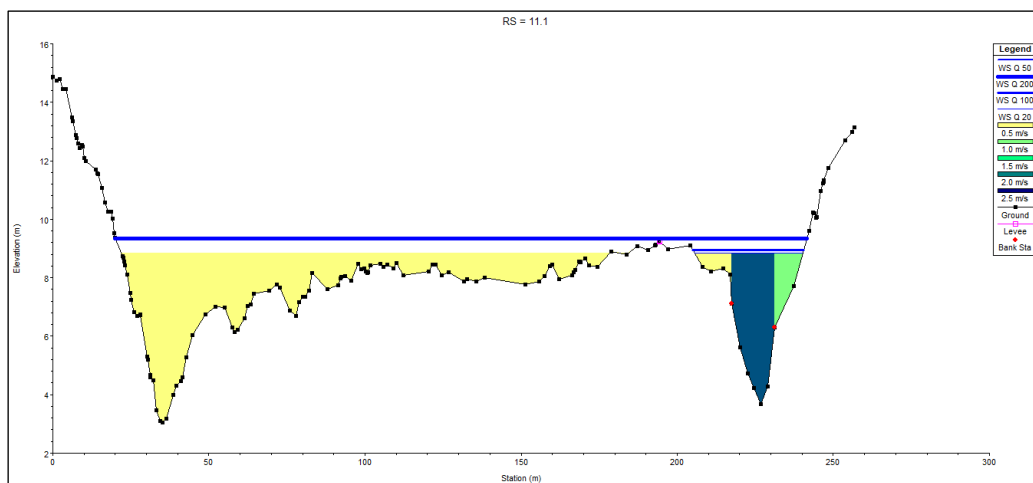
Figure 52: Cross section 11.1

- The bridge of Via San Lorenzo (section 11.65) is completely submerged for each of the investigated discharges which furthermore flood the area on the orographic right side. The result was confirmed by the 2015 event.
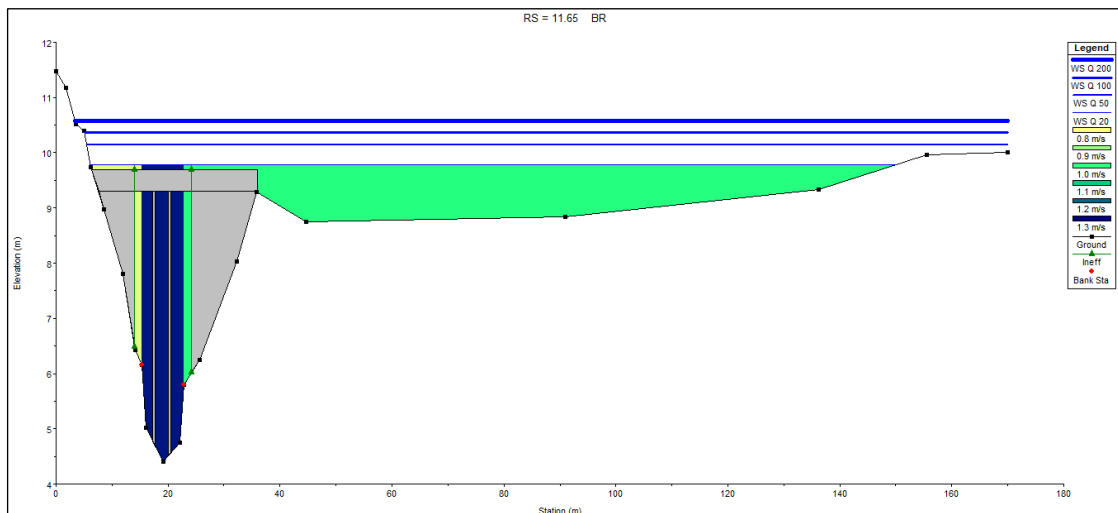
Figure 53: Cross section of the bridge of Via San Lorenzo
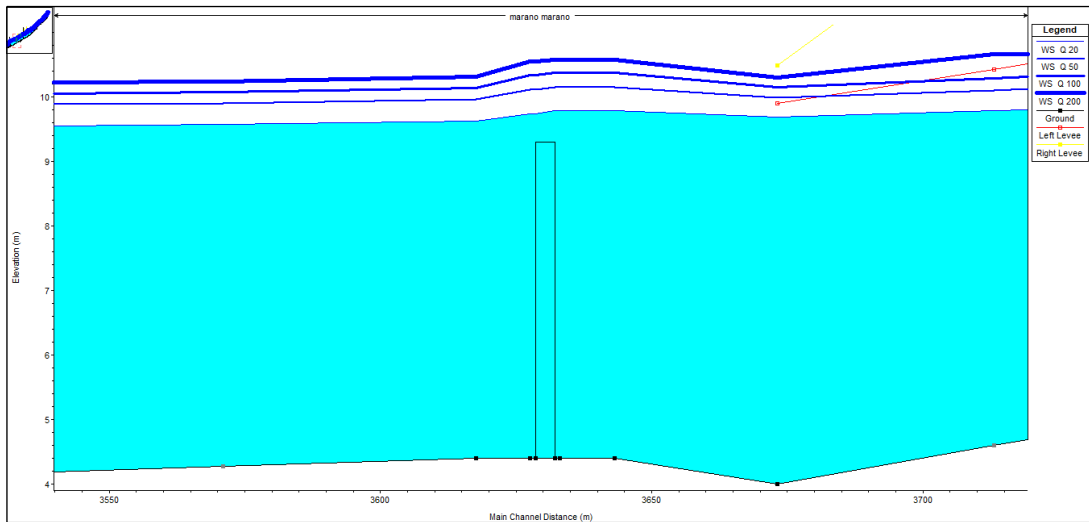
Figure 54: Longitudinal profile of the bridge of Via San Lorenzo
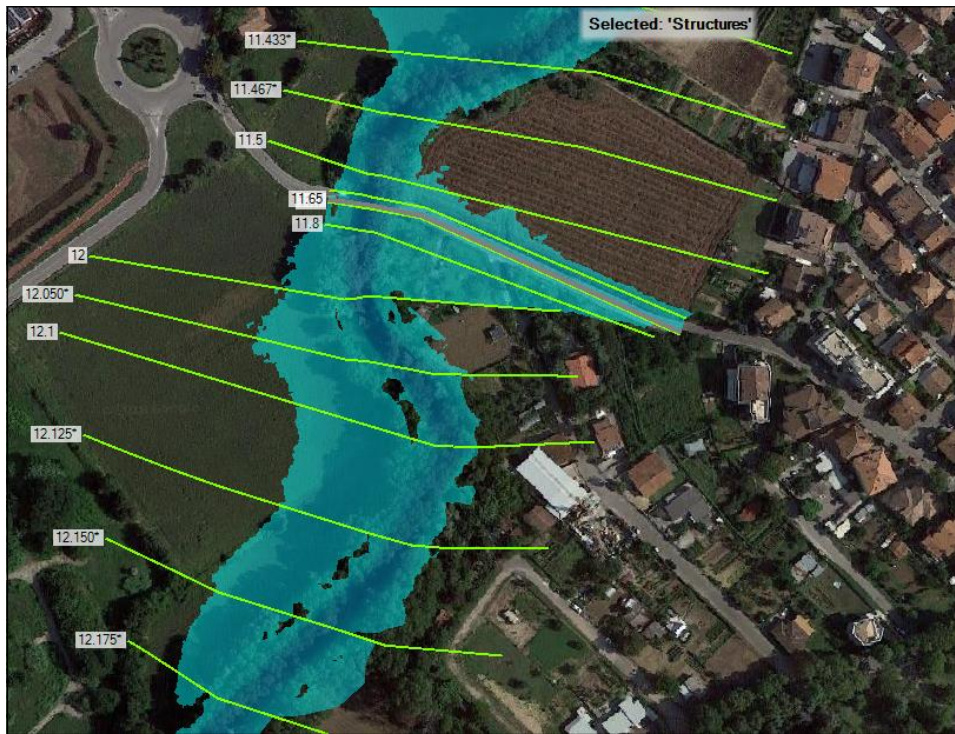
Figure 55: View of the flooded area (Q$_{200}$) in correspondence of the bridge of Via San Lorenzo (section 11.65 BR)

- The meandering area between the bridge of Via San Lorenzo (section 11.65 BR) and the Highway bridge (section 14.75 BR) is flooded, but no building is reached by the water.
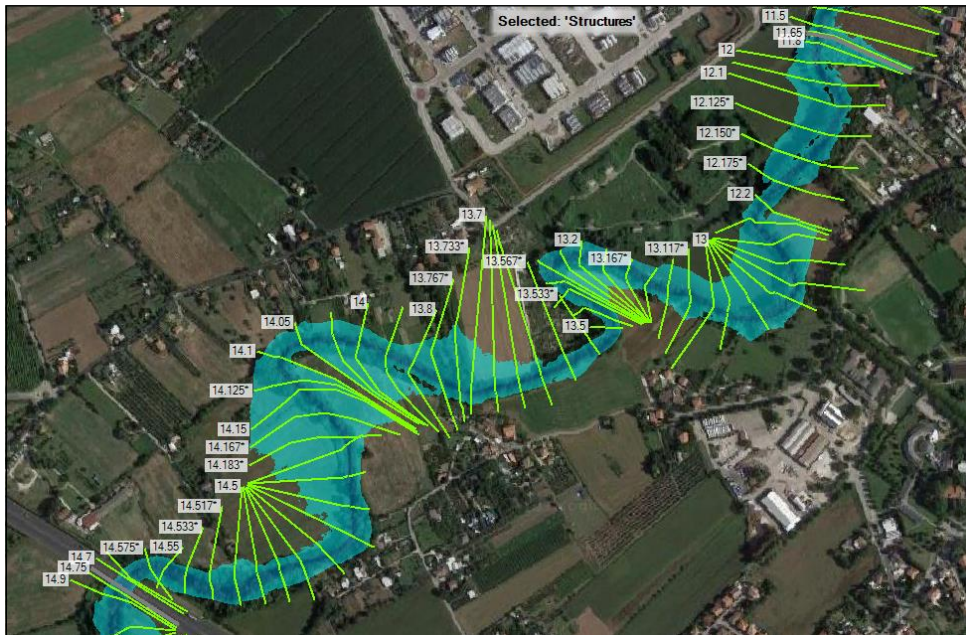
Figure 56: Flooded (Q_{200}) meandering area between the bridge of Via San Lorenzo (section 11.65 BR) and the Highway bridge (section 14.75 BR)

- A group of buildings at Case del Molino, located on the orographic right side between the Highway bridge (section 14.75 BR) and the bridge of the provincial road 31 (section 20.45 BR), are flooded for discharges equal to Q_{20}. The odd inundation map is due to the intrinsic nature of the 1D model, since the flow can overtop the levee at one cross section and remain in the main channel at the next one.
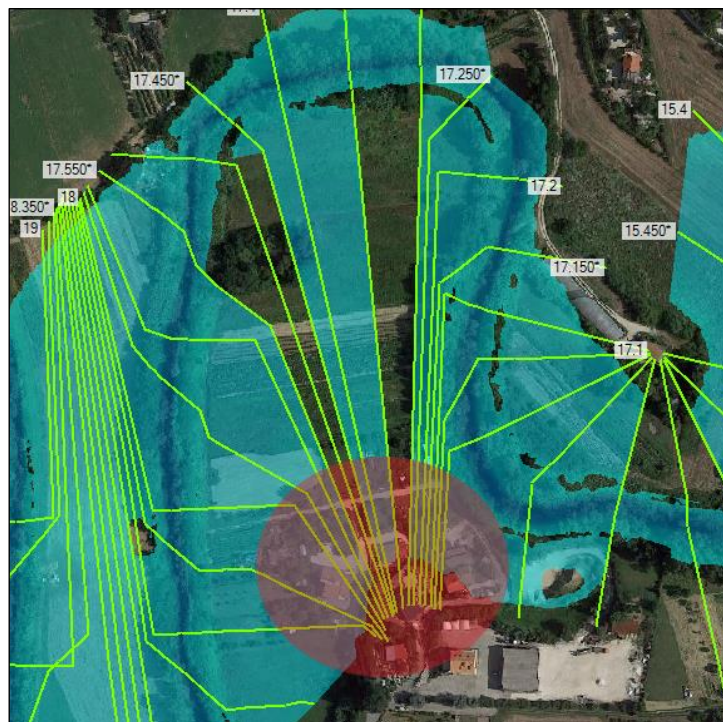
Figure 57: Highlighted in red the buildings flooded by the discharge Q_{20}
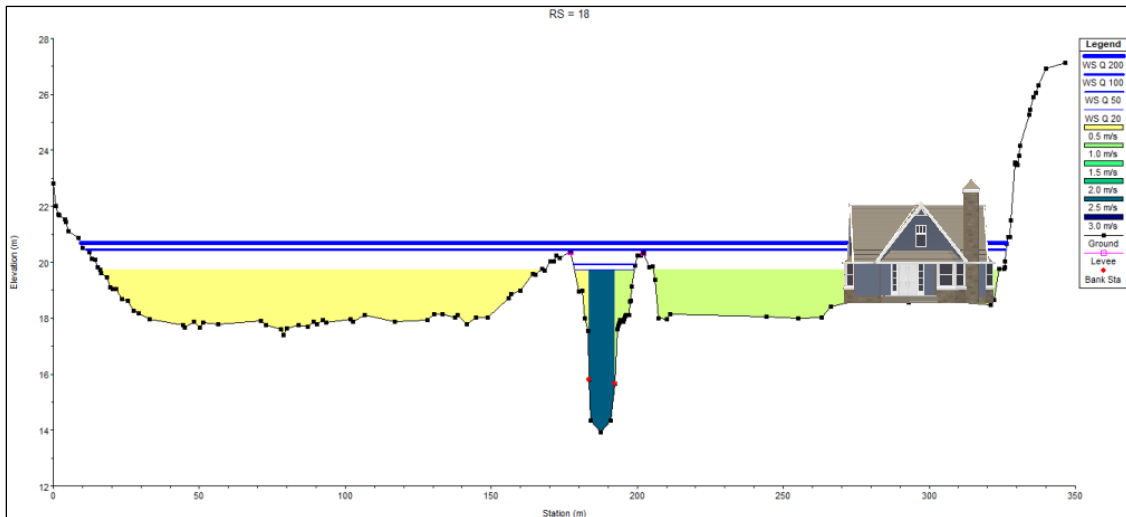
Figure 58: Cross section 18, schematic representation of the buildings at risk, not to scale

- Three buildings at Case del Molino, located on the orographic left side downstream of the bridge of the provincial road 31 (section 20.45 BR) are reached by the water (Q_{20}) flooding at the cross section 20.1.
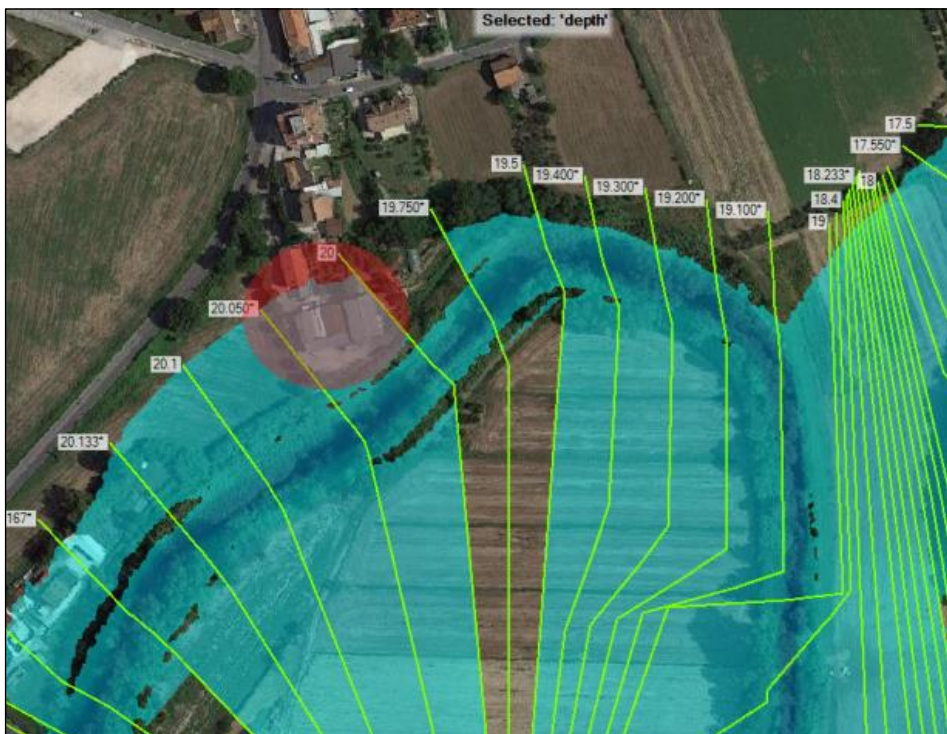
Figure 59: Highlighted in red the buildings flooded by the discharge Q_{20}
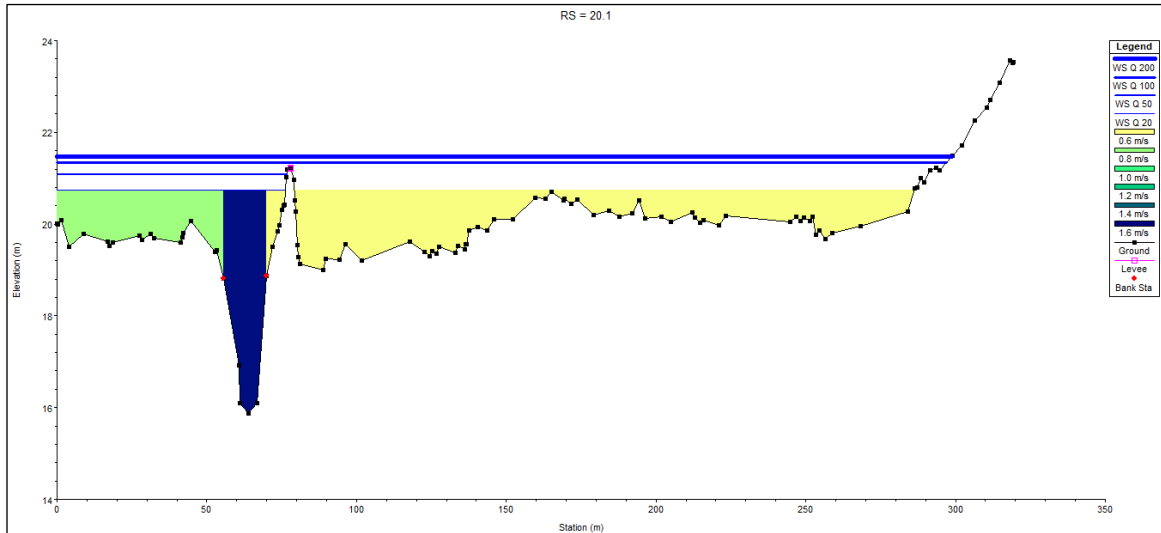
Figure 60: Cross section 20.1, upstream of the buildings
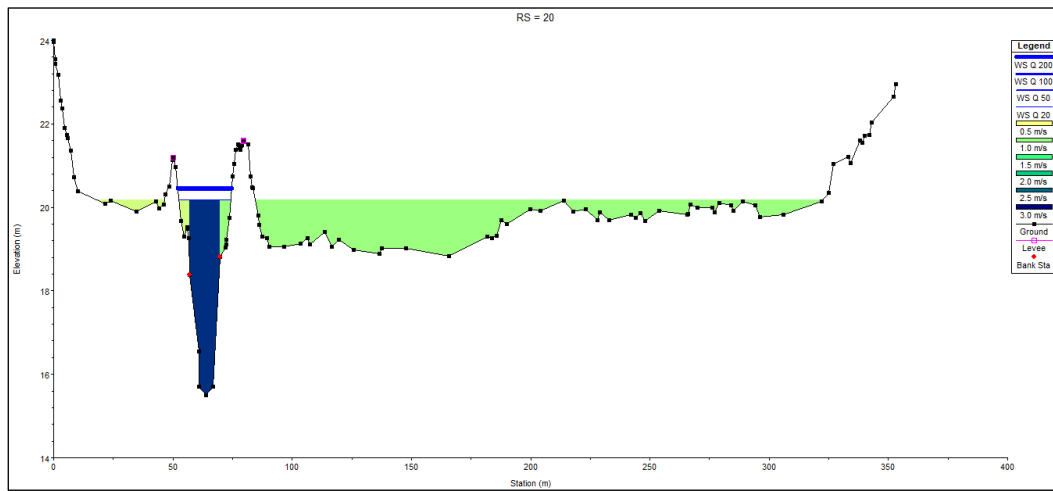
Figure 61: Cross section 20, just downstream of the buildings

- At the bridge of the provincial road 31 (section 20.45 BR), each of the investigated discharges flood, reaching a group of buildings located just downstream of the bridge, on the left orographic side.
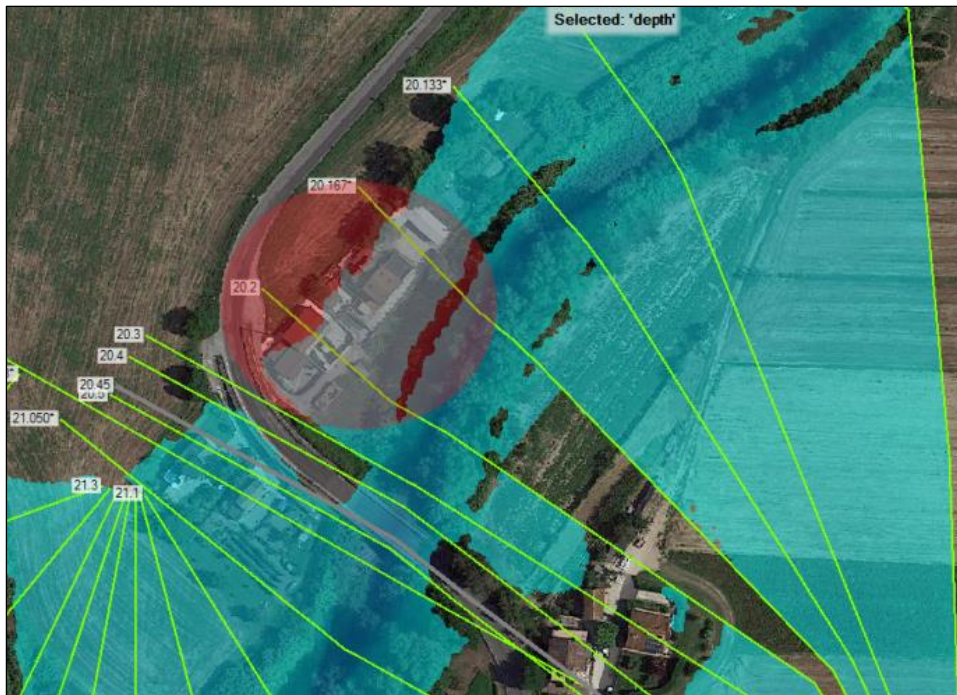
Figure 62: Highlighted in red the flooded buildings (Q$_{200}$)
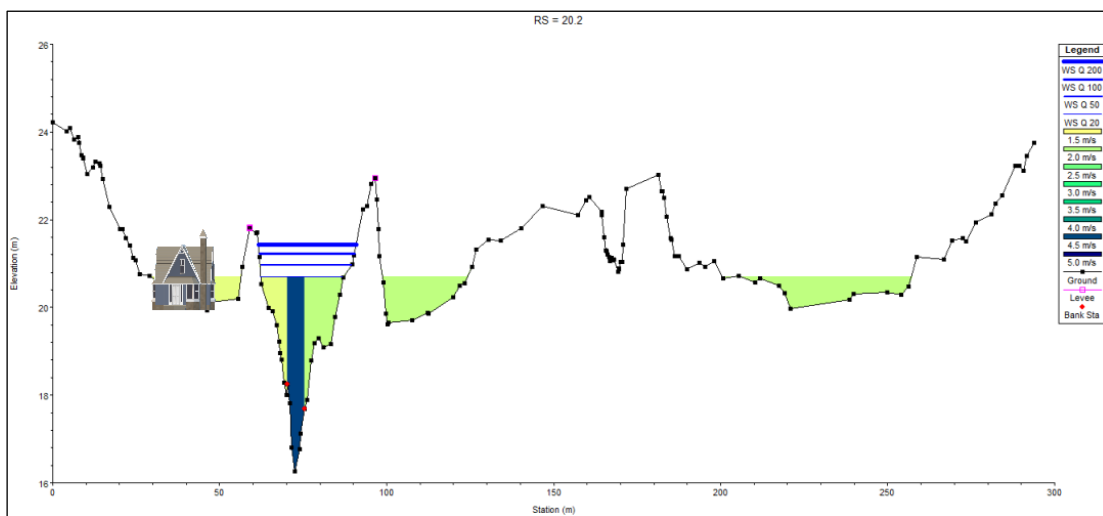
Figure 63: Cross section 20.2, schematic representation of the buildings at risk, not to scale

- At the bridge of the provincial road 31 (section 20.45 BR), the discharge Q_{200} reaches the intrados, while for the other three discharges investigated, results a freeboard lower than 1.5 m.
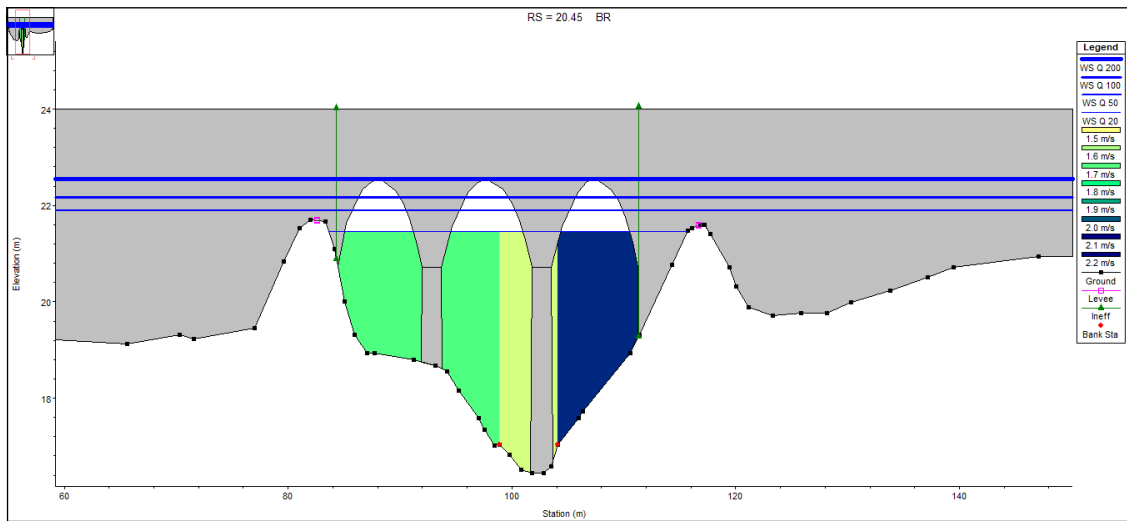
Figure 64: Cross section of the bridge of the provincial road 31 (section 20.45 BR)
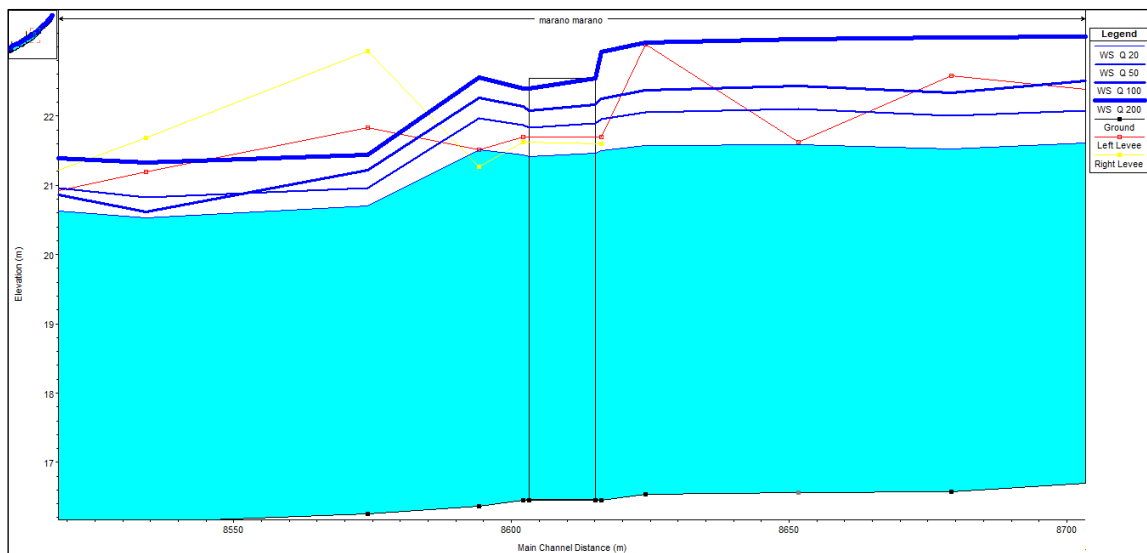
Figure 65: Longitudinal profile of the bridge of the provincial road 31 (section 20.45 BR)

70

- A group of buildings located on the orographic left side just upstream of the bridge of the provincial road 31 (section 20.45), is reached by the water flooding at the bridge (Q_{50}).
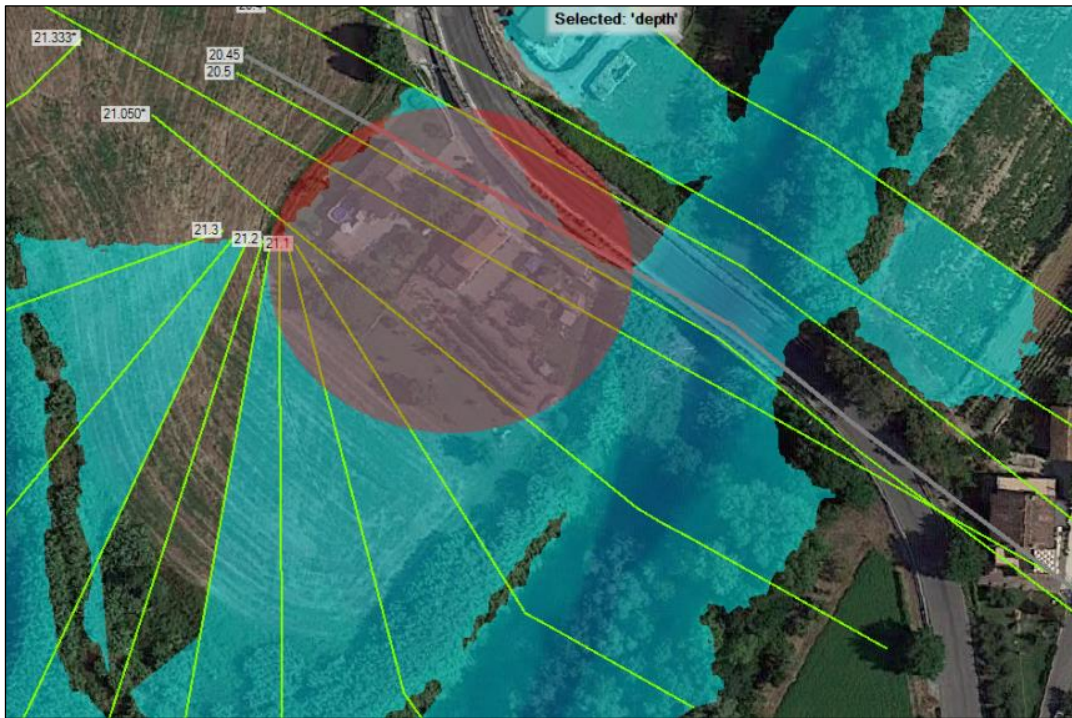
Figure 66: Highlighted in red the flooded buildings (Q_{200})
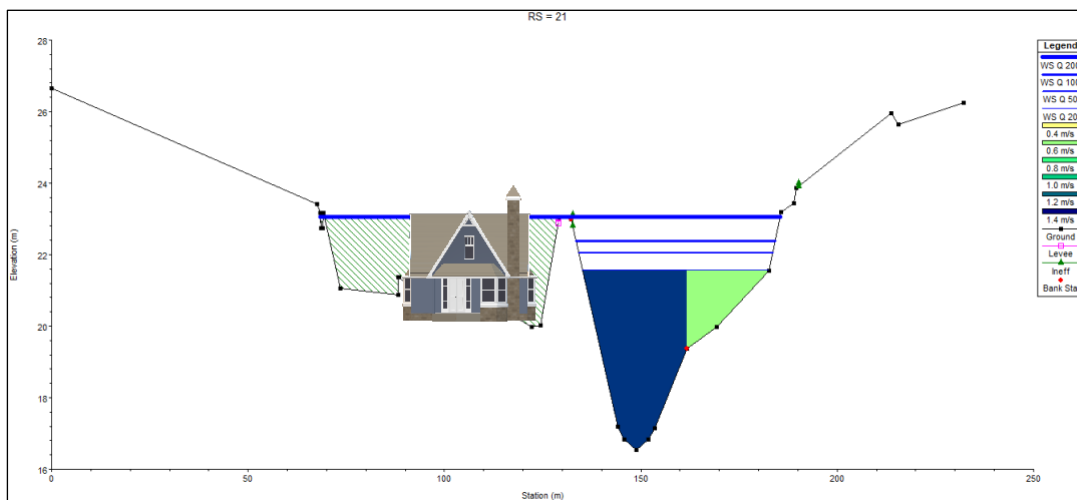
Figure 67: Cross section 21, schematic representation of the buildings at risk, not to scale

- The meandering area between the bridge of the provincial road 31 (section 20.45 BR) and the bridge of the provincial road 41 (section 32.15 BR), is flooded. At Ospedaletto, there is a levee protected area on the orographic left side, in which are located fields of crops and a group of greenhouses, which is not flooded but it is located at an altitude lower than the water stage.
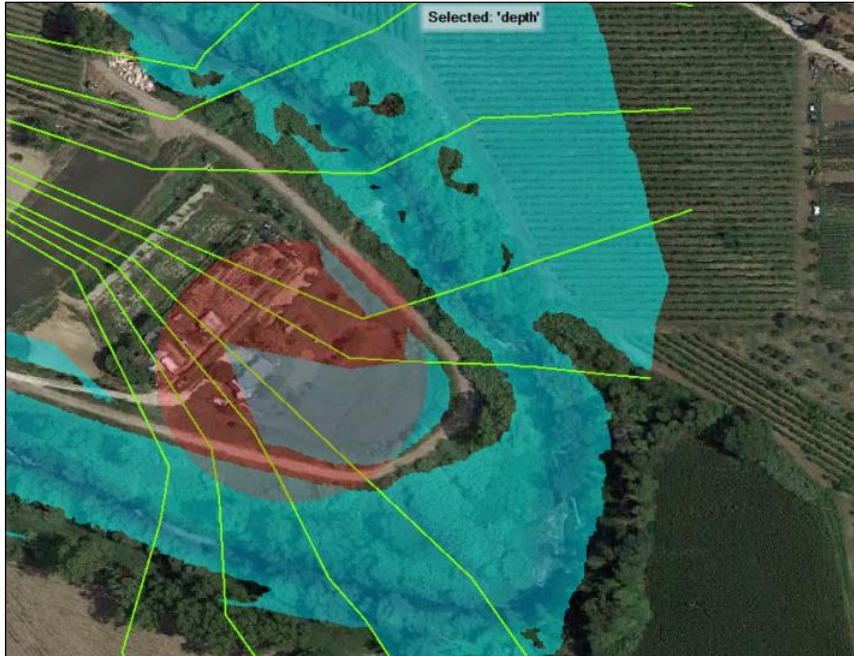
Figure 68: Highlighted in red the area beyond the levee
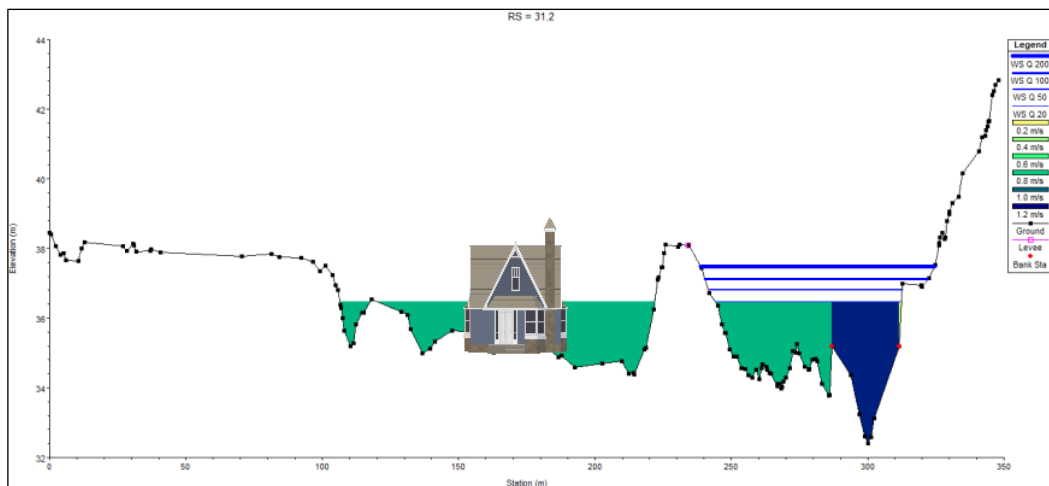
Figure 69: Cross section 31.2, schematic representation of the buildings beyond the levee, not to scale

- At Ospedaletto, there is a group of buildings on the orographic left side just downstream of the bridge of the provincial road 41 (section 32.15 BR), which is not flooded but it is located at an altitude lower than the water stage.
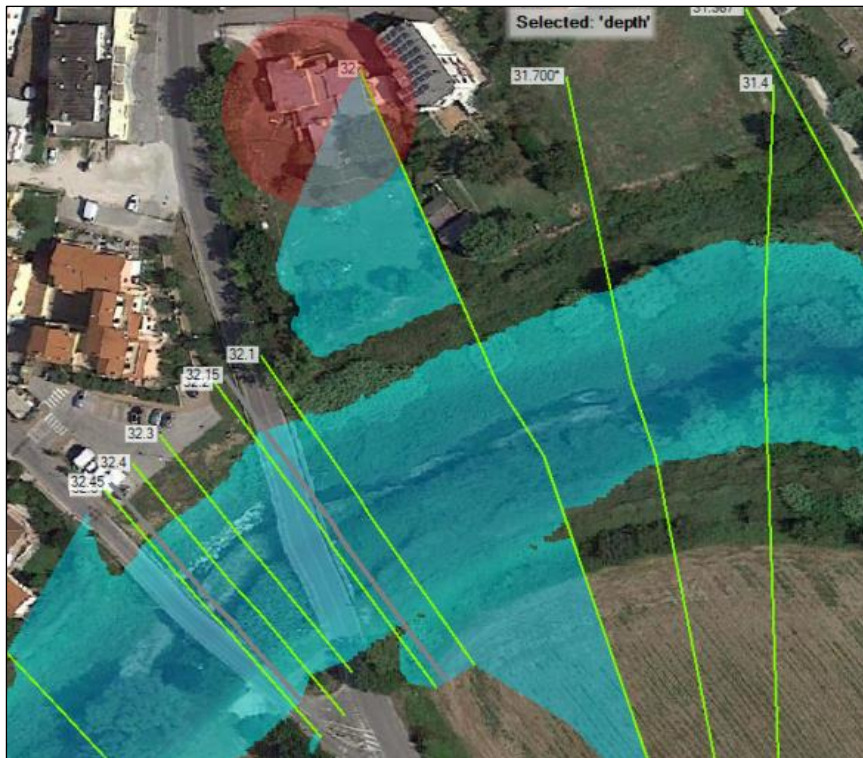
Figure 70: Highlighted in red the buildings beyond the levee
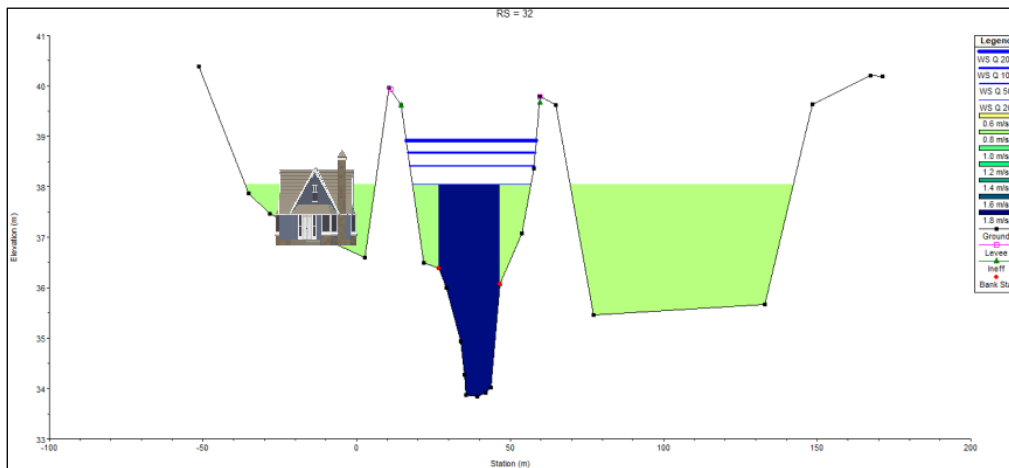
Figure 71: Cross section 32, schematic representation of the buildings beyond the levee, not to scale

73

- At the bridge of the provincial road 41 (section 32.15 BR), the discharge Q_{200} reaches the intrados, while the freeboard is lower than 1.5 m for the other three design discharges.
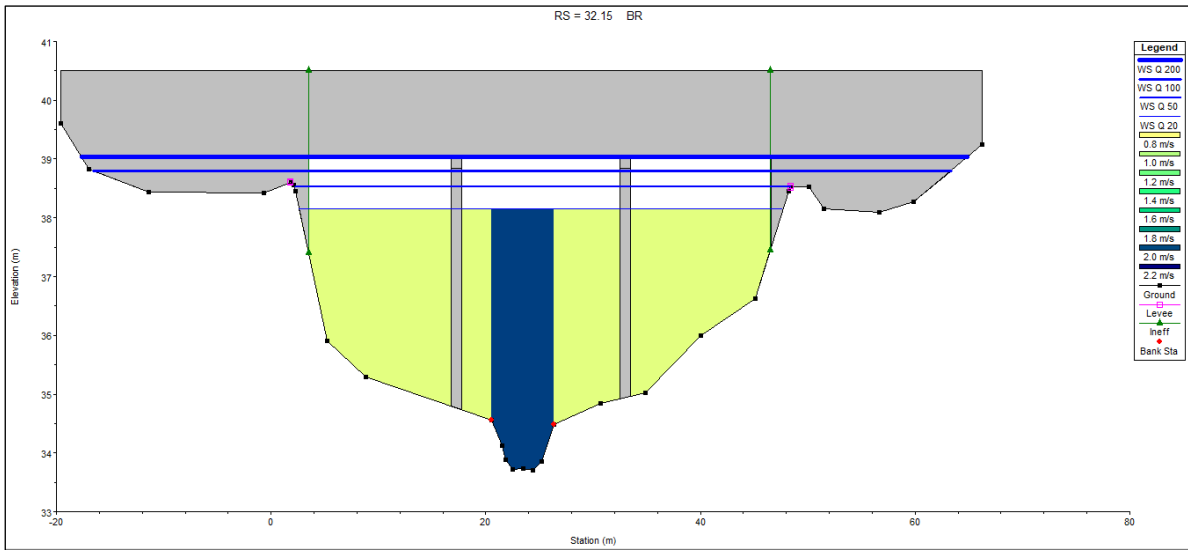
Figure 72: Cross section of the bridge of the provincial road 41 (section 32.15 BR)

- At the bridge of Via Marzabotto (section 32.45 BR), the discharge Q_{50} reaches the intrados, while for discharge Q_{20}, it results a freeboard lower than 1.5 m.
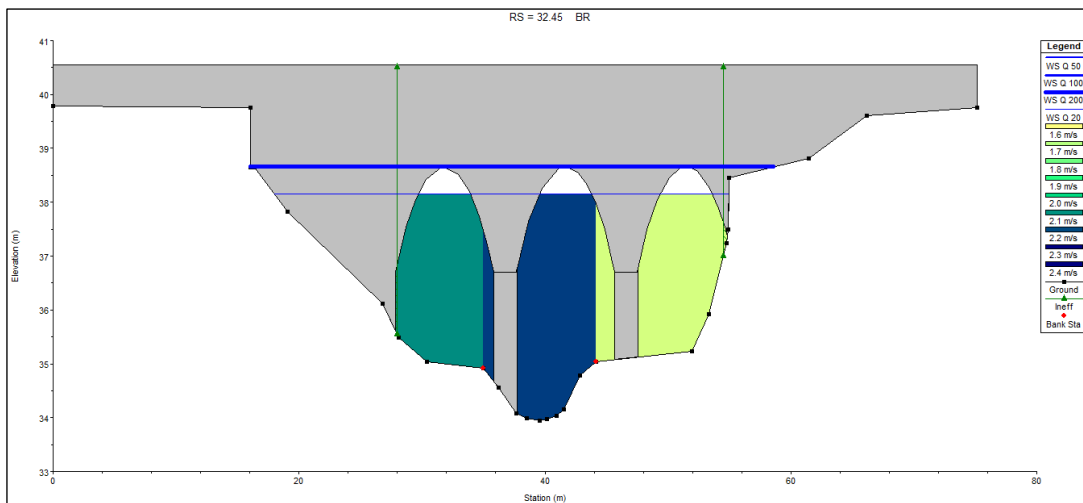
Figure 73: Cross section of the bridge of Via Marzabotto (section 32.45 BR)
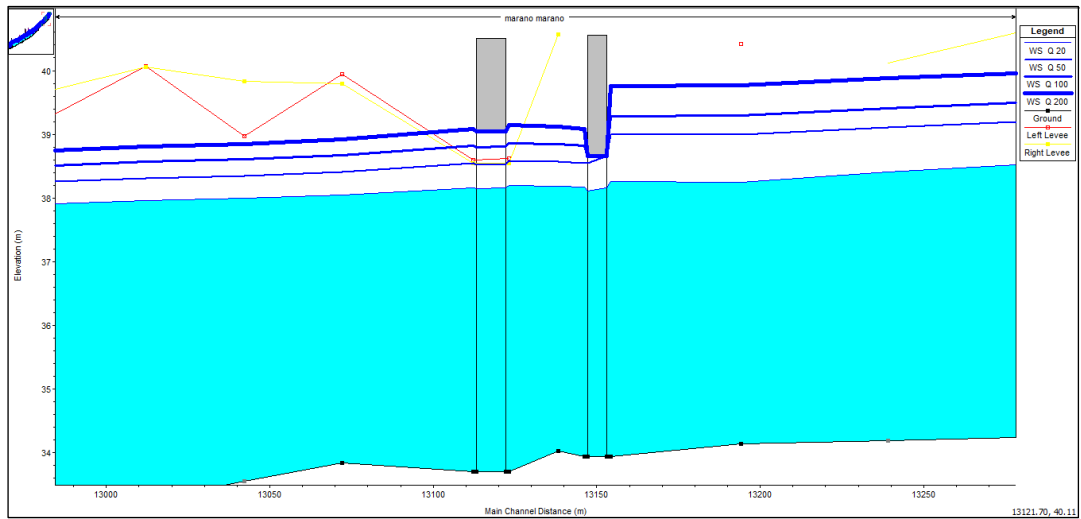
Figure 74: Longitudinal profile of the two bridges (section 32.45 BR and section 32.15 BR)

- At Ospedaletto, there is a building on the orographic left side upstream of the bridge of Via Marzabotto (section 32.45 BR), which is not flooded but it is located at an altitude lower than the water stage.

Figure 75: Highlighted in red the building beyond the levee

- The meander between the bridge of Via Marzabotto and the ford crossing with culverts of Via Cella, is flooded; the result was confirmed by the 2015 event. In the area there are three buildings, one is flooded for discharges equal to Q_{50}, while the other two are at risk for discharge Q_{200}.
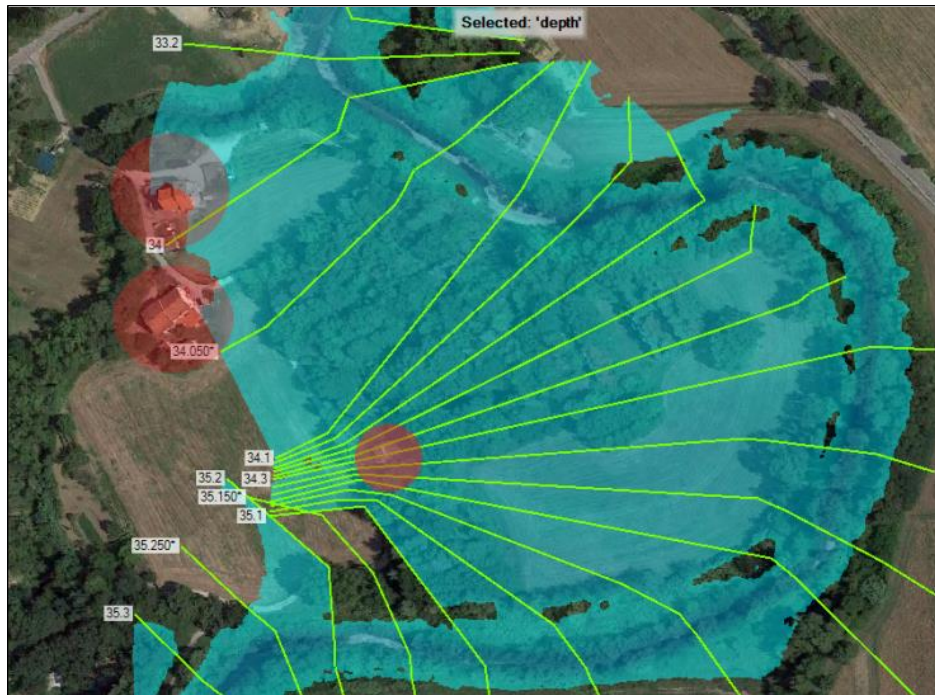
Figure 76: Highlighted in red the buildings at risk

- The ford crossing with culverts of Via Cella is completely submerged by any investigated discharge.
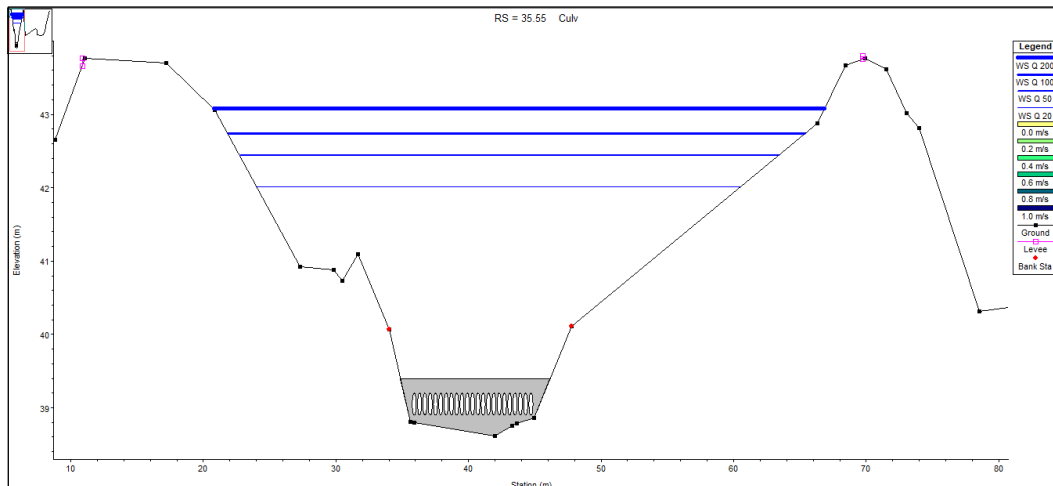
Figure 77: The ford crossing with culverts of Via Cella

- An equestrian center, located on the orographic left side, upstream of the ford crossing with culverts of Via Cella, is located at an altitude lower than the water stage, but it is not flooded by any of the investigated discharges.
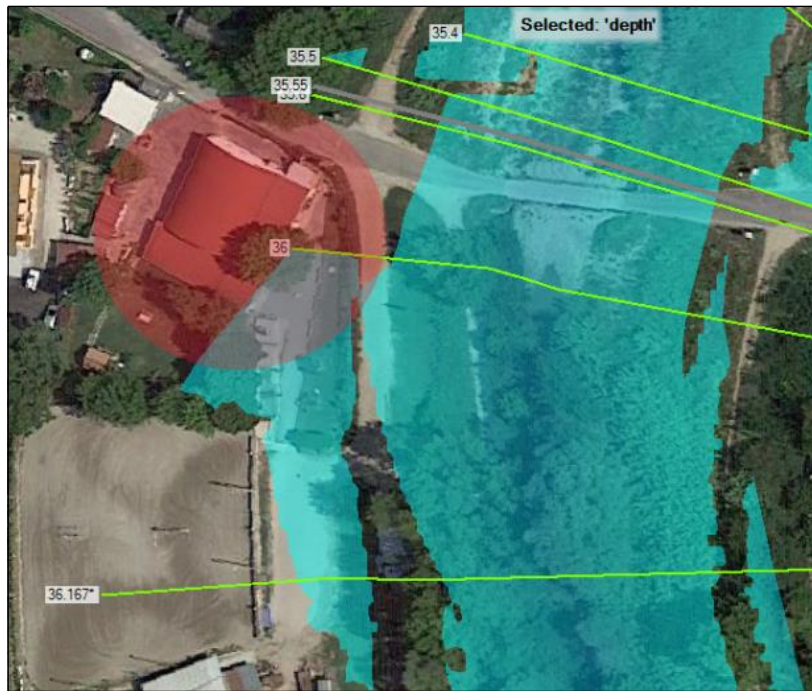
Figure 78: Highlighted in red the equestrian center beyond the levee

- A group of buildings located on the orographic right side, upstream of the ford crossing with culverts of Via Cella, is located at an altitude lower than the water stage, but it is not flooded by any of the investigated discharges.
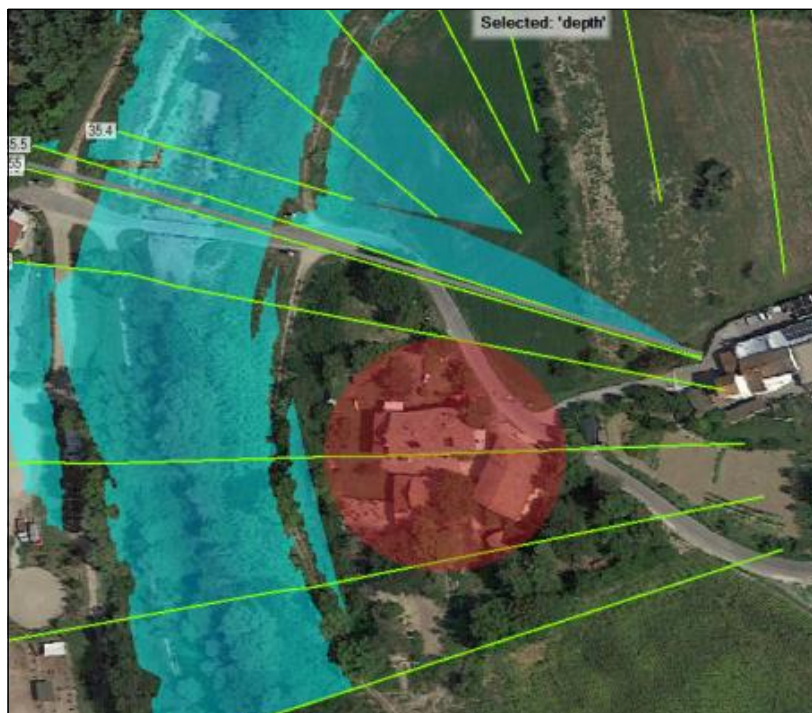
Figure 79: Highlighted in red the buildings beyond the levee
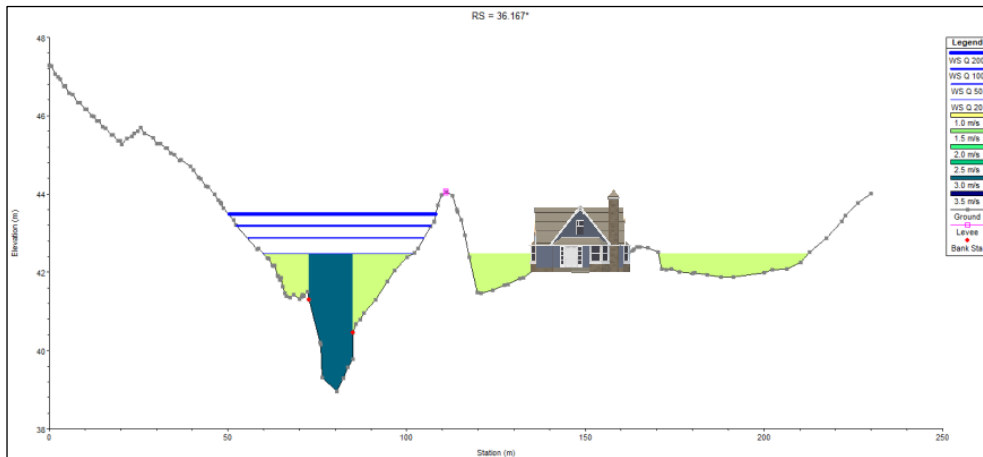
*Figure 80: Cross section 36.167, schematic representation of the buildings
beyond the levee, not to scale*

In conclusion, by analyzing the steady flow simulation results, it can be said that along the first stretch of the stream, from the first downstream bridge (section 1.05 BR) to the bridge of Via Tortona (section 6.35 BR), there are different areas at flood risk in correspondence of which the levees should be heightened. The critical areas are the following: the residential area downstream of the pedestrian bridge, the beverage warehouse, the go-kart track and the residential area just upstream of the bridge of Viale Portofino.

Moving upstream, the floodplains located along the meandering stretch, between the bridge of Via Tortona (section 6.35) and the first upstream cross section (section 36.5), are flooded. Despite this, it is important to emphasize that the flooding of these area contributes to reduce the flood risk at the downstream urbanized area. Therefore, it would be better to allow flood expansion where possible, keeping and heightening only the levees which protect buildings or farming activities.

Concerning the hydraulic infrastructures, the bridges of Via Tortona (section 6.35 BR) and Via San Lorenzo (section 11.65 BR), are the most critical since result to be completely submerged. Thereafter, in order of decreasing criticality there are respectively: the bridge of the railway line (section 3.15 BR), in correspondence of which any of the investigated discharge reaches the intrados; the bridge of Via Marzabotto (section 32.45 BR), intrados reached for discharges equal to Q_{50}; the bridges of the provincial road 31 and 41 (sections 20.45 BR and 32.15 BR), intrados reached for discharges equal to Q_{200}.

The longitudinal profile of the stream, subdivided in stretches, is reported below.
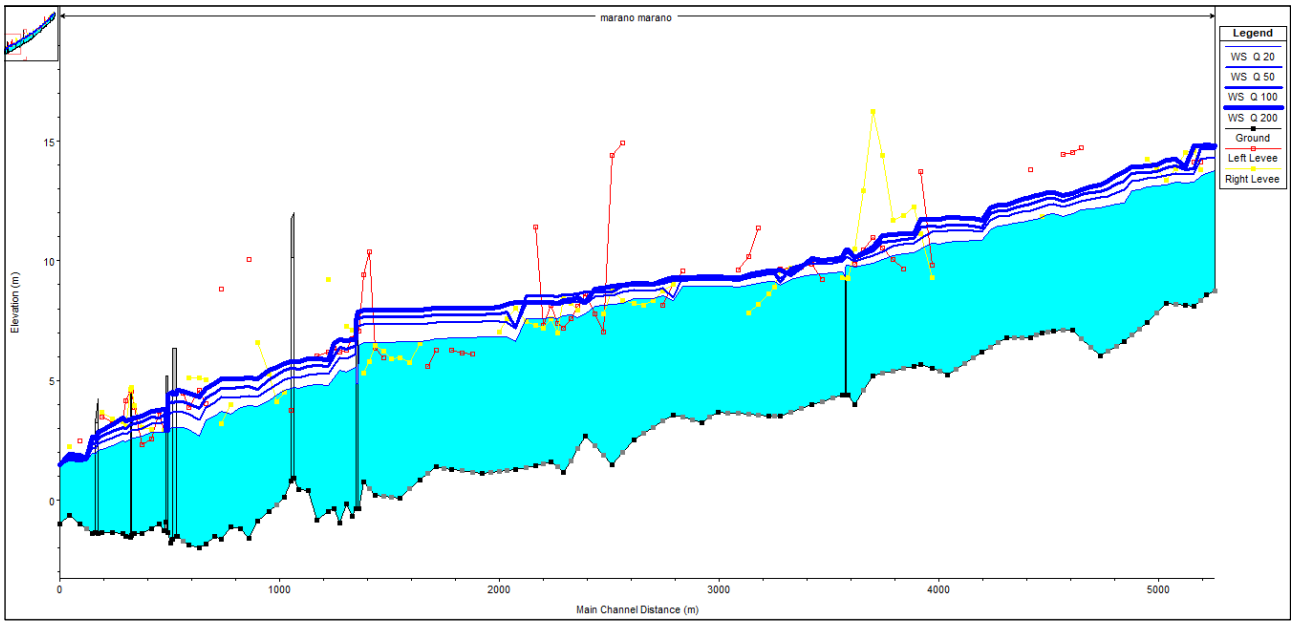
Figure 81: Longitudinal profile of the stream from cross section 0 to 14.15
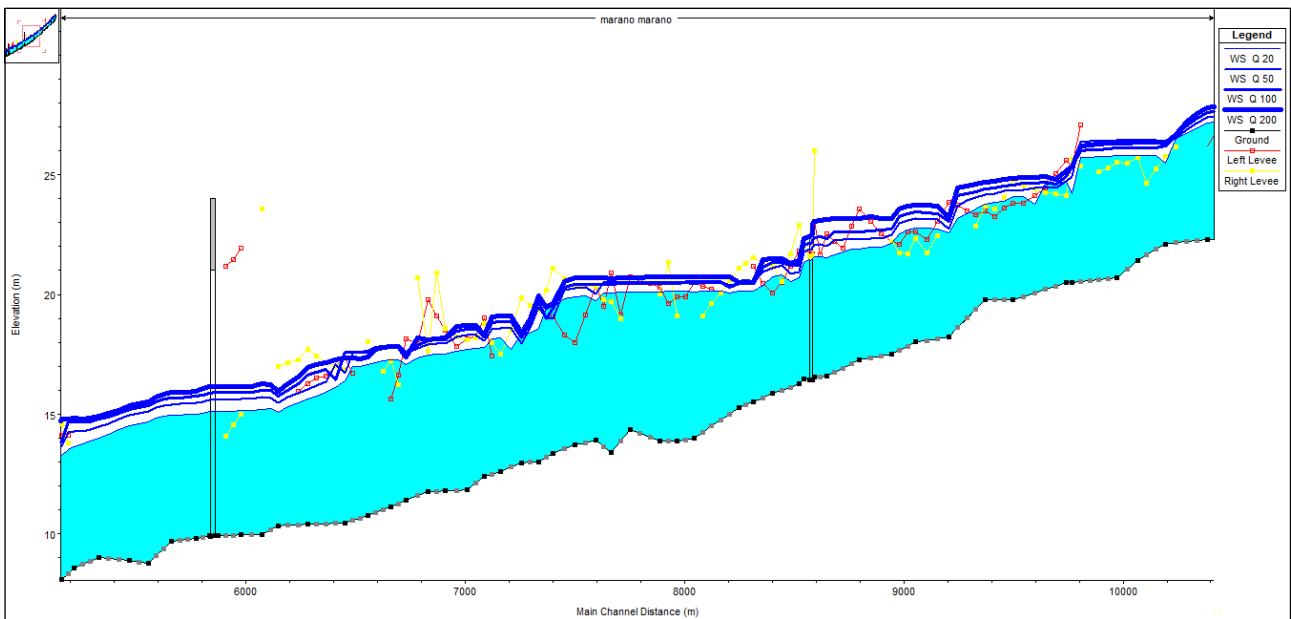
Figure 82: Longitudinal profile of the stream from cross section 14.15 to 23.3
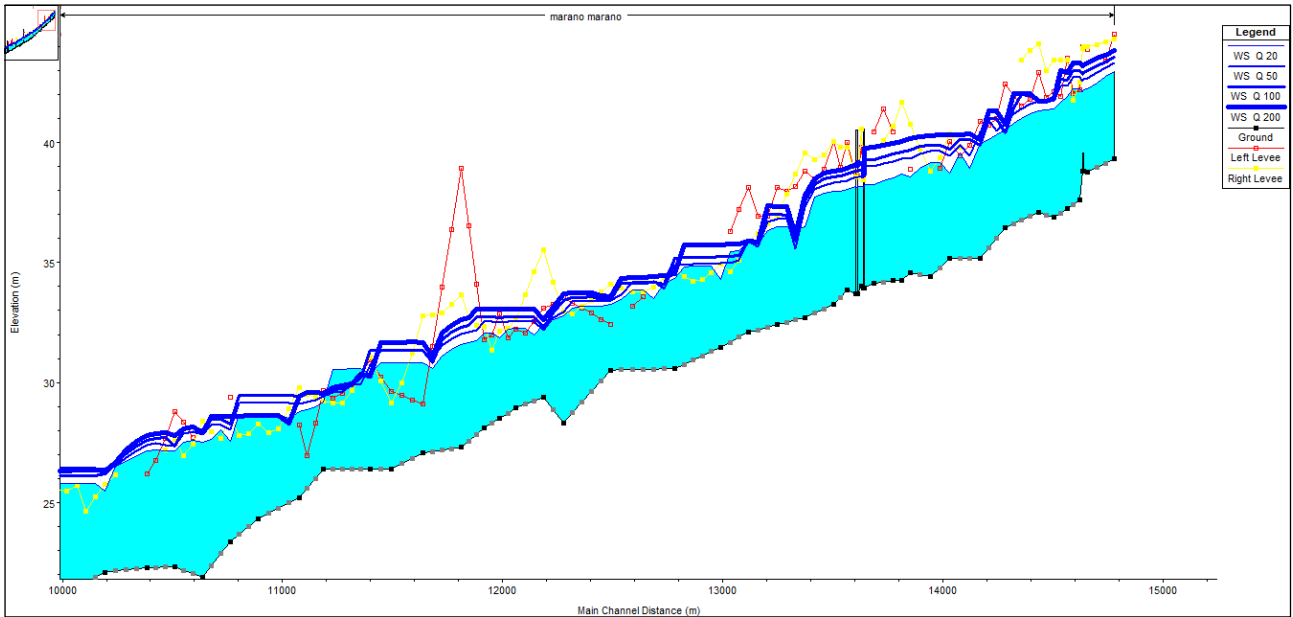
Figure 83: Longitudinal profile of the stream from cross section 23.3 to 36.5

Figures 84-87 are presented the flood inundation maps generated for each examined peak discharge. The maps can be used to update the flood hazard and risk maps of the Marano stream.
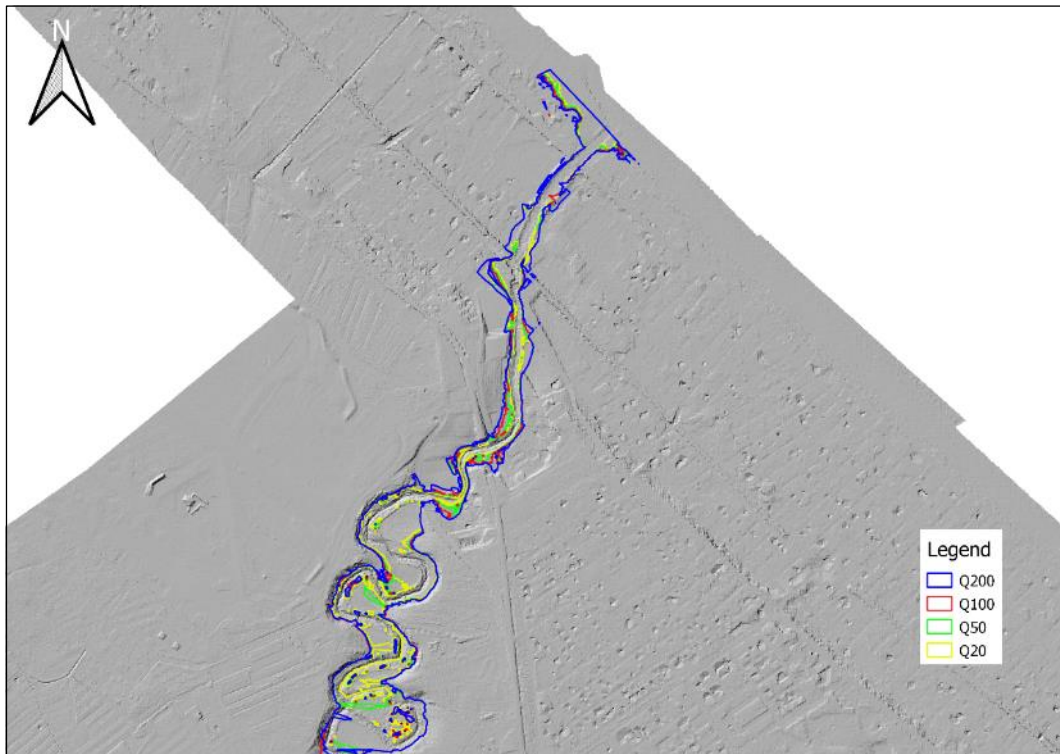
Figure 84: Flood inundation map (first downstream stretch)
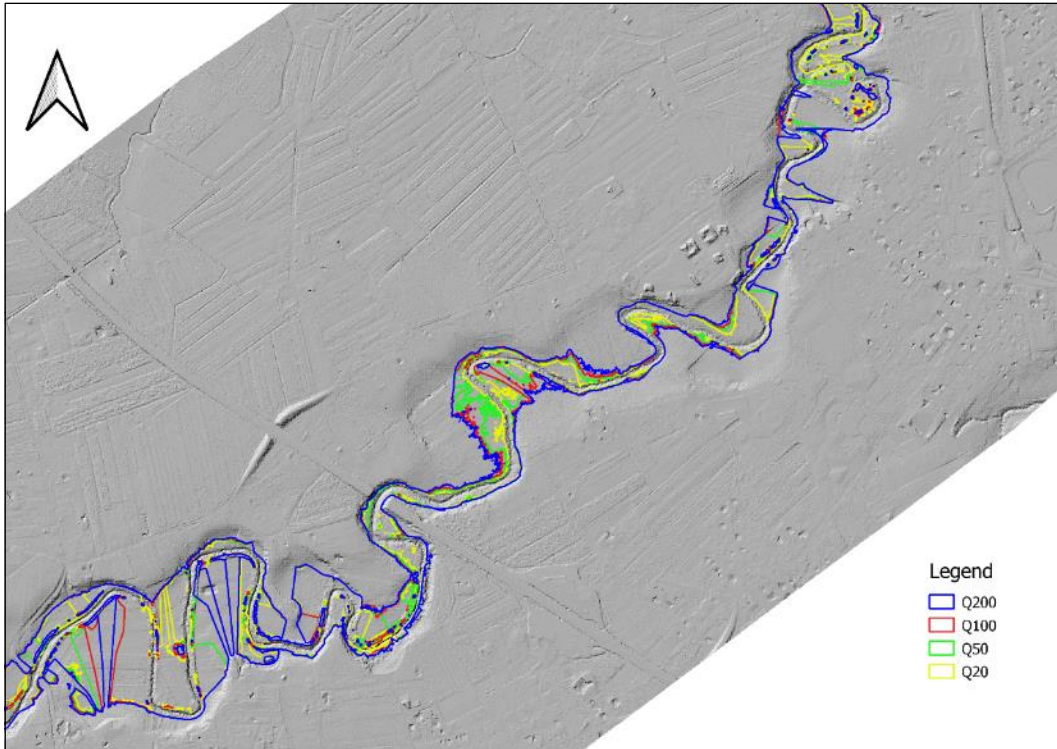
Figure 85: Flood inundation map (second stretch)
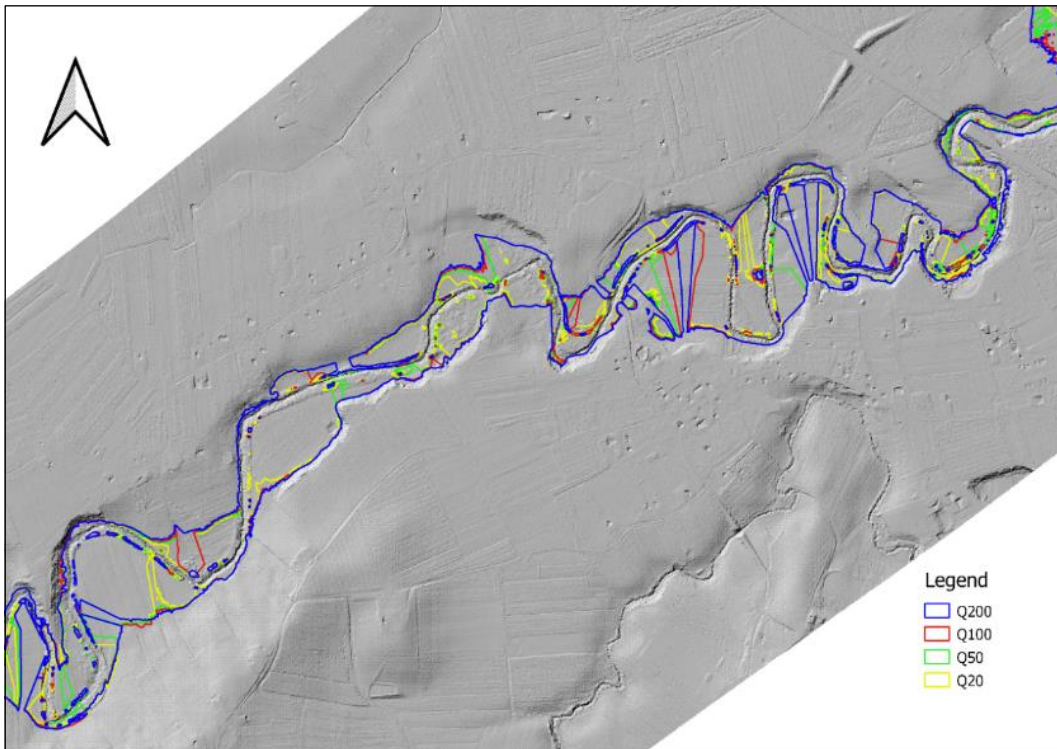
Figure 86: Flood inundation map (third stretch)
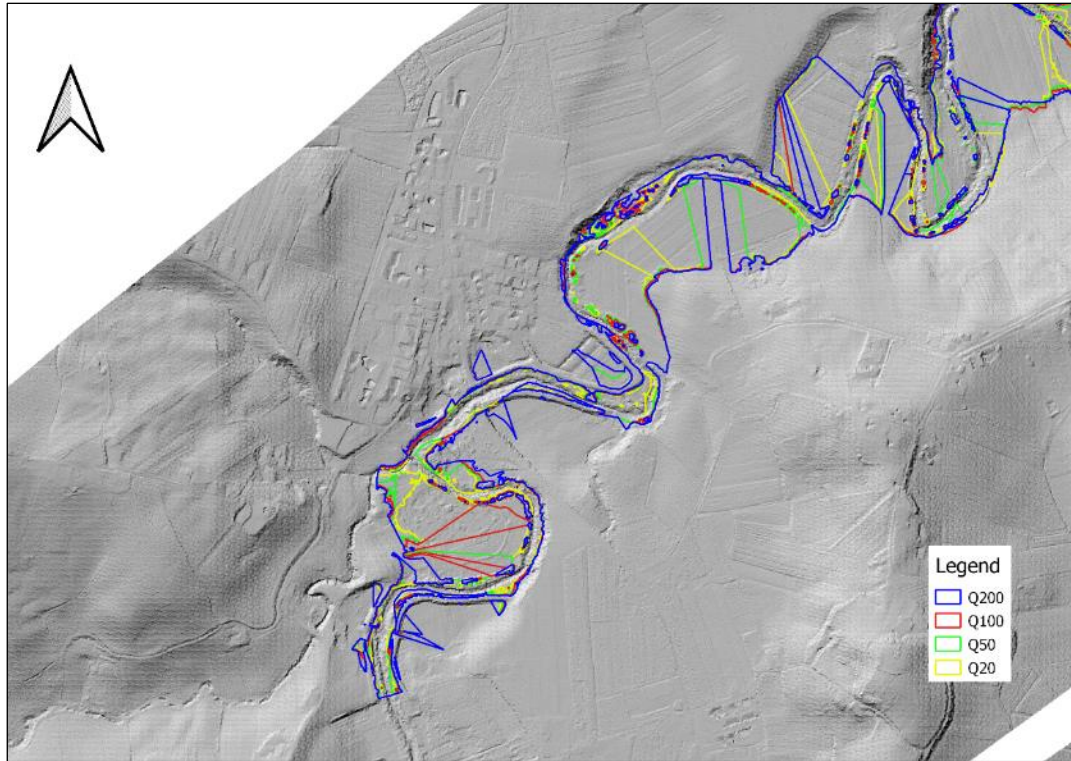
Figure 87: Flood inundation map (fourth stretch)

8. Unsteady flow hydraulic analysis of the Marano stream

The aim of the unsteady flow hydraulic analysis is to quantify the flood peak reduction and to assess the floodplains inundation dynamics with all four hydraulic models. The results of each model will then be presented and compared to evaluate if and how much they differ from each other. Obviously, measurements of real flood discharges will be needed to evaluate which model best fits the reality.

The next chapter describes the procedure to determine the synthetic design hydrographs for the return periods of interest (20, 50, 100, 200), starting from flood discharges data and catchment characteristics.

8.1 Definition of the design hydrographs

The method proposed by Majone et al. (2000a; 2000b), which generates the synthetic design hydrograph starting from the regional estimation of the flood reduction curve and of the peak position for each duration, is described below.

The flood reduction curve is defined by the average flood peaks for each duration assigned:

$$\overline{Q_D} = \max\left(\frac{1}{D}\int_{t-D}^{t} Q(\tau)d\tau\right), \quad t \in [0\,;D]$$

For gauged catchments, the flood reduction curve can be derived by the statistical analysis of the average flood peaks with assigned durations, extracted from historical flood waves (Annual Maximum Series or Peaks Over Threshold). The durations must be included between 0 (instantaneous discharge) and a value D_{max} long enough to represent the flood wave duration of the catchment studied. Once the flood reduction curve is obtained, the synthetic design hydrograph is determined

by imposing the average flood peaks for each assigned duration equal to the ones of the reduction curve. The shape of the hydrograph is defined by a coefficient $r_D \in [0\,;1]$, expressing the position of the flood peak, computed as the ratio between the time interval before the peak and the duration D of the related average flood peak. The value of r_D is computed for each historical hydrograph and the mean value of r_D is then used to determine the synthetic hydrograph.

The synthetic design hydrograph is then defined by the following conditions:

$$\int_{-r_D D}^{0} Q\,(\tau\,;T)\,d\tau = r_D \overline{Q_D}\,(T)D \qquad \int_{0}^{(1-r_D)D} Q\,(\tau\,;T)\,d\tau = (1 - r_D)\overline{Q_D}(T)D$$

The expressions of the two branches of the synthetic design hydrograph are obtained by differentiating the two equations with respect to the duration D:

$$Q(t;T) = \frac{\frac{d}{dD}(r_D \overline{Q_D}\,(T)D)}{\frac{d}{dD}(r_D D)}, \quad t = -r_D D \quad (r_D D_{max} \le t \le 0)$$

$$Q(t;T) = \frac{\frac{d}{dD}((1 - r_D)\overline{Q_D}\,(T)D)}{\frac{d}{dD}((1 - r_D)D)}, \quad t = (1 - r_D)D \quad (0 \le t \le (1 - r_D)D_{max})$$

For ungauged catchment, such as the one of the Marano, both $\overline{Q_D}\,(T)$ and r_D can be determined by means of regionalization techniques.

To estimate the flood reduction curve, it is convenient to link $\overline{Q_D}\,(T)$ and Q_T by means of the reduction ratio:

$$\varepsilon_D = \frac{\overline{Q_D}(T)}{Q_T}$$

and:

$$\overline{Q_D}(T) = \varepsilon_D Q_T$$

consequently, the average flood peaks $\overline{Q_D}(T)$, can be determined once that the function ε_D has been identified. Generally, the reduction ratio is considered not dependent on the return period, whereas it is dependent on the duration D and on the catchment characteristics influencing the flood event. In literature there are many formulations for the determination of ε_D, the main ones are presented below:

- $\varepsilon_D = (1 + bD)^{-c}$

  where:

    $$b = \frac{1}{2t_R};$$

    t_R is the lag time of the catchment evaluated with the moments method;

    $c = 1 - n(T)$, with $n(T)$ exponent of the monomial rainfall depth-duration-frequency curve (*Silvagni, 1984*).

The formulation has been proposed by NERC (1975) as empirical-derived, but can also be derived conceptually (*Fiorentino, 1985*).

A similar expression is proposed by the "Piano Stralcio di Bacino Marecchia-Conca":

$$\varepsilon_D = (1 + D/b)^{-c}$$

where:

$$b = a_1 \left(\frac{L}{\Delta H}\right)^{a_2}, \text{ with } a_1 = 84.0 \text{ and } a_2 = 0.768$$

- $\varepsilon_D = \left(\frac{k}{D}\right)\left(1 - \exp\left(-\frac{k}{D}\right)\right)$

where:

$$k = 1.027 \cdot t_R \cdot \exp(2.277 \cdot n) \qquad\qquad (\textit{Fiorentino e Margiotta, 1997})$$

The expression has been proposed by Fiorentino (1985), obtained under the assumption of rainfall-runoff models with linear reservoir. Its calibration and regionalization are easier, since it has one parameter (k).

- $\varepsilon_D = \sqrt{\Gamma(D)} = \sqrt{\frac{\theta}{2D}\left(2 + \exp\left(-\frac{4D}{\theta}\right) - \frac{3\theta}{4D}\left(1 - \exp\left(-\frac{4D}{\theta}\right)\right)\right)}$

where:

$\Gamma(D)$ is the variance function (i.e. the ratio between the variance of the process aggregated to the scale D and the variance of the instantaneous process);

$\theta = 0.985 \cdot t_R$, expression proposed for the catchments of southern Italy (*Brath et al., 1994*)

This formulation has been proposed by Bacchi e Brath (1990), based on the analysis of the crossing properties of the two standardized processes with reference to a given threshold.

To compute r_D the following expressions are available:

- $r_D = b_1 + \dfrac{b_2}{b_3 + \left(\frac{D}{k}\right)^{b_4}}$ \qquad\qquad (*Tanda, 2001*)

where:

$k = 0.424 \cdot L^{1.05}$, obtained using a monomial formula:

$k = c_0 x_1^{c1} x_2^{c2} \dots x_n^{cn}$, where c_i is the generic coefficient and x_i is the generic morphometric index, in this case the length of the main channel; the coefficients value has been determined by means of the least square method based on local estimation of k, obtained from historical flood series recorded by 14 hydrometers of central-northern Italy, with at least 20 years of observations;

b_i parameters to be determined with least square method.

- $r_D = r_{Dlim} + (0.5 - r_{Dlim}) \cdot \exp\left(-\frac{D}{k}\right)$

  where r_{Dlim} and k are parameters to be determined with least square method.

Once the reduction ratio ε_D and the coefficient r_D have been computed, the synthetic design hydrograph can be determined by solving the differential equations written above. In this case, the software Matlab (script provided in the Appendix) was used to discretize and solve the differential equations, considering a temporal step $\Delta D = 1$ hour and the maximum duration of the event $D_{max} = 72$ hours, chosen according to the characteristic meteorological events of the catchment.

The flood peaks Q_T are the same used for the steady flow hydraulic analysis. The reduction ratio ε_D and the coefficient r_D, were computed with two different methods. Afterwards, the hydrographs resulting from the two methods were compared, in order to choose the one showing the most similar trend to the observed flood waves of the gauged catchments near the Marano.

The figures below show the synthetic hydrographs (T=20, 50, 100, 200 years) generated by the two different methods. In the first case (Figure 88), the reduction ratio ε_D were computed with the expression of Bacchi e Brath (1990), while the coefficient r_D with the second formula listed above. The values of the parameters r_{Dlim} and k were calibrated with the least square method.
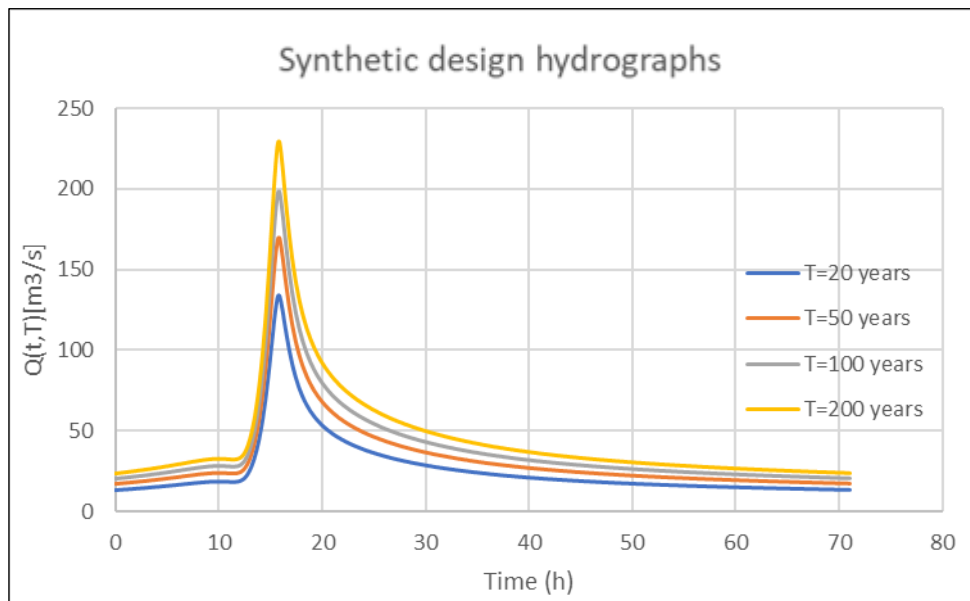
Figure 88: Design hydrographs for T = 20, 50, 100, 200

In the second case (Figure 89), the formula proposed by the "Piano Stralcio di Bacino Marecchia-Conca" was used for the computation of ε_D; and the formula proposed by Tanda (2001), for the computation of r_D. As mentioned above, the parameters of the formula for r_D computation, were calibrated using historical flood series recorded by 14 hydrometers of central-northern Italy.
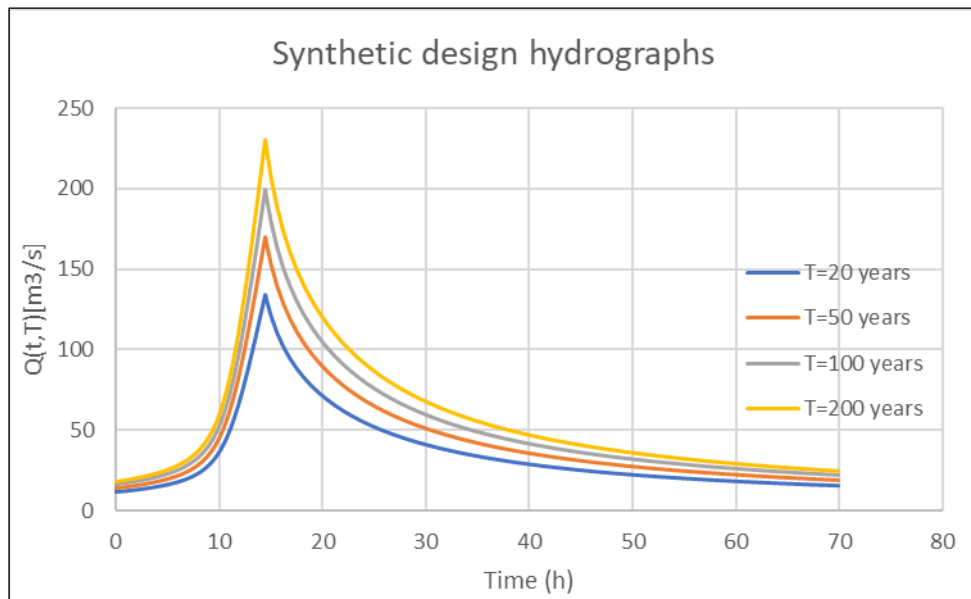
Figure 89: Design hydrographs for T = 20, 50, 100, 200

Figure 90 shows a comparison between the synthetic design hydrographs for T = 200 years, computed with the two methods.
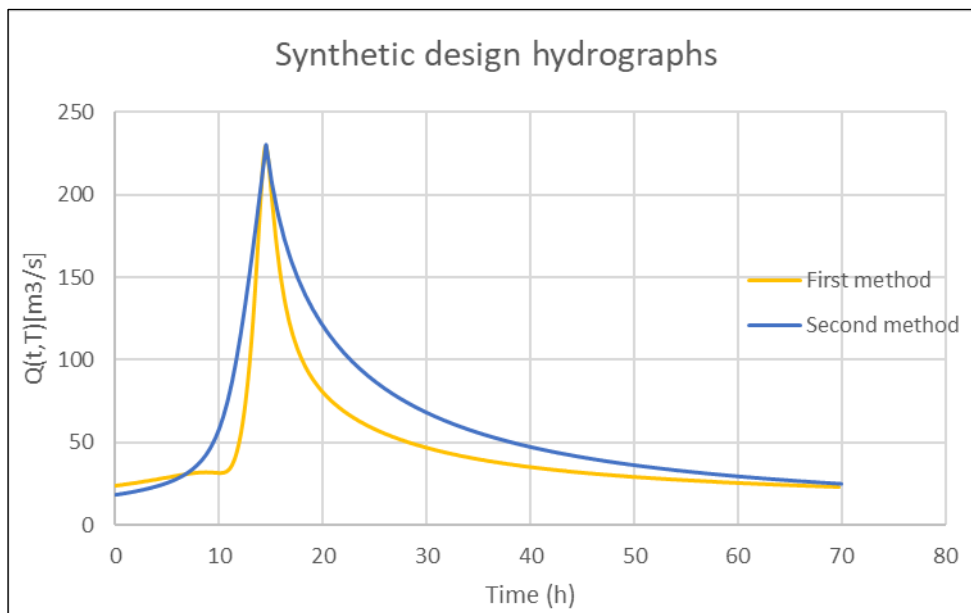
Figure 90: Synthetic design hydrographs comparison for T= 200 years

As it is possible to see in Figure 90, the synthetic design hydrograph determined with the second method is more precautionary since it returns the largest volumes, consequently, the second method was chosen

	Total volume (hm^3) for T=200 years
First Method	11.669
Second Method	15.191

Table 6: Comparison of the total volume stored

Table 7 shows the hydrographs volumes for each return period considered.

	T=20	**T=50**	**T=100**	**T=200**
Section 36.5	9.206 hm^3	11.507 hm^3	13.319 hm^3	15.191 hm^3

Table 7: Hydrographs volumes

8.2 Initial and boundary conditions

The synthetic design flow hydrographs (T=20, 50, 100, 200) and a stage hydrograph (equal for each return period), with a constant stage of 1.49 m, were entered respectively as upstream and downstream boundary conditions. As previously mentioned, 1.49 m results from the simultaneous effects of the flood wave and of the tide with a return period of 10 years. The boundary conditions were set equals in all the modelling schemes. It is reminded that all the simulations were run on a time period of 72 hours.

The first value of the upstream flow hydrograph was entered as flow initial condition, whereas the stage initial condition at each cross section was set by the program, computing a steady flow backwater run. The initial water stages of the *Storage Areas* and of the *2D flow areas* (second and third modelling scheme) were left blank. In this way, if the initial stage in the main channel is higher than the *Lateral Structure* there will be water in the areas, otherwise they will start dry. In the fully 2D model, the *Initial Condition Ramp Up Time* option was used in order to have flow through the *2D flow area* before the start of the simulation. In particular, the program performs a warm up period of five hours, increasing linearly the flow from zero to the first value of the hydrograph. In this way the 2D simulation will start with the same conditions set in the other models.

To ensure the best possible comparison between the results, all the simulations were run with a computational time interval of 4 seconds respecting the Courant-Friedrichs-Lewy condition.

8.3 Unsteady flow simulations results

In the following, the results for three stretches of the stream are shown. The first stretch goes from the upstream boundary cross section 36.5 to cross section 20.3, located in the middle of the meandering stretch; the second from cross section 20.3 to cross section 4.6 located downstream the end of the meandering stretch; the third from cross section 4.6 to the mouth at cross section 0.

Stretch	**1°**	**2°**	**3°**
Sections	36.5-20.3	20.3-4.6	4.6-0

Table 8: Stretches considered

8.3.1 1D hydraulic model

The simulation took 55 seconds, returning a mass balance error of 0.02%. Graphs 1-6 show the flood peaks reductions, for each stretch and for each return period considered.
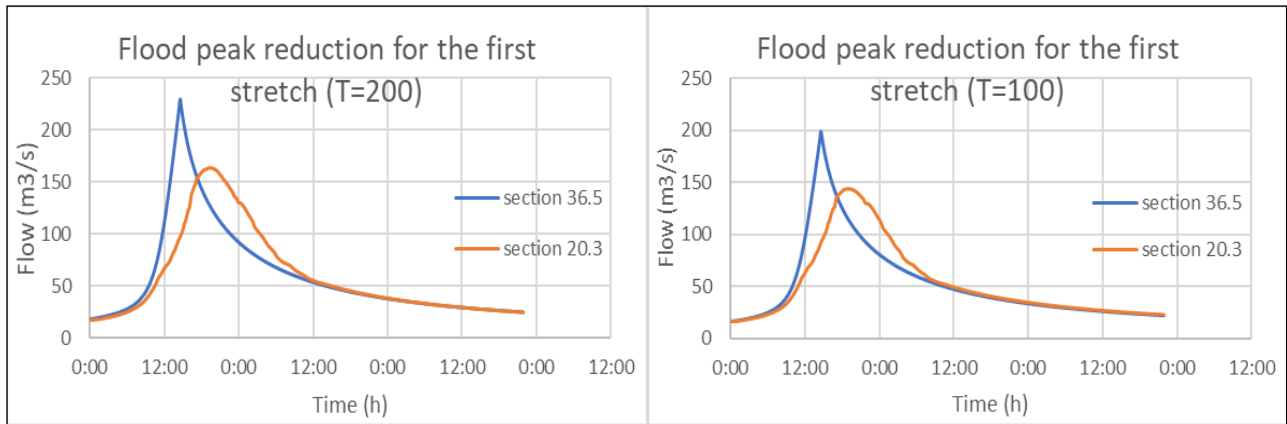
Graph 1: Flood peak reduction for the first stretch (T = 200 and 100 years)
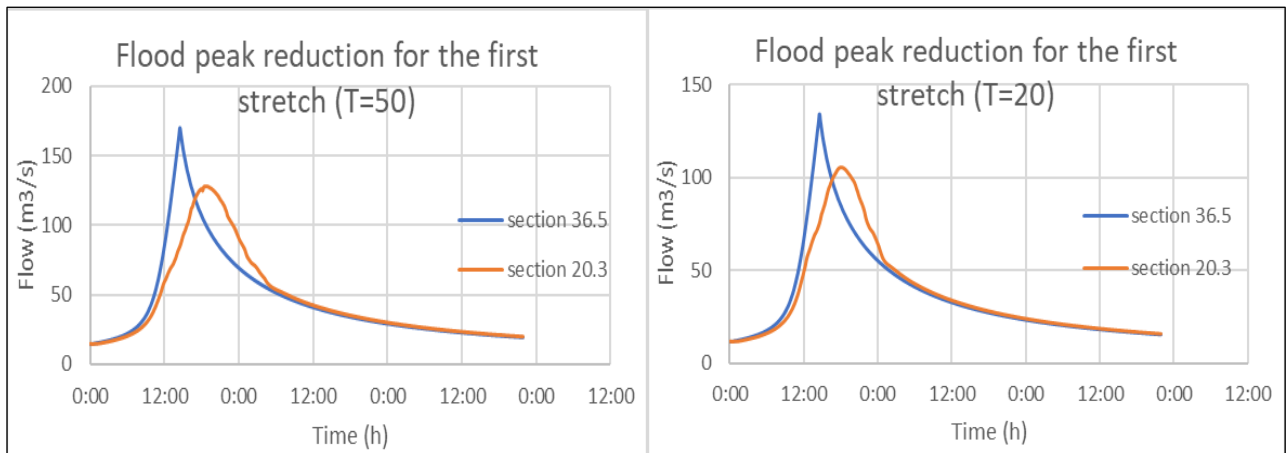
Graph 2: Flood peak reduction for the first stretch (T = 50 and 20 years)
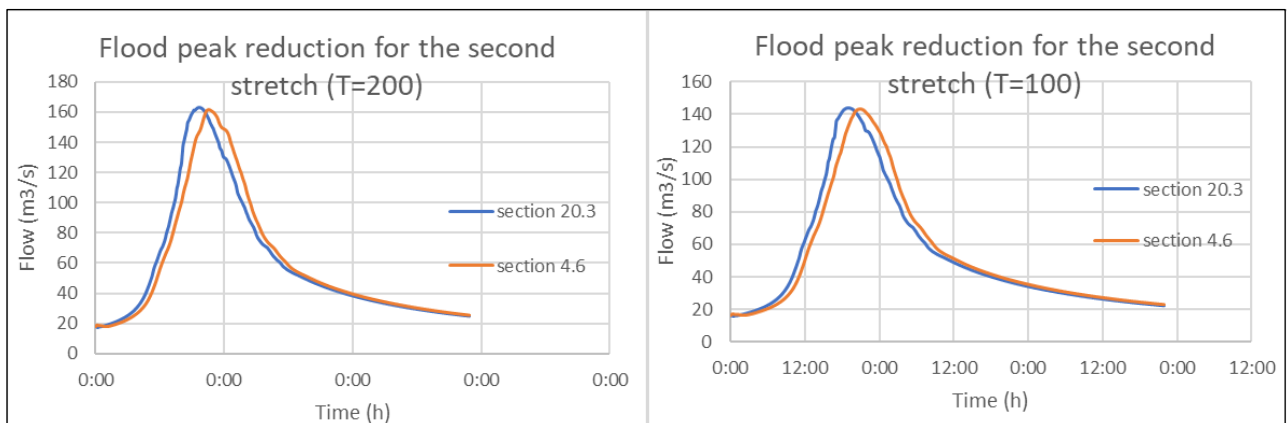
Graph 3: Flood peak reduction for the second stretch (T = 200 and 100 years)
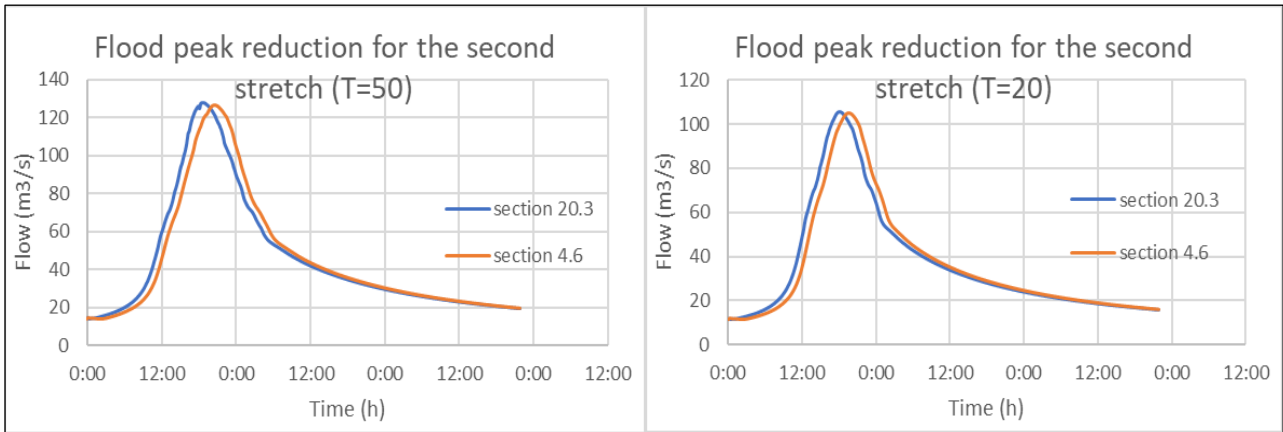
Graph 4: Flood peak reduction for the second stretch (T = 50 and 20 years)
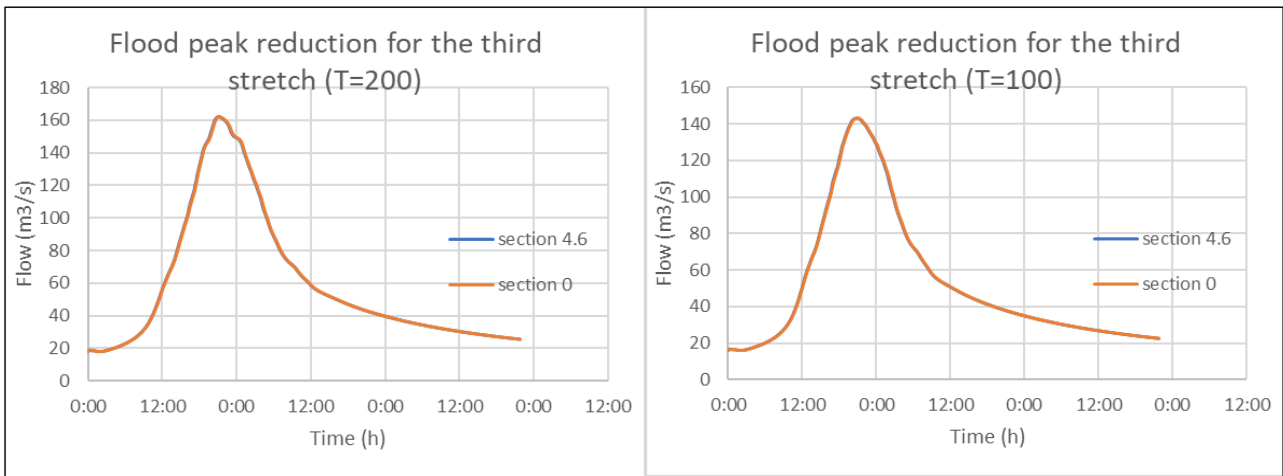
Graph 5: Flood peak reduction for the third stretch (T = 200 and 100 years)
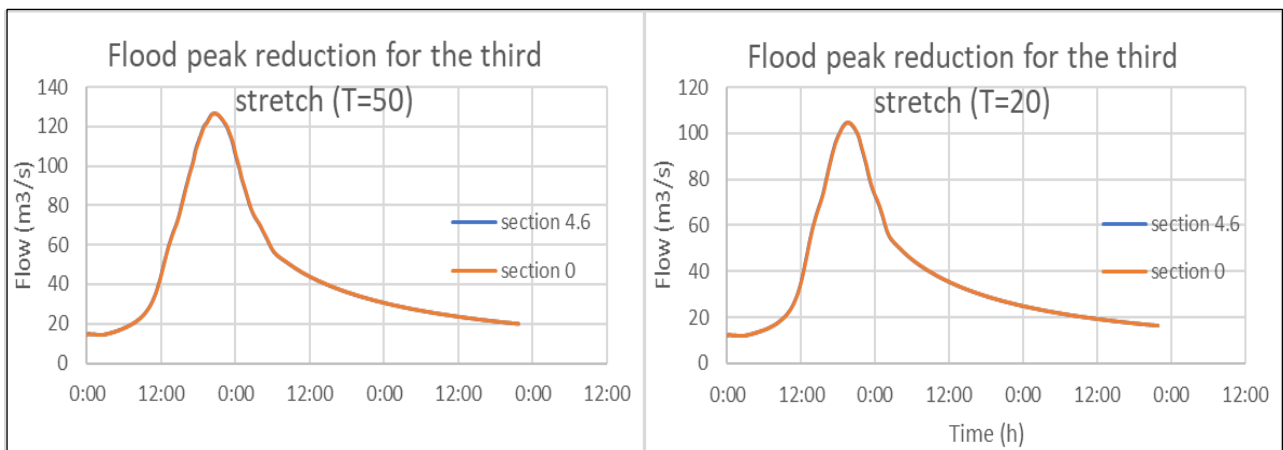
Graph 6: Flood peak reduction for the third stretch (T = 50 and 20 years)

Figures 91-93 show a comparison between the maximum water levels, at three critical bridge, resulting from the steady and unsteady flow simulations. The results are consistent between each other, even if, the water levels computed by the unsteady flow simulation are lower as a result of the natural flood peak reduction.
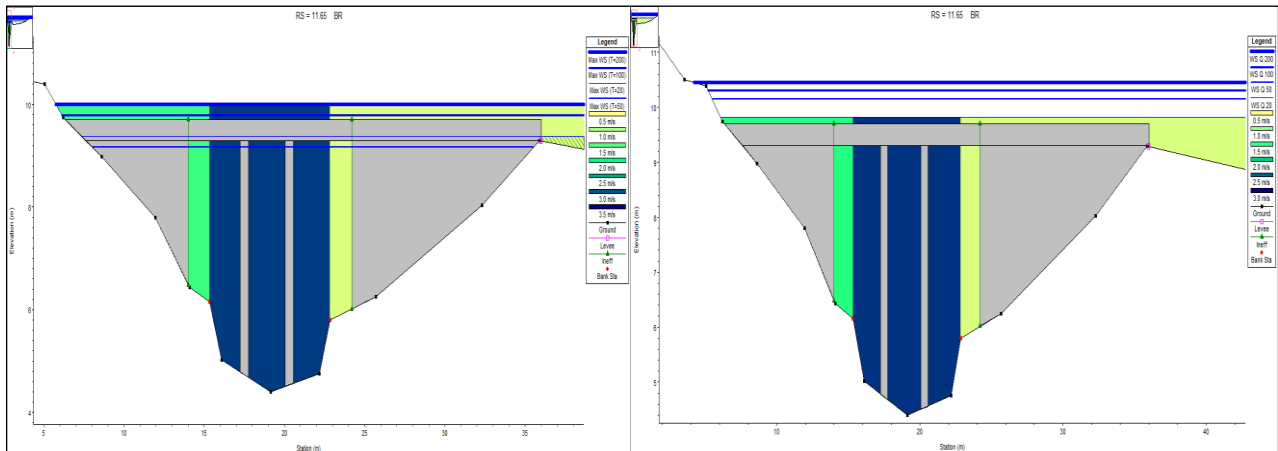
Figure 91: Comparison between the maximum water levels at the bridge of via San Lorenzo resulting from the unsteady flow simulation (left) and steady flow simulation (right)
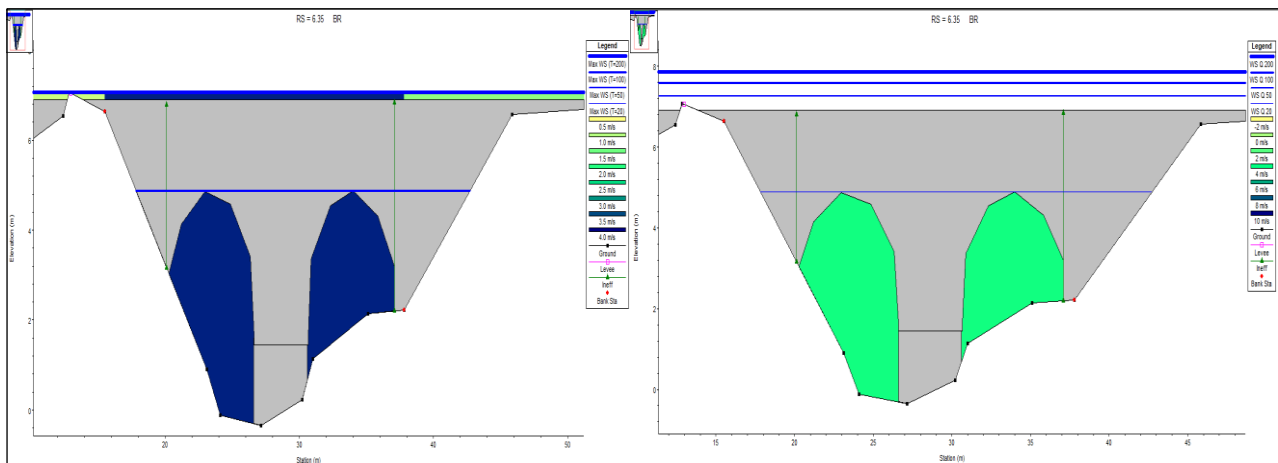
Figure 92: Comparison between the maximum water levels at the bridge of Via Tortona resulting from the unsteady flow simulation (left) and steady flow simulation (right)
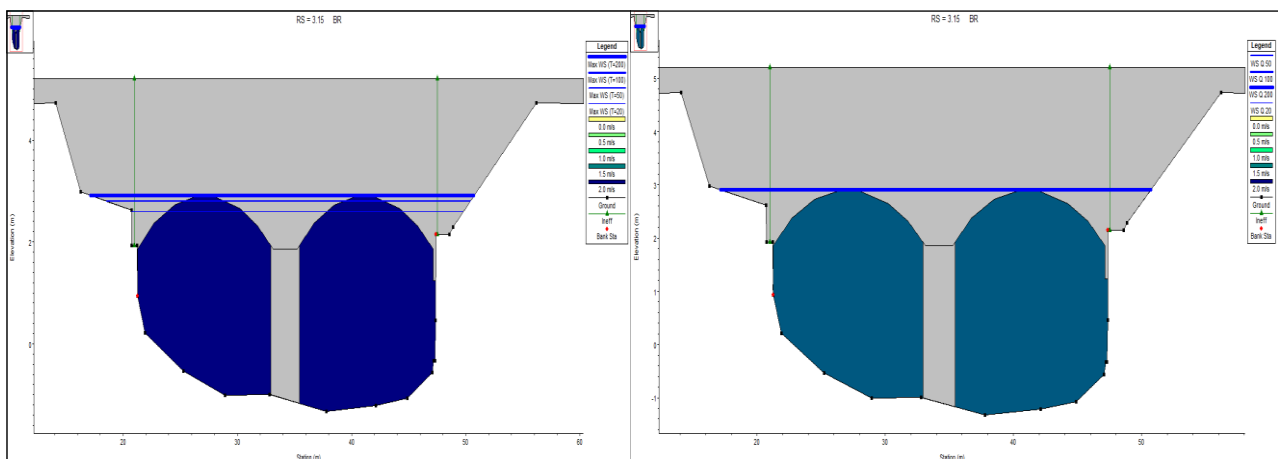
Figure 93: Comparison between the maximum water levels at the bridge of the railway line resulting from the unsteady flow simulation (left) and steady flow simulation (right)

8.3.2 1D hydraulic model with storage areas

The simulation took 1 hour and 3 minutes, returning a mass balance error of 0.47%. Graphs 7-12 show the flood peaks reductions, for each stretch and for each return period considered.
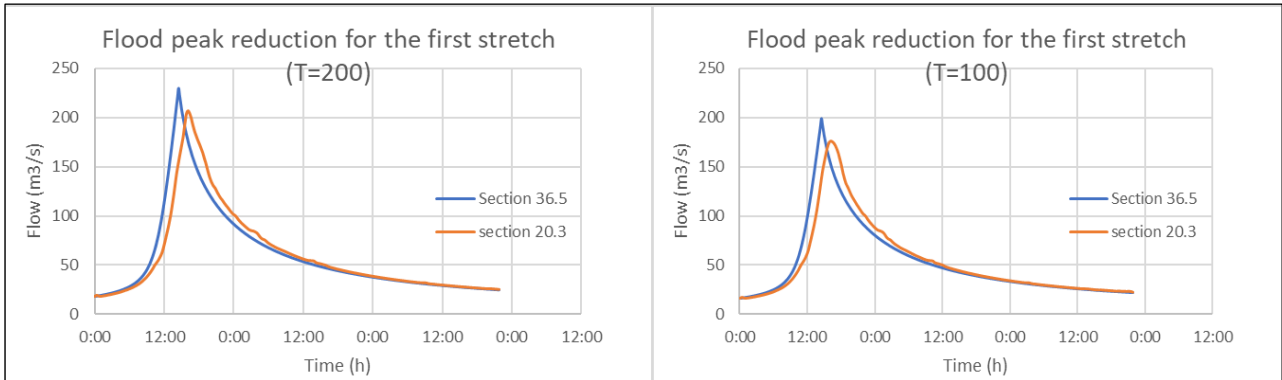
Graph 5: Flood peak reduction for the first stretch (T = 200 and 100 years)
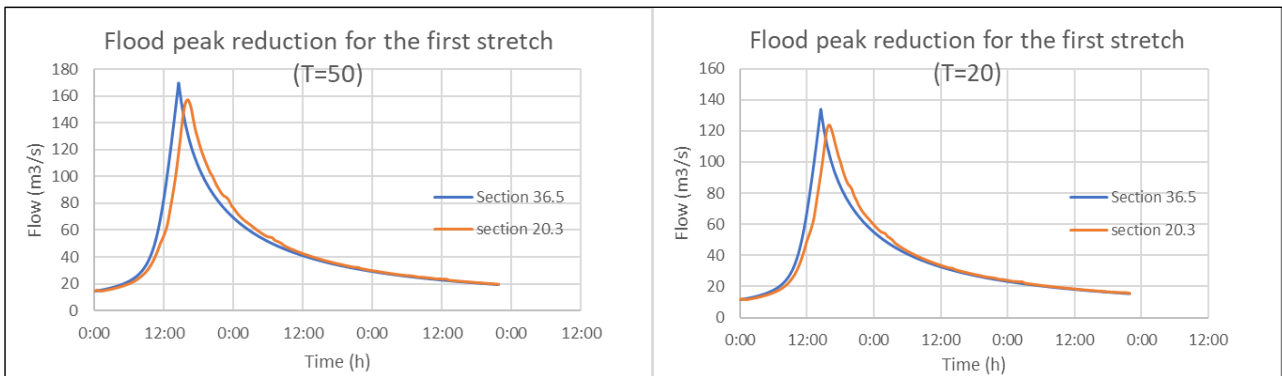
Graph 6: Flood peak reduction for the first stretch (T = 50 and 20 years)
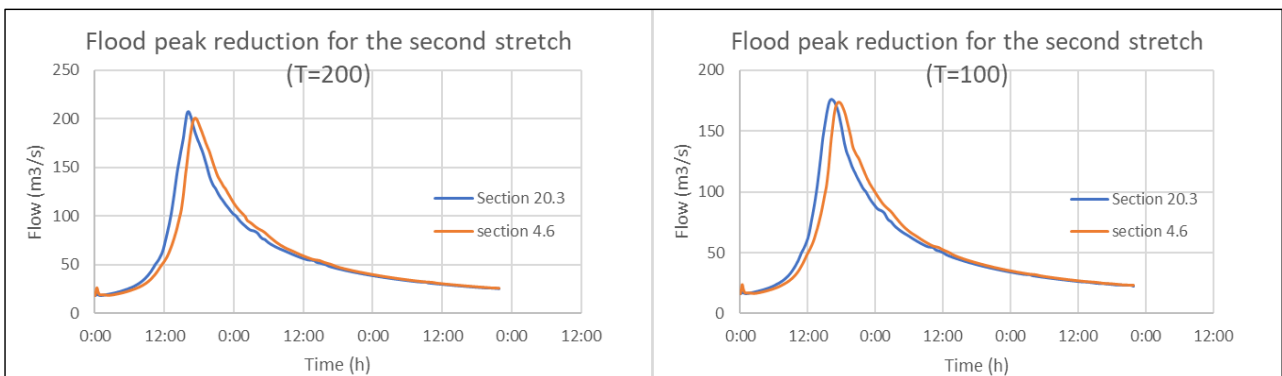
Graph 7: Flood peak reduction for the second stretch (T = 200 and 100 years)
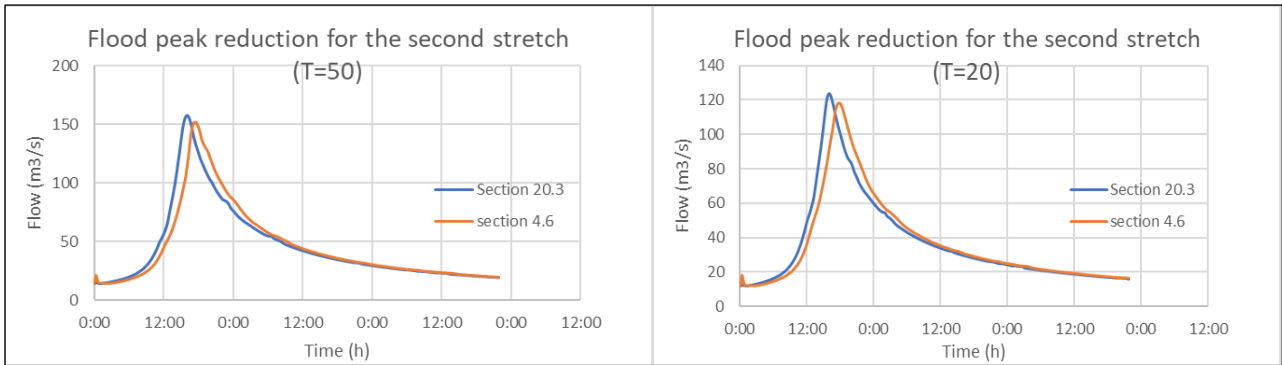
Graph 8: Flood peak reduction for the second stretch (T = 50 and 20 years)
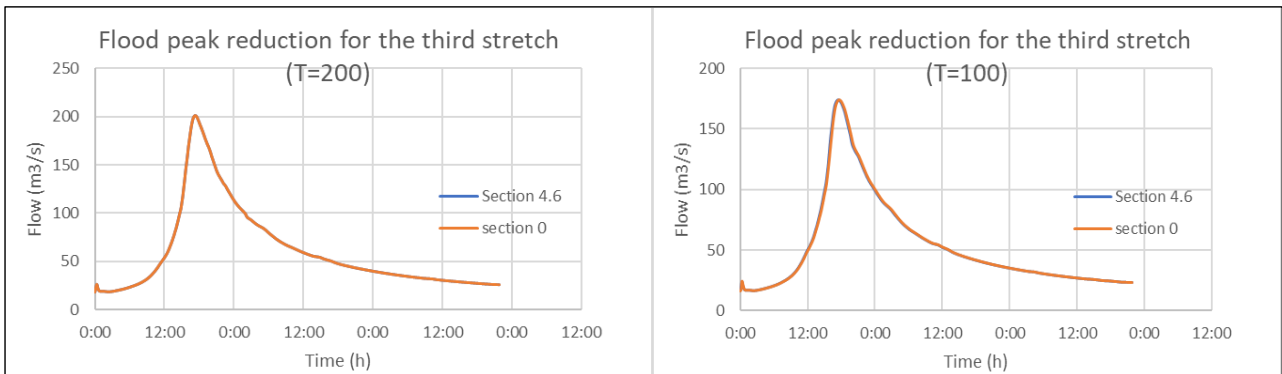
Graph 9: Flood peak reduction for the third stretch (T = 200 and 100 years)
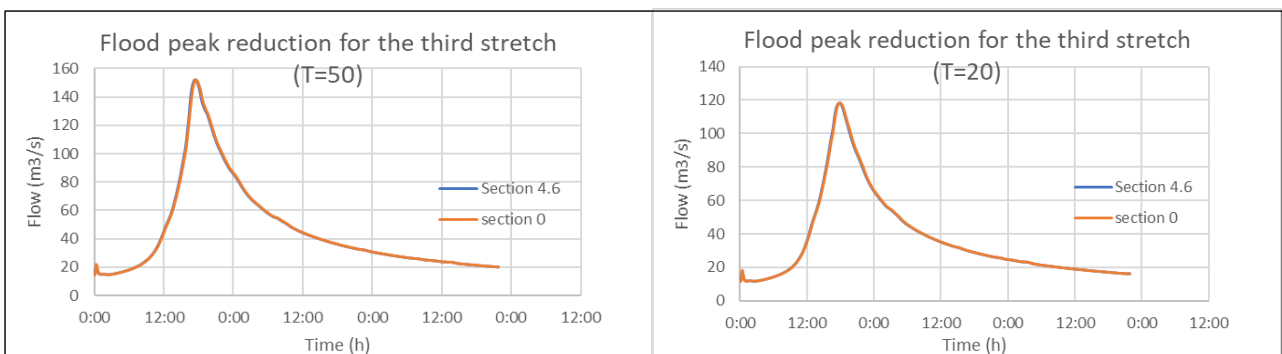
Graph 10: Flood peak reduction for the third stretch (T = 50 and 20 years)

Table 9 shows the *Storage Areas* storing the largest volumes for T=20 years.

ID number	32	31	35	17
Area (1000 m²)	64.89	45.4	41.23	22.32
Volume (1000 m³)	61.96	36.81	34.12	25.92
Volume at the end of the event (1000 m³)	3.46	0.02	0.01	0.01

Table 9: Storage Areas storing the largest volumes

The hydrographs presented in Graph 13 show the interaction between the main channel and the *Storage Area* 21.
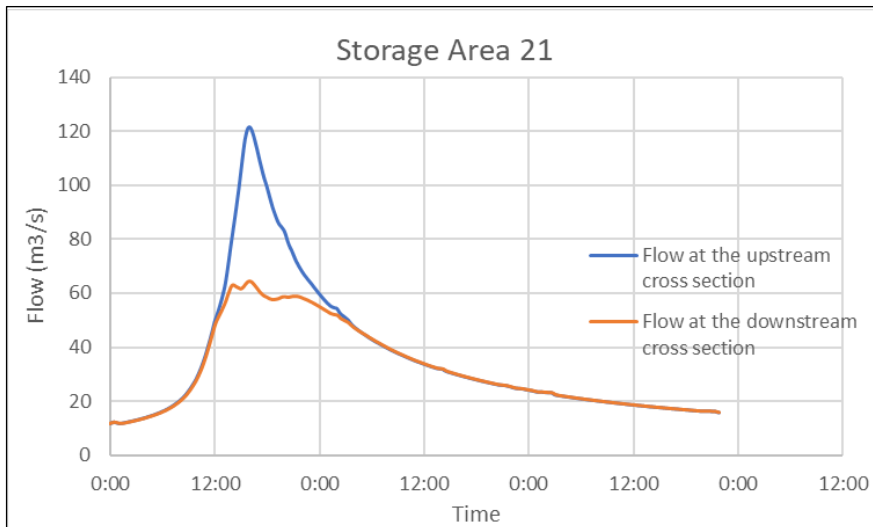
Graph 11: Hydrographs of the Lateral Structure 20.15 associated to Storage Area 21

The excessive flood peak reduction shown in Graph 13, is a result of a by-pass phenomenon made possible by the alignment of the *Lateral Structures* of two consecutive *Storage Areas*.
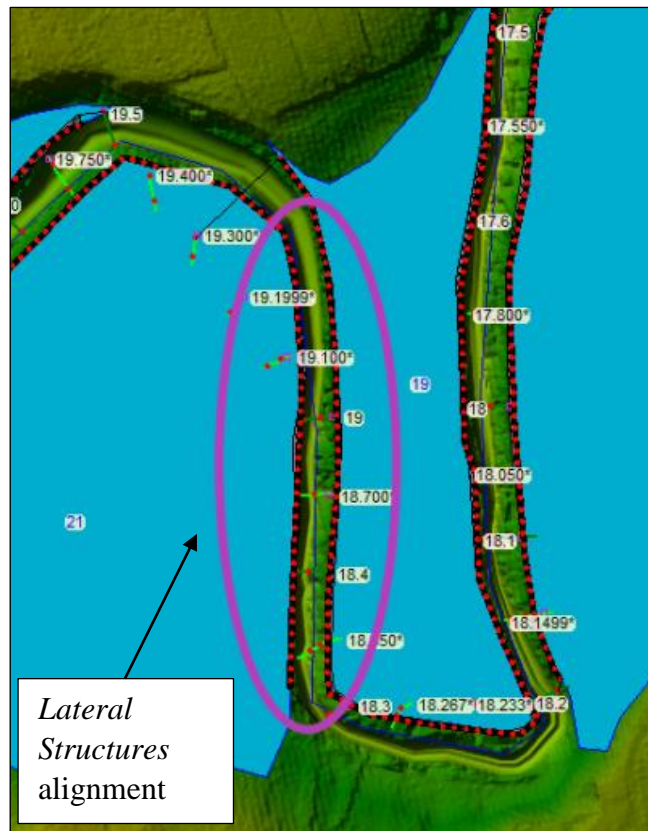
Figure 94: Lateral Structures alignment

This phenomenon is widespread along the entire meandering stretch. Therefore, it is only possible to quantify the flood peak reduction induced by a series of Storage Areas and not by a single one.

8.3.3 Coupled 1D/2D hydraulic model

The simulation took 2 hour and 42 minutes, returning a mass balance error of 34%. Graphs 14-19 show the flood peaks reductions, for each stretch and for each return period considered.
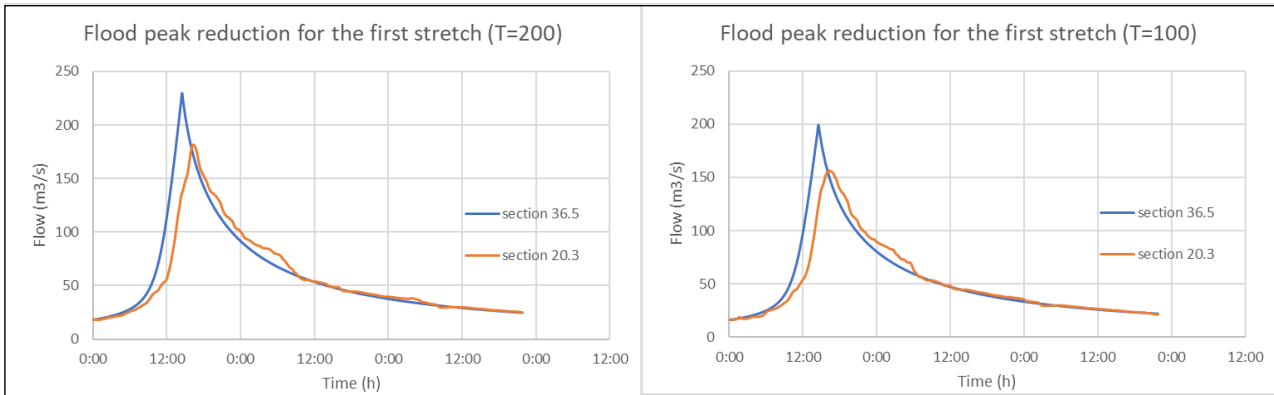
Graph 12: Flood peak reduction for the first stretch (T = 200 and 100 years)
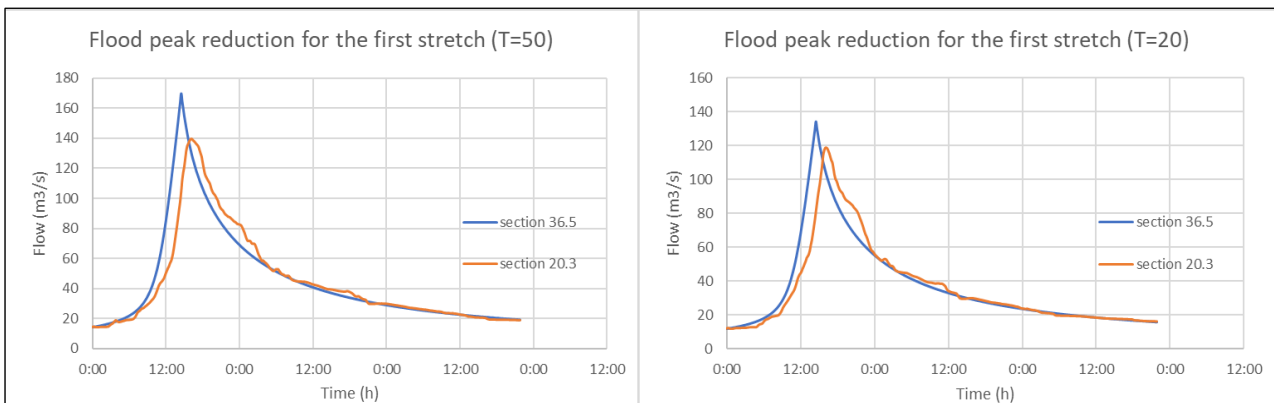
Graph 13: Flood peak reduction for the first stretch (T = 50 and 20 years)
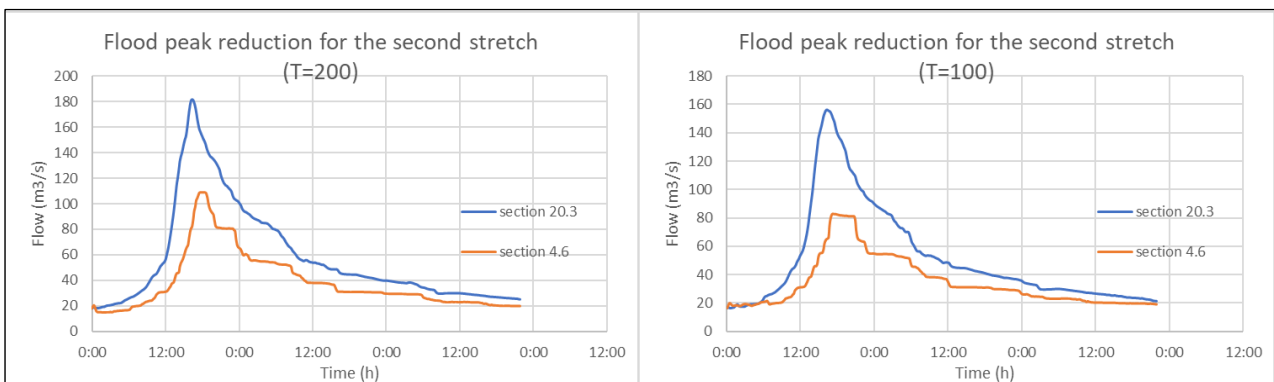
Graph 14: Flood peak reduction for the second stretch (T = 200 and 100 years)
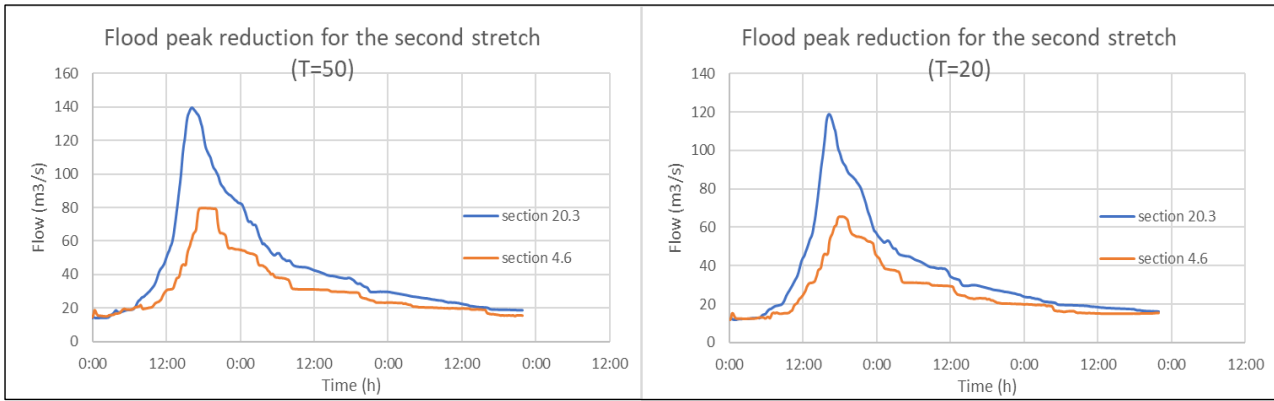
Graph 15: Flood peak reduction for the second stretch (T = 50 and 20 years)
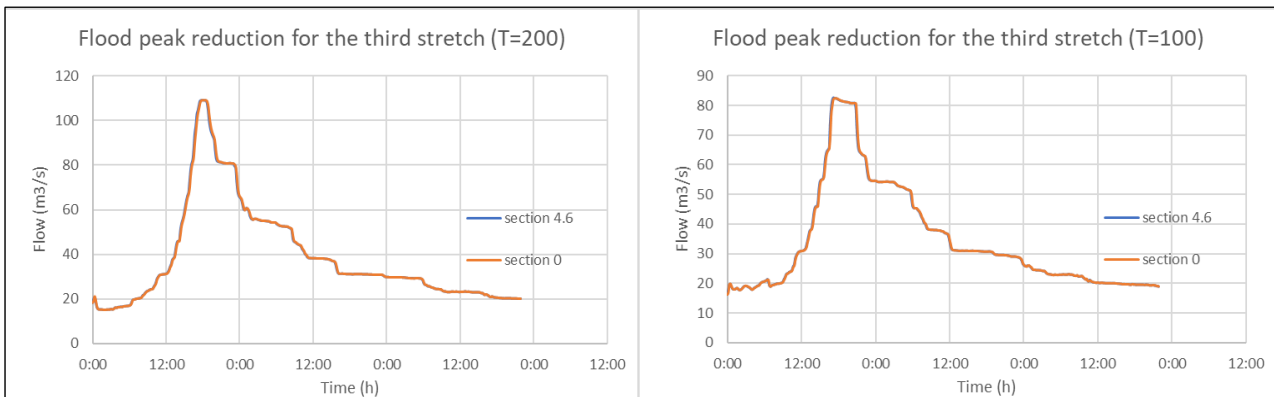
Graph 16: Flood peak reduction for the third stretch (T = 200 and 100 years)
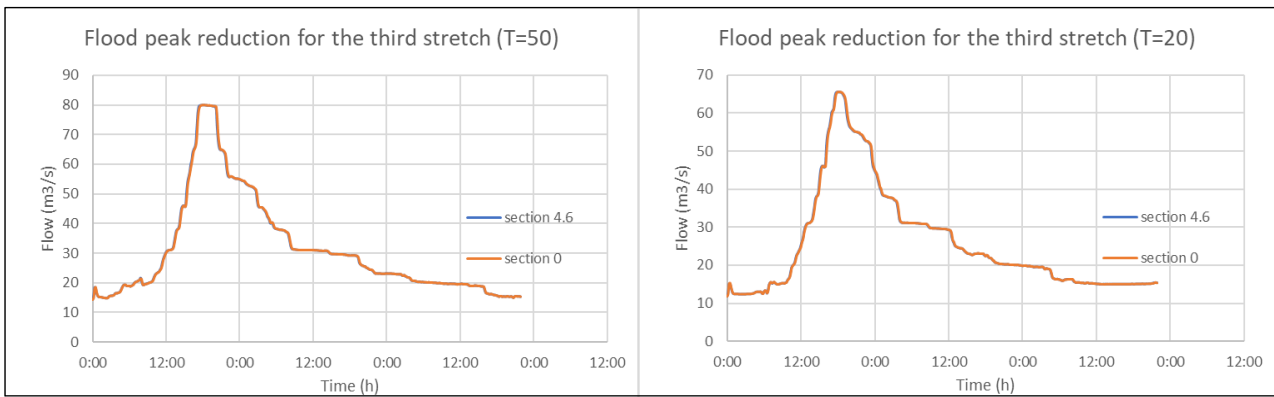
Graph 17: Flood peak reduction for the third stretch (T = 50 and 20 years)

As can be seen in graphs above, the results are affected by numerical instabilities. The simulation returns a mass balance error of 34%, which explains the excessive flood peak reduction. Further considerations will be presented later.

By looking at the flow lines resulting from the coupled 1D/2D simulation, it is possible to see the by-pass phenomenon described above.
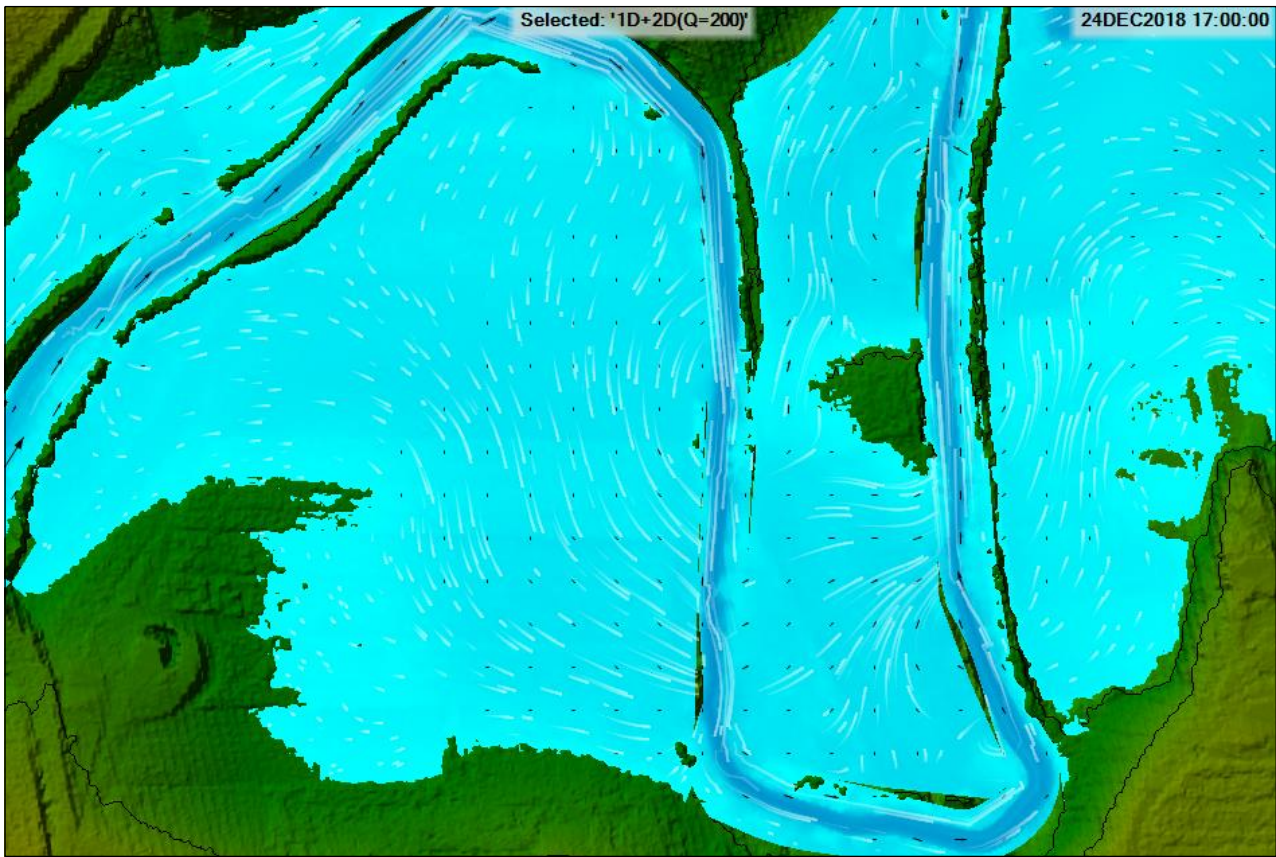
Figure 95: Flood inundation map of the coupled 1D/2D model, in white the flow lines, in black the velocity vectors

8.3.4 Fully 2D hydraulic model

The first 2D simulation was run with the Diffusion-Wave equations taking 4 hours and 34 minutes and returning a mass balance error of 3.65%. Graphs 20-25 show the flood peaks reductions for each stretch and for each return period considered.
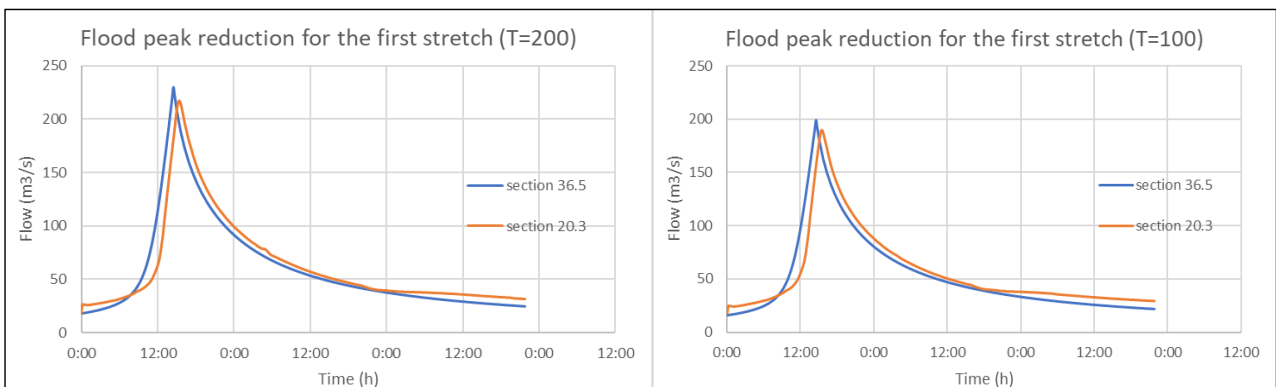
Graph 18: Flood peak reduction for the first stretch (T = 200 and 100 years)
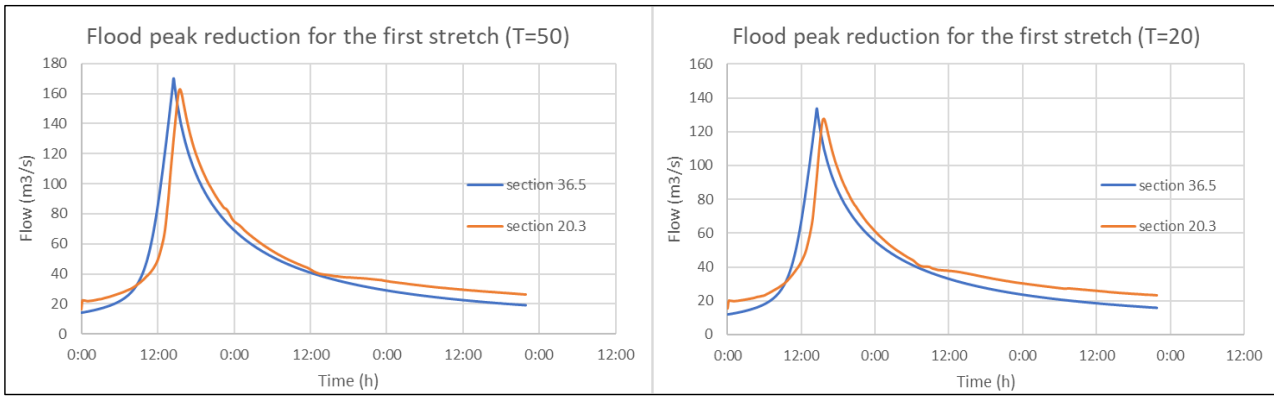
Graph 19: Flood peak reduction for the first stretch (T = 50 and 20 years)
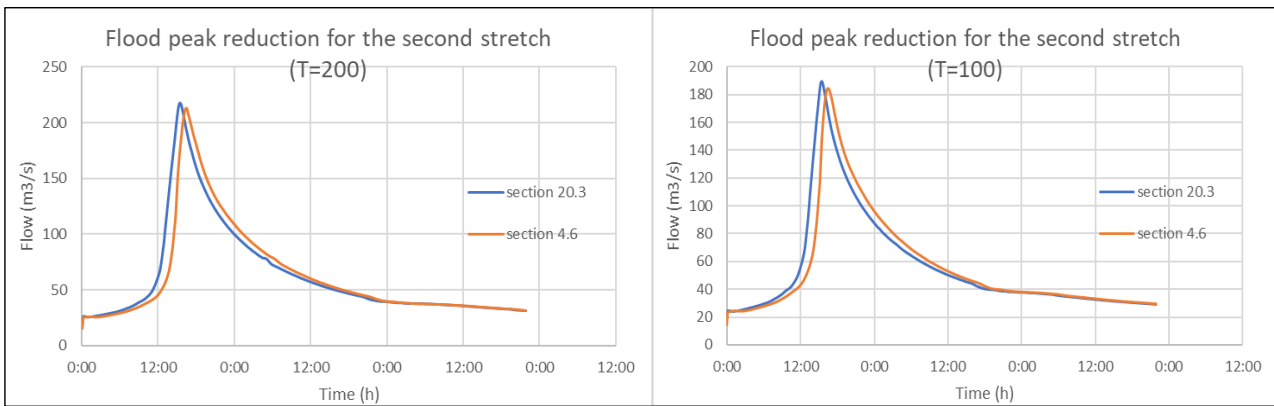
Graph 20: Flood peak reduction for the second stretch (T = 200 and 100 years)
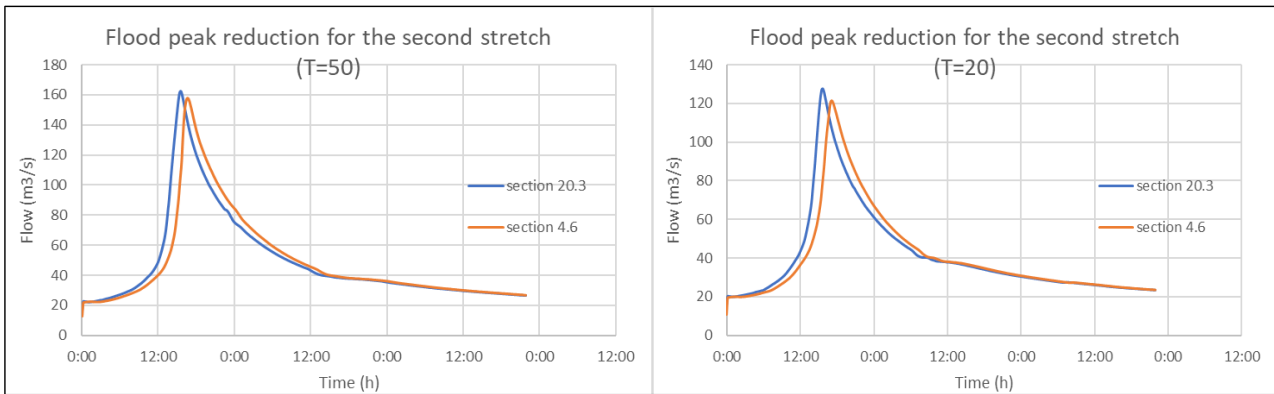
Graph 21: Flood peak reduction for the second stretch (T = 50 and 20 years)
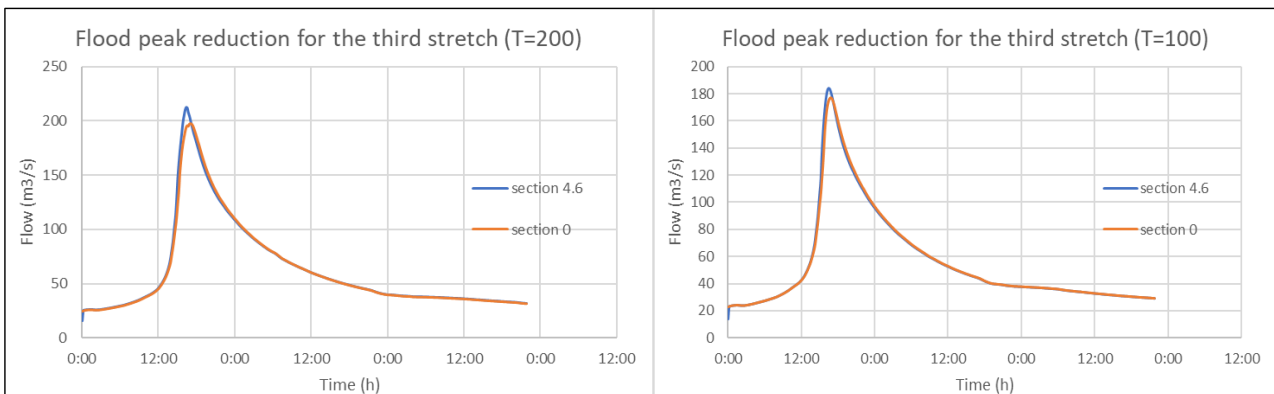
Graph 22: Flood peak reduction for the third stretch (T = 200 and 100 years)
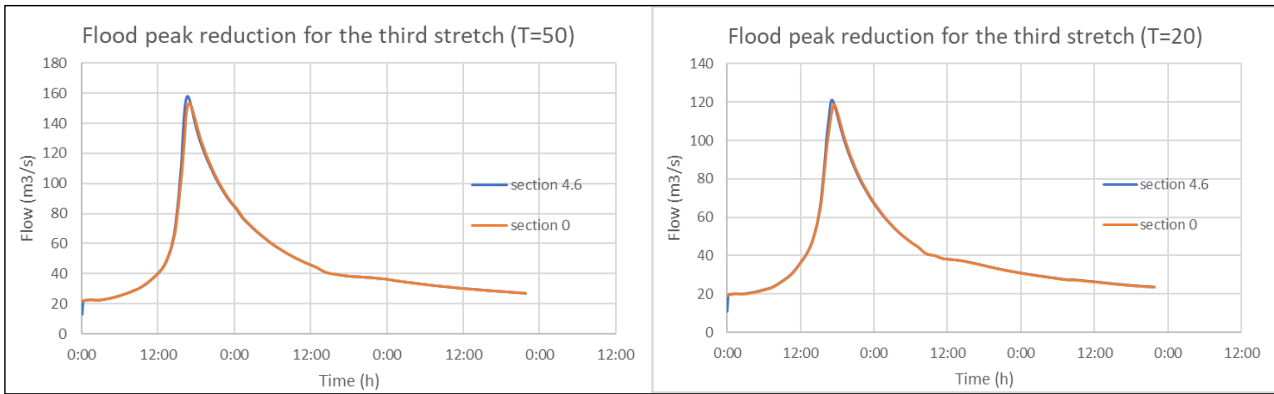
Graph 25: Flood peak reduction for the third stretch (T = 50 and 20 years)

As previously mentioned, to obtain flow results in correspondence of the *Lateral Structures* defined in the previous models, *2D Flow Areas Connections* were entered. These connections are defined by the elevations data of the levees as the *Lateral Structures* and can be modeled using either weir flow equation or 2D equations. In the two previous models (1D+SA and 1D/2D), the weir equation was used. For the 2D model both 2D and weir equations were used, finding no significant differences in term of flood peaks reduction, but much more numerical instability with the weir equation. Therefore, if as in this case, there are no continuous levees defining a clear barrier between river flow and overland flow, it is more advisable to use 2D equations. Graph 26 shows the hydrograph related to the Lateral Structure 26.15 as an example.
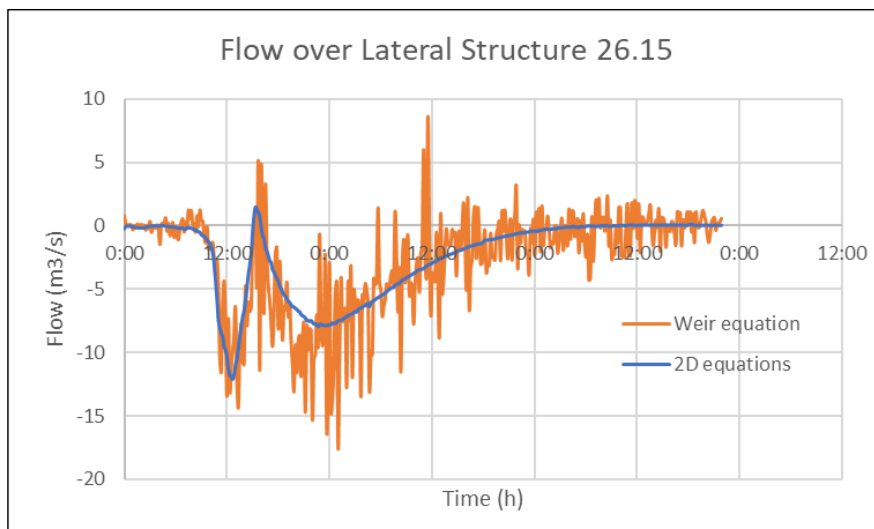
Graph 26: Flow over Lateral Structure 26.15, the negative flow is due to the sign convention (negative flow towards the main channel)

The 2D simulation was also run with the full momentum equations, taking 7 hours and 15 minutes and returning a mass balance error of 2.35%. The graphs below show a comparison between flow and stage hydrographs for T=200, obtained from the two 2D simulations.
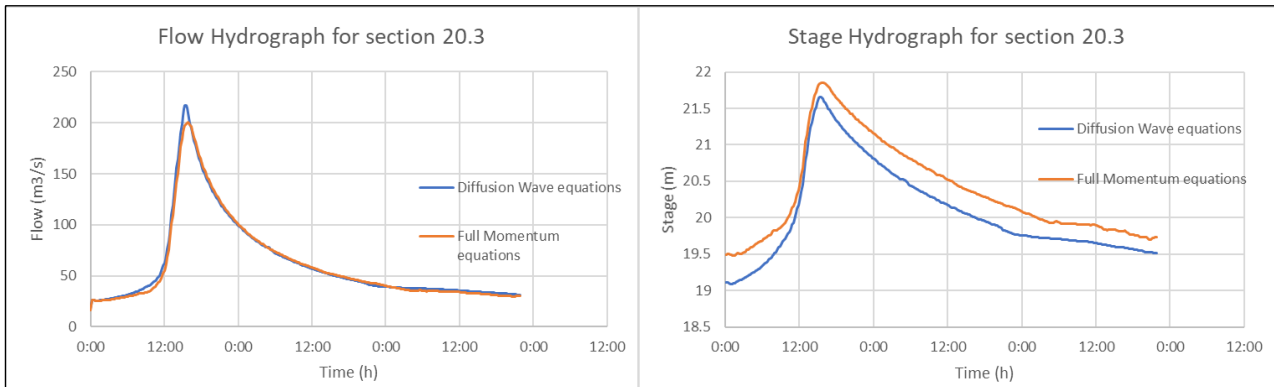
Graph 27: Flow and stage hydrographs for section 20.3, obtained from the two 2D simulations
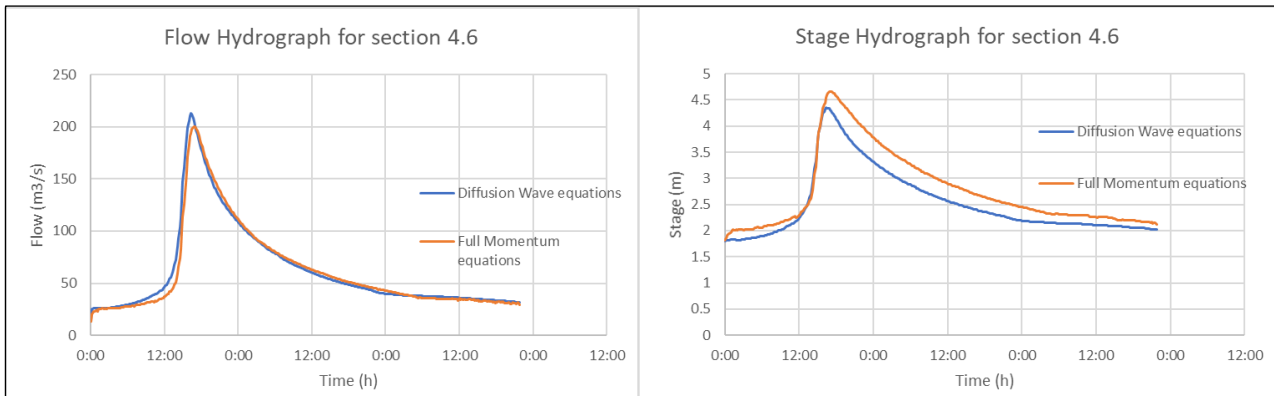
Graph 28: Flow and stage hydrographs for section 4.6, obtained from the two 2D simulations28

As it is noted in the graphs above, for both cross sections, the flow hydrographs are similar except for the flood peaks, which result higher in the 2D simulation run with the Diffusion-Wave equations. On the other hand, the water stages computed with the Full Momentum equations are generally higher, especially at the beginning of the event and during the recession period. Therefore, it follows that the 2D simulation run with the Diffusion-Wave equations, returns generally higher water velocities. This can be due to the different characteristics of the two sets of equations. Indeed, the Diffusion-Wave equations do not consider the Coriolis effect, the Eddy viscosity and the Acceleration terms.

Figures 96-97 show the velocity distribution maps for both simulations.
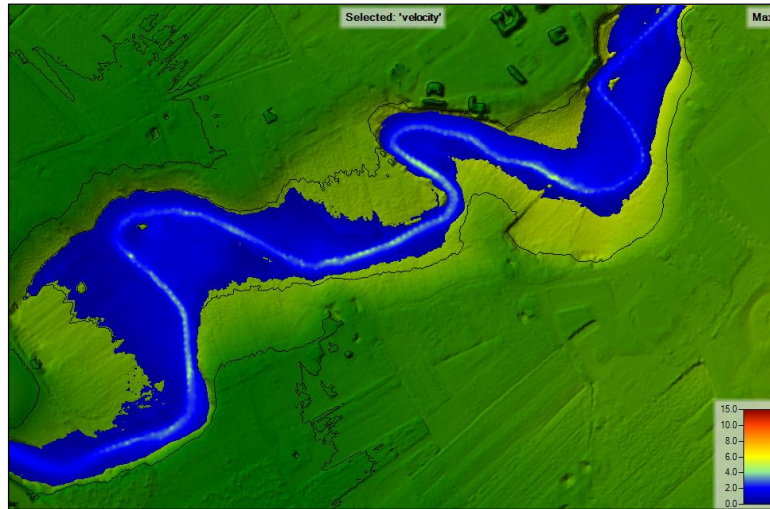
Figure 96: Velocities distribution for the 2D simulation run with the Diffusion-Wave equations

Figure 97: Velocities distribution for the 2D simulation run with the Full Momentum equations

Given the longer computational times and the uncertainties related to the overestimation of energy losses in the main channel *(Betsholtz & Nordlöf, 2017)*, it was concluded that the diffusive model represents an acceptable first step in 2D hydraulic modeling of the Marano stream.

8.3.3 Comparison between the unsteady flow simulations results

In the following, a comparison between the results of all the simulations run is presented.

The graphs below show the resulting percentage reductions in flood peaks for each stretch analyzed and for each return period and model considered.
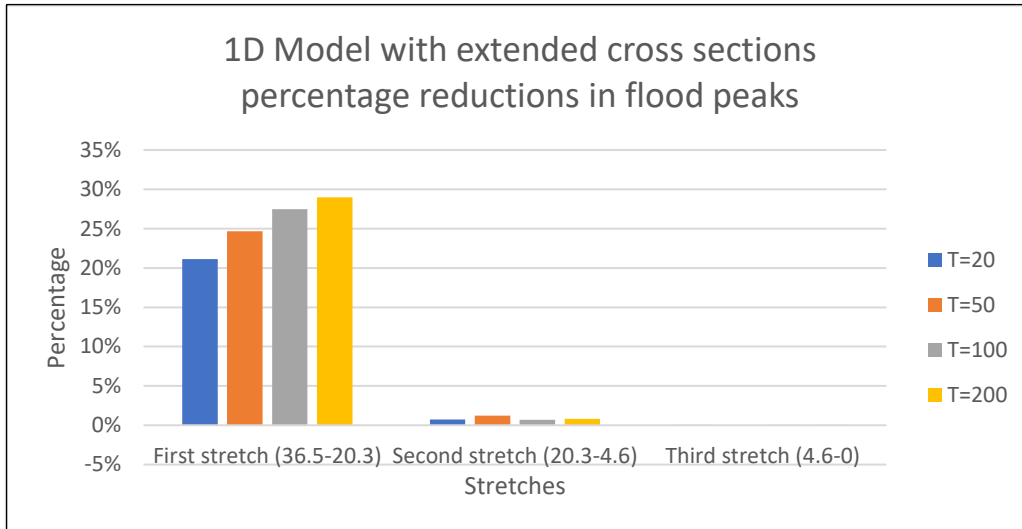
Graph 29: Flood peak dampening (in %) for the 1D Model with extended cross sections
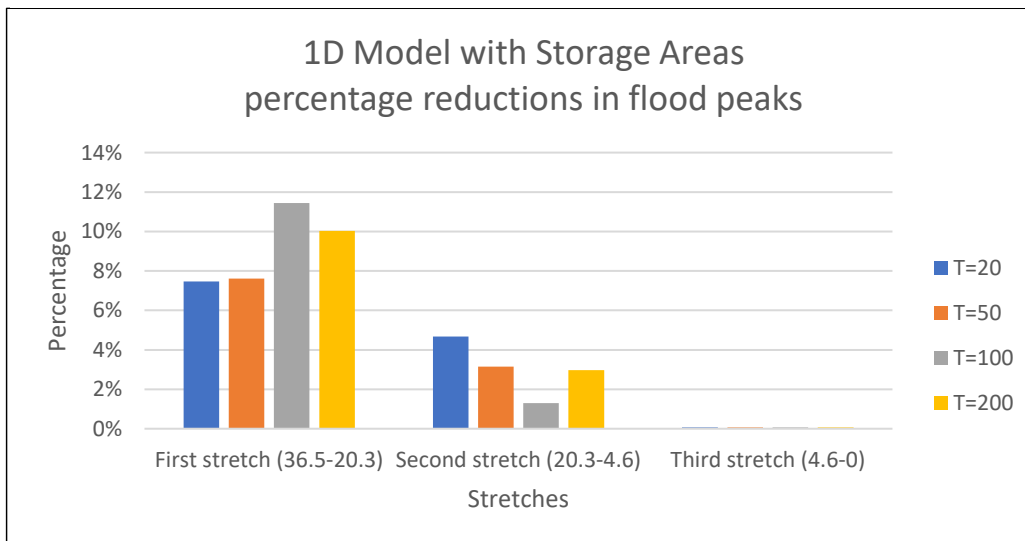
Graph 30: Flood peak dampening (in %) for the 1D Model with Storage Areas
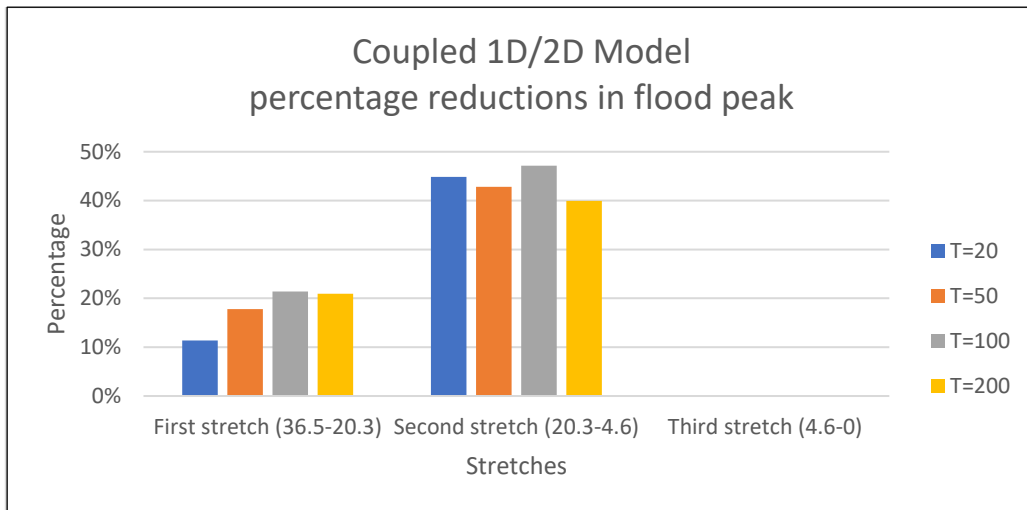
Graph 31: Flood peak dampening (in %) for the Coupled 1D/2D Model
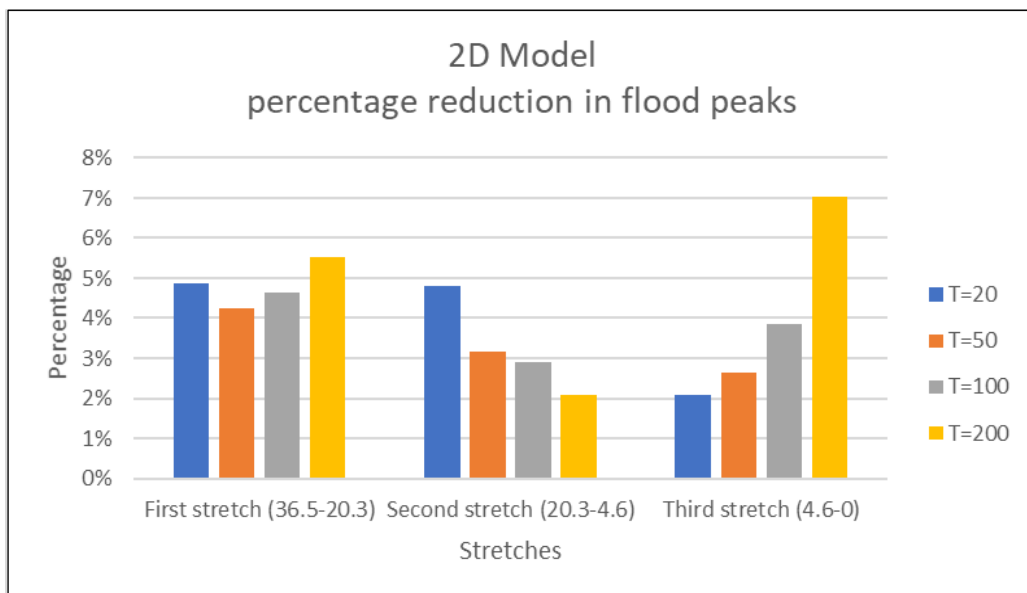
Graph 32: Flood peak dampening (in %) for the Fully 2D Model

By looking at the graphs presented above, it is noted the substantial difference between the results of each model. Both 1D and 1D with *Storage Areas* models return decreasing flood peaks reductions from upstream to downstream. The coupled 1D/2D model returns the largest flood peaks reductions in correspondence of the second stretch, but this is mostly due to the high numerical diffusion. The 2D model is the only one reducing the flood peaks along the third stretch. It is worth emphasizing that models 1D with *Storage Areas* and 2D return similar results in terms of overall flood peaks reductions.

For the first stretch, the 1D Model with extended cross sections returns the largest percentage reductions, with a maximum of 29% for T=200 years and a minimum of 21% for T=20 years. For the second stretch, a maximum reduction of 47% for T=100 years and a minimum of 40% for T=200, is given by the coupled 1D/2D model. The 2D model is instead the only one returning significant flood peaks reductions for the third stretch, with a maximum of 7% for T=200 and a minimum of 2% for T=20.

The graphs presented below, show a comparison between flow and stage hydrographs resulting from each model, at two significant cross sections, for T=20 years.
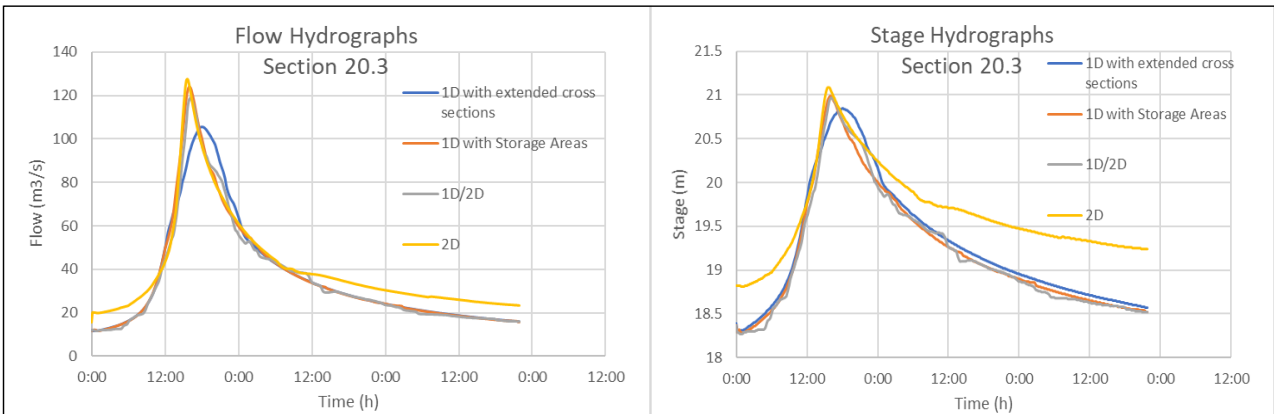
Graph 33: Flow and Stage hydrographs for section 20.3
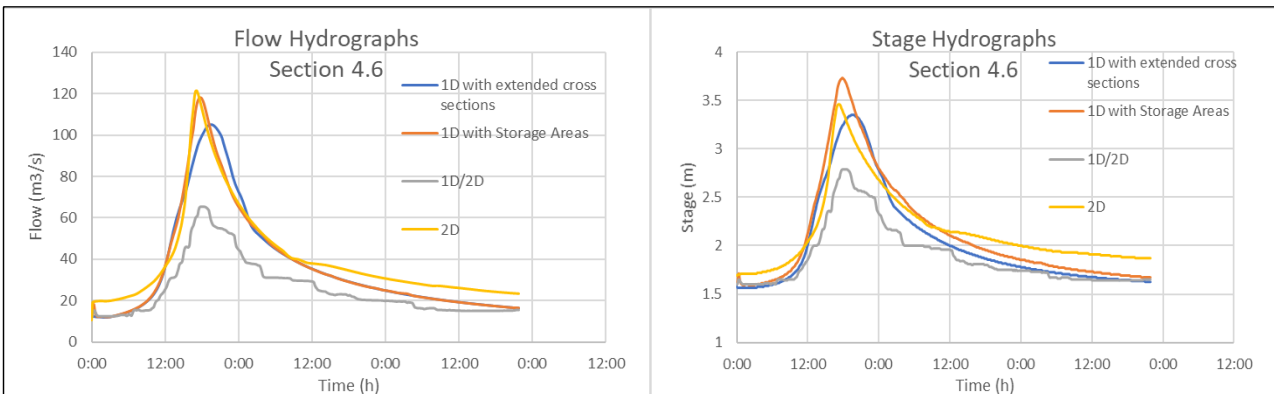
Graph 34: Flow and Stage hydrographs for section 4.6

The flow hydrographs of section 20.3, show that three models out of four return similar results, except for the values at the beginning and at the end of the event, which result higher for the 2D model. The 1D model with extended cross sections, shows instead the lowest flood peak and the largest flood wave dispersion. This trend is similar for the stage hydrographs.

Regarding the flow hydrographs at cross section 4.6, it is noticed the dramatic flood peak reduction for the coupled 1D/2D model mostly due to numerical diffusion. The results of the other models follow instead the same trend shown at cross section 20.3. On the other hand, stage hydrographs result rather different from each other. The lowest stage is again returned by the coupled 1D/2D model, while the highest by the model with *Storage Areas*. It is interesting to note that the 2D model has the steepest rising limb and the least steep falling limb.

The graphs below show the maximum discharges as a function of the cross sections (upstream end on the right, downstream end on the left). The discharges resulting from the 2D model are not presented, since they can be compared with the ones resulting from the other models only at three cross sections (where flow results almost entirely mono dimensional).
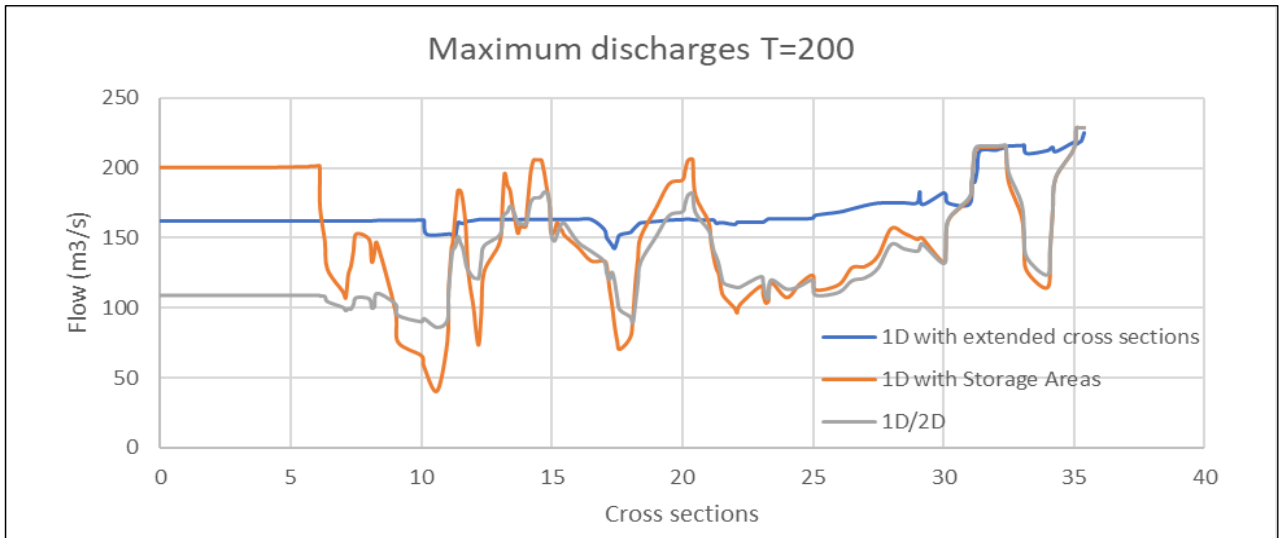
Graph 35: Maximum discharges for T=200 years
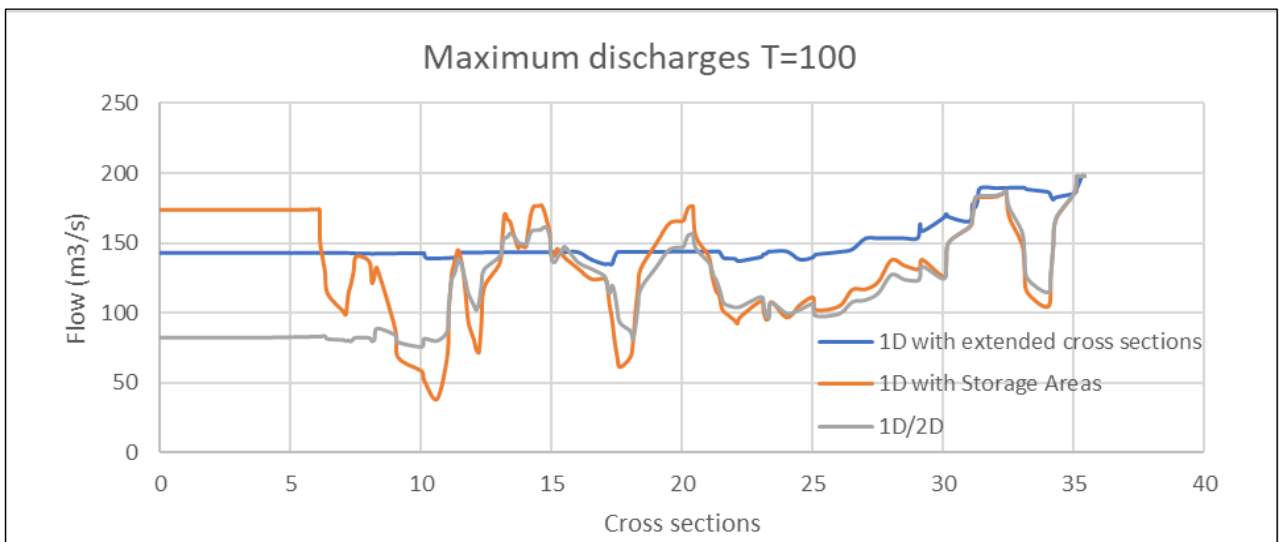
Graph 36: Maximum discharges for T=100 years
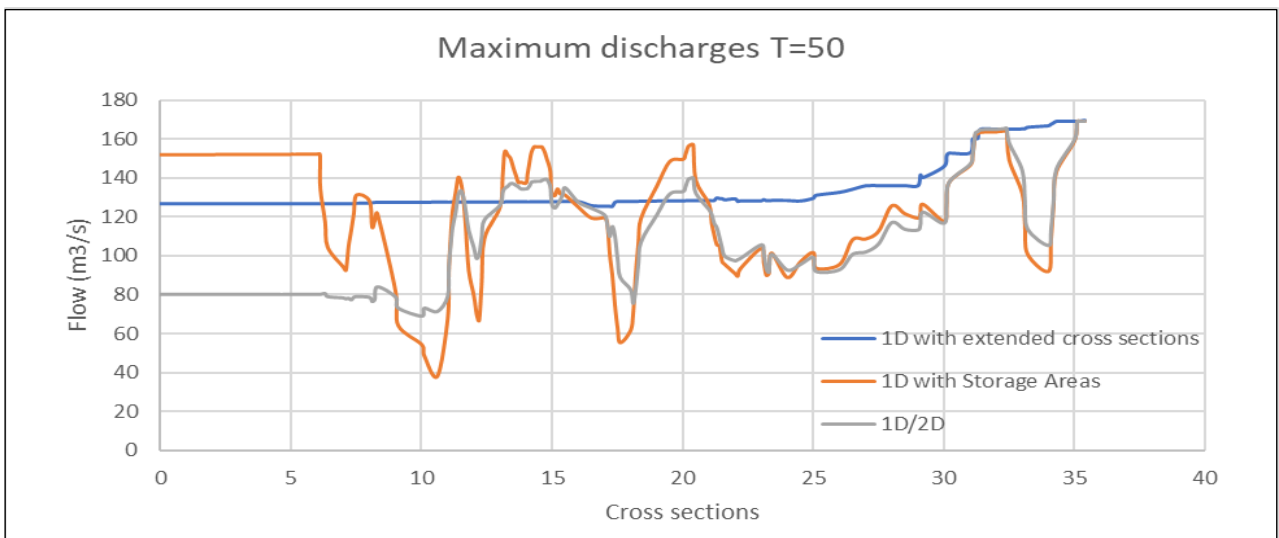
Graph 37: Maximum discharges for T=50 years
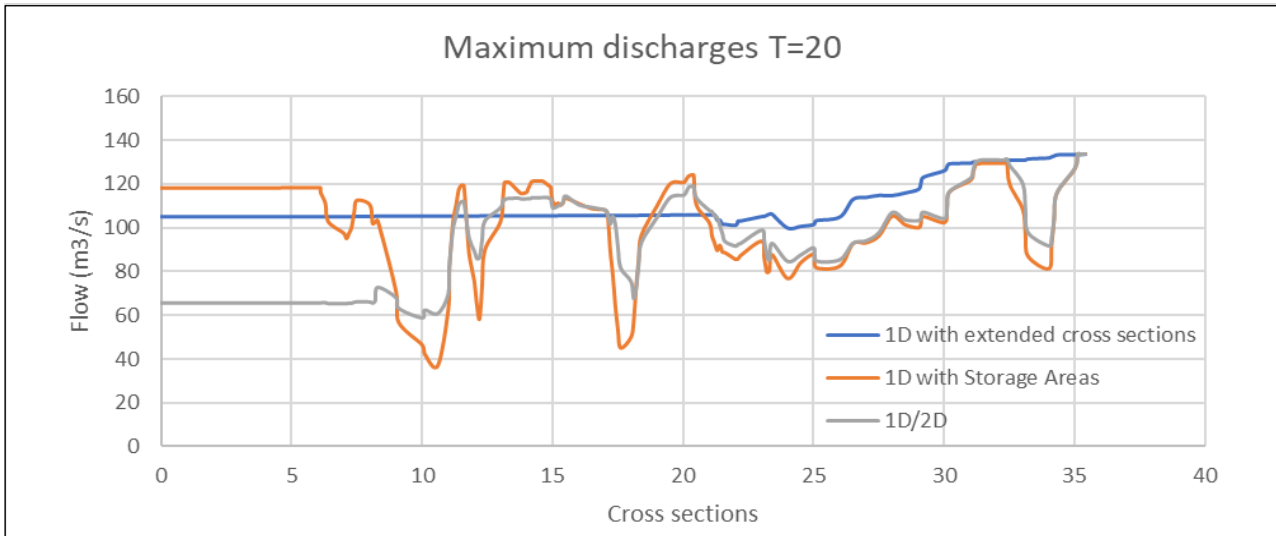
Graph 38: Maximum discharges for T=20 years

As can be seen in the graphs above, the peak discharges trends of the coupled 1D/2D model and of the 1D model with *Storage Areas* present many discontinuities (in part removed), as a result of the by-pass phenomena previously described. The difference between the two trends increases moving downstream, returning a difference of almost 50% at the last downstream stretch.

On the other hand, the results of the 1D model with extended cross sections have a decreasing trend up to cross section 26, from here onwards the values remain steady.

The graphs below show the maximum water depths as a function of the cross sections.
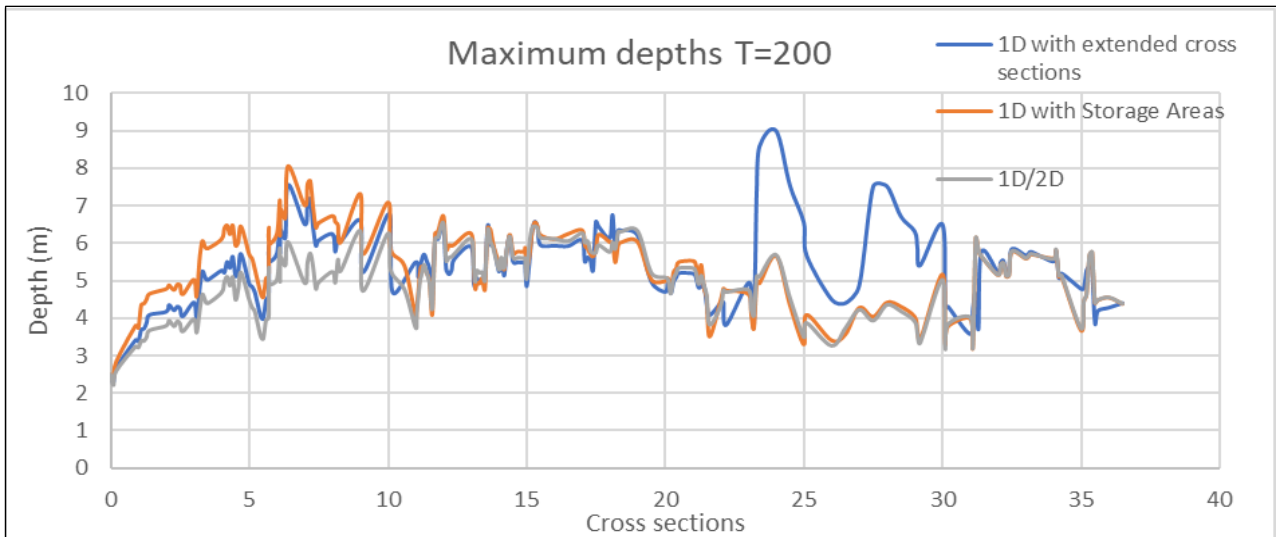
Graph 39: Maximum depths for T=200 years
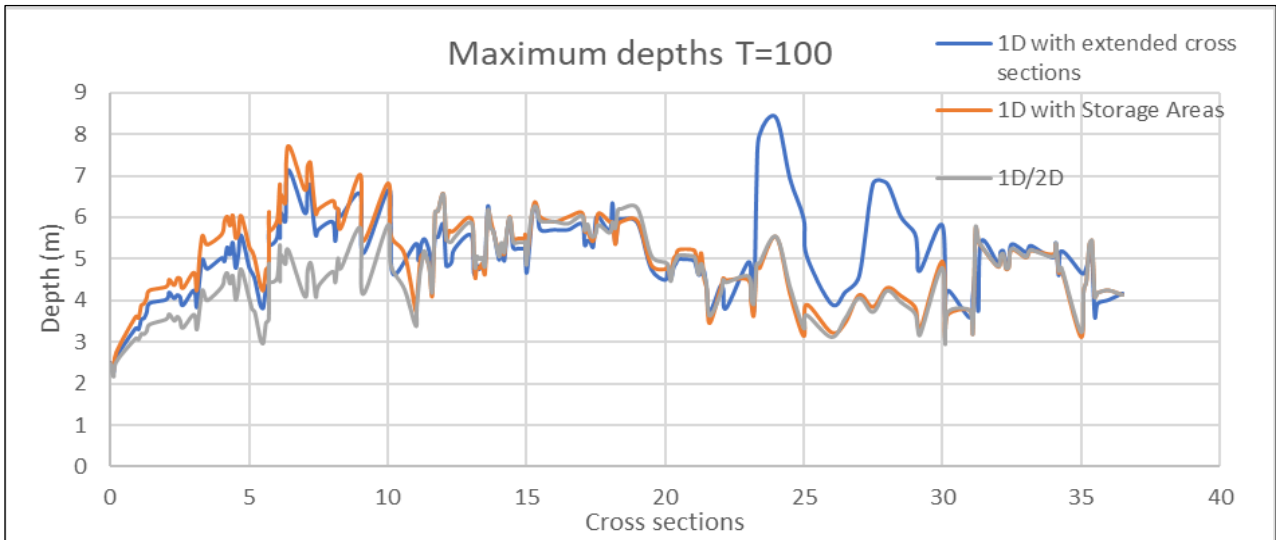
Graph 40: Maximum depths for T=100 years
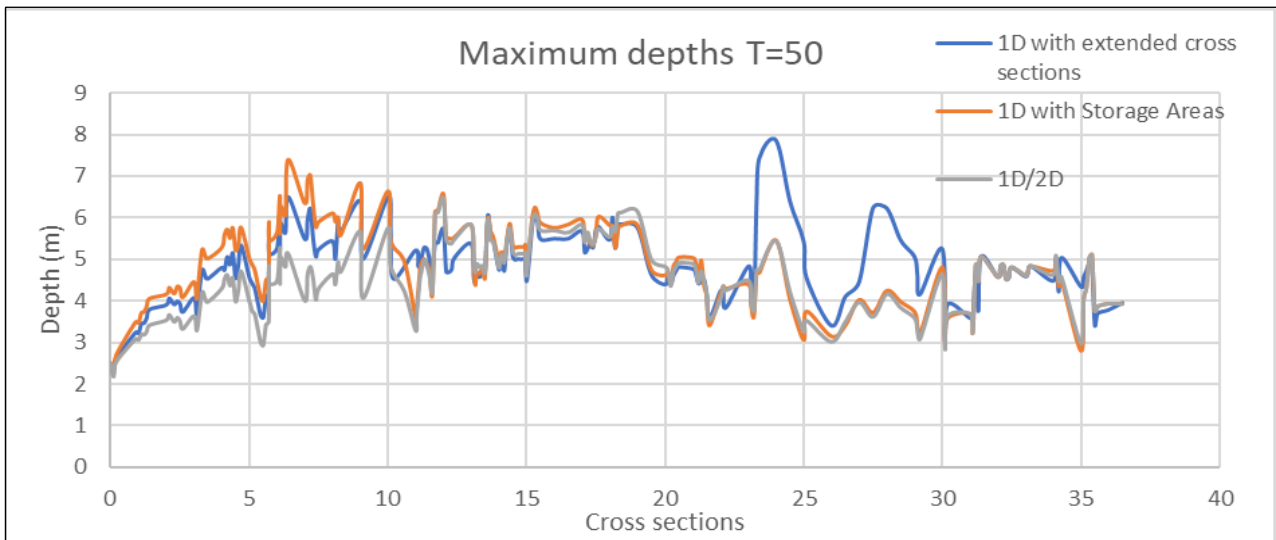
Graph 41: Maximum depths for T=50 years
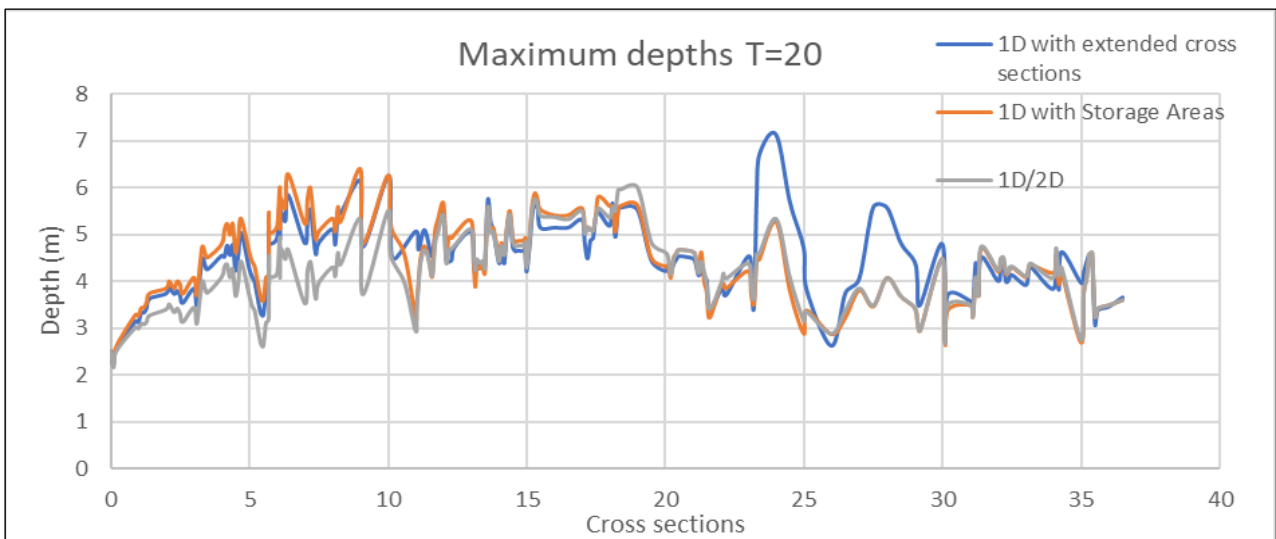
Graph 42: Maximum depths for T=20 years

106

The graphs below show a comparison between the water depths (for T=200 years) resulting at different points of the three floodplains storing the largest volumes. The results are presented for two points of each floodplain, a point at low elevation and a point at a higher elevation. In this way, it is possible to assess the different floodplains flooding and emptying dynamics resulting from each model.
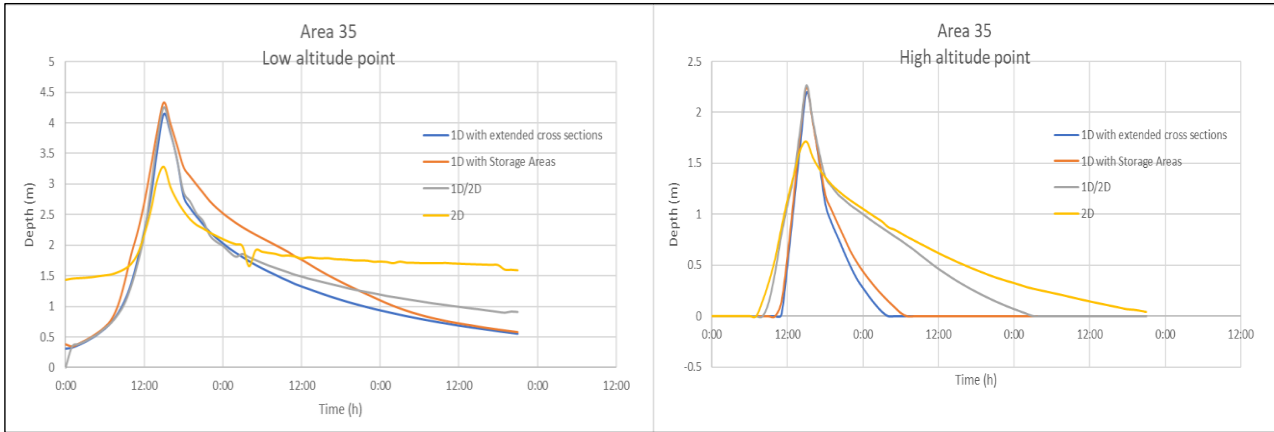
Graph 43: Water depths at two points of the area 35
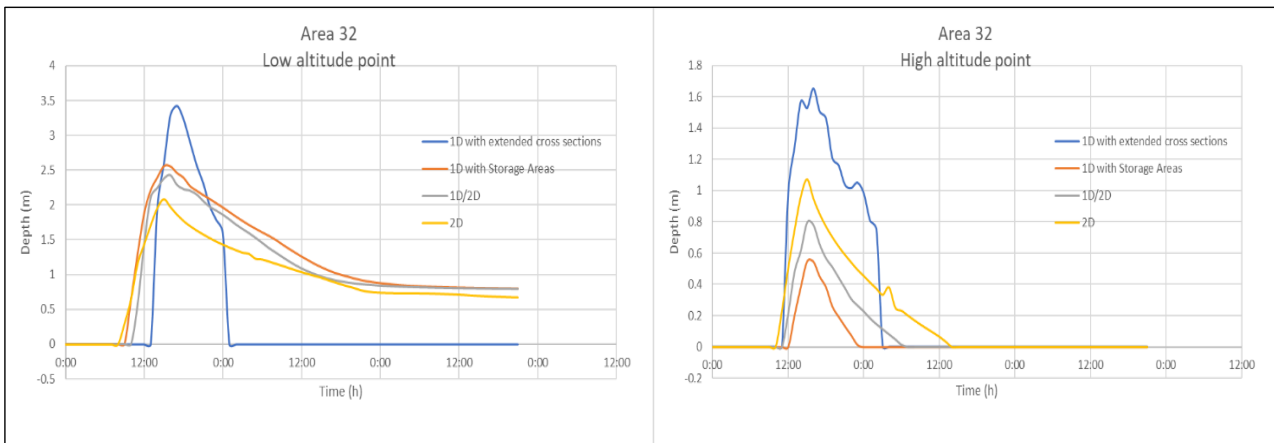
Graph 44: Water depths at two points of the area 32
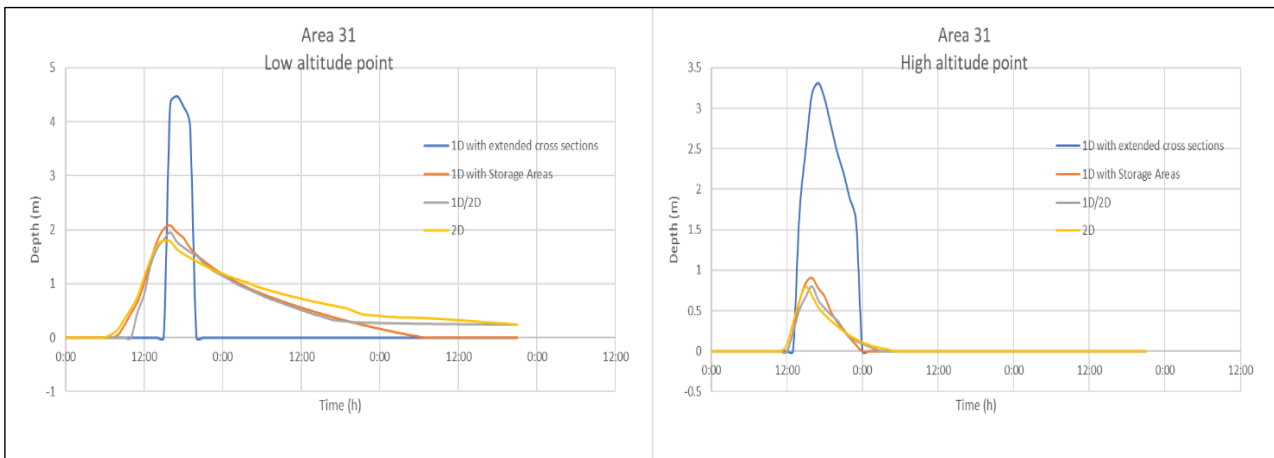
Graph 45: Water depths at two points of the area 31

As can be seen in the graphs above, the water depths computed by the 1D model with extended cross sections, rise and drop very quickly, reaching very high values. This is due to the incorrect

representation of floodplains inundation dynamics. In fact, this model does not consider any lateral flow over levees, when the main channel water level rises above the levee level the floodplain is inundated instantaneously.

Instead, by comparing the results of the other three models, it can be noted that the model with *Storage Areas* returns the greatest water depths at low elevation points. This is a consequence of floodplains hydrostatic representation made by the model. Indeed, when the water overtops the levees, regardless of where this occurs, it floods firstly and instantaneously the zone at the lowest elevation.

Lastly, the 1D/2D and 2D models return water depths trends with "smooth" recessions as a result of the floodplain dynamic representation.

In support of the considerations reported above, the different floodplain inundation dynamics, due to the conceptualizations made by each model, are illustrated below. The figures show the floodplain inundation (*Area 35*, T=200 years), at the time when water starts to inundate the floodplain.
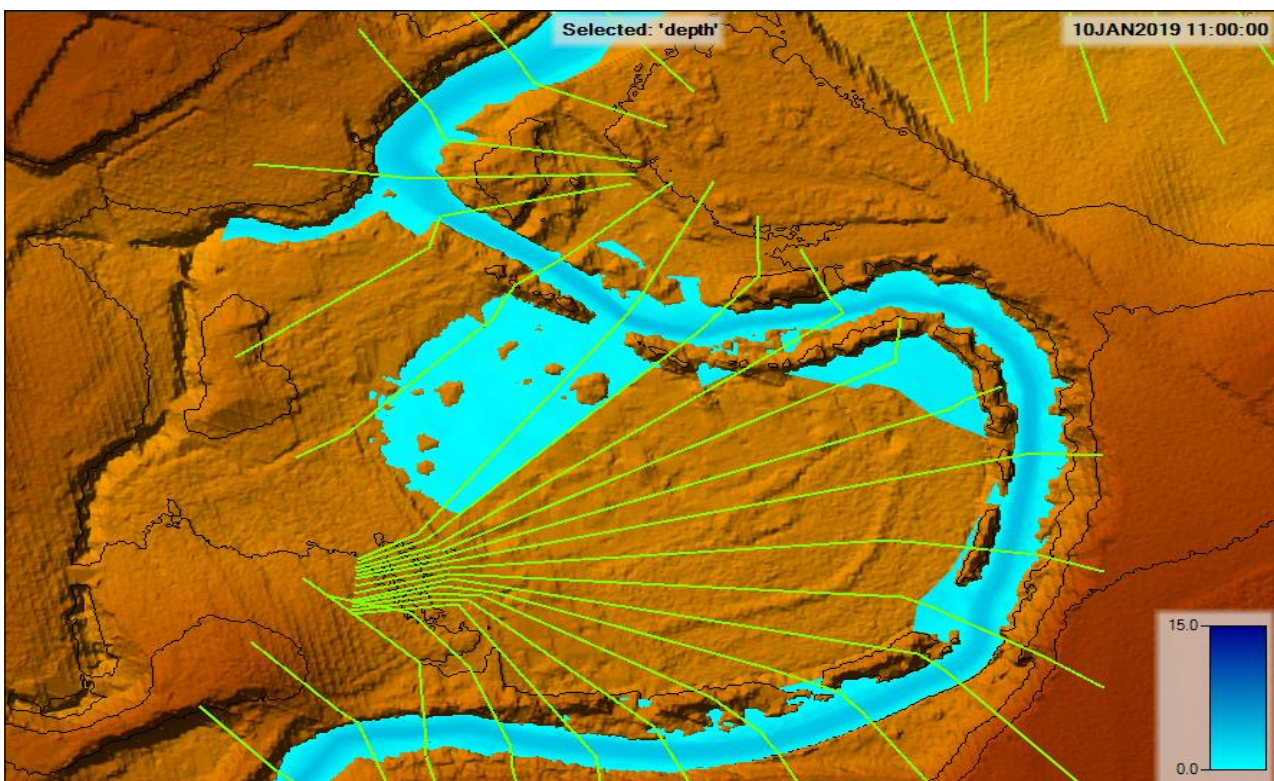
Figure 98: Floodplain inundation (1D model)
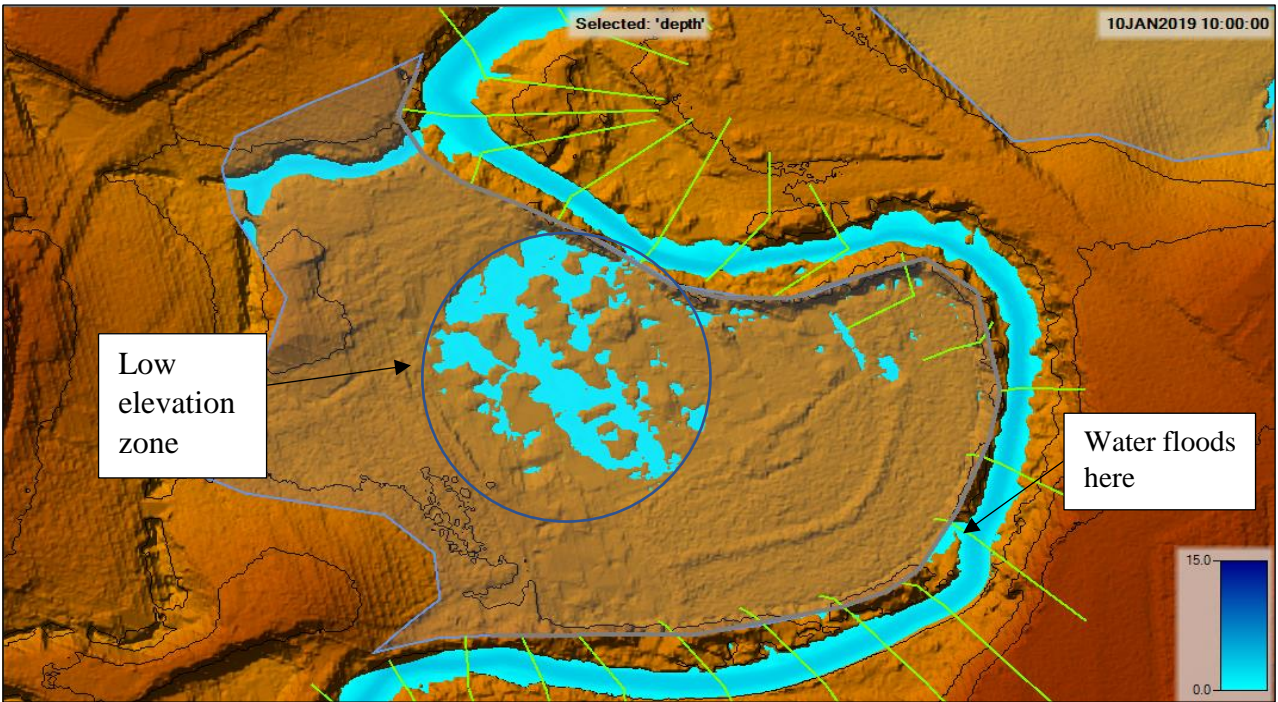
Figure 99: Floodplain inundation (1D model with Storage Areas)
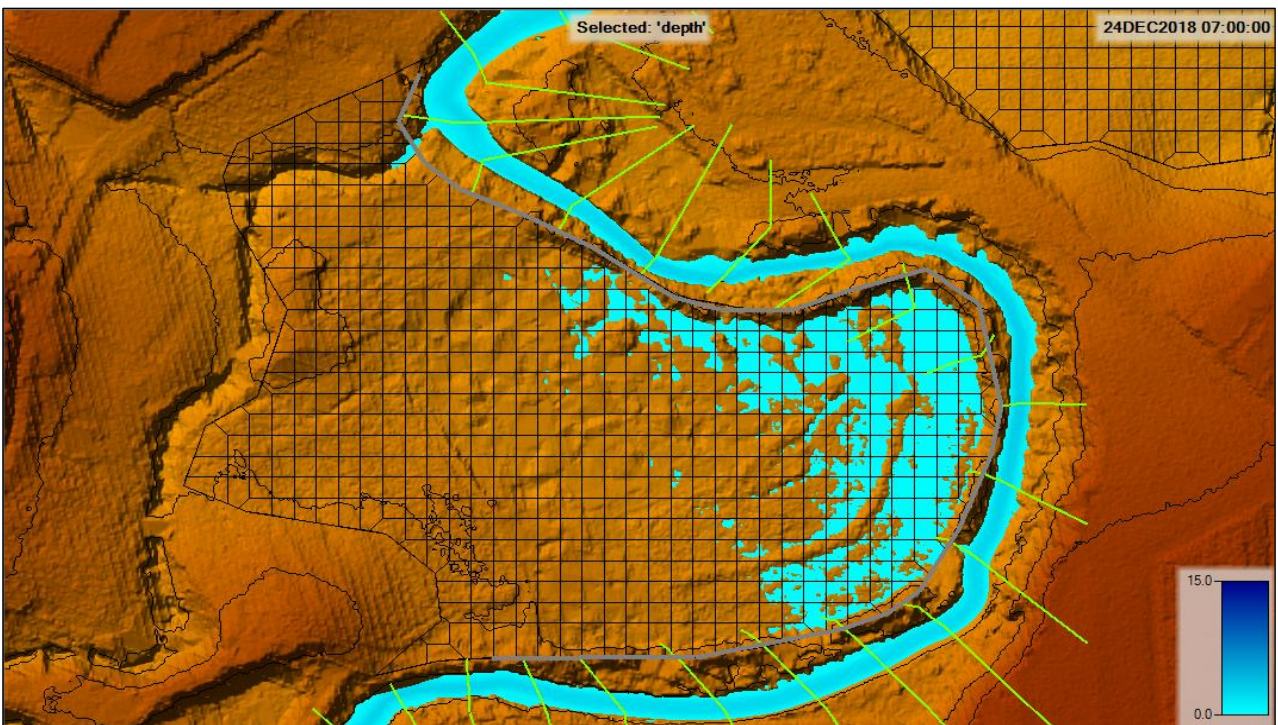
Figure 100: Floodplain inundation (coupled 1D/2D model)
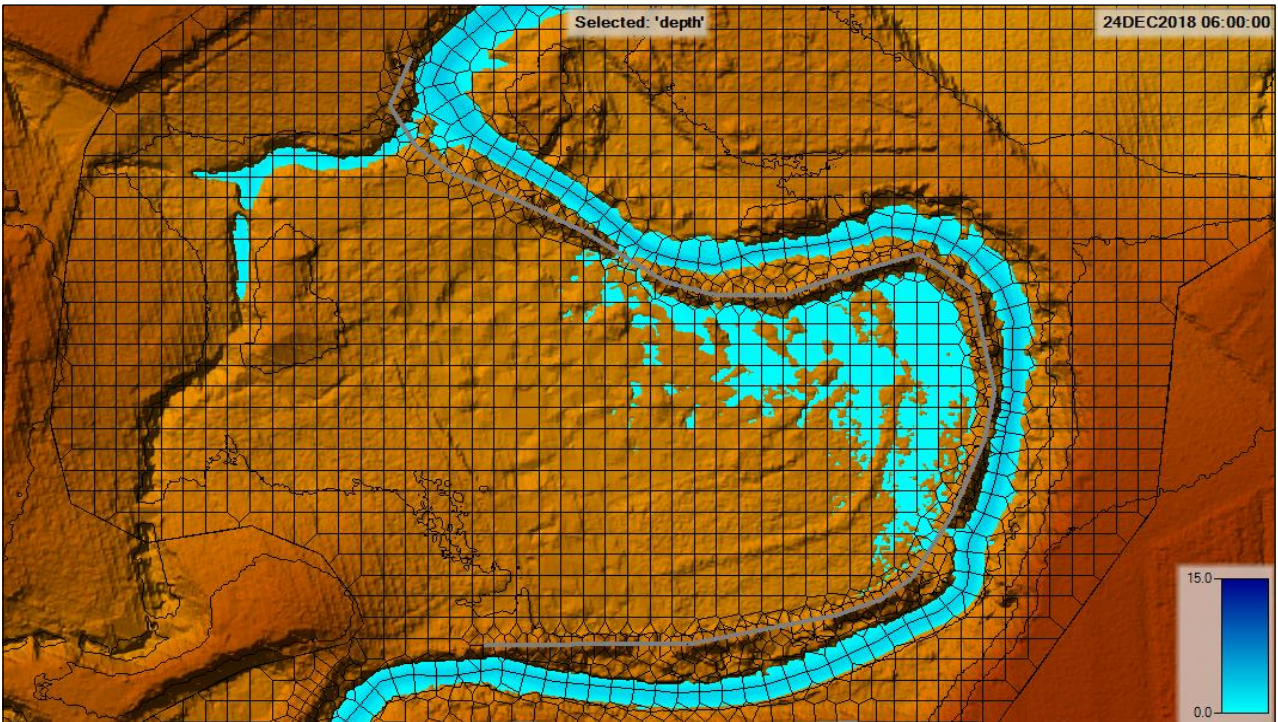
Figure 101: Floodplain inundation (2D model)

As can be seen in the figures above, each model is characterized by different times and dynamics of inundation. Coupled 1D/2D and 2D models show similar inundation dynamics (the most realistic ones), since both models represent the floodplain as dynamic *2D Flow Area*. Concerning the 1D model, it is noted a fragmented inundation due to the representation of floodplain through cross sections; indeed, water can flood at one cross section but not at the next one. The 1D model with hydrostatic *Storage Areas*, on the other hand, inundates firstly the zone at the lowest elevation.

Graph 46 shows the flow hydrograph related to the *Lateral Structure 35.15* connecting the main channel to the *Area 35*.
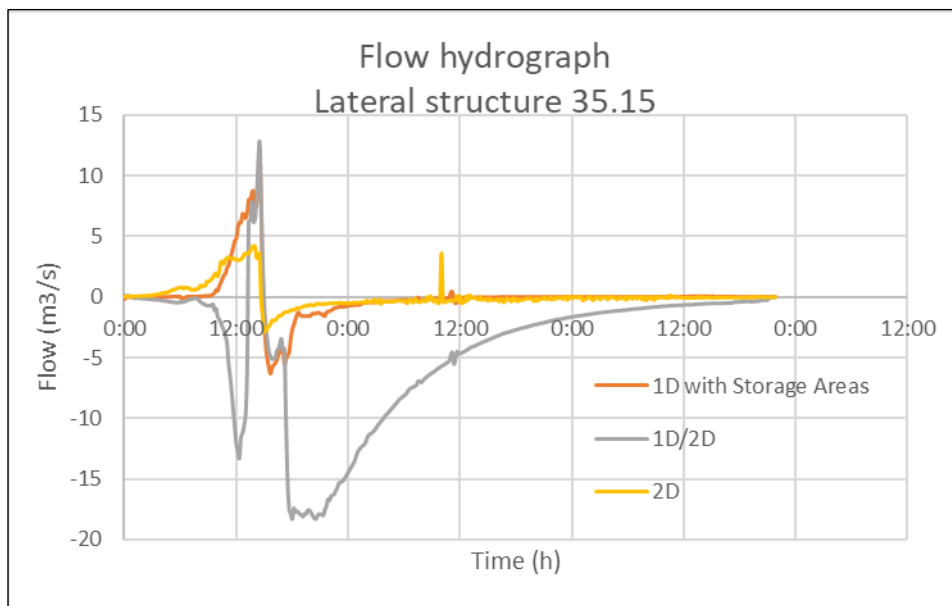
Graph 46: Flow hydrographs of Lateral structure 35.15 (negative flow towards the main channel)

By looking at Graph 46, it is possible to quantify the floodplain inflow and outflow, together with the floodplain activation time. First, the diagrams point out the unreliability of the coupled 1D/2D model results, due to the numerical stability issues; indeed, it is noted the pronounced fluctuation during the inflow phase and the excessive outflow. Second, the 2D model returns the smallest volume stored and the shortest floodplain activation time.

The graphs below show a comparison between flow and stage hydrographs resulting at the five most critical bridges, for T=200 years. It is reminded that in the 2D model, the bridges were represented as culverts or gates, depending on their shape.
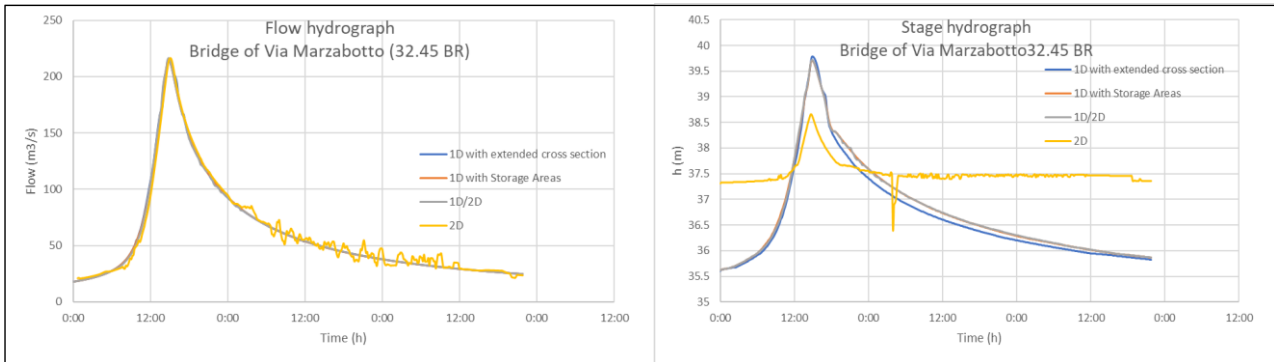
Graph 47: Flow and Stage hydrographs at the bridge of Via Marzabotto (section 32.45 BR)
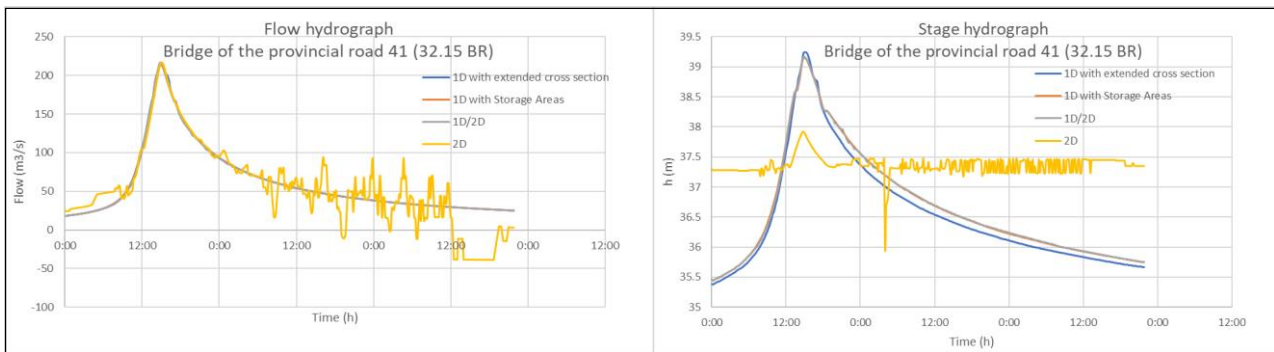
Graph 48: Flow and Stage hydrographs at the bridge of the provincial road 41 (section 32.15 BR)
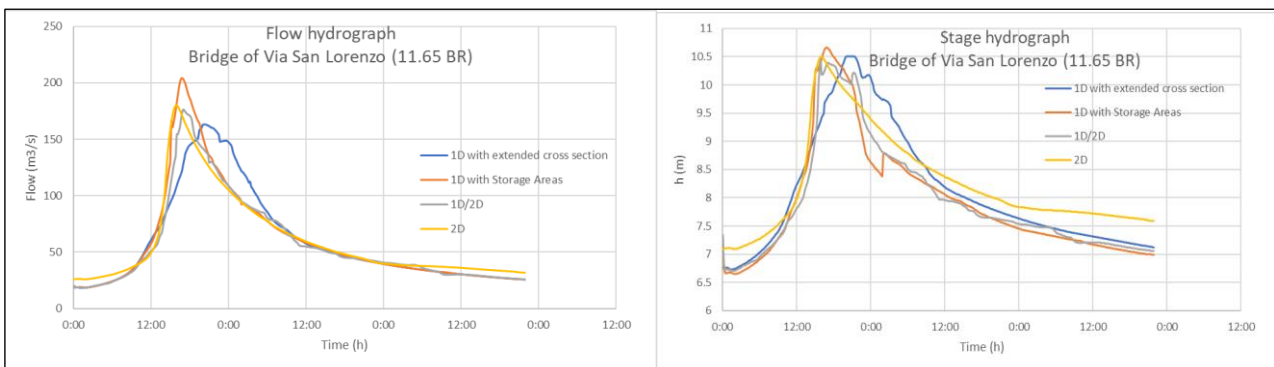
Graph 49: Flow and Stage hydrographs at the bridge of Via San Lorenzo (section 11.65 BR)
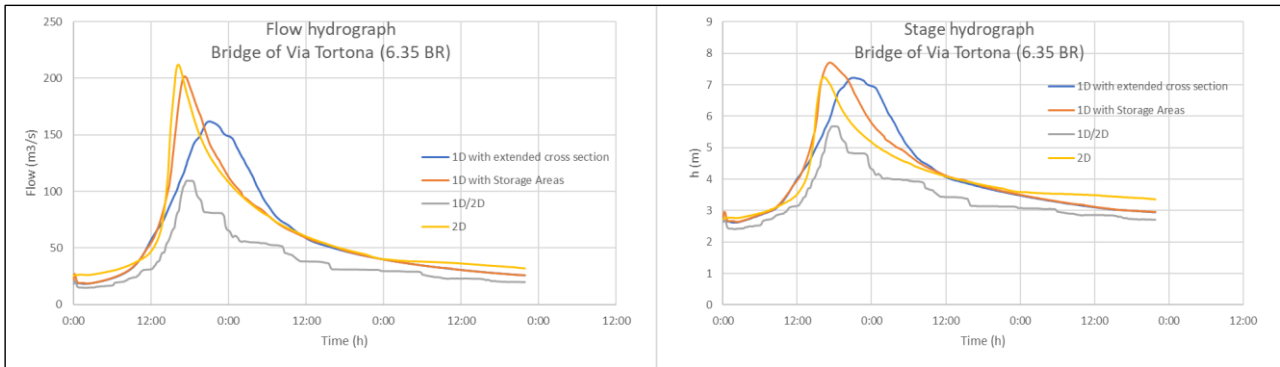
Graph 50: Flow and Stage hydrographs at the bridge of Via Tortona (section 6.35 BR)
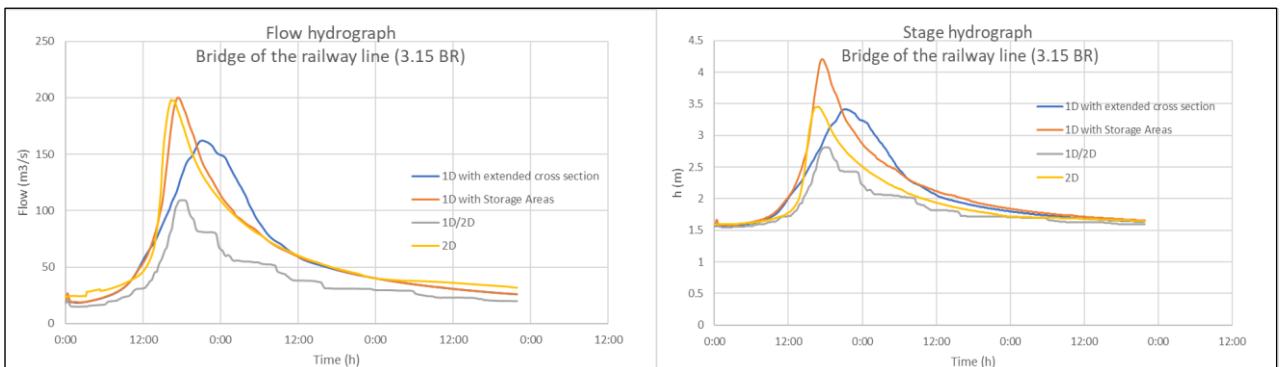
Graph 51: Flow and Stage hydrographs at the bridge of the railway line (section 3.15 BR)

By looking at the graphs above it is noted that the flow and stage hydrographs computed by the 2D model, at the bridge of Via Marzabotto and at the bridge of the provincial road 41, are affected by some instabilities (due to the structures proximity) which, however, do not affect downstream results.

As can be seen in graph 26 and 27, the most significant differences between the results of the 2D model and the results of the other three models, are at the bridge of Via Marzabotto and at the bridge of the provincial road 41. The flow hydrographs are consistent between them, while the water stages computed by the 2D model, are rather steady, rising only of half a meter in correspondence of the flood peak.

8.3.4 Comparison between flood inundation maps

The figures below show the maximum inundation extents resulting from each model, for T=200 years.
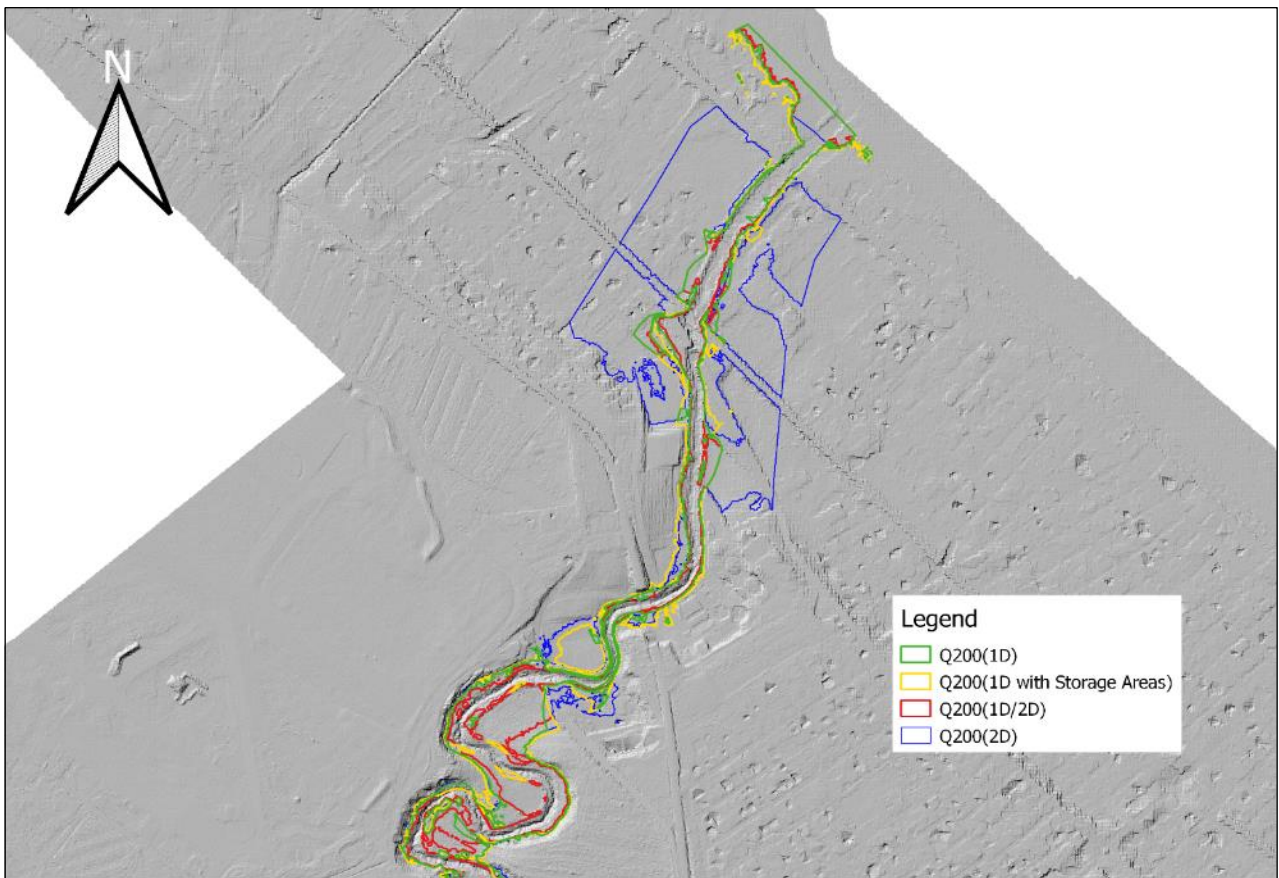
Figure 102: Flood inundation map (first downstream stretch)
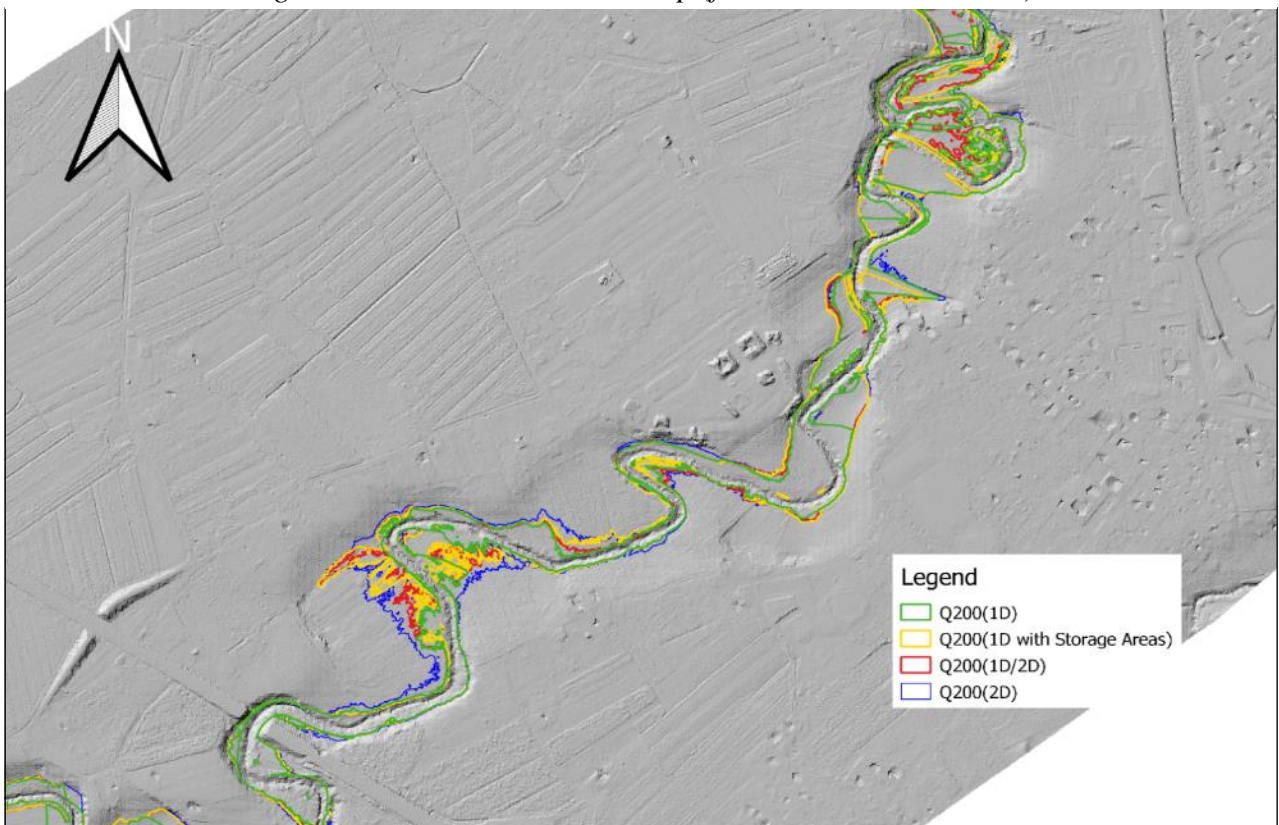
Figure 103: Flood inundation map (second stretch)
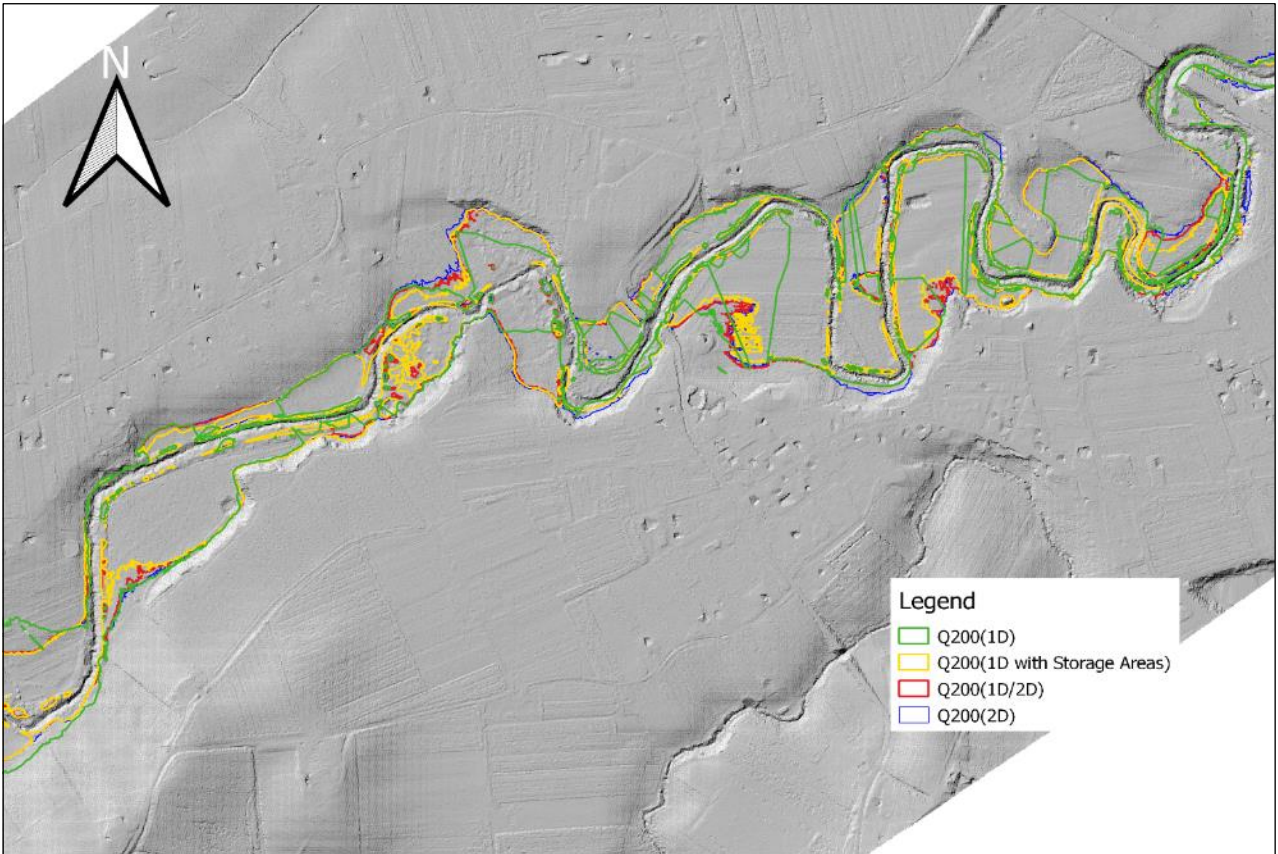
Figure 104: Flood inundation map (third stretch)
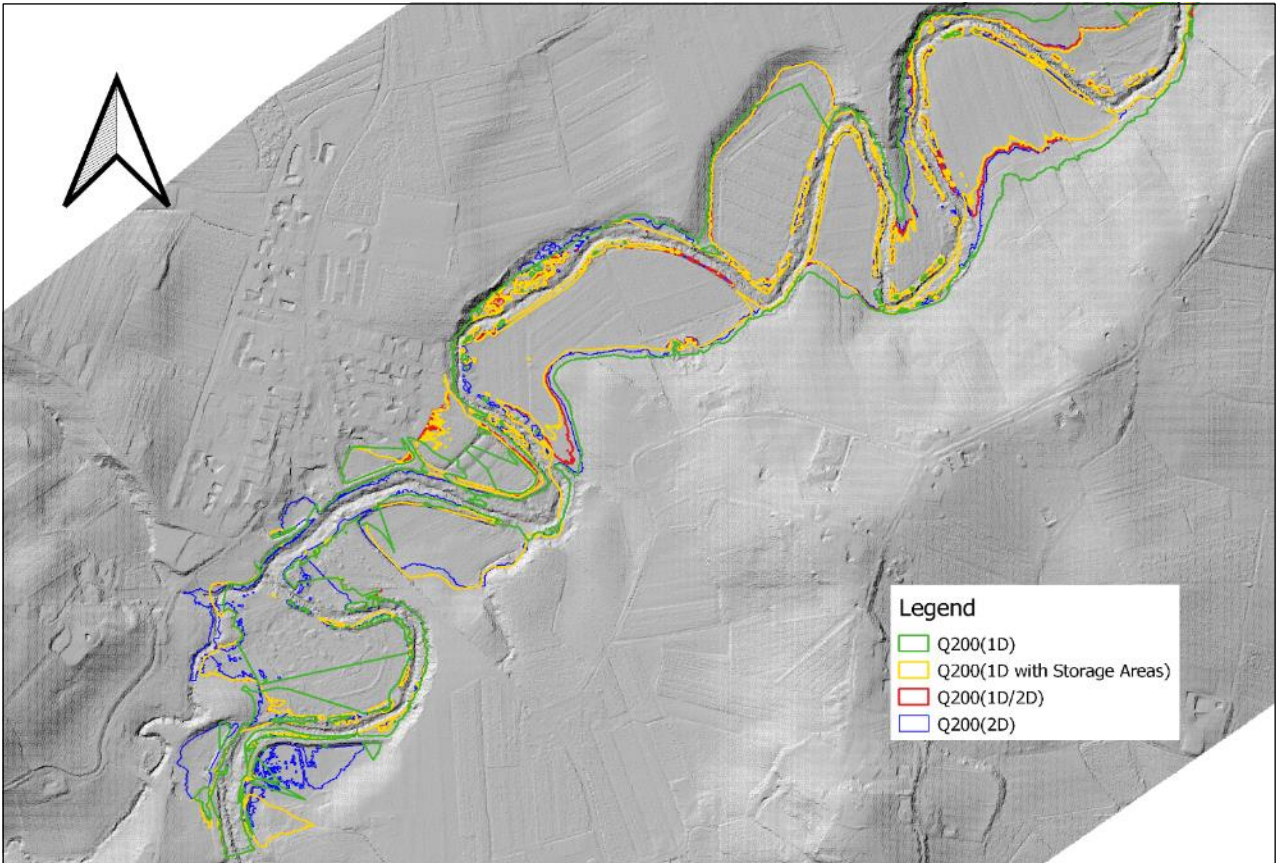
Figure 105: Flood inundation map (fourth stretch)

As it can be seen in the figures above, 1D model returns odd inundation maps as a result of its intrinsic limits explained before. On the other hand, the 2D model shows the largest inundation extent, particularly along the first upstream stretch and along the last downstream stretch (explaining the significant flood peak reduction occurring between cross sections 4.6 and 0, showed in Graph 32).

8.3.5 Comparison between velocity maps

The figures below show the different velocities distribution resulting from the four models at a stretch of the stream.

Figure 106: Velocities distribution (1D model with extended cross sections)

Figure 107: Velocities distribution (1D model with Storage Areas)

Figure 108: Velocities distribution (Coupled 1D/2D model)
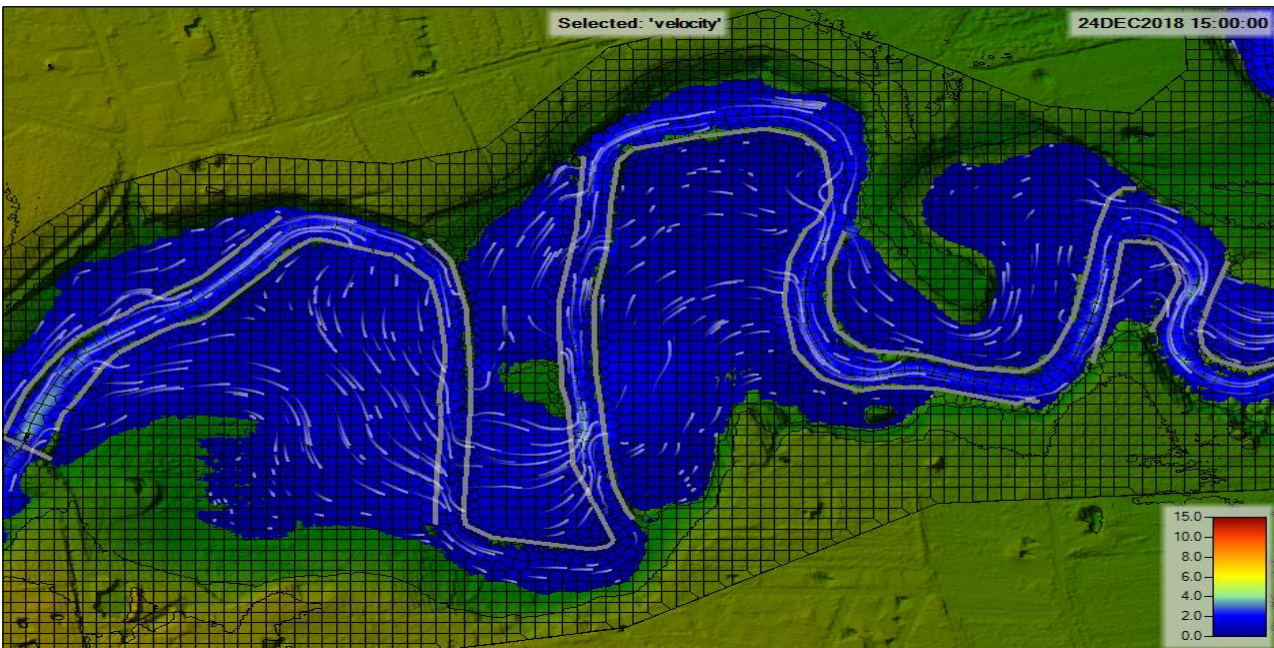
Figure 109: Velocities distribution (2D model)

As can be seen in the figures above, the 2D model returns the most accurate representation of the velocities distribution, in both main channel and floodplain. 1D model results, on the other hand, are rather inaccurates since are based on interpolation of 1D velocities computed at the cross sections. Consequently, it is not possibble to map velocities around features located between cross sections.

8.3.6 Final considerations about the unsteady flow simulation results

Observing the results of the four hydraulic models, substantial differences are noted in terms of flood peaks reductions, flood inundation extents and dynamics; consequently, flood hazard assessment of the Marano stream, changes according to the hydraulic model considered. In the future it is hoped that flood peaks measurements at different river sections together with observations of flood inundation extents will be available. With real observations it would be possible to calibrate the models, assessing which one returns the most realistic results.

Having said that, according to the mass balance errors, only three of the four models analyzed returned reliable results. In particular, for T=200 years, the percentage errors of 1D, 1D with *Storage Areas,* 1D/2D and 2D models are 0.02%, 0.47%, 34.63% and 3.65% respectively. The large error returned by the coupled 1D/2D model can be explained by the numerical stability issues. In particular, the irregular elevations profile of the *Lateral Structures* connecting the main channel (1D) to the floodplains (2D), had a strong impact on the model stability. By looking on stage hydrographs and profile plots, it is noted that the model becomes unstable when the water level in the main channel is approximately equal to the elevation of the *Lateral Structures*. In this case, given the irregular shape of the *Lateral Structures* it is common to have 1D water levels close to the level of the structure.

9. Conclusions

The results of the steady flow simulations enabled us to evaluate conservatively the flood prone areas and the hydraulic adequacy of the structures present along the stream, for return periods of 20, 50, 100, 200 years. Six bridges resulted inadequate, since flow reaches the intrados or, as it happens in two cases, submerges the entire structure. It is noticed that most of the natural floodplains of the stream are inundated. Along the stream some residential areas together with commercial and craft activities are potentially flooded. However, it is worth emphasizing that the widespread floods along the upstream stretch decrease the flood risk at the downstream urbanized area.

The unsteady flow simulations allow one to quantify the flood peaks reductions and to represent the floodplains inundation dynamics with four different hydraulic models. However, comparing the results of the four models, substantial differences are noted in terms of flood peaks reductions, floodplains inundation extents and dynamics. Therefore, it is hoped that in the future flood peaks measurements at different river sections, together with observations of flood inundation extents would be available in order to assess which of the four models return the most reliable results.

Having said that, in flood hazard assessment context, where local water depths, velocities and discharges are primary concerns, 2D hydraulic models seem to represent the best option. In fact, by representing flood propagation through a computational mesh, it is possible to obtain detailed results on the entire topographic surface. This issue takes on particular importance for a river characterized by a complex geometry and discontinuous levees such as the one studied.

In view of the findings of this case study, some considerations related to the four hydraulic models used are reported below.

1D models are not suitable for modeling channel-floodplain interactions and floodplain inundation dynamics, not even for small streams/torrents, as in this case. These models compute two separate parallels flow, one in the main channel and one in the floodplain, not considering lateral flows occurring when the stream overflows its banks. At each cross section a single water level is computed, therefore, when the main channel water level rises above banks level, the entire floodplain is

instantaneously inundated. Furthermore, it was observed that the water may overtop the banks at one cross section but not at the next one, generating odd inundation maps such as the one showed above. In flood hazard assessment, mapping velocity distribution is one of the main concerns. In this regard, it is underlined that 1D velocity maps are based on interpolation of 1D results, therefore, it is not possible to obtain accurate velocity distribution. In conclusion, 1D models can perform well when modeling flow restricted between channel banks. On the other hand, limitations of 1D models might become evident when modeling overland flow.

1D models with floodplains represented as hydrostatic *Storage Areas* might be suitable for studying the flood peak reduction induced by the introduction of levees separating the floodplain from the main channel. Moreover, when the timing of levee-overtopping is of interest, this approach represents a valuable alternative to 1D/2D and 2D models because of shorter computational time. On the other hand, the schematization of floodplains as hydrostatic areas leads to an unrealistic representation of floodplains inundation dynamics.

Coupled 1D/2D models allow to represent main channel flow in 1D and floodplain flow in 2D. It was noted, however, that if there is not a clear continuous barrier separating the main channel from the floodplains, the model might have great stability issues. Filtering elevations data can increase computational stability but in this way the results accuracy decreases. Therefore, coupled 1D/2D models appears to be more suitable for modeling areas where 1D and 2D flow areas are separated by a continuous and smooth levee.

2D models represent flood diffusion through a continuous surface, returning the most accurate representations of the flood propagation. In order to obtain reliable results, however, it is important to accurately design the computational mesh. Therefore, cell faces have to be aligned with the highest elevation of the barriers and have to be perpendicular to the main flow. Moreover, cell sizes have to be small enough to allow the fulfillment of the previous two conditions. Despite this, with the sub-grid approach used in Hec-Ras, it is possible to use a relatively coarse computational grid which however incorporates the finer resolution topography. 2D models require a terrain model which is not always available. Furthermore, river bathymetry should be always incorporated in the terrain model in order to obtain reliable results (*Cook & Merwade, 2009*). Another issue of 2D approach highlighted in this study, is the longer computational time in respect of 1D and coupled 1D/2D models. This problem might become more important when real time flood risk estimations are needed. Lastly, it is worth to emphasize that there are some uncertainties related to 2D bridge modeling, since Hec-Ras allows one to represent bridges as simpler structures, such as culverts or gates and this approximation might lead to inaccurate results.

In addition to the information obtained from the four hydraulic models used, as future studies, the exploration of the following topics shall contribute to achieve a more complete response to flood hazard assessment issue:

- the inclusion of the levee breach option in hydraulic models, in order to detect possible levees failures along the stream;
- the sediment transport analysis, which allow to study changes in main channel geometry during a flood event.

10. Appendix

10.1 Script in Matlab 1

```matlab
% genera l'idrogramma di portata per eventi con determinato tempo di ritorno T
% 2 è la sezione di ospedaletto di coriano
passoD = 1; %Passo di discretizzazione (ore)
Dmax = 72;%Durata massima (ore)
D = (0:passoD:Dmax)';
T = [20,50,100,200]; %Tempi di ritorno
passot=5/60; %ore necessario per avere intervalli di tempo regolari per HEC-RAS
%Dati bacino %km^2
A2=54.3;
A=A2;
L2=16.79; % ospedaletto di coriano (sez 14_2016 HECRAS 33.1)
L=L2;
n = [0.3012, 0.2932, 0.2871, 0.2810];
Pma=880; %mm
P1g=76.5; %mm
%m s.l.m. quota media dei sottobacini, valori presi dal PAI
Hm2=229;
Hm=Hm2;
%m quota della sezione di chiusura presa da rilievi
qsc2=36.1;
%m dislivello medio dei sottobacini rispetto alla relativa sezione di chiusura
DHm2=Hm2-qsc2;
DHm=DHm2;
a=84;
b=0.768;
c=a*(L./DHm).^b;
d=n;
for i=1:length(T)
epsD2(:,i) = (1+D/c(1)).^(d(i)-1);
end
QT=[134 170 199 230];
k2=0.424*L(1)^1.05;
rD2=0.184+0.374./(1.33+(D/k2).^1.25);
for i=1:length(T)
F21(:,i)=rD2.*D;
F22(:,i)=F21(:,i).*epsD2(:,i);
F23(:,i)=(1-rD2).*D;
F24(:,i)=F23(:,1).*epsD2(:,i);
end
%Calcolo delle derivate centrate
for i=1:(length(D)-2)
Der21(i,:)=(F21(i+2,:)-F21(i,:))/(D(i+2)-D(i));
Der22(i,:)=(F22(i+2,:)-F22(i,:))/(D(i+2)-D(i));
Der23(i,:)=(F23(i+2,:)-F23(i,:))/(D(i+2)-D(i));
Der24(i,:)=(F24(i+2,:)-F24(i,:))/(D(i+2)-D(i));
107
end
QTm2=repmat(QT(1,:),length(D)-2,1);

% SEZIONE 2
% Costruzione della porzione sinistra dell'idrogramma
Qsx=[QTm2(1,:) ; QTm2.*(Der22./Der21)];
tsx=-F21(1:length(D)-2,1);
% Costruzione della porzione di destra dell'idrogramma
Qdx=[QTm2(1,:) ; QTm2.*(Der24./Der23)];
tdx=F23(1:length(D)-2,1);
% unione idrogrammi
```

```matlab
t=[tsx ; tdx];
Qsx=Qsx(1:length(Qsx)-1,:);
Qdx=Qdx(1:length(Qdx)-1,:);
Q2=[Qsx ; Qdx];
Q2=sortrows([t Q2]);
col=find(ismember(Q2(:,1),0),1);
Q2(col,:)=[];
% necessario per inserire l'onda di piena in HEC-RAS (vuole passo t costante)
tmin=min(Q2(:,1));
tmax=max(Q2(:,1));
clear tint
tint=unique(sort([0:passot:tmax 0:-passot:tmin])');
Qreg2=zeros(length(tint),length(T)+1);
Qreg2(:,1)=tint;
for h=2:length(T)+1
j=1;
for i=1:length(tint)
k=length(Q2(:,1));
if tint(i)==0
Qreg2(i,h)=max(Q2(:,h));
j=j+1;
else
while tint(i)-Q2(j,1)>=0 && tint(i)-Q2(j+1,1)>0
j=j+1;
end
tm=Q2(j,1);
Qm=Q2(j,h);
109
while Q2(k,1)-tint(i)>=0 && Q2(k-1,1)-tint(i)>0
k=k-1;
end
tM=Q2(k,1);
QM=Q2(k,h);
alfa=(tM-tint(i))/(tM-tm);
Qreg2(i,h)=alfa*Qm+(1-alfa)*QM;
end
end
end


% Grafici
% Idrogrammi Q2(t,T)
figure(2)
plot(repmat(Q2(:,1),1,length(T)),Q2(:,2:end))
% Formattazione Figura
legend(strcat('T= ',string(T),' anni'))
xlabel('Time [h]','FontSize',12)
ylabel('Q(t,T) [m^3/s]','FontSize',12)
title(['MARANO AT OSPEDALETTO: synthetic hydrographs'],'FontSize',14)
set(gca,'Xgrid','on','YGrid','on')
axis([min(Q2(:,1))-10 max(Q2(:,1))+10 min(min(Q2(:,2:end)))-10
max(max(Q2(:,2:end)))+10])
% Q_D(t,T)
figure(5)
plot(repmat(D,1,length(T)),repmat(QT(1,:),length(D),1).*epsD2)
% Formattazione Figura
legend(strcat('T= ',string(T),' anni'))
xlabel('D [ore]','FontSize',12)
ylabel('Q_D(T) [m^3/s]','FontSize',12)
title(['Curva di riduzione di piena Q2_D(T)'],'FontSize',14)
set(gca,'Xgrid','on','YGrid','on')
% eps_D(T)
figure(6)
```

```matlab
plot(repmat(D,1,length(T)),epsD2)
% Formattazione Figura
legend(strcat('T= ',string(T),' anni'))
xlabel('D [ore]','FontSize',12)
ylabel('eps_D(T)','FontSize',12)
title(['Fattore di riduzione eps2_D(T)'],'FontSize',14)
set(gca,'Xgrid','on','YGrid','on')
% r_D
figure(7)
plot(D,rD2)
% Formattazione Figura
xlabel('D [ore]','FontSize',12)
ylabel('r_D(T)','FontSize',12)
title(['Parametro di posizione del picco r2_D'],'FontSize',14)
set(gca,'Xgrid','on','YGrid','on')
% Esportazione Q
xlswrite('Q2_regolare.xlsx',{'t' 'Q20' 'Q50' 'Q100' 'Q200'},'Foglio1','A1')
xlswrite('Q2_regolare.xlsx',Qreg2,'Foglio1','A2')
```

10.2 Script in Matlab 2

```matlab
% Tracciamento delle onde di piena di progetto sulla base del metodo proposto
% da Maione, Mignosa e Tomirotti (2000, Acqua)
% Dati e parametri finali:

clear all % Cancella lo spazio delle variabili
set(0,'ShowHiddenHandles','on'); delete(get(0,'Children')) % Chiude tutte le
figure


% Parametri del programma
T = [20 50 100 200]'; %Tempi di ritorno
QT = [134 170 199 230]'; %Portate al colmo di assegnato T
Theta = 2.893371791; %Parametro per la curva di riduzione dei volumi di piena
(Bacchi e Brath, 1992)

%PARI A 1.54*Tc per i sottobacini
Dmax = 72; %Durata massima
passoD = 1/12; %Passo di discretizzazione
rDlim= 0.22  % rD ad andamento esponenziale a due parametri, rD minimo
k=     8.19  % rD ad andamento esponenziale a due parametri, parametro di
smorzamento
Onde_Uscita= 'OP_MARANO.txt'; %File di testo per l'uscita delle onde
Nomestaz=['MARANO AT OSPEDALETTO: synthetic hydrographs'];%Titolo Figura

% Variabili del programma
% D:= Vettore durate considerate
% npti:= Numero punti della discretizzazione
% rD:= Vettore rD interpolati (linearmente)
% EpsiD:= Curva di riduzione dei volumi di piena (Bacchi, Brath)

% F1:= Vettore rD*D
% F2:= Vettore rD*D*EpsiD
% F3:= Vettore (1-rD)*D
% F4:= Vettore (1-rD)*D*EpsiD
% DerX:= Derivata centrata di FX
% Onda:= Matrice a due righe contenente l'idrogramma adimensionale di progetto
(riga 1)
```

```matlab
% e le ascisse temporali corrispondenti (riga 2)


D = (0:passoD:Dmax)';
npti = length(D);
% I METODO
% Con interpolazione dei dati sperimentali
%rD = interp1(rDsper(1,:),rDsper(2,:),D,'spline');

% II METODO
% Con andamento esponenziale a due parametri:
rD = rDlim + (0.5-rDlim).*exp(-D./k);

EpsiD = sqrt(Theta./(2.*D).*(2+exp(-4/Theta.*D)-(3*Theta)./(4.*D).*(1-exp(-
4/Theta.*D))));
EpsiD(1)=1;

F1=rD.*D;
F2=F1.*EpsiD;
F3=(1-rD).*D;
F4=F3.*EpsiD;

%Calcolo delle derivate centrate
for i=1:npti-2
   Der1(i)=(F1(i+2)-F1(i))/(D(i+2)-D(i));
   Der2(i)=(F2(i+2)-F2(i))/(D(i+2)-D(i));
   Der3(i)=(F3(i+2)-F3(i))/(D(i+2)-D(i));
   Der4(i)=(F4(i+2)-F4(i))/(D(i+2)-D(i));
   Der1=Der1';Der2=Der2';Der3=Der3';Der4=Der4';
end

% Costruzione della porzione sinistra dell'idrogramma
Onda(1,:)=Der2./Der1; % valori di portata
Onda(2,:)=-F1(2:length(F1)-1)'; %ascisse temporali
%Identificazione eventuali valori non congruenti
PosMin=find(Onda(1,:)==min(Onda(1,:)));
if PosMin~=1 | PosMin~=length(Onda(1,:))
 Onda(:,PosMin:length(Onda(1,:)))=[]; clear PosMin; % Rimozione dei valori non
congruenti
end

Onda=fliplr(Onda); % Ordinamento per ascisse temporali crescenti
dimSx=length(Onda');
Onda(1,dimSx+1)=1;
Onda(2,dimSx+1)=0;

% Costruzione della porzione di destra dell'idrogramma
OndaDx(1,:)=Der4./Der3;
OndaDx(2,:)=F3(2:length(F3)-1)';
dimDx=size(OndaDx');

Onda(:,dimSx+2:dimSx+2+dimDx-1)=OndaDx; clear OndadDx;
%Riporto a 0 le ascisse temporali del primo valore utile dell'idrogramma
%Partendo dal minimo
Onda(2,:)=Onda(2,:)-min(Onda(2,:));
%Partendo da -20
%Onda(2,:)=Onda(2,:)-(-20);

figure(1)
hold on
```

```matlab
StileLinea=['k-'
            'k:'];
for i=1:length(QT)

plot(Onda(2,:),QT(i)*Onda(1,:),StileLinea(round(1+abs(sin(i*pi/2))),:),'LineWidt
h',3*(i/length(QT)));
end

% Formattazione Figura

title(Nomestaz,'FontSize',14)
set(gca,'Xgrid','on','YGrid','on')
% Generazione della griglia equispaziata per le X
Xgriglia=0:10:1000;
Xsuper=find(Xgriglia>max(Onda(2,:)));
set(gca,'XLim',[0 Xgriglia(min(Xsuper))],'XTick', 0:10:Xgriglia(min(Xsuper)) )
% Generazione della griglia equispaziata per le Y
Ygriglia=0:100:1E6;
Ysuper=find(Ygriglia>max(QT));
set(gca,'YLim',[0 Ygriglia(min(Ysuper))],'YTick', 0:100:Ygriglia(min(Ysuper)))
set(gca,'GridLineStyle','-')
xlabel('Time (h)','FontSize',12)
ylabel('Q(t,T) m^3/s','FontSize',12)
set(gcf,'PaperPositionMode','auto','PaperType','A4','PaperUnits','normalized','P
aperOrientation','Landscape','Units','normalized','Position', [0 0 1 1]);
%legend(['T = ' num2str(T(1)) ' anni'],['T = ' num2str(T(2)) ' anni'],['T = '
num2str(T(3)) ' anni'],['T = ' num2str(T(4)) ' anni'],['T = ' num2str(T(5)) '
anni'],1);

saveas(gcf,'OP_MARANO.tif'); %File per uscita grafica

% Uscita delle onde di progetto su file di testo
Dtxt=0:1/12:floor(max(Onda(2,:)));
Ondatxt(2,:)=Dtxt;
Ondatxt(1,:)=interp1(Onda(2,:),Onda(1,:),Dtxt);

fid = fopen(Onde_Uscita,'w');
fprintf(fid,'D (ore)   T (anni)
%8d%8d%8d%8d%8d%8d%8d%8d%8d%8d%8d%8d%8d%8d%8d%8d\n',T);
fprintf(fid,'\n');
for iprint=1:length(Ondatxt)
   fprintf(fid,'%10.3f
%8.1f%8.1f%8.1f%8.1f%8.1f%8.1f%8.1f%8.1f%8.1f%8.1f%8.1f%8.1f%8.1f%8.1f%8.1f
\n',Ondatxt(2,iprint),Ondatxt(1,iprint)*QT);
   fprintf(fid,'\n');
end
fclose(fid);
```

11.   References

Abbott M. B., Basco D. R., Computational fluid dynamics. An Introduction for Engineers, Longman, New York, 1989.

Babister M., Ball J., Barton C., Bishop W., Gray S., Jones R. H., McCowan A., Murtagh J., Peirson B., Phillips B., Rigby T., Retallick M., Smith G., Syme B., Szylkarski S., Thompson R., and Weeks B. (2012). Australian Rainfall & Runo Revision Project 15: Two dimensional Modelling in Urban and Rural Floodplains. Number November.

Bacchi B. e Brath A. 1990. Stima delle leggi di attenuazione delle massime portate in assegnata durata. L'Energia Elettrica, n.67(4), 157-170.

Betsholtz A., Nordlöf B., 2017. Potential and limitations of 1D, 2D and coupled 1D-2D flood modelling in HEC-RAS. Master Thesis.

Brath A., Fiorentino M. e Villani P. 1994. Valutazione dei volumi di piena a frequenza assegnata. In V. Copertino e M. Fiorentino, (a cura di), Valutazione delle piene in Puglia, GNDCI-CNR, Potenza.

Brunner G.W., 2016, Hydraulic Reference Manual, US Army Corps of Engineers, Hydrologic Engineering Center, HEC-RAS, River Analysis System, Version 5.0.

Brunner G.W., CEIWR-HEC, 2016, User's Manual, US Army Corps of Engineers, Hydrologic Engineering Center, HEC-RAS, River Analysis System, Version 5.0.

Brunner G.W., CEIWR-HEC, 2016, 2D Modeling User's Manual, US Army Corps of Engineers, Hydrologic Engineering Center, HEC-RAS, River Analysis System, Version 5.0.

Chow V.T., 1959, Open channel hydraulics. McGraw-Hill.

Cook A., Merwade V., 2009. Effect of topographic data, geometric configuration and modeling approach on flood inundation mapping. Journal of Hydrology 377 (2009) 131-142.

Fiorentino M. 1985. La valutazione dei volumi di piena nelle reti di drenaggio urbano. Idrotecnica, n.3, 141-152.

Fiorentino M. e Margiotta M. R. 1997. La valutazione dei volumi di piena e il calcolo semplificato dell'effetto di laminazione di grandi invasi. In G. Frega, (a cura di), Tecniche per la difesa dall'inquinamento, Ed. Bios, 203-222.

Fiorentino M., Rossi F. e Villani P. 1987. Effect of the basan geomorphoclimatic characteristics on the mean annual flood reduction curve. In Proc. Of 18th Annual Pittsburgh Modelling and Simulation Conference, part 5, 1777-1784, April 23-24.

Fread D.L., 1974, Numerical Properties of the Implicit Four Point Finite Difference Equations of Unsteady Flow, NOAA Technical Memorandum NWS Hydro-18, U.S. Department of Commerce, NOAA, NWS, Silver Spring, MD, 123pp.

Fread D.L., 1976, Theoretical Development of an Implicit Dynamic Routing Model, Hydrologic Research Laboratory, Office of Hydrology, U.S. Department of Commerce, NOAA, NWS, Silver Spring, MD., presented at Dynamic Routing Seminar, Lower Mississippi River Forecast Center, Slidell, LA., 13-17 Dec 1976.

Horrit M.S., Bates P.D., 2002. Evaluation of 1D and 2D numerical models for predicting river flood inundation. Journal of Hydrology 268 (2002) 87-99.

IRP CNR, 2019, Rapporto Periodico sul Rischio posto alla Popolazione italiana da Frane e Inondazioni, Anno 2018.

Ispra. 2018. I dati sul consumo di suolo in Italia. Roma.

Le buone pratiche per gestire il territorio e ridurre il rischio idrogeologico, 2007, Legambiente, Operazione fiumi e Protezione Civile.

Liggett, J.A., e Cunge, J.A., 1975, Numerical Methods of Solution of the Unsteady Flow Equations, in Unsteady Flow in Open Channels, edited by K. Mahmood and V. Yevjevich, Vol. I, Chapter 4, Water Resources Publications, Ft. Collins, CO.

Macchione F., Costabile P., Costanzo C & De Santis R., 2018, Fully-Hydrodynamic Modelling Supporting Flood Hazard Assessment and Communication: A Reference Framework. Italian Journal of Engineering Geology and Environment, Special Issue 1 (2018), 101-121.

Majone U., Mignosa P., Tomirotti M. 2000a."Synthetic Design Hydrographs for Flood-Control Reservoirs and Flood-Plain Management", Proceedings of the International Conference New Trends in Water and Environmental Engineering for Safety and Life: Eco-compatible Solutions for Aquatic Environments, Capri, July 3-7 2000, Balkema, Rotterdam, The Netherlands.

Majone U., Mignosa P., Tomirotti M. 2000b. "Sul calcolo del volume degli invasi di laminazione", L'Acqua, (5), pp. 19-28.

Marcher C. 2007/2008. Applicabilità degli idrogrammi sintetici di progetto nello studio del comportamento idraulico dei corsi d'acqua naturali, Tesi Magistrale.

Miotto F., Laio F. e Claps P. 2004. Sulla valutazione indiretta delle curve di riduzione dei colmi di piena. Dipartimento di Idraulica, Trasporti ed Infrastrutture Civili, Politecnico di Torino.

NERC (National Environmental Research Council). 1975. Flood Studies Report, London.

NTC (Norme Tecniche Costruzioni) 2008. Norme tecniche per le costruzioni. D.M. 14/1/08.

Piano Stralcio di Bacino per l'assetto idrogeologico. 2004. Autorità Interregionale di Bacino Marecchia-Conca.

Pollicino G., 2007. Digitalizzazione e Analisi Numeriche di Serie Idrometriche per Corsi d'Acqua Emiliano-Romagnoli. DISTART- Università di Bologna, Rapporto Interno.

Prestininzi P. & Fiori A., 2006. A Two-Dimensional Parabolic Model for Flood Assessment. Italian Journal of Engineering Geology and Environment, 1 (2006). 5-18.

Rapporto dell'evento meteorologico del 5 e 6 febbraio 2015. ARPA Emilia-Romagna, Servizio IdroMeteoClima.

Regione Emilia-Romagna. 2017. Progetto Generale Preliminare torrente Marano e Rio Melo - Relazione Tecnica Generale.

Rossi F. e Villani P. 1987. La valutazione della piena media annua istantanea e di assegnata durata attraverso le caratteristiche geomorfoclimatiche del bacino. In F. Rossi, (ed.), Rapporto annuale Linea 1, GNDCI-CNR.

Rossi F., Fiorentino M., Versace P. 1984. Two component extreme value distribution for flood frequency analysis, Water Resour. Res., Vol. 20, n.7.

Silvagni G. 1984. Valutazione dei massimi deflussi di piena, Pubblicazione n.489 dell'Istituto di Idraulica, Università di Napoli.

Singh V. P. 1998. Two-Component Extreme Value Distribution. In: Entropy-Based Parameter Estimation in Hydrology. Water Science and Technology Library, vol 30. Springer, Dordrecht.

Stambazzi L. 2016/2017. Analisi del comportamento idraulico del torrente Marano tramite modello idrodinamico. Tesi Magistrale.

Tanda M. G., Mignosa P., Tomirotti M., Gardelli R. e Adami S. 2001. Caratterizzazione idrologica dell'asta principale del fiume Po nel tratto che va dalla confluenza della Dora Baltea all'incile del Po di Goro, Dipartimento di Ingegneria Idraulica, Ambientale e del Rilevamento, Politecnico di Milano.